A Holistic View on Aquaporins:
Production, Structure, Function and Interactions

Florian Schmitz

PhD thesis

Department of Chemistry and Molecular Biology

University of Gothenburg

UNIVERSITY OF GOTHENBURG

Gothenburg 2020

Cover illustration: Model of human aquaporin 4, PDB: 3GD8

Thesis for the degree of Doctor of Philosophy
In the Natural Sciences

A Holistic View on Aquaporins: Production, Structure, Function and Interactions

florian.schmitz@gu.se

ISBN 978-91-8009-068-1 (PRINT)
ISBN 978-91-8009-069-8 (PDF)
Available online at: http://hdl.handle.net/2077/66539

Department of Chemistry and Molecular Biology
Division of Biochemistry and Structural Biology
University of Gothenburg
SE-405 30 Göteborg, Sweden

Borås, Sweden 2020
Printed by Stema Specialtryck AB

“The secret of life, though, is to fall seven times and to get up eight times.”

Paulo Coelho, The Alchemist

ABSTRACT

Aquaporins are specialised membrane proteins, which regulate the water homeostasis of cells. In eukaryotic organisms, this process is tightly regulated, and aberrations in aquaporin functionality lead to severe pathologies in humans. The aim of this thesis is to shed light on the aquaporin function and regulation, both as individual protein targets and in the cellular context, as well as exploring various applications for human aquaporin 4, specifically. A wide range of biochemical methods have been applied, ranging from the importance of robust protein production methods, for targets as well as for their complexes, to functional and structural characterization.

For biochemical characterization and structural analysis, large amounts of pure, homogeneous and stable recombinant protein are needed. The methylotrophic yeast *Pichia pastoris* was utilized for the overproduction of the soluble protein Sirtuin2, an indirect up-regulator of Aquaporin4 in humans. The highest yet-reported yield of the protein (40 mg/l) was achieved, facilitating modulation trials of the potential drug target. The *P. pastoris* overproduction system was also employed for the expression of human AQP4, facilitating new research applications, such as improved Neuromyelitis Optica diagnosis, and a better understanding of the intermolecular binding between the monomeric subunits.

In addition, the novel structural characteristics of AQP1 from the fish *Anabas testudineus* was studied in this thesis and key residues responsible for the molecular mechanisms for osmoregulation were identified by mutational analysis combined with functional studies. By combining stopped-flow assays and molecular dynamics simulations, a novel extracellular gating mechanism could be elucidated for this particular aquaporin isoform, being less efficient in water transport than AQP4 and phosphorylation of Tyrosine 107 leads to a closed conformation involving loop C.

Functional studies were also performed for the development of a new method for testing the transport specificity of aquaporins regarding hydrogen peroxide. The transport rate can be standardized in relation to protein quantity, resulting in a more accurate determination of transport rates as compared to cell growth assays.

Interactions between proteins are difficult to evaluate, but using bimolecular fluorescence complementation, membrane protein complexes could be quantified and screened *in vivo* in a high-throughput manner. During the course of this work, we standardized sample preparation and defined criteria which allow the discrimination between constructive and random interactions. Taken together, the results presented in this thesis lay the fundament for future screening for novel interaction partner using a cDNA library, a method that is not limited to aquaporins.

SAMMANFATTNING PÅ SVENSKA

Vatten är nödvändigt för alla livsformer på jorden och transporten av vattenmolekyler in i celler är tajt reglerad av en speciell typ av membranbundna proteiner: aquaporiner. Icke fungerande aquaporiner ligger bakom flera av människans sjukdomar, så som utveckling av tumörer, diabetes insipidus och Alzheimers sjukdom. Innan vi kan utveckla specifika läkemedel finns det fortfarande mycket att lära när det gäller den grundläggande molekylära mekanismen som kan kopplas till olika sjukdomar. Resultaten som presenteras i denna avhandling fördjupar vår förståelse, inte bara för aquaporinerna i sig, men också för hur de regleras, som en del av de cellulära nätverk som de är del av. Det är oftast inte bara en metod som behövs för att belysa komplexa frågeställningar, det är därför målmolekylerna studeras utifrån olika perspektiv och med hjälp av olika metoder inom proteinforskning. Tillgången till stora mängder av stabilt och rent protein är en vanlig begränsning för strukturell och biokemisk karakterisering. I arbetet som beskrivs i den här avhandlingen har den metylotrofa jäststammen Pichia pastoris använts för att producera lösliga såväl som membranbundna proteiner från olika organismer; AtPIP2;4 och SoPIP2;1 från växtriket samt SIRT2 and AQP4 från människa och AQP1 från fisk. Pålitlig proteinproduktion var förutsättningen för att lösa strukturerna av AtPIP2;4 och cpAQP1aa, där den information som erhölls användes för att utvärdera olika funktionella aspekter hos dessa två aquaporiner. Genom att sedan kombinera mutations- och funktionsstudier med molekylsimuleringar kunde en ny regleringsmekanism hos aquaporinet från fisken belysas och en modell för dess varierande osmoreglering presenteras. Funktionsstudier användes också för att utveckla en ny metod för att utvärdera transportspecificiteten för aquaporiner med avseende på väteperoxid. I den här metoden kunde transporthastigheten standardiseras i relation till mängden protein vilket gav en mer exakt uppskattning jämfört med helcellsstudier. Slutligen är interaktioner mellan proteiner svåra att utvärdera, men med hjälp av bimolekylär fluorescens komplettering kunde membranproteinkomplex kvantifieras och screenas med stor genomströmning in vivo. Sammantaget så lägger resultaten från denna avhandling grunden för framtida screening av nya interaktionspartners från ett cDNA bibliotek, en metod som inte är begränsad till aquaporiner.

LIST OF PUBLICATIONS

This thesis is based on the following studies, referred to in the text by their Roman numerals.

I. **Schmitz F**, Luthman K, Jarho E, Hedfalk K, Seifert T (2020) Efficient production of pure and catalytically active SIRT2 in *Pichia pastoris*. *Manuscript*

II. Zeng J, **Schmitz F**, Isaksson S, Arbab O, Andersson M, Sundell K, Eriksson L, Swaminathan K, Törnroth-Horsefield S, Hedfalk K (2020) Novel structural mechanism of extracellular gating of aquaporin from the fish climbing perch (*Anabas testudineus*). *Manuscript*

III. Wang H, Schoebel S, **Schmitz F**, Dong H, Hedfalk K (2020) Characterization of aquaporin-driven hydrogen peroxide transport. *Biochimica et Biophysica Acta* (BBA)-Biomembranes, 1862(2), 183065.

IV. Wang H, Schoebel S, **Schmitz F**, Dong H, Hedfalk K (2020) Quantitative analysis of H_2O_2 transport through purified membrane proteins. *MethodsX*, 7, 100816.

V. **Schmitz F***, Glas J*, Neutze R, Hedfalk K (2020) High-throughput screening combining bimolecular fluorescence with flow cytometry reveals constructive membrane protein complex formation. *Manuscript*

* These authors contributed equally

CONTRIBUTION REPORT

Referred to publications by Roman numerals

I. I performed the production and purification of SIRT2. I quantified the protein expression levels and took part in writing the article and the making of the figures.

II. I produced and purified all mutated variants of cpAQP1aa and performed all functional experiments on water and glycerol transport. I took large part in curating the data, formal analysis, methodology and visualization.

III. I performed the majority of the experiments for water transport. I took large part in curating the data, formal analysis, methodology and visualization.

IV. I performed the majority of the experiments for water transport. I took large part in curating the data, formal analysis, methodology and visualization.

V. I performed the majority of the experiments and was involved in the development of the flow cytometry assay for membrane complexes. I took large part in curating the data, formal analysis, methodology and visualization. I wrote the original draft and took part in the editing.

TABLE OF CONTENT

ABBREVIATIONS

SDS-PAGE	Sodium dodecyl sulfate polyacrylamide gel electrophoresis
NPA	Asparagine, Proline, Alanine signature motif in aquaporin structures
RAB	Ras-related protein in brain
SNARE	Soluble N-ethylmaleimide-sensitive-factor attachment receptor
ROS	Reactive oxygen species
PPI	Protein:protein interaction
AQP	Aquaporin
TM	Transmembrane
NF-kB	Nuclear factor 'kappa-light-chain-enhancer' of activated B-cells
SIRT	Sirtuin
NAD	Nicotinamide adenine dinucleotide
CNS	Central nervous system
PD	Parkinson's disease
PAMP	Pathogen-associated molecular pattern
OAP	Orthogonal arrays of particles
NMO	Neuromyelitis optica
NMOSD	Neuromyelitis optica spectrum disorders
GLT-1	Glutamate transporter 1

CFTR	Cystic fibrosis transmembrane conductance regulator
Å	Ångström (10^{-10} m)
ar/R	Aromatic / Arginine restriction site in aquaporins
FDA	Food and drug administration
GRAS	Generally recognised as safe
CHO	Chinese hamster ovary cell
CMC	Critical micelle concentration
MST	Microscale thermophoresis
SEC	Size-exclusion chromatography
IEX	Ion-exchange chromatography
HIC	Hydrophobic interaction chromatography
MAD	Multi-wavelength anomalous dispersion
SAD	Single-wavelength anomalous dispersion
DWI	Diffusion-weighted magnetic resonance imaging
DLS	Dynamic light scattering
HTS	High-throughput screening
GFP	Green fluorescent protein
YFP	Yellow fluorescent protein
PALM	Photoactivated localization microscopy
FAST	Fluorescence-activating and absorption-shifting tags
FACS	Fluorescence-activated cell sorting

PDB	Protein data bank
NMR	Nuclear magnetic resonance
PAL	Photoaffinity labeling
IMAC	Immobilized metal ion affinity chromatography
MRI	Magnetic resonance imaging
BCR-Seq	B-cell repertoire sequencing
Ig-Seq	Immunoglobulin sequencing
POPC	Phosphatidylcholine = 1-palmitoyl-2-oleoyl-sn-glycero-3-phosphocholine
TEOS	Tetraethyl orthosilicate
MAS	Magic angle spinning (solid-state NMR)
MD	Molecular dynamics
HOLE	A program for the analysis of pore dimensions[1]
ITC	Isothermal titration calorimetry
SC	Synthetic complete
kDa	Kilo Dalton
AOX	Alcohol oxidase
OD	Optical density at wavelength 600 nm

1. INTRODUCTION

One of the key factors in the evolution of biological life on Earth was the development of a separate environment in which catalytic reactions could take place, biotic information was saved for replication and energy from the outside could be stored in chemical molecules.[2] The convergence of these factors was the start point for the successful biological trial-and-error process we now call evolution. Without the differentiation between an outside and an inside, defined by the very first lipid bilayer, the separated Darwinian biochemical adaption processes would have never appeared.[3] The diversity of life in a broad range of abiotic conditions is possible because the early membrane vesicles, through interactions of free lipids, have formed a thermodynamically stable assembly so that their hydrophilic parts are exposed to the surrounding water and internal solutions.[4] Between the bilayer, the hydrophobic core prevents the diffusion of hydrophilic solutes, while gases can diffuse through the barrier.[5] The active transport of molecules was already assumed in the 1940s of the last century, but a first valid model, the fluid mosaic model, considering proteins as the driving force for membrane transport, was developed 1972.[6, 7]

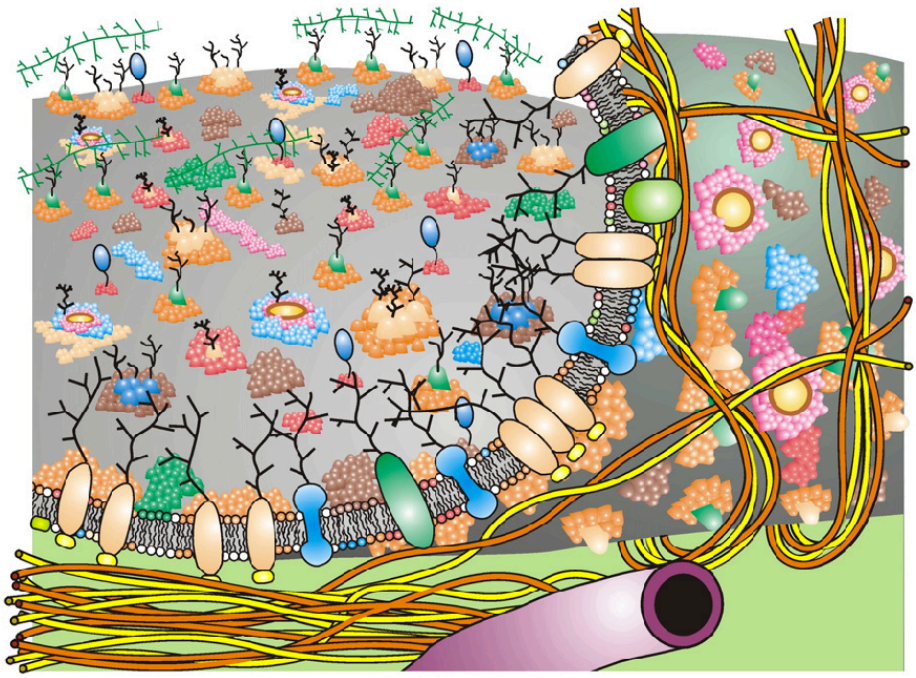

Figure 1: A schematic presentation of a cell membrane from an intracellular perspective, containing membrane domain structures and membrane-associated cytoskeletal elements.[7]

Today we know that the membrane is not only a floating sea of lipids, it is much more complex and it is crowded with specialized proteins, which typically make up 50 % of the membrane mass (see figure 1).[8,9]

The lipid composition of membranes in organisms is highly specific in different cell types, among organelles and varies depending on the functionality.[10] The lipid backbone is much more than a backdrop for the incorporated proteins; instead, it can enhance the formation of oligomers or effect the function of proteins.[11, 12] Due to the low passive diffusion rate of molecules through the lipid bilayer, rapid responses to environmental changes and the control of gradients are associated with the functionality of the membrane-integrated proteins.[13]

1.1. MEMBRANE PROTEINS

Proteins are essential for life, which is expressed in their nickname "building blocks of life". Literally, proteins shape our bodies (cytoskeleton), make us fall in love (oxytocin) and catalyze reactions, that enabled life on earth for us humans (rubisco).[14-16]
As we saw in the previous chapter, cell membranes are important for building a compartment and essential for the reactions that take place for survival.[2]
A closed cell, on the other hand, would deprive the organism of water and energy. As a consequence, specialized proteins are embedded in the phospholipid bilayer, which act as gatekeeper for the cells. These integral membrane proteins are important, among other things, for controlling the in- and outflux of molecules, either passively or by using energy as well for dynamic reactions by cascade signalling.
The versatile role of membrane proteins for cellular function makes them important targets for drug development. While only 26 % of all genes are encoding for membrane proteins, they are targeted by more than 50 % of all available drugs.[17] Membrane proteins are also crucial for the constitution of proton gradients for energy production and regulation of the osmotic balance of cells.[18] Fulfilling both roles, guiding water through the plasma membrane, while stabilizing a proton gradient at the same time, needs a highly specialized protein. Evolution shaped a class of membrane proteins for this task: the aquaporins.

1.2. AQUAPORINS

Organisms began colonizing the land side of the Earth about 3.5 billion years ago, and although evolutionary progress has produced a huge variety of life forms, they all rely on the same old dependency: They need water to survive.[19] Water enables cell biochemistry, but the flux inside and outside of biological systems through membranes must be tightly controlled. Water homeostasis is passively regulated by aquaporins along an osmotic gradient, a functionality which makes them ubiquitous in all kingdoms of life.[20]

For a long time, it was unclear how the water transport in cells is controlled. A solely passive transport could be excluded in 1957, by measuring the high water flux rates of human red blood cells.[21]

Since a passive transport through the bilayer is not capable of sustaining the water household of a cell, in the absence of an alternative theory, the presence of aqueous pores with a diameter of 3.5 Å in the membranes was initially suspected.[22] It took until 1970, when Macey and Farmer proved that mercury-sensitive proteins must be responsible for the flow of water across the cell membrane, and another 23 years before the amino acid that is mercury-sensitive in human AQP1 (cysteine 189) was discovered.[23, 24] Patience is definitely required in structural biology, which can be illustrated by the discovery of the first aquaporin, which began in 1988 as a persistent 28 kDa SDS-PAGE band in the laboratory of Prof. Peter Agre when working with human erythrocytes.[25]

It took another four years until the then so-called CHIP28 protein could finally be isolated, which filled the role of the "water-filled channels in the membrane" and was awarded the Nobel Prize in 2003.[22, 26] Compared to their soluble counterparts, membrane proteins are more challenging to classify.[27] Aquaporins, which are classified as part of Major Intrinsic Proteins (MIPs) can be roughly divided into two major groups due to their specificity not only for water (orthodox aquaporins) but also for small solutes such as glycerol and urea (aquaglyceroporins).[28, 29] Mammalian AQP11 and AQP12, the so-called superaquaporins, form yet another subclass. Their water permeability is still being discussed, while their intracellular distribution indicates a role other than just water transport.[30, 31]

1.2.1. STRUCTURAL CHARACTERISTICS

Although the basic structure of membranes is formed by the lipid bilayer and the varying content of phospholipids, glycolipids and sterols, the specific function of each membrane segment is defined by the incorporated protein. Since the function of a protein is directly linked to its structure, high resolution structures give valuable insights into the underlying molecular mechanisms. In aquaporin research, the first high-resolution structure of human AQP1 (hAQP1) in 2000 supported the previously predicted "hourglass" shape of the central water pore.[32-36] Structural biology methods have made enormous progress since the beginning of the millennium, and all revealed structures share a structural homologues design: an assembled homotetramer, consisting of individually functional monomeric subunits (see figure 2).

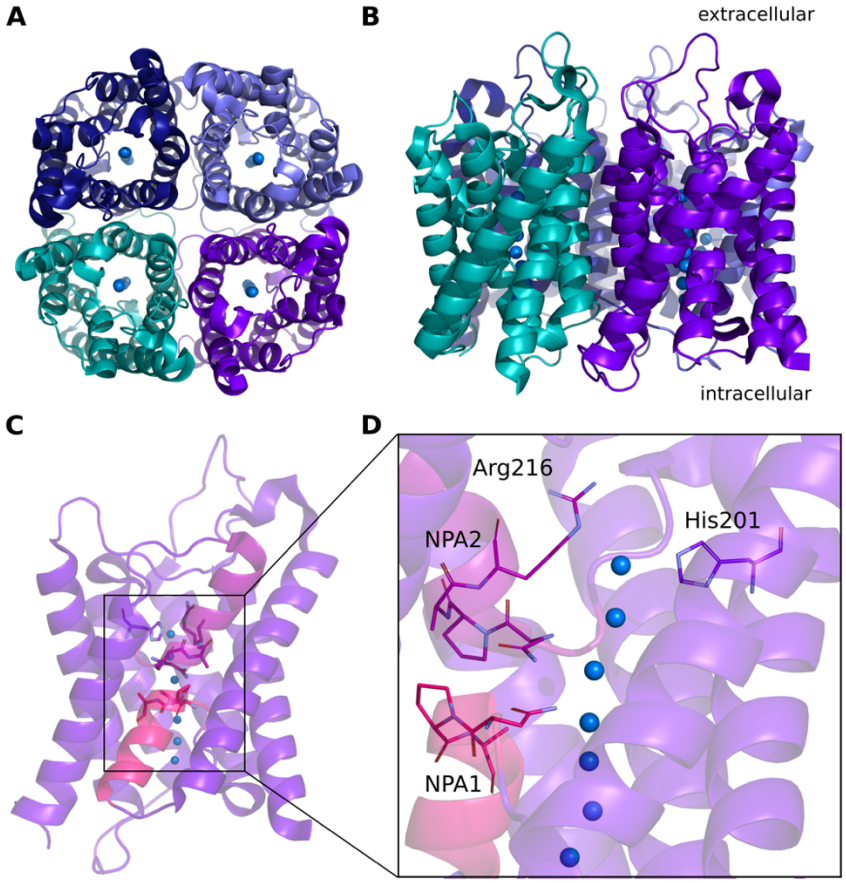

Figure 2: A) Top view of the AQP4 tetramer (PDB: 3GD8), showing four monomeric subunits and the single file water transport in each pore. B) Side view of A, indicating the orientation of AQP4 in the membrane. C) AQP4 monomer with highlighted half helices, containing the NPA motifs. D) Zoom in the constriction region, containing the R/Arg selectivity filter.

The position of these subunits also creates a pseudo- or central pore, which can have additional transport features as CO_2 permeation and ion transport.[37-39] The co-transport function of aquaporins beside water in the putative central pore is controversially discussed, one reason for this could be the general structural similarity between aquaporin isoforms, which is not a single factor for the observed effect.[40, 41] There is strong evidence that multiple factors determine the function and specificity of the different aquaporins subclasses, so that it is important to know the structural characteristics that aquaporins have in common.[42] From there, structural deviations give insight in cellular physiology, something that will be discussed in this thesis.

Each water pore is folded by six surrounding transmembrane helices, connected by five loops and the N- and C-termini are located on the cytosolic side of the membrane.

Two elongated loops fold back into the membrane from the intra- and extracellular side and form a seventh pseudo transmembrane helix. Water molecules entering the pore will first pass an arginine (R/Arg) selectivity filter, impairing the entrance of high molecular weight and charged molecules.[43] The filter is the narrowest part of the protein and positioned 8 Å away from the highly conserved part of the protein, which contains the two characteristic NPA (N/asparagine, P/proline, A/alanine) motifs.[44]

In orthodox aquaporins, single water molecules with a diameter of 2,7 Å are forced to squeeze through a pore with a diameter of about 3 Å, thus ensuring the exclusion of protons and ions by electrostatic repulsion.[45] This feature is crucial for preserving the gradient disparities across the membrane, e.g. for photosynthesis or mitochondrial respiration.

The diameter of the constriction region in aquaglyceroporins, however, is more variable, ca. 0,5 Å - 1 Å wider than in orthodox AQPs, to allow larger solutes to pass the hydrophobic barrier.[46] Additionally, the more hydrophobic amino acid lining in the pore leads to an optimized passage of larger and more hydrophobic solutes such as glycerol.[47]

Aquaporins facilitate the rapid transport of water molecules while being repulsive to protons and solutes being repulsive to protons and solutes, when they are not required.[48] Each individual aquaporin subunit is able to mediate the transport of up to 3×10^9 water molecules per second, and although water is elementary for the cell, there are situations where the flux must be controlled.[49] Although aquaporin production can be regulated at the level of gene transcription, it is a complex and slow process.[50] In the next chapter, posttranslational pathways for regulating aquaporin activity are discussed, with gating and trafficking being the most important ones. Another important factor is the interaction of aquaporins with other regulation proteins, and the usage of PPIs as complementation marker.

1.2.2. AQUAPORIN REGULATION AND INTERACTIONS

The water transport function of aquaporins is beneficial to all organisms, but the intrinsic waterflow itself cannot be actively controlled in response to environmental signals. In the course of evolution, cells have adopted three main regulatory strategies to regulate the flux of water through the membrane. While the regulation of water flow is slow at the transcriptional and translational gene level, post-translational regulations such as trafficking and gating allow for a more rapid response at the molecular level.[51]
Basically, eukaryotic cells either store inactive aquaporin molecules in intracellular vesicles (trafficking), or they manipulate the functionality of the proteins to restrict the waterflow (gating).
These two processes can be triggered by the binding of regulatory proteins, modifying the target protein inducing a conformational change. As a result, either the diameter of the central pore in the transmembrane region becomes narrower (pinching effect), or an external loop of the protein plugs the central pore (capping effect).[52]

The regulation of aquaporin by trafficking was described before gating as a way to regulate eukaryotic water transport. The activity of water transport from the membrane is reduced by the storage of inactive aquaporins in intracellular vesicles in response to environmental stress. The mechanism was first described for AQP2 in human kidney, responsible for the absorption of water from pre-urine.[53] The relocating of proteins to the cell membrane can be triggered by various compounds. In eukaryotic cells, hormones are often involved (vasopressin in the case of AQP2), but also soluble proteins (RAB and SNARE proteins) and modifications of the proteins themselves (S-acylation) can regulate the trafficking.[54-56] The abundance and identity of membrane and surface proteins is crucial for cell functionality and deviations from the transport mechanism can lead to severe disorders. Abnormal trafficking is evident in several neurodegenerative disorders such as Alzheimer`s disease, but it is also the cause of diabetes insipidus by affecting the ability to concentrate primary urine.[57, 58]

Gating of aquaporins, which is especially relevant in plants, is a response to changes in environmental conditions (presence of ions, draught), or as reaction to signaling intermediates such as pH changes in the vacuole or ROS.[59]
Spinach aquaporin SoPIP2;1 is such a gated water channel, triggered by flood and drought, a conformational change is induced involving phosphorylation and changes in pH.[60, 61] It is important to note that gating is an equilibrium state, and the plugging mechanism is hence reversible.[62]

AQP0 is an example of a gated mammalian aquaporin, which is present in the eye lens where it mediates cell junctions. The regulation of AQP0 is Ca^{2+} dependent, inducing the binding of the regulatory protein calmodulin (CaM) to the C-terminus of AQP0, resulting in a pore closure.[63, 64] It has been shown that cooperative complex formation exhibits 1:2 stoichiometry by a single Ca^{2+}-activated CaM binding to two adjacent AQP0 monomers.[65]
Aquaporin gating has also been an established regulatory mechanism for other mammalian aquaporins, such as AQP1, AQP3, AQP4, AQP5, AQP10, as well as for AQPZ from Escherichia coli.[52, 66-72]

Aquaporin interactions and cellular function

Since proteins and PPIs are crucial for the cellular functionality of all living organisms, deviations from normal protein function and patterns of PPI can lead to disease states. Examples are disturbances in the p35 suppressor protein interactome, resulting in tumor genesis or the development of neurodegenerative diseases like Alzheimer`s disease.[73, 74]
Most often, these pathological conditions are related to key proteins and multi-protein complexes involved in a variety of fundamental processes like the modification of other proteins (sirtuins) or water homeostasis in cells (aquaporins).
Protein-protein interactions of aquaporins are crucial for their underlying functions and several physiological processes in humans relate to them.[75] An aberration of these mechanisms has significant consequences for the organism, resulting in a variety of severe pathologies.[76, 77] The diversity of clinical syndromes cannot be explained with the passive transport mechanisms of aquaporins alone, indicating the importance of the regulatory role of these membrane proteins.[78] Since the intrinsic structural features of aquaporins are highly identical between different organisms, the various functionalities can be explained by the different types of interactions aquaporins form with proteins.[44]
The structurally most important interactions of aquaporins involve the formation of quaternary structures as tetramers. These arrangements might consist of the same monomeric subunit, which is the most common abundance pattern, or different AQP monomer isoforms assembly into hetero-tetramers (such as TIPs and PIPs in plants; AQP0 in mammalia).[79-82]
Some aquaporins are able to form supramolecular assemblies, orthogonal arrays which form interactions between cells. AQP0 and AQP4 are known for not only transporting water, but also for the formation of these orthogonal arrays as cell-adhesion junctions.[83]
Another form of PPIs are Transient interactions for AQP regulation in higher eukaryotes, which are mediated by post-translational modifications.[84, 85]

On the molecular level, these interactions are mainly facilitated by the C-terminus of the aquaporins, accompanied by the more flexible extracellular loops A and E.[86, 87] The stabilization of aquaporin tetramers in the membrane is mainly maintained by the interaction of transmembrane (TM) helices 1 and 2 in conjunction with TM 4 and 5, showing the diverse range of possible interaction properties.[87]
The diversity of potential aquaporin interaction partner, especially in view of potential drug development, indicates the importance of methods, which are able to detect these PPI networks.
The pathology of diseases on a molecular level is complex and cannot be traced back to single PPIs, hence existing methods for detection must be improved.

Aquaporin function in their cellular context

Noteworthy, it is not only the direct interactions between two proteins that are important for the regulation of a certain protein target, in the larger cellular context, indirect interactions are also of major importance. One example is the indirect effect of sirtuins on the regulation of aquaporins.
Sirtuins control a broad spectrum of cellular processes through their ability to suppress gene transcription by epigenetic mechanisms.[88] SIRT2 is one of the nuclear sirtuins (beside SIRT1, 6 and 7), and its inhibition leads to the up-regulation of AQP4 through enhanced NF-kB activation.[89] The regulation, co-expression and localization of sirtuins together with aquaporins have been reported earlier, but the exact details are still unclear.[90-92] To shed further light on these processes and to characterize the sirtuin and the interactions involved, the production of a sirtuin homologue, in *P. pastoris* will be discussed. Importantly, the availability of high-quality protein samples is crucial for biochemical characterization and medicinal development of putative drug targets, like SIRT2.

The effects of the seven mammalian SIRT isoforms on various disorders depends on their modulation as well as their up- and downregulation of the proteins which have different consequences on the progress of various diseases (see figure 3).

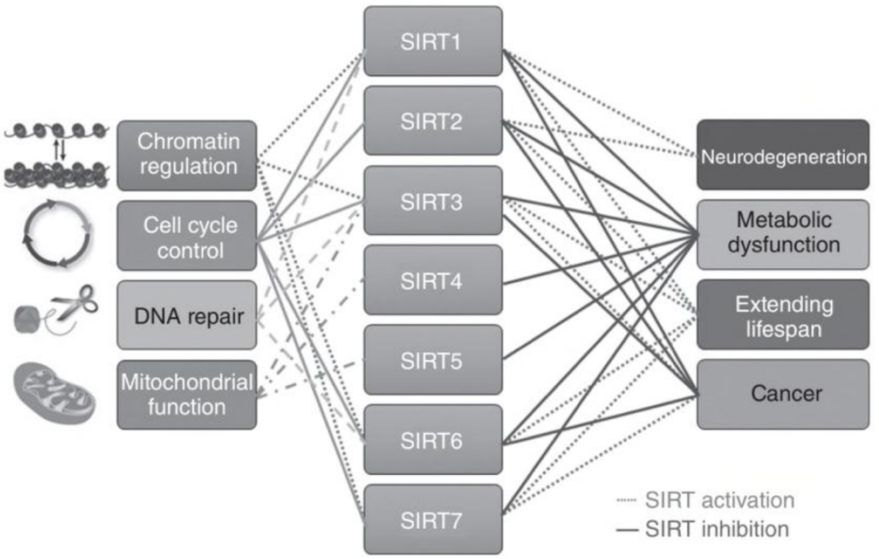

Figure 3: Sirtuins: Biological functions and influences on various disorders related to specific SIRT homologues.[93]

While the activation of sirtuins in general is associated with a positive impact on metabolic and age-related diseases, the inhibition of the enzymes shows beneficial effects for cancer treatment, infectious and neurodegenerative disorders.[94]

Understanding the mechanisms behind sirtuin modulation is the first step towards the development of drugs selectively targeting the effects of their regulation.[95]

SIRT2 is a cytosolic NAD^+ dependent protein deacetylase, which is mainly expressed in the mammalian CNS. The enzyme is involved in crucial physiological functions and a key player in tumorigenesis.[96-98]

SIRT2 is a promising drug target, since its inhibition attenuates the toxicity of α-synuclein in Parkinson's Disease (PD), but also the development of tumors.[97, 99] In addition, the development of a potent and selective inhibitor is crucial for the investigation of further cancer control strategies based on SIRT2 modulation.[100] Interaction and structural studies require a high yield supply of pure and homogeneous protein sample.

1.2.3. PLANT AQUAPORINS

One of the key characteristics of living organisms is their ability to move. From the six main kingdoms of life, plants are the least mobile subclass. While other eukaryotic organisms, such as mammalians, are able to change their environmental biosphere, *plantae* have had to adapt to their habitat. Since water is a volatile resource, plants developed a complex water uptake system to sustain their cellular homeostasis.
In 1893, Böhm postulated the cohesion-tension theory, which provided a mechanism for how plants supply their cells with water and nutrients.[101] The theory has been updated over the years, but the use of the capillary effect is still an essential factor for water transport in plants.[102-104] Another factor in water transfer is the use of osmosis for water flow between the cells to maintain cell turgor pressure.[105]
Aquaporins in the membranes of plants facilitate the flow of water and allow the cells to build up the turgor necessary to expand the hydraulic pressure to supply upper plant parts against gravity. Maintaining an optimal level of osmosis is existentially important for plants, and the variability of aquaporins enable plants to adapt to different niches and physiological conditions.[59] Plant aquaporins are not only involved in osmosis regulation, but also in leaf hydraulics, stomata movements and responses to environmental stimuli.[106-109]
While humans have a variety of 13 aquaporin isoforms, plants developed between 30 and 70 aquaporin homologues, adopted to specific environmental needs.[59, 110]
Among others, gene duplication has led to the high variety of homologues and the aquaporins of vascular plants can be assigned to five subfamilies: Plasma membrane intrinsic proteins (PIPs), the tonoplast intrinsic proteins (TIPs), the nodulin-26 like intrinsic proteins (NIPs), the small basic intrinsic proteins (SIPs) and the X-intrinsic proteins (XIPs).

The versatility of aquaporin phenotypes is shown by the different substrates that are transported into the cell. Plant aquaporins have been shown to transport gases, metalloids (e.g. boric acid and arsenite) and small dissolved substances such as urea and NH3.[107, 111, 112] They also play a vital role in the protection against pathogens, namely in the pathogen-associated molecular pattern (PAMP) immune response of plants. PIPs mediate the translocation of externally applied hydrogen peroxide (H_2O_2) from the apoplast in the cytoplasma, a signal for the presence of pathogens.[113, 114] H_2O_2 is a reactive oxygen species (ROS) and involved in many signalling processes related to stress response and regulation of the programmed cell death program in plants.[115]

The transport specificity of plant and mammalian aquaporins for hydrogen peroxide has so far been tested with cell based cultures.[116-118] In this thesis we present a method to evaluate the H_2O_2 transport on protein level.

1.2.4. HUMAN AQUAPORINS

Aquaporins occur in all tissues of the human body and conduct the functionality of single cells up to organs. In mammals, 13 AQPs (AQP0-12) have been identified and historically they have been divided into subclasses, related to their substrate specificity. Classical, or orthodox, aquaporins (hAQP0, 1, 2, 4, 5, 6, and 8) transport water, while the specificity of hAQP3, 7, 9, 10 and 12 includes small solutes beside water.[119, 120] Based on their versatility these so called aquaglyceroporins become an interesting drug target.[121-123] A third class comprises the superaquaporins hAQP11 and 12, which are not investigated in detail, but recent studies indicate a correlation with cyst-like disease and pancreatitis.[124, 125]

Since aquaporins exist in all tissues, misfunction of the transport effect has direct implications on health.

This can, for instance, be the case with uncontrolled influx of water into cells after injuries (edema). In the brain, AQP4 is related to critical tissue swelling and a potential drug candidate must inhibit uncontrolled waterflux, while being a non-toxic alternative to the heavy metal salts used at the moment.[126, 127]

Table 1 shows diseases linked to aquaporins, while the function and medical aspects of AQP4 are discussed in more detail in the next chapter.

Table 1: Diseases linked to aquaporins and their specificity for transport. [78, 128-151]

Aquaporin	Specificity	Related disease
AQP0	**Water, CO_2**	**Congenital lens cataract**
AQP1	**Water, H_2O_2, gases**	**Cancer development**
AQP2	**Water**	**Nephrogenic diabetes insipidus, water balance disorders**
AQP3	**Water, urea, glycerol, small solutes, metal ions**	**Gastric cancer regulation, skin tumorigenesis**
AQP4	**Water**	**NMOSD, brain oedema, brain cancer, Alzheimer`s disease**
AQP5	**Water, CO_2**	**Sjögren`s syndrome**
AQP6	**Water, anions, small solutes, gases**	**Unknown**
AQP7	**Water, ions, small solutes**	**Obesity, metabolic abnormalities**
AQP8	**Water, glycerol, H_2O_2, small solutes**	**Bowel syndrome, polycystic ovary syndrome**
AQP9	**Water, glycerol, metal ions, small solutes, gases**	**Polycystic ovary syndrome, insuline resistence, Alzheimer`s disease**
AQP10	**Water, glycerol, small solutes**	**Pompholyx, psoriasiform acanthosis**
AQP11	**Water, glycerol**	**Polycystic kidneys, hepatocyte vacuolization**
AQP12	**Unknown yet, secretion function suspected**	**Unknown**

1.2.5. AQP4

As described before, aquaporins are essential for the water supply of cells, which also applies to the central nervous system (CNS). Since the brain consists of about 80 % water, and its function inextricably coupled to water homeostasis, the three brain water-channels (AQP1, 4 and 9) must play central roles in brain functionality and physiology.[152, 153]

Aquaporin 4 is mainly expressed in the astrocyte end-feet of glia cells, facilitating the movement of water out and into the cells.[154] The polarization of AQP4 is strongly correlated with its ability to supply the astrocytes with water from the blood vessels, so called blood-brain-barrier transport. At the structural level, the orthodox AQP4 hosts a classic NPA motif and selectivity filter as described in chapter 1.2.1 (refer properly). AQP4 has the ability to form higher order structures, so-called orthogonal arrays of particles (OAP), a property, it shares with AQP0.[75] The size of these OAPs is defined by the ratio of the mainly expressed AQP4 isoforms M1, (323 amino acids) and M23 (301 amino acids), which differ in their translation and splicing lengths.[155-157] The AQP4 splice variant M23 is mainly responsible for OAP formation, while a mixture of the two isoforms, depending on the ratio of the isoforms, still promotes array formation.[158] OAP formation is an exclusive feature of AQP4 and clinically relevant, by being the target of anti-AQP4 immunoglobulin G autoantibodies (NMO-IgG), involved in NMOSD.[159, 160] An important factor for the distribution and anchoring of AQP4 in the membrane is the expression of the recently discovered extended form of AQP4 (exAQP4).[161] Translational readthrough expands the regulatory potential of AQP4 and ensures the correct polarization of the protein at the astrocytes.[162] All these multifactorial dependencies, such as the translation of AQP4 at the molecular level, the correct physiological localization in the membrane and the formation of higher structural features, increase the risk that AQP4 is associated with various diseases.

Today we know that AQP4 is involved in many clinical symptoms, from Alzheimer's disease to neuropsychiatric disorders and brain edema.[163-166] AQP4 is also the key protein for understanding the auto-immune disease Neuromyelitis optica spectrum disorder (NMOSD), affecting the CNS and optical nerves.[167] In their pathogenesis, patients show the development of aquaporin4 antibodies (AQP4-IgG) that bind to the water channel in their astrocytes. In the final stage of the disease, the complementing reaction following the binding of the antibody to the AQP4 antigen leads to blindness and paralysis. A major challenge in the diagnosis of NMOSD is the ability to detect the AQP4-IgG in patient serum, which is the first step towards diagnosis and accurate treatment of the disease.[168, 169]

AQP4 is a membrane protein and water channel of great interest for medical and technical research. Hence, the majority of the work presented in this thesis is focusing on this specific target where (un-, once-, and double-) labeled human AQP4 (hAQP4) has been produced for various research applications, all aiming towards an increased understanding of the AQP4 molecular mechanism. These include the characterization of intermolecular AQP4 homotetramerization, the characterization of circulating AQP4-IgG on molecular level and the utilization of silica-stabilized AQP4 as a technical water filter. Another topic is the larger physiological function in the cellular context being exemplified by the interaction of AQP4 with calmodulin and the relationship of AQP4 to sirtuin 2 (SIRT2), a deacetylase which is involved in many physiological processes and a potential anti-cancer drug target.[100, 170]
Aquaporin interactions are fundamental for cellular function with AQP4 being no exception. Interactions of hAQP4 were identified with $K_{ir}4.1$, a potassium channel in astroglias, GLT-1, SUR1-TRPM4, Alpha-1-Syntrophin and CFTR.[171-175]
In this thesis we lay the fundament for methods able to screen and verify novel interaction partner of (membrane) proteins, with a focus on aquaporins.

2. METHODOLOGY

Back in 1838, when chemistry was a dirty and hand-made business, the Dutch scientist Gerardus Johannes Mulder published his results of working with egg-white-like substances, which he extracted from plants and animals.[176] He "asserted that this material was the essential general principle of all animal body constituents…".[177] Mulder worked with albumin, fibrin and casein and named the identical organic base material *protein*, a word he adopted from the Swedish chemist Jacques Bursailleus. Basically, researchers from the 19th century had the same problems we face today in our professional routine: 1.) We have to isolate sufficient amounts of **pure protein**. 2.) Our senses are not able to investigate the **structure** of our molecular target, with the consequence that 3.) the **function** of a protein cannot be explained. The correlation between the structure and function is fundamental in protein science, especially in protein-protein interactions. One of the first regulatory interaction pairs discovered was trypsin with its inhibitor in 1906.[178] It took decades of technological development to investigate protein-protein interactions in routine applications.[179, 180] The nature of protein interactions and their networks is still relevant in modern biochemistry, and a separate chapter will deal with the question: 4.) how do we **detect protein interactions**?
The next chapters will deal with the challenges associated to protein production, focusing on membrane proteins for various analytical purposes.

2.1. PRODUCTION AND PURIFICATION OF MEMBRANE PROTEINS

Nowadays we can no longer imagine the laborious work of scientist 200 years ago to obtain the objects of their studies. Compared to their colleagues in the fields of botany and zoology, they were unable to study proteins in the wild. On the other hand, our curious predecessors were still dependent on plants and animals as production hosts. It was not uncommon to find the first biochemists (chemist at that time) to extract their study objects in slaughterhouses or in production plants. These roots are still present in the names of the amino acids. In the case of the first discovered amino acid asparagine, the name derivates from the plant *Asparagus officinalis*, which naturally contained a higher yield of the amino acid. These yields were not high in modern terms, for example, the Italian chemist Arnaldo Piutti reported that he had to process 6500 kg germ buds to gain enough protein crystals to perform his experiments.[181]

Today, we also need large quantities of pure and functional protein, but the development of recombinant production techniques has substantially simplified the entire process from gene to target protein.
From my experience it is well invested time to consider the production, purification and characterization process as a holistic strategy. The entire setup for producing and purifying a specific target is unique and cannot simply be replicated for two proteins, even though there are high similarities. The most important steps in (membrane) protein production that need to be considered are shown in figure 4. In the next chapter I will first discuss different expression systems, followed by the review of the production host *Pichia pastoris*, used for the bulk protein production in this thesis. Then we will learn more about protein purification and the use of the pure protein for structural and functional analysis, before we finally deal with methods of protein interaction.

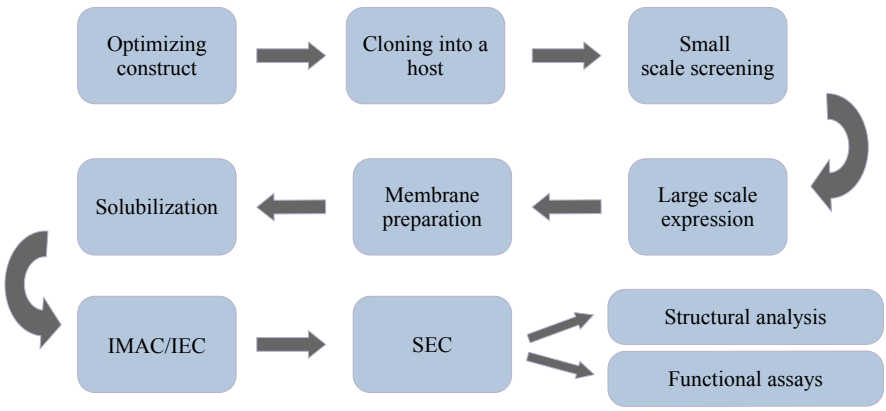

Figure 4: Flowchart of the typical steps towards structural and functional analysis of a protein target.

2.2. PROTEIN PRODUCTION HOSTS

Today, a wide variety of hosts are available for recombinant protein production; mainly bacterial, yeast and mammalian / higher eukaryotic host systems. The choice of a production system to a large extent depends on the target which should be obtained in the end. All expression systems have their intrinsic advantages and disadvantages, but the first thing to consider is the origin of the protein target itself.

Working with eukaryotic proteins requires the presence of post-translational modifications (PTMs), and the host used for expression must be able to perform glycosylation, phosphorylation, while providing a eukaryotic cell like machinery for the correct folding of the functional protein, especially valid for membrane protein targets.
Prokaryotes do not provide this, but are cheap and easy to modify and are used as a pre-host for cloning and plasmid preparations.[182] There have been efforts to enable *E.coli* to express suitable membrane protein targets, overcoming the lead to toxicity and low yields of the prokaryotic host system.[183-185] Thus, if a new expression set-up needs to be created, different expression hosts, including prokaryotic hosts, can be screened. Other popular membrane protein expression hosts for structural and functional characterization are yeasts, including *Saccharomyces cerevisiae* and *Pichia pastoris* (*Komagataella phaffii*).[186, 187]
There are benefits offered by yeast systems; well-known genetics, high growth rates and densities of prokaryotic systems together with a posttranslational modification machinery which is similar to expression in higher eukaryotes. In addition, yeast is able to perform disulfide bond formation, acetylation, phosphorylation as well as certain O- and N-linked glycolysation patterns, which is the most complex protein modification and important for a human-like protein functionality.[17] There are a variety of protein based drugs that are produced recombinantly in yeast, e.g. the hormones insulin and glucagen are produced in *S. cerevisiae*.[188] Nevertheless, attention is required because the glycolysis pattern of a protein affects the stability and metabolism of the drug in the patient.[189, 190] Even though yeast is able to perform post translational modifications similar to mammalian cell lines, especially in *S. cerevisiae*, the recombinant protein is enriched with up to 200 high-mannose glycan residues (mostly N-linked glycosylation), since a smaller variety of utilisable sugars is available compared to mammalian cells.[191] *P. pastoris*, on the other hand, is known to add less mannose residues to the expressed protein target, resulting in protein targets suitable for human drug delivery, such as human insulin, hepatitis B vaccine and protein polymers among others as a result of recombinant optimization.[191-193]

The ability to study human protein related diseases is based on the access to the proteins of interest and the proteins related to them in the PPI network dynamics.[194, 195] Before interaction targeting therapies are developed, the related proteins must be produced. The production host *Pichia pastoris* is capable to produce both, the disease target for basic medical research, and the compatible biopharmaceuticals.[196-198] Protein-based drugs produced in *P. pastoris* are approved by the U. S. Food and Drug Administration (FDA) since 2009, such as the plasma kallikrein inhibitor Kalbitor®.[199]

The use of recombinant produced proteins for medical purposes is an indication for proper PTMs performed by the production host.
For pathological related experiments it is crucial to use protein source material, which shows the same properties as the native protein. Structural clarification, functionality and understanding of interactions of the target depend on the proper initial production.
The proteins produced for the studies in this thesis are possible drug targets, since they are among others relevant for metabolic and aging-related diseases (hSIRT2) or autoimmune diseases (hAQP4). We used the benefits of protein production in *P. pastoris*, to obtain highly pure, stable and biological relevant material for our studies.
The advantages of *P.pastoris* as an expression host for several projects of this thesis are discussed in more detail in the next section.

2.3. OVERPRODUCTION IN *P. PASTORIS*

P.pastoris offers an ideal compromise between growth performance, high cell titer, secretory expression and mechanisms of protein expression comparable to mammalian cells. These benefits are complemented by the possibility to introduce linearized foreign DNA into the chromosome.[200] In addition to the expression similarities with eukaryotic cells, the work with *P.pastoris* offers practical advantages such as high growth rates, simple genetic manipulation and GRAS status (generally recognized as safe).[200, 201] Mammalian cell expression of recombinant proteins, in contrast, can be challenging due to high system costs, potential contamination with animal viruses, capacity limitations and selection difficulties.[202, 203]
The usage of *P. pastoris* for the production of integral membrane proteins for structural determination has been proven many times.[204] In this thesis, the targets hAQP4, hSIRT2, AtPIP2;4, SoPIP2;1 and cpAQP1aa (plus mutants) were produced in high yields and high quality, sufficient enough for crystallization and functional assays.
Since *P. pastoris* is a methylotrophic yeast, we use its ability to metabolize methanol as the only carbon source. The metabolism switch is coupled to the strongly and strictly controlled alcohol oxidase 1 promoter (AOX1), which enables the operator to decouple the growth and replication phase from the induction phase of the protein target. The alcohol oxidase of the yeast cells oxidizes the added methanol to formaldehyde and hydrogen peroxide as the first products, which requires large amounts of oxygen and generates heat.[205]

The cells compensate the low affinity of alcohol oxidase to oxygen with the overproduction of the enzyme, which it can account for up to 30 % of cell mass and can be seen as impurities during purification.[206] The high demand for oxygen flow, temperature and feed management makes the usage of bioreactors advisable.[207, 208]

It has been shown, that the usage of bioreactors can improve the yield up to a factor of eight compared to shaking flasks.[209] A favourable feature for this efficiency is the high titer of the cells and possible multicopies of the target gene in the genome.[210, 211] Because *P.pastoris* is a Crabtree negative yeast, it does not lose carbon under respiratory conditions through ethanol production, which prevents autotoxicity and greater efficiency compared to other hosts such as *S. cerevisiae.*[212]
In practical terms, the process from gene or plasmid to high-expression cloning is a streamlined process using commercially available selection kits (such as Invitrogen EasySelect™ Pichia). The linearized pPICZ vector with the target gene can be transferred by electroporation into a X-33 *P.pastoris* strain, where it is integrated into the genome via homologous recombination.[213] A Zeocin resistance on the plasmid allows iterative screening with advanced antibiotic concentrations to find highly expressing clones selected for multicopy insertion of the gene.[214]
In a subsequent small-scale expression test, zeocin-resistant clones from the previous step are compared with regard to high target expression.[215] A subsequent immunoblot analysis against the target protein from the cell lysates indicates the suitable clone for a large-scale growth in a bioreactor under controlled and optimized conditions regarding oxygen supply, temperature and pH adjustments.
The large-scale expression efficiency and quality of the protein target should be evaluated by immunoblotting to confirm identity and the stability of the target.[216]

2.3.1. THE IMPORTANCE OF PTMs FOR PROTEIN OVERPRODUCTION

The importance of PTMs cannot be underestimated for the insight into molecular mechanisms and the explanation for pathologies. The human genome encodes for around 20 000 nonmodified (canonical) proteins.[217] Interestingly, these coding regions occupy only 1-2 % of the entire genome, while the remaining regions hold structural and functional information.[218]

Several factors such as alternative splicing, nucleotide polymorphism and PTMs ensure, that as many as 100 different protein variants, "proteoforms", can be produced from a single gene.[219]
Three subtypes of protein candidates carry out PTMs, which can be classified as "writing", "reading" and "erasing".[220-222] Typically, each of these modifications is carried out by a specific protein class, but the sirtuin family is unique in the way, that they can act as both, writer and eraser.[223]
These proteins fulfill the writing role by putting a ribose on target protein side chain (ribose transferase), but they are also able to remove acyl groups from proteins (deacetylase). The NAD^+ dependent reversible (de-)acetylation of Lys side-chains effects all types of cellular proteins and is an ancient and highly conserved posttranslational modification. With more than 6800 protein acetylation sites in mammalians, acetylation rivals phosphorylation in prevalence and malfunctioning of the acetylation machinery is involved in several severe diseases such as cancer development, neurodegenerative diseases and cardiovascular diseases.[224-226]

Since SIRT2 plays a significant role in several pathological pathways, the recombinantly produced protein should share the same translational characteristics as the native mammalian protein.[227-230] Additional PTMs from alternative hosts such as *S. cerevisiae* could influence the outcome of clinical tests, e.g. by modifying the glycosylation composition of the protein. In comparison, glycosylation occupancy in *P. pastoris* can be modified to be comparable to mammalian cells (CHO).[231] These improvements are not guaranteed for every protein target, but at the same time the higher yields of the yeast host are utilized for protein overproduction.

2.4. MEMBRANE PROTEIN PURIFICATION

The selection of a suitable expression host for your protein target is the first step towards characterization. This chapter will focus on how to get rid of the host proteins while retaining the protein needed for further studies.
The isolation of the desired protein target from the mass of unwanted co-expressed proteins and cell debris is not trivial and an often-underestimated step towards structural analysis.[232, 233] The process of membrane acquisition and the final protein purification is unique for every protein, but similar objectives must be followed.

Several steps are required to extract the membrane proteins from the natural environment in which they are incorporated. Membranes are first isolated by lysis of the cells, sometimes followed by various washing steps to remove unwanted peripheral membrane proteins. Initially, the cells have to be disintegrated, which can be done with different methods.
Cells are commonly lysed either by enzymatic and chemical techniques, or by mechanical cell disruption.[234]
As each technique has its advantages and disadvantages, the method chosen must fit to the physical attributes of the host (e.g. the presence of a cell wall or cuticle), but also to the sensitivity of the target protein.[235, 236]

Various physical methods can be used to open the cells, considering the robust cell wall of some hosts and the impact of the method on the quality of the protein. In particular, the heat-formation of a chosen method might have a degradation effect on thermolabile biomolecules.[237]
In a subsequent centrifugation step (~10.000 x g) cell debris and unbroken cells are removed, and finally the crude membranes, containing the target protein, are obtained from the supernatant by ultracentrifugation (~100,000 x g). The extracted crude membranes pass through several washing steps, and while it can be sufficient to clean the membranes with urea, it may be necessary to add a subsequent NaOH washing step, in those cases it does not interfere with the stability of the target protein. The latter step reduces the yield of the remaining target protein, but removes peripheral proteins, which are less tightly associated with the membrane.[238]
Membrane proteins are adapted to their natural lipid environment, and if the embedded proteins should be extracted from the previously isolated membranes, they have to be solubilized from their environment (figure 5). Membrane solubilization is another critical (and underestimated) step in the process of extracting the target protein from its environment, and it is not advisable to take shortcuts to find the right detergent for this task. Even for the same class of membrane proteins, preferences may differ, and initial detergent screening may point the way to efficient extraction while the protein remains stable in the new environment.[239, 240]

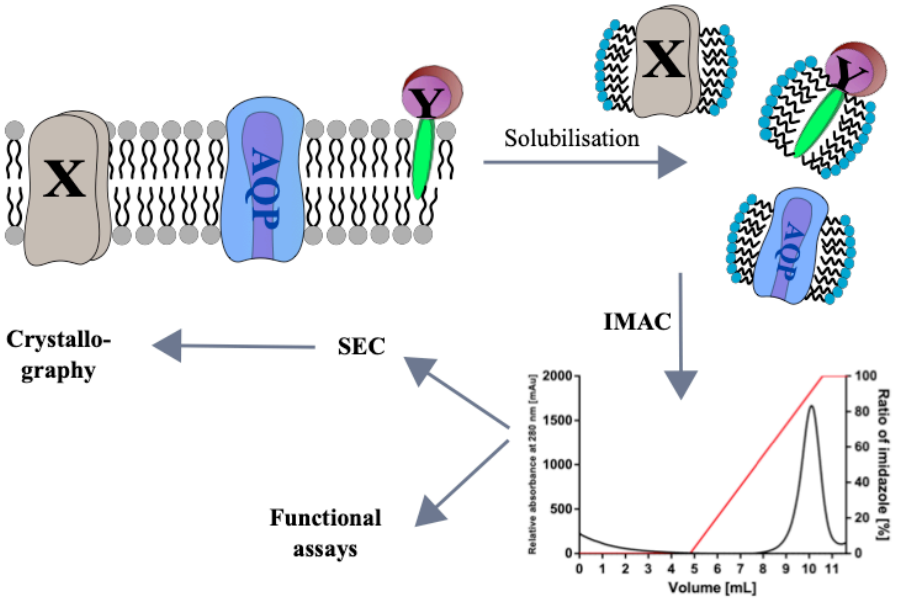

Figure 5: Solubilisation process as a pre-requisite for the isolation and purification of membrane proteins for different analytical purposes.

Since the extraction from the membrane is a first purification step, the detergent screening process should include different critical micellar concentrations (CMC) of the detergents, as well as the monitoring of purity and stability/functionality if possible (for example by microscale thermophoresis (MST)).[241]

Once the target is solubilized, typically three main steps of protein purification can usually be performed: In a first step, we want to extract our protein target from the mixed protein solution and for this purpose $Ni2^{+}$-affinity or ion exchange chromatography is applied depending on the design of the expression construct for the target protein. Sometimes, second intermediate step is applied, if an excess of bulk impurities needs to be removed, and commonly an extra run of the first method is then applied. Finally, size exclusion chromatography (SEC) ensures a high-quality sample for further applications such as structural and functional analysis.[242]. A separation based on size is usually performed as the last polishing step in a purification routine to check the sample for homogeneity and monodispersity.[243] Size Exclusion Chromatography (SEC) allows to avoid aggregations and ensures comparable protein batches for further investigations.[244, 245]

By using recombinant technology, it is possible to modify the protein target with tags, i.e. by inserting amino acid patterns, which facilitates the purification process using affinity chromatography.[246-248]

The use of an additional tag for proteins can have an impact, as the off-standing amino acids may interfere with crystal formation.[249-251] If potential implications should be avoided, purification can be performed based on the specific properties of the protein, e.g. by Anion Exchange Chromatography (IEX), using the charge of the protein. Another separation property is hydrophobicity, used in Hydrophobic Interaction Chromatography (HIC), which is beneficial after salt precipitations.

2.5. X-RAY CRYSTALLOGRAPHY

In the last section, the process of obtaining a high-quality protein sample was discussed. The molecular mechanism of proteins can only be explained with the knowledge of their structure. Unfortunately, we cannot derive the three-dimensional model of a protein by examining it with a conventional light microscope. The physical resolution limit for microscopes using visible light is $\lambda/2$. This allows us to distinguish objects or structural features with a size of about 200 nm, while the bond-length between the atoms of the protein molecules is around 1 Å.

Electromagnetic radiation of shorter wavelengths must be used to reveal the protein structures. The discovery of X-rays by Wilhelm Conrad Röntgen in 1895 enabled the detection of molecule structures, but several advanced techniques are needed to overcome the limitations of classical magnification.[252] In traditional microscopes optical lenses are used to focus, respectively magnify the scattered light of objects. X-ray radiation cannot be focused with a traditional lens, and we need the help of a mathematical lens – Fourier transformation – to reconstruct the image of an object.[253] The scattering of X-rays at the electron density of the atoms in the protein solution is not sufficient to obtain structural information. The additional effect of radiation damage compelled the use of protein crystals as object. The highly-ordered arrangement of protein molecules in a lattice offers the advantage of a possible constructive interference between the molecules and, as a consequence, an increased scattering of the radiation that has occurred. Sir William Lawrence Bragg formulated the requirements for constructive interference in his famous law of 1914:[254]

$$n\lambda = 2dsin(\theta) \qquad \text{(Equation 1)}$$

The incoming radiation with the wavelength λ and an angle θ is only interfering in a constructive way with the lattice planes with distance d, if the path length difference between two waves is a multiple n of wavelength λ (see figure 6, A).

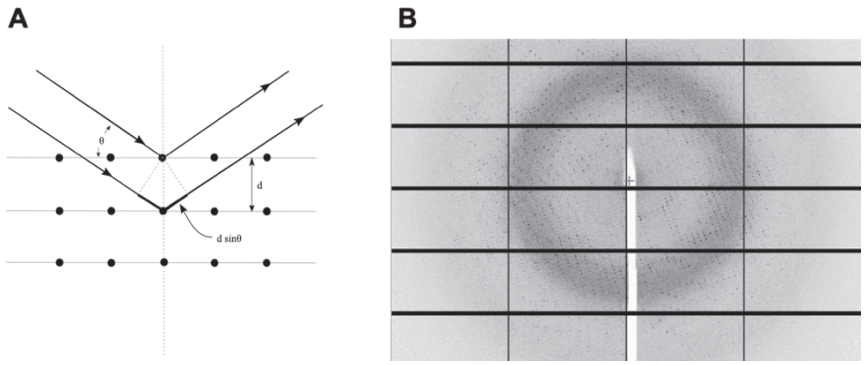

Figure 6: A) Bragg diffraction: Constructive interference of an X-ray beam at the electron density of molecules in a crystal lattice. B) Constructive interference pattern as a result of Bragg diffraction in a SoPIP2;1 crystal, detected by Jessica Glas.

One might notice, that this formula is independent of the content of the lattice. Bragg`s law was originally invented with inorganic salts as a background, but any kind of molecule can meet these criteria to show reflection patterns.
Biochemists take advantage of this property, to force protein molecules in lattice structures to determine their structures. The Bragg reflections do not produce a traditional (virtual) image as we know it from light microscopes. Instead, a unique diffraction pattern can be detected (see figure 6, B) which ideally should be focused to obtain a reconstructed image of the unit cell electron density inside the crystal. This type of lens does not exist, which means that structural biologists have to deal with the intrinsic crystallography dilemma called phase problem.
In order to reconstruct the electron density of the molecule, the experimentally recorded reflection points need to provide information about the related intensities and their phases. Since we detect the spots on the screen, we know the amplitudes (= intensities) of each spot. At the same time, the phase information gets lost, which represents the position of the peak of electron density in the unit cell (= positions of the atom). In a diffraction experiment we therefore collect inverted information about the reciprocal space of the crystal, which can be transformed into real space (electron density) by Fourier transformation, the “lens” of the crystallographers.

The phase problem with macromolecule crystals can be solved individually for every experiment as a direct method, which can be very time-consuming and requires small molecules and high resolution (> 1.2 Å). Other established methods include isomorphous replacement, MAD, SAD and molecular replacement, and they offer elegant solutions to speed up the phasing. Isomorphous replacement paved the way for solving the first protein structure at atomic level and has been developed by Max Perutz.[255] The method is based on the idea of attaching heavy metals to the macromolecular structure of the protein, without altering it. The additional atoms will contribute to the structure factors of the whole molecule, and by comparing the reflection data to the unmodified molecule the phase problem can be solved.

MAD and SAD are experimental methods, which also use heavy metal molecules to obtain phase information, but rather use the characteristic capacity of the metals to absorb X-rays of certain wave lengths. Lighter atoms of the macromolecule, such as carbon, oxygen and nitrogen, do not contribute to this type of resonance phenomenon, and the contribution of the anomalous scattering of heavy atoms can be used to derive the protein substructure.[256, 257]
The most popular phase method is the so-called molecular replacement, which accounts for more than 70% of the deposited macromolecular structures and offers several advantages such as speed, cost-effectiveness and a high degree of automation.[258] As with any technique there are a number of requirements, the most important of which are sequence identity (> 25-50 %) and structural identity.[259, 260] In molecular replacement, a protein with a known structure is used as a template for the initial phases of the unknown protein.
Many classes of proteins, such as aquaporins, share common structural features and by translating and rotating the obtained diffraction data into the template, unknown structural features can be obtained.

2.6. PROTEIN CRYSTALLIZATION

X-ray crystallography has been the most successful technique for the determination of three-dimensional structures of (membrane) proteins for the last hundred years.[261] The largest number of Nobel price laureates is directly or indirectly related to the field of crystallography, while new emerging techniques like cryogenic electron microscopy continue the trend towards structural discoveries.[262, 263]

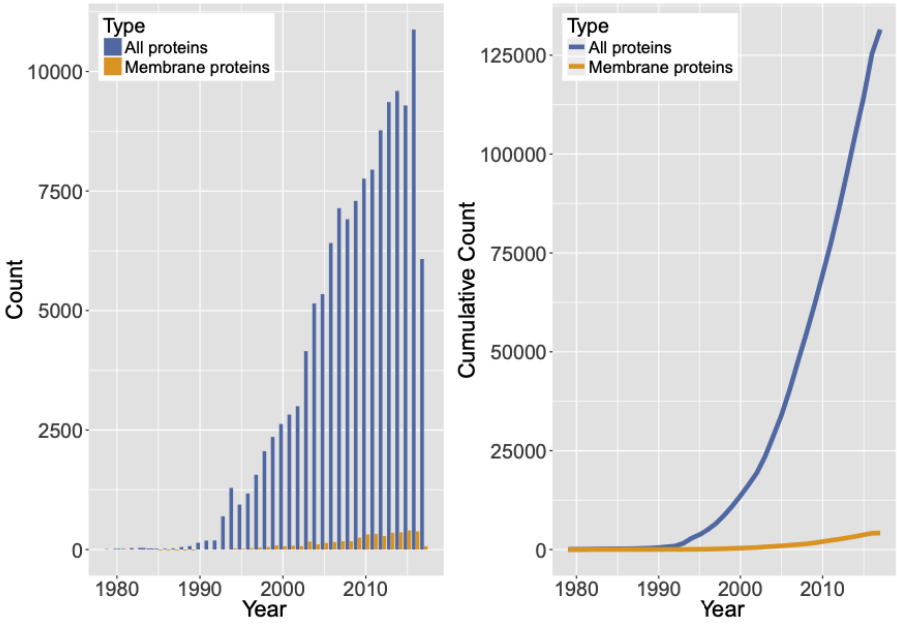

Figure 7: PDB entries of 3D structures in the year 2017 by year of deposition (left) and cumulative numbers (right).[264]

While the cumulative number of all protein structure entries in the pdb-database is increasing every year (see figure 7), the proportion of membrane proteins is less than 1 %.[264]

This "membrane gap" can be explained by the additional complexity of membrane crystallography, resulting from its amphiphilic nature, intrinsic instability and the need for detergents, suitable protein expression hosts and purification efforts.[265, 266] The crystallisation of soluble proteins is a complex matter in itself, and while inorganic chemicals can easily be obtained by evaporation of a supersaturated solution, more effort is required for (membrane) protein solutions. The first reported protein crystallization (haemoglobin) happened by chance in the year 1840, and the author of the publication stated, that he had problems to replicate the discovered process with the assumed chemicals.[267, 268] Today's crystallographers know this problem very well, and although the physical principles of structure determination have been known for more than a hundred years, the process of protein crystallization still cannot be rationalized in advance.[269] What we have is a basic understanding of the process leading to the formation of crystals in a protein solution.

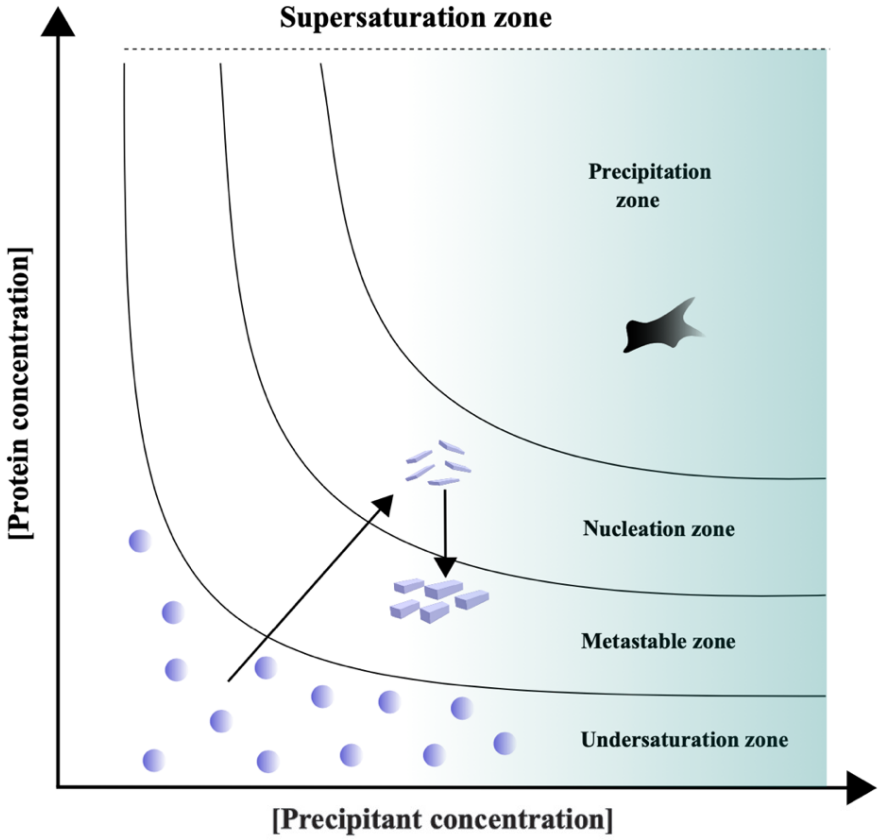

Figure 8: The phase diagram: A theoretical concept for protein crystal growth in a vapor diffusion experiment. Starting from a protein solution in the undersaturation zone, the evaporation of liquid from the drop leads to a higher protein and precipitant concentration. Initial crystal growth occurs, if the nucleation zone is reached. Afterwards, crystal growth is continued in the metastable zone.

In order to achieve crystal growth, our highly pure and monodisperse protein solution must undergo several phase changes, which depend on the protein concentration and the content of different salts and precipitants (see figure 8). At the beginning, in the undersaturated zone, the proteins are dissolved in liquid solution. Primary nucleation, the starting point for crystal growth, can only be initiated in a supersaturated state, the labile zone (nucleation zone). But how to get there? One way to increase the protein concentration is to add more protein molecules, but the supply from our side is limited and we learned before that it is difficult to obtain more base material. An easier way is the evaporation of water from the aqueous protein solution, by altering the osmotically conditions in the environment.

There are several techniques available for manipulating the water content, one of the most commonly used systems is called vapor diffusion via hanging drop (see figure 9). The protein is kept soluble in a volume of precipitant solution which is placed atop a reservoir solution containing a higher concentration of salts and precipitants. In a hanging drop experiment, the reservoir is located under a glass lid, where the protein drop is sitting. Other variations include an elevated placement on a platform inside the reservoir solution (sitting drop), or the use of microdialysis.

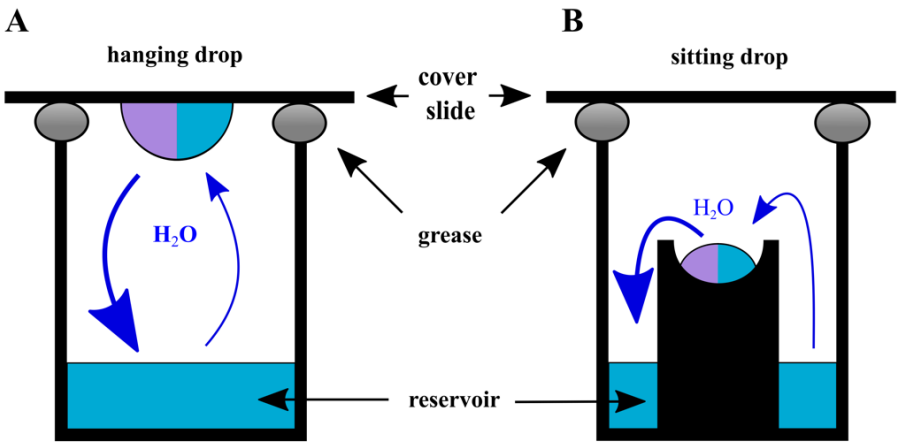

Figure 9: Two different vapor diffusion methods. A) The hanging drop method, where the protein/precipitant solution is placed under a cover slip, and hold in position by surface-tension. B) The sitting drop method, where the protein/precipitant solution placed on a pedestal to avoid contact with the reservoir.

Regardless of the method used, the closed system ideally reaches an equilibrated state over time. The initial protein solution becomes more concentrated and the nucleation zone is reached.
The formation of the initial crystals is accompanied by a decrease of free and available protein molecules and the growth of the final crystal will continue in the metastable phase of the diagram. This optimal sequence of molecule arrangement happens rarely, and in most cases many different starting conditions must be varied in terms of pH, salt, precipitant, temperature and additive, otherwise the proteins are likely to reach the unstable precipitation zone and end up in amorphous degradation. The appearance of first crystals after several batches of purification and screening events is a remarkable moment in a project, but not the end of a journey for a better understanding of the structural properties of a protein.
Well diffracting crystals require optimization of the crystallization conditions, altering the starting conditions, detergents and the addition of specific substances.

Finally solving the structure of a protein will give us an idea about the function of the target, which we can validate with (biophysical) methods presented in the next chapters, complementing our understanding of the underlying molecular mechanisms.

2.7. FUNCTIONAL STUDIES OF AQUAPORIN TRANSPORT

The structural elucidation of aquaporin macromolecules enabled the development of theories of how water molecules are transported through the cell membrane. The transport process itself is difficult to observe, since the transport of a single water molecule is a fast and shielded process inside the aquaporin. Additionally, the proteins are present in aqueous solution, which makes it difficult to identify and track the individual molecules. Recent developments in diffusion-weighted magnetic resonance imaging (DWI) have determined the exchange time of water from the intracellular to the extracellular space of human AQP4 expressing cells to be 43 ms, an improvement over the non-facilitated diffusion time of the molecules of 100 ms.[270-272]

Understanding the function of proteins is an essential part of biophysical studies, and the fast nature of biological processes has accelerated the development of feasible tools to study the function of proteins that our senses are unable to do. The analysis of rapid biological processes depends on the kinetics of the underlying mechanisms, for example the binding of an enzyme to its substrate.

The examination is compounded by the fact that many biological processes are irreversible, which made mixing depending techniques necessary. Previously done by hand, the mixing time before evaluation was in the range of seconds, and the deadtime made it impossible to observe many processes. The manual mixing process can also cause individual operator errors, which are easily observed when evaluating titration studies from student laboratories in basic chemistry.

In 1923 the invention of automated mixing led to the development of the first continues flow instrument, used for the binding analysis of carbon monoxide to hemoglobin.[273] The mixing time was reduced to 1 ms, but the size of the reaction chamber resulted in a sample consumption of 7.5 l for a single measurement only.[274] The situation improved with the development of the first stopped-flow instrument in 1943, combining low sample consumption with rapid mixing times.[275]

Instead of detecting reaction signals along the length of the reaction tube, the monitoring system was fixed at a specific point in the mixing chamber and defined volumes of reactants were induced and ejected.[276]

The advantages of using stopped-flow measurements to analyze the rapid transport of water molecules by aquaporins are obvious, but the transport process cannot be directly monitored with this technique.
Since the passive water transport across the cell membrane depends on an osmatic gradient, this dependency is used to create a natural environment for the membrane proteins to detect an indirect signal for the kinetic measurements. By incorporating the aquaporins into liposomes while exposing them to a hyperosmotic gradient, the shrinkage of the vesicles can be detected as a variation in light scattering intensity.
The reconstitution of membrane proteins, such as aquaporins, into liposomes requires the transfer of the protein from its micelle environment into an artificial lipid vesicle. Initially, a high detergent concentration keeps the protein completely solubilized in aqueous micelles. By reducing the detergent concentration, the solubilized protein spontaneously reconstitute into liposomes and form proteoliposomes.[277] The removal of the initial detergents can be done by various methods, such as hydrophobic interactions with polymer beads, dilution or dialysis.[278]
The size distribution of the (proteo-)liposomes can be determined by Dynamic Light Scattering (DLS), since a monodisperse vesicle distribution is a prerequisite for subsequent calculation of water transport rates.
The testing of aquaporin functionality in a stopped-flow experiment is performed by loading one syringe in the sampler with a proteoliposome solution and another with a hyperosmotic buffer (see figure 10).
Rapid mixing of these two solutions creates an osmotic gradient between the inside of the vesicles and the outside, resulting in a flow of water outside the proteoliposomes. As a result, the shrinkage of the vesicles can be recorded as light scattering, typically measured over time at a 90° angle to increase the signal to noise ratio.

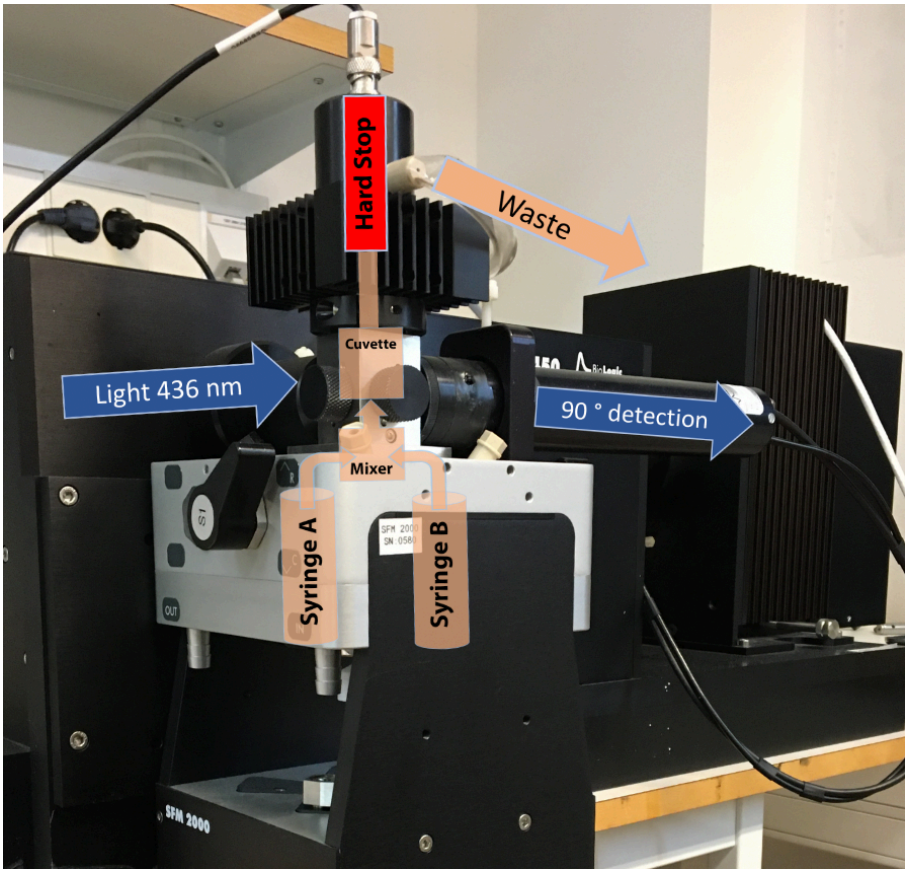

Figure 10: Stopped-flow equipment used for experiments presented in this thesis, with overlaid functionality features. The 90° light-scattering from a mixed sample is detected in a hard-stop defined time frame.

Several mixing experiments are replicated, averaged, normalized, time truncated and finally fitted with a single or double exponential function. Since a single exponential function is only suitable for uniform proteoliposomes with exactly the same number of functional proteins evenly distributed over the surface (which rarely occurs in experiments), a double exponential fitting is used to derive the constants of the water transport rate for quantitative comparison between different aquaporin species.[279]

2.8. PROTEIN:PROTEIN INTERACTIONS AND BIFC

From a historical perspective, it was a path of trial and error from the first extraction of proteins and their purification to the recombinant production and analysis methods we use today. Not to mention the collaboration needed to develop techniques, that allow us to observe proteins at the atomic level. For a long time, and even today, scientists in the field of structural biology were forced to concentrate their effort on a single protein target. It could take years for a research group to resolve the structure of a protein target, even longer when interaction partners were involved. The process from protein of interest, its purification, characterization, structural analysis and interaction studies can be seen as a linear progression towards the goal of understanding the fundamental processes of life. Years of fundamental research have revealed that basically all biochemical cycles in our cells depend on the interaction of proteins. Before we can target single proteins for further structural analysis, we have to reveal the interaction network the protein is incorporated in.

The importance of proteins and their interaction for the complexity of organisms, especially humans, was addressed in the context of the human genome project.[280] It was shown that proteins and their (transient) complexes are responsible for the complexity of an organism and the diseases associated with it. It was the dawn for the field of proteomics, the interdisciplinary scientific domain of understanding the proteome of organisms and their underlying protein-protein interactions (PPI). Proteomics is a relatively new scientific field, but the starting point for PPI studies can be traced back to the systematic evaluation of yeast two hybrid assays to generate a protein interaction library, an interactome, in the year 2000.[281] Over the last twenty years, several methods for the detection of PPIs have been developed (see table 2 and 3), which led to the discovery of a large number of protein networks.[282] These are deposited in databases and are accessible for search queries.[283-285]

Table 2: Different PPI detection methods and their application for HTS of (novel) protein:protein interactions.[286-292]

	Method	Advantages	Disadvantages	Sample preparation (pure protein/*modus-operandi*); ability to screen for novel interactions
Biophysical	**Microscale Thermophoresis (MST)**	• Label free detection • Low protein quantities needed • Contact free	• Depending on autofluorescent aminoacids, otherwise labeling needed • Interaction kinetic information are depending on equilibrium formation	• HTS possible in protein-targeted drug discovery • Labeling enables *in situ* measurements of interaction affinities in cell lysates
Biochemical	**Co-Immunoprecipitation (Co-IP)**	• Key technique for PPI confirmation, especially complex targets • Proteins are in physiological conditions • High specificity	• Insufficient sensitivity for low affinity PPIs and short timeframe interactions • Selection and quality of antibody is critical for success • Information about the target needed	• Gold standard for screening novel interaction partner • Must be processed *in vitro,* support for *in vivo* interactions
	Bimolecular Fluorescence Complementation (BiFC) = Protein-fragment complementation assay	• Intrinsic fluorescence of complex formation • Locking of transient PPI events • Location of complex formation *in vivo* • Correlation between fluorescence intensity and complex formation • Can be utilized for membrane protein targets	• Independent complementation promotes background signal • Fluorophores are not functional in aerobic hosts • BiFC mechanism complicates dynamic protein interactions	• Works in different (prokaryotes, eukaryotic) model hosts under cellular conditions *in vivo* • Detection of novel interaction partner via cDNA screening
	Förster Resonance Energy Transfer/ Bioluminescence Resonance Energy Transfer (FRET/BRET)	• Fast energy transfer enables detection of rapid PPI events • High sensitivity due to nanoscale D/A (donor/acceptor) separation • Independent targets detectable with different reporter fluorophores	• Low signal intensity requires proper control experiments • Depending on accurate image processing for high signal to noise ratio • A/D stoichiometry is critical for valid results	• Works in different host systems *in vivo* • HTS with cDNA libraries practicable

Table 3: Continuation from table 2.

	Method	Advantages	Disadvantages	Sample preparation (pure protein/*modus-operandi*); ability to screen for novel interactions
Biochemical	**Phage display**	• Rapid screening of peptide libraries • Ideal for antibody binding studies or identification of substrate specificity • Connection between displayed protein information and encapsulated DNA	• Verification of results with protein-level methods • Random presentation of peptides may lead to random protein interactions not representing *in vivo* formation	• *In vitro* only and designed rather for affinity screening, stability and enzymatic activity than novel interaction detection • cDNA screening practicable
	Far western blot	• Cell lysates can be used, purified protein not needed • Detection of indirect binding complex partner • Detection of transient PPIs	• Denaturing process prevents detection of complexes depending on native protein state or refolding process • Indirect protein interactions are not detectable	• *In vitro* only, also in lysated cell samples • HTS not possible, due to a long experimental time
	Enzyme-Linked Immunosorbent Assay (ELISA)	• Highly specificity/sensitivity due to usage of specific antibodies • Easy to perform and economic	• One target (antigen) must be known beforehand • Method relies on the quality of the antibody • High false-positive rate, especially if washing is insufficient	• HTS of novel interactions possible • Best performance with purified protein, analysis with (diluted) cell lysates possible
	Protein chip	• Parallel automated analysis of multiple PPIs • Versatile: used for PPIs; protein-DNA interactions; RNA-protein interactions • Interactome mapping • Large-scale	• Correct data analysis is crucial to avoid a high false-positive rate • Misleading surface interaction of bait and chip	• Invented for HTS • Microarrays for lysate screening are in development, but are sensitivity insufficient
Genetical	**Two-hybrid systems**	• Scalable and economic • Possibility to screen interactomes • Bacteria two hybrid preferable for membrane proteins	• Expression levels of protein targets determine sensitivity and specificity of the screen • Missing post translational modifications increase false-positive hit rate	In vivo; screening of novel interactions via cDNA libraries is possible

Membrane protein networks, including aquaporins, are the main target for therapeutics and a database search for experimentally validated protein interaction highlights the problem scientists are facing:[293]
Far more potential protein interaction targets are being discovered than are evaluated by traditional experimental methods, mainly due to advances in the field of bioinformatics.[294-296] The examination of these potential targets in the same linear way as before (target by target) is inefficient, instead existing experimental PPI detection methods are used for large-scale screening to evaluate potential interaction partner.
There are several methods available to screen for protein:protein interactions, whereby the intrinsic disadvantages must be weighed against the potential benefits. A significant amount of actual PPI networks has been discovered by the yeast two-hybrid (Y2H) approach, which fuses cleaved transcription factors to proteins of interest.[297] The physical interaction of these proteins leads to the reconstitution of the functional transcription factor, and the expressed reporter gene enables the detection of positive cells. Since this technique is based on the manipulation of DNA, protein purification is not necessary for further analysis. This benefit allows automated high-throughput screening (HTS) of host libraries to find potential *in vivo* PPIs.[298] In contrast, Y2H screens show a high false-negative rate on the order of 70-90 % (not detected true interactions), and a false-positive rate of 25-45 % (detection of non-interaction partners).[299, 300] As a consequence, potential hits of each PPI detection method must be verified by further studies or the detection can be improved by using complementary methods in combination.[301]
The use of protein complementation as a reporting tool for protein interactions goes back to a publication from 1958, explaining the self-organisation of two individual peptide residues of ribonuclease A into their native and functional structure.[302] From there it took another 36 years to develop the first in vivo of the first *in vivo* proximity sensor, based on the split ubiquitin pair fused to proteins of interest, which "makes it possible to monitor a protein-protein interaction as a function of time, at the natural sites of this interaction in a living cell".[303] The detection was based on induced chemiluminescence, but the basic idea of protein complementation as a monitoring tool for interaction studies was coherent.
The fusion of nonfunctional cleavage parts of the green fluorescent protein (GFP) to a potential interaction partner and the monitoring of the autofluorescence of the complemented reporter protein was the next evolutionary step towards the development of a technique which is routinely used as Bimolecular Fluorescence Complementation (BiFC).[304]

The use of GFP, a 26.9 kDa protein from the jellyfish *Aequorea victoria*, as a reporter sensor was a milestone not only for cell biology, but also for protein scientist, who were able to monitor their object of interest from the cell to purification. This important protein was a by-product of the luminescence research of the protein aequorin from Osamu Shimomura, and the discovery was rewarded with a Noble Price in 2008, although these "unusual proteins…had no particular importance when we first reported them".[305]

The use of BiFC was an elegant solution to visualize protein interactions directly. In addition, information on the strength of the interaction could be obtained, as the intensity of the signal correlates with the strength of the molecular interactions.[306] The efficiency of the fluorescence complementation assay is directly related to the fluorescent proteins used. A higher quantum yield from the fluorophores increases the signal to noise without the need for better detectors or changes in methodical routines. As a consequence, modified GFP versions were soon developed, which not only have a higher fluorescence intensity per protein, but also improved properties with regard to their range of application under physiological conditions. One example is the improved yellow fluorescent protein SYFP2 (see figure 11), hereinafter YFP, which has a 204% higher relative brightness compared to the related GFP version.[307]

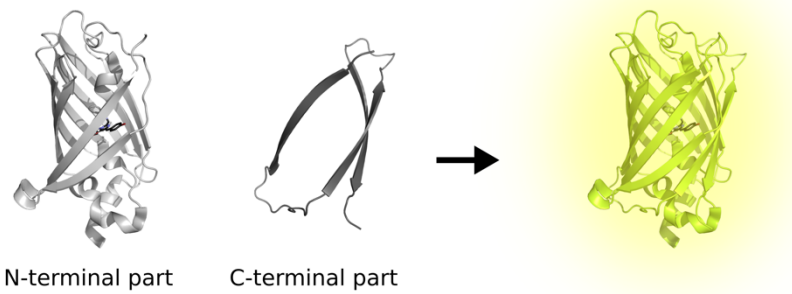

Figure 11: Fluorescence protein complementation of YFP. Non fluorescent parts of YFP (YFPN1-154/YFPC155-239) were designed by a split at a position between the 7th and 8th ß-strand of the protein for efficient reconstitution and less background fluorescence.[308] The chromophore region, origin of the fluorescence signal, is highlighted in the middle of the protein.

In recent years, protein engineering efforts have led to the design of a wide variety of available fluorescent proteins (FP), providing a toolbox for different needs in microscopy and PPI studies.[309]

BiFC experiments can be designed to to study pH changes or multiple protein-protein interactions, and in combination with Photoactivated Localization Microscopy (PALM) the spatial resolution of interactions has been improved down to the nanoscale.[310-312]
The BiFC assay offers several advantages (see table 2), that can be used for screening PPI networks. The irreversibility of the complementation process is a beneficial feature of the method, which simplified the purification and study of locked complexes.[313]
On the other hand, the detection of dynamic protein interactions required the development of fluorescence reporter tags that bind the complementation partner in a short-term and reversible manner. Recently introduced Fluorescence-Activating and absorption-Shifting Tags (FAST) could complement the traditional BiFC assay, by avoiding the extended maturation times of BiFC formation.[314]
The benefits of BiFC for detecting and screening PPIs such as high specificity and sensitivity, signal stabilization, localization of complementation, availability of different screening host systems and easy applicability have made this technique popular with researchers in different fields of life sciences.[315-319]
Nevertheless, any method can be extended and the next chapter will discuss the fundamental technology to automate BiFC verification for high-throughput screening of protein interactions.

2.9. FLOW CYTOMETRY

The principle of BiFC indicates the existence of protein interactions and where these are located in the cell. The extraction of this and the readout of the fluorescence intensities was done by light microscopes with fluorescence detection systems in the rise of technology. There are still arguments in favour in daily routine work, such as the easy availability of fluorescence microscopes, a short learning curve for their handling and the optical importance of fluorescence images for cell growth control.
The fusion of high throughput routines with fluorescence microscopic evaluation fails due to the time-consuming microscopic preparation as well as the induced subjectivity by choosing the right cell targets for intensity analysis. HTS and population analysis of BiFC depend on the readout of a statistical number of samples as well as a fast and objectively correct readout of the fluorescent cells.

Molecular biologists used flow cytometry, a technology originally derived from cell biology, to evaluate (and sort) cells with specific characteristics. The basic idea of single cell analysis in suspensions dates back to 1934, when Andrew Moldavan reported a technique, in which cells were counted on the basis of the photoelectric effect.[320] More than 30 years of technological improvements passed from counting to sorting the cells, first on the basis of cell volume, later the evaluation was based on the intrinsic fluorescence.[321, 322] The commonly used term Fluorescence Activated Cell Sorting (FACS) was introduced in 1972 by the group around Len Herzenberg.[323] They reported an experimental system, which is able to sort 2000 fluorescing cells per second using a fluorescence threshold. Although modern FACS machines are able to sort up to 34000 (FACSMelody) drops per second, the general design is the same as 40 years ago (see figure 12).

In the beginning of a sorting or analysis process, the cells are first organized in buffer droplets by hydrodynamics in the fluid system. Directed towards the flow chamber, the cells get spotlighted by one or several lasers, and an optical analysis system in modern FACS is able to verify the size (forward scattering) and complexity (side scattering) of the cell targets. Interesting fractions of the population, based on uniformity, shape and fluorescence, are selected by the electronics for further analysis and sorting, based on an electrostatic deflection system. The entire process of sample preparation, droplet formation, excitation with the laser system, analysis and sorting takes less than a second.
These advanced machines initially facilitated the purification of antibody solutions, but today flow cytometry and FACS are used in many scientific fields, from physics to food science.[324]

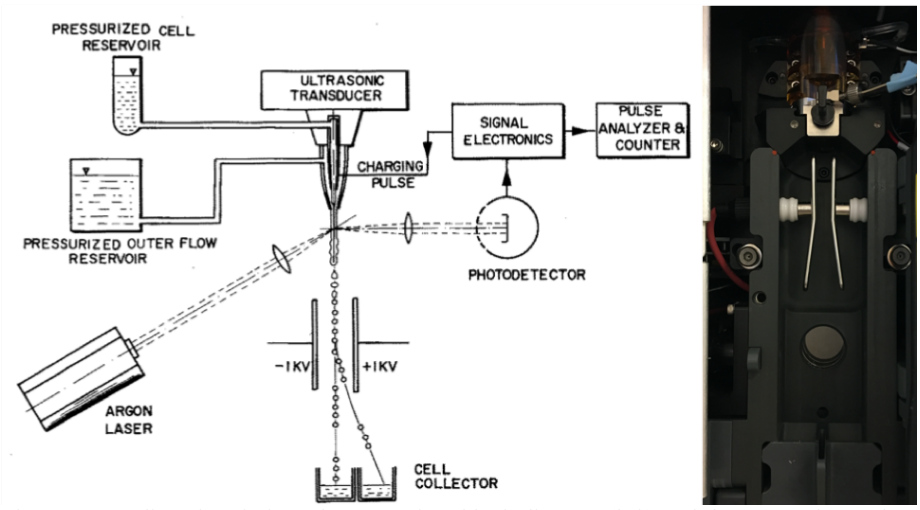

Figure 12: Earliest description of a FACS in a block diagram (left) and the setup of a modern FACS (right), showing the same essential components, such as the charged plates.[323]

With regard to fluorescence from protein complementation, the intensity and population characteristics of growth assays can be read out. The electronic system converts the diffraction scattering and fluorescence intensities into dimensionless values, which are presented to the user as dot plots or histograms. Based on pre-selection (gating) of functional, equally fluorescing cells, from a transformed population, statements about successful protein interactions can be made from the statistics obtained.

3. SCOPE OF THE THESIS

Working with membrane proteins, the "wild west" of structural biology, is not only a challenge on its own.[325], it involves different fields of science, biophysics, molecular and experimental biochemistry among others to characterize the molecular mechanisms of proteins.

The function of a protein cannot be explained theoretically from the amino acid sequence, as a consequence the protein targets must be produced and characterized. In this thesis, aquaporins and other potential drug targets from different species were produced and characterized to get a holistic picture of their function, while methods were developed or enhanced to facilitate future experiments.

Before the structure or functionality of a protein can be determined, the protein of interest must be produced in high yields and adequate quality. The overproduction of protein targets in the host *P. pastoris* was used to overcome the bottleneck of insufficient protein yield for further studies of the soluble protein SIRT2 (**Paper I**), an enzyme involved in various biological processes like tumor development, neurodegenerative diseases, inflammatory responses and a valuable target for drug development. The membrane protein human aquaporin 4 was produced in high yields in *P. pastoris* to improve the diagnosis of neuromyelitis optica, the development of more efficient water filter and to reveal the intermolecular binding between AQP4 molecules and potential interaction partner. The structure of aquaporins determine their function and in **Paper II** the effect of mutations in the novel structure of cpAqp1aa were investigated, leading to a hypothesis for a novel extracellular gating mechanism of a fish aquaporin.

Beside protein purification, method development for protein characterization was a focus of this thesis. A novel assay for the determination of H_2O_2 transport on protein level was developed in **Paper III** and **Paper IV**. The inclusion of structural features of plant aquaporins presume the involvement of outer membrane domains in transport specificity of this protein class.

The importance of protein:protein interactions for protein functionality becomes more evident in the recent years. We improved the BiFC system in **Paper V** for HTS screening of novel PPIs in a standardized assay, with the ultimate goal to screen for AQP4 interaction partners.

4. RESULTS AND DISCUSSION

4.1. HIGH-LEVEL PROTEIN PRODUCTION

The proteins produced in this thesis were one soluble target of medical relevance; SIRT2, and two aquaporin targets; hAQP4, cpAQP1aa, with the aim to elucidate their structure and function. All targets were produced in the yeast host *P. pastoris* and the results are described in Paper I-IV.

4.1.1. SOLUBLE PROTEIN SIRT2 (PAPER I)

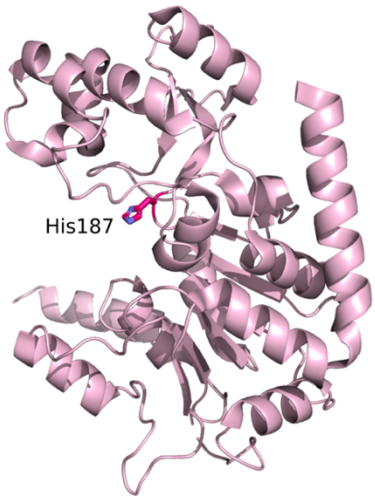

The importance of (human) sirtuin modulation for the pathogenesis of molecular mechanisms was discussed in chapter 1.2.2. Especially the inhibition of SIRT2 has recently attracted attention, since the binding of selective chroman-4-one derivates to SIRT2 has shown a significant reduction of proliferation in human cancer cell lines.[326]

Figure 13: Side-view of the apo-form of SIRT2 (PDB: 3ZGO), with the potential inhibition site with His187 highlighted.

Figure 13 highlights the conserved active site residue His187, where chroman-4-one-based SIRT2 inhibitors are proposed to bind.
The continuation of inhibition studies and the establishment of co-crystallization experiments requires the availability of pure, homogeneous sample of the protein in high yields.
A literature search on the expression and purification of sirtuin leads to a bipartite usage. The medical implications of sirtuins are often tested *in vitro* in different mammalian cell lines.[88, 327-331]

The recombinant expression of sirtuins for molecular characterization is often carried out in the prokaryotic host *E.coli*.[332-334] The structure of SIRT2 was discovered in the year 2001, and *E.coli* has since been the dominant host for recombinant protein production.[335-340]
The choice of a specific expression host influences the protein target, the importance of PTMs has already been discussed (see chapter 2.3.1) and is a crucial factor in the regulation of sirtuin activity.[341-343]
The achievable yields are also influenced by the choice of hosts. There is little information on SIRT2 yields in terms of media volumes, one source states 13-15 mg/L of a truncated isoform from minimal media for NMR studies.[344] These amounts were achieved with *E. coli* as the expression host. In a second source from another doctoral thesis, a yield of 2.5 mg/L was obtained for SIRT2 purification.[345]

In **Paper I** we describe in detail, how we increased the yield to 39 mg/L in minimal media by taking advantage of the *P. pastoris* expression. The increase in yield is sufficient for supplying photoaffinity labeling experiments (PAL) and potential crystallization setups.

From a practical point of view, the high expression yields in *P. pastoris* are not only a result of technical advanced growth systems (bioreactor), but also the result of iterative screening for high expression clones.
The screening process started with the linearization and transformation of the SIRT2 construct into *P. pastoris*. Resulting clones were screened with increasing concentrations of the selection marker Zeocin.
The selection process is a first indication of protein expression, but there are more criteria required for large-scale fermentation. Selection screening on Zeocin plates cannot replace a small-scale expression test in shaking flasks, where the largest colonies from the previous step, which showed high expression, are compared in terms of replication and growth behaviour, including a methanol induction phase. A subsequent immunoblot analysis against the fused His affinity tag of SIRT2 from the cell lysates indicated the appropiate clone for a large-scale growth in 3 L fermenter.

The cell yield for each fermenter run is individual and can vary from 300 g to more than 700 g, depending on various factors such as nutrition availability, pH stability and air supply. SIRT2, used in **Paper I** for PAL studies, is derived from a growth batch that yielded 342 g of cell mass with a SIRT2 expression level of 5% of total protein content.
The expression efficiency and quality of the protein target were evaluated by immunoblotting. Especially when methanol is added at the toxicity limit, there is a risk that H_2O_2-induced oxidative stress is induced, which cannot be compensated by the cells, resulting in protein degradation.[346]

A subsequent three-step protein purification, including IMAC to remove mass impurities and two SECs to increase purity and homogeneity, was performed to obtain SIRT2. The purification of SIRT2 can be adapted to the needs of subsequent experimental setups. The purity of SIRT2 after the first gel filtration may be sufficient for enzymatic assays or initial activity measurements of SIRT2. For crystallization setups, e.g. in combination with potential inhibitors, the homogeneity is not sufficient (see figure 14, A).
A second SEC, using pooled SIRT2 samples from the previous gel filtration, was performed to verify, if a monodisperse and pure sample can be obtained for crystallization experiments (see figure 14, B).

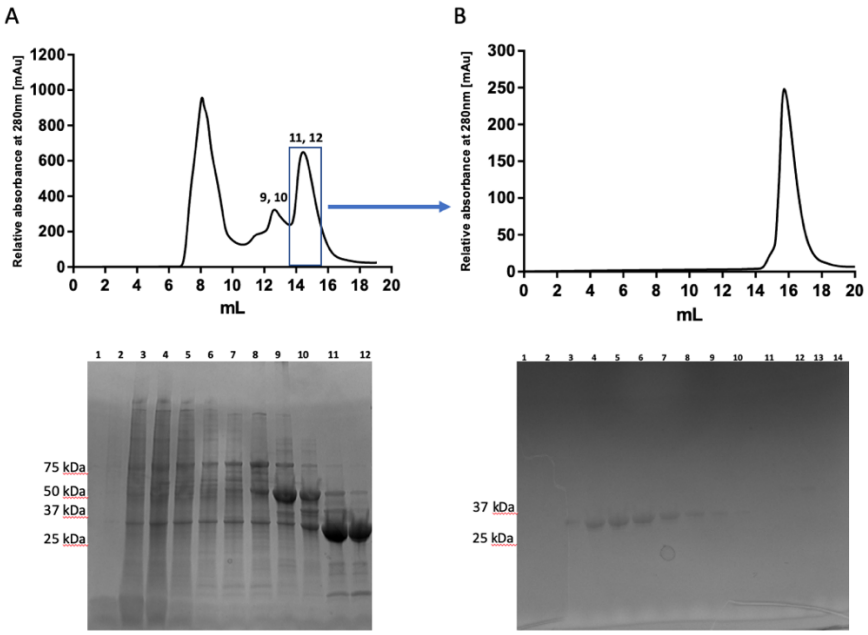

Figure 14: Two-step purification of SIRT2. The protein purity of an initial SEC (A) was enhanced by a subsequent SEC (B) run, removing potential impurities seen in SDS-gels.

The additional purification step resulted in highly pure, uniform and monomeric SIRT2, resulting in an 89% protein loss. Nevertheless, a 20-fold increase in SIRT2 concentration can be achieved compared to lysate and the final protein yield after two SECs is at least 2.6 times higher than previously reported.
The (structural) stability of proteins is a basic prerequisite for crystallographic studies, and the thermodynamic stability of proteins is a qualitative characteristic with regard to purification success.[347]

The stability of proteins can be quantified by various methods such as Nuclear Magnetic Resonance (NMR) or thermofluor assys.[348-350]
Purified and concentrated samples of SIRT2 from both size exclusion runs were analyzed regarding their thermodynamic stability by means of microscale thermophoresis (see figure 15).

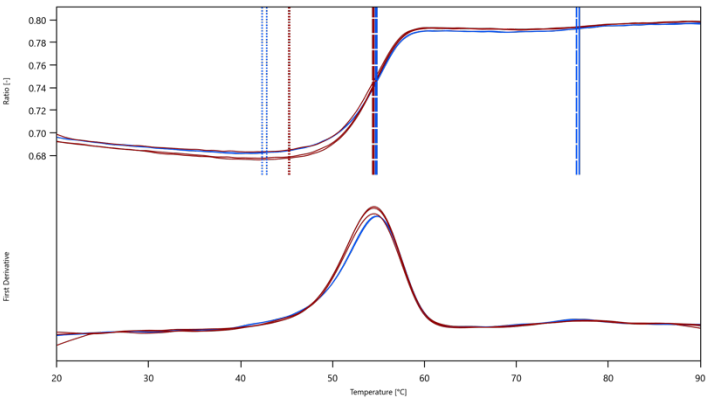

Figure 15: Thermostability evaluation of two SEC runs via MST. A second gel filtration run (red line) increased the thermostability in comparison to the initial gel filtration (blue line).

The thermostability of SIRT2 after SEC 1 (blue line, figure 15) and SEC 2 (red line, figure 15) of the purification was improved by an average of 2.36 °C at the expense of protein yield.
The high SIRT2 expression level in *P. pastoris* compensates for the lower protein yield after a second gel filtration run, when a highly pure and monodisperse protein sample is required.

4.1.2. MEMBRANE PROTEIN AQP4

The diverse role of aquaporin 4 in health and pathological disorders has increasingly attracted the attention of the research community in recent years (see chapter 1.2.5). There is a broad spectrum of medical applications for purified AQP4, especially for protein produced in high yields with suitable and diagnostically conclusive PTMs. The established improved recombinant overexpression of AQP4 in *P. pastoris* has been used to obtain high amounts of the membrane protein for different applications.

For overexpression, a His tag fused AQP4 construct with a triple amino acid mutation (M48N, L50K, N185D) was cultured in a 3 l bioreactor with minimal media.[351] The overexpression feature of the M1 construct was intensified by codon optimization and proper clone selection for high-yielding transformants.[352]
A single step IMAC purification was used to obtain protein of sufficient purity for use in the desired applications (see figure 16). An extrapolated yield of 108 mg/l medium or 0.35 mg/g cells was obtained.

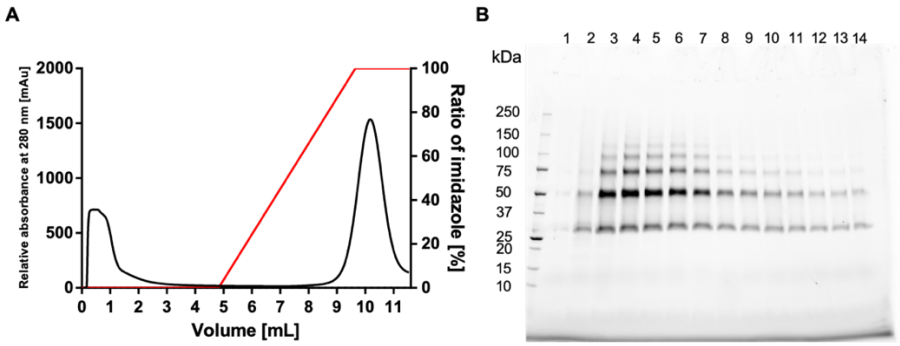

Figure 16: A) Ni-NTA-purification of hAQP4. B) The related SDS-gel of the peak fractions shows a typical hAQP4 degradation pattern.

The high-purity AQP4 obtained was used for a wide variety of application including the improvement of diagnostic techniques for autoimmune diseases, development of stable artificial membranes in the development of water filters and method development for NMR studies on AQP4 itself, a method of potential use for hAQP4 protein complexes.

4.1.3. MANUSCRIPTS IN PREPARATION

1. Improving the diagnosis of Neuromyelitis Optica Spectrum Disorder

Neuromyelitis Optica Spectrum Disorder (NMOSD) is an immune-mediated inflammatory condition, often involving the CNS, with a high affinity for affecting the optic nerves and the spinal cord.[353] A major advance for clinical diagnosis of the disease was the presence of detectable antibodies against AQP4 (AQP4–immunoglobulin G [IgG]) in the serum of patients.[354]
The occurrence of AQP4-IgGs is correlated with pathogenic potential and patients with NMOSD show syndromes or lesions of the spinal cord, optic nerve, brainstem, diencephalon, area postrema and cerebral presentations on Magnetic Resonance Imaging (MRI) screenings.[355]

The severity of disease progression cannot be linked to the abundance (titer) of AQP4-IgGs, indicating the molecular diversity of the constituents which comprise the AQP4-IgG titer as a pathological origin.[356]
Recent developments in bioinformatics and proteomics have made it possible to profile humoral immunity and the repertoire of human antibodies at the molecular level.[357] The analysis of the circulating AQP4-IgG repertoire is possible by combining two key techniques, B-cell repertoire sequencing (BCR-Seq) and Immunoglobulin sequencing (Ig-Seq).[358]
BCR-Seq enables the analysis of the acquired immune response of patients by sequencing B cells at the bulk and single cell level with regard to the antibody information presented on the cell surface.[359] As part of the adaptive immune system, these B cells from the patient serum are responsible for the secretion of antibodies as an immune response.
Ig-Seq is a proteomics tool that enables the analysis of the dynamics of the antibody repertoire based on the obtained BCR-Seq data (= encoded by the individual B cells) of the patient.[360, 361]
These methods were used in combination, to specify the AQP4-IgG polyclonal serum repertoire of NMOSD patients. We produced AQP4 to facilitate two aspects of the project: The recombinantly produced protein was immobilized on a chromatography column to purify the AQP4-IgG polyclonal serum repertoire. Based on the BCR-seq/Ig-seq platform analysis of the circulating AQP4-IgGs in patients, monoclonal antibodies (mAbs) were designed and expressed for verification. A binding assay of the mAbs with AQP4 confirmed the AQP4-IgG profiles obtained by using high-throughput sequencing and quantitative immunoproteomics in combination.
These results provide new insights into our understanding of humoral immune responses and for a better diagnosis of NMOSD in patients.

2. AQP4 stabilization for technical applications

The interest in aquaporins is not only limited to biomedical research, the versatile role of the membrane protein is also utilized in material science to enable new applications for waste water treatment and purification.
Drinking water production from seawater or the preparation of pure water for industrial usage is mainly achieved by a polymer based reverse osmosis.[362, 363]
The purification process works against the osmotic gradient, which is compensated with the use of pumps to drive the filtration process.
Large amounts of energy is needed to meet the increasing demand for pure and fresh water, making up to 45% of the total permeate production cost for desalination.[364]

The use of renewable energy for desalting sea water has improved the ecological footprint for seawater reverse osmosis.[362] Previous attempts for improvements were mostly focused on the specific energy consumption, not on the water selection process itself.[365]
Since most of the biological cells have the ability to facilitate water transport, attempts to mimic this process with human technology were carried out.[366] The incorporation of aquaporins into filter membranes would combine the proteins high selectivity for water molecules with a self-driven flux without the need for high external support pressure.[367] A limited factor for this approach is the stability of the protein, and previous attempts were mainly focused on aquaporin stabilization by polymerization.[368-370] Hence, the stable hAQP4 produced in this thesis, could also be used in the development of a suitable membrane matrix for water filters. Specifically, the stabilization of AQP4 in silicon dioxide (nanostructured glass) is explored, offering new perspectives for the development of efficient water filter for real-world use.
The usage of aquaporins in technical applications is limited by the need of the protein for a natural environment to prevent functionality. As a membrane protein it can be transferred into liposomes (see chapter 2.7) to keep its functionality, but these vesicles lack structural integrity for technical purposes. Proteoliposomes can be stabilized within a silica matrix, with implications in protein accessibility.[371] An alternative is the coating of the proteoliposomes with a layer of silica, resulting in a better accessibility of the aquaporin and higher diffusion rates of molecules.

A novel method was developed to coat proteoliposomes with silica (see figure 17). The silicification process of the organic-inorganic material was characterized with different biophysical and structural methods to gain insight into the mechanisms of silica shell growth.

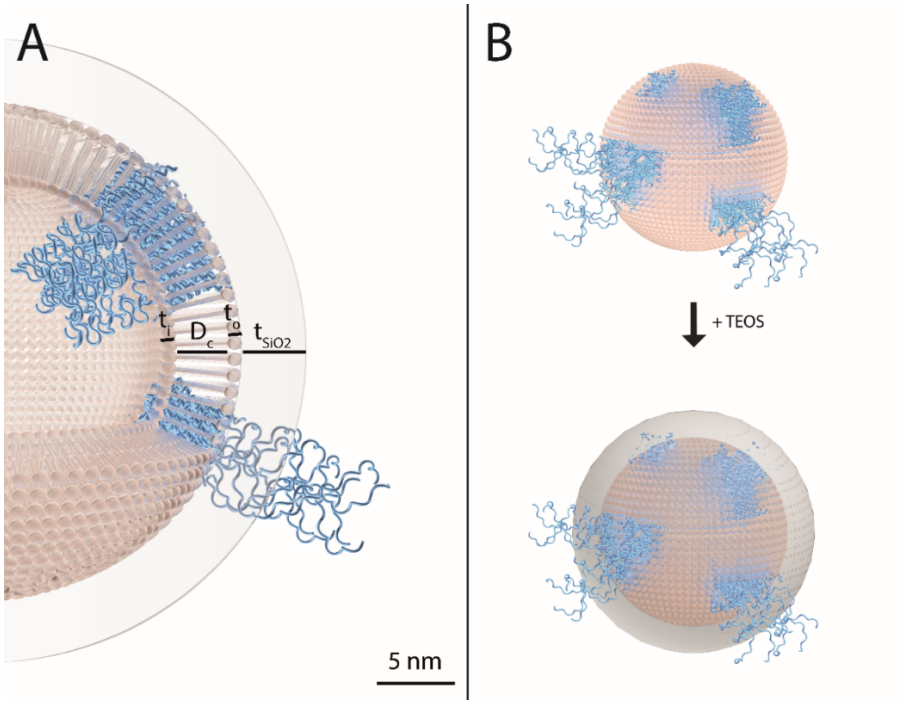

Figure 17: A) Schematic illustration of the silicification process of hAQP4 proteoliposomes. The protein is presented in blue, POPC lipids in brown, and silica in grey. B) Formation of the silica layer after the addition of tetraethyl orthosilicate (TEOS). Modelling performed by Simon Isaksson, Chalmers university.

Notably, the stabilization process of AQP4 proteoliposome coating with a silica shell does not have any negative impact on the native confirmation of the reconstituted protein, a promising prospect for future functionality tests.

3. Method development for NMR studies on AQP4 interactions

The potential of AQP4 as a drug target for various diseases has been discussed in chapter 1.2.5. The evaluation of potential pharmaceutical interaction candidates heavily relies on high resolution structures of the protein in combination with the binding partner.[372] To date, X-ray crystallography accounted for the greater part of the structures (90 %), with the remainder produced by NMR (9 %) and Three Dimensional Electron Microscopy (3DEM, 1 %).[373]

The development of Magic Angle Spinning (MAS) solid-state NMR (ssNMR) has facilitated the investigation of structural, dynamical and interaction properties of membrane proteins in a lipid bilayer environment.[374]

Here we present preliminary results of MAS ssNMR studies on the homotetramerization of AQP4. Several main goals were achieved to be able to detect and assign the signals of AQP4. First of all, we demonstrated the feasibility of producing milligrams of isotopically labelled AQP4 (^{15}N, ^{13}C) in high purity in the host *P. pastoris* (see figure 18).

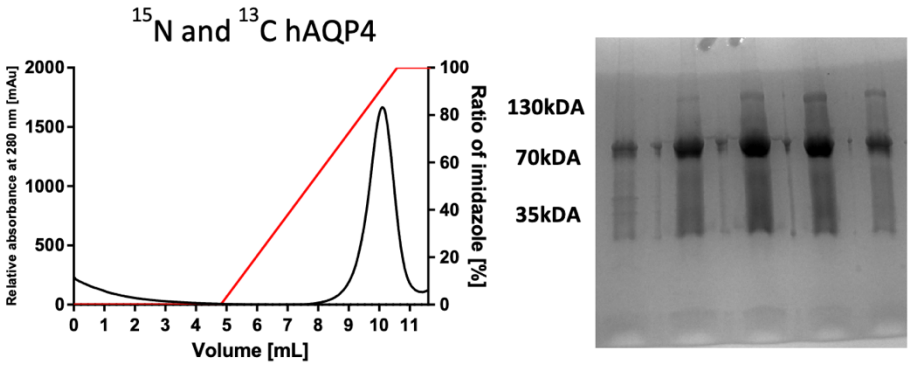

Figure 18: Ni-NTA-purification of 15N- and 13C labelled hAQP4 shows a chromatogram with a peak fraction containing 8mg protein. The double-labelled hAQP4 appears mainly as dimers in the related SDS-gel.

Second, we established a methodology to reconstitute AQP4 in lipid bilayers for MAS ssNMR measurements, by mixing the detergent-solubilized and purified protein with preformed POPC liposomes at a protein-to-lipid ratio of 2:1 (w/w).

After removing the detergent by dialysis, the sample precipitate was transferred into MAS NMR rotors and a set of 2D and 3D correlation spectra of AQP4 were obtained (see figure 19).

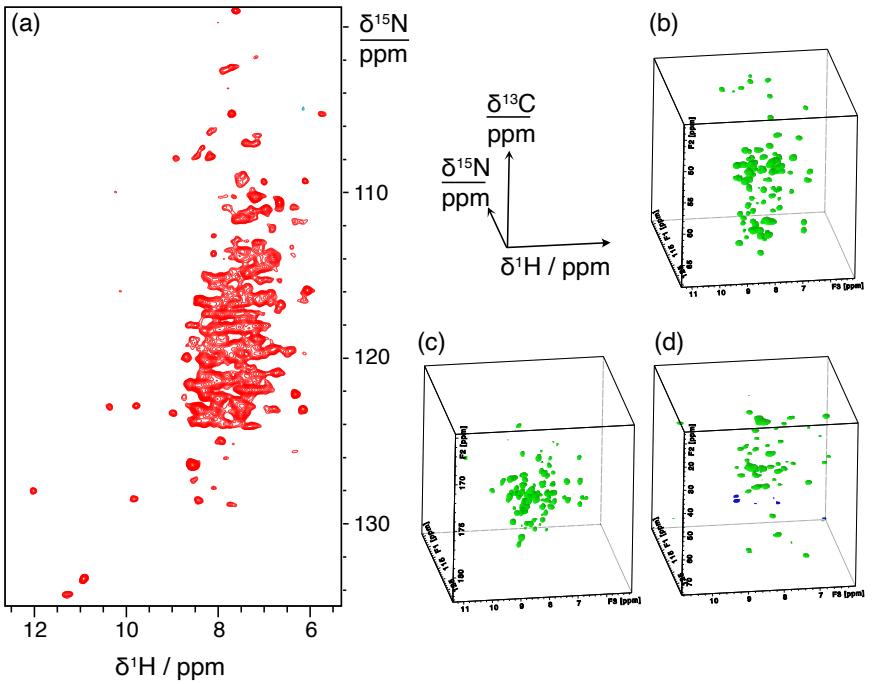

Figure 19: MAS NMR spectra of [^{15}N, ^{13}C]-labelled hAQP4 in POPC bilayers. (a) 2D ^{1}H-^{15}N correlation spectrum of hAQP4 obtained at 60 kHz MAS on a 23.5 T spectrometer. (b-d) 3D ^{1}H-^{13}C-^{15}N correlation spectra for resonance assignment obtained at 100 kHz MAS on a 18.8 T spectrometer: (b) (H)CANH, (c) (H)CONH, (d) (H)(CA)CB(CA)NH. Spectra were obtained and evaluated by Tanguy Le Marchand, Centre de RMN à Très Hauts Champs.

The high quality 2D spectrum of (^{15}N, ^{13}C) labelled AQP4 (see figure 19, a) indicates a very homogeneous environment for the proteins incorporated in lipids, comparable to similar experimental conditions observed for other membrane proteins.[375] Subsequent 3D (^{1}H-^{13}C-^{15}N) correlation spectra (see figure 19, b-d) were recorded to automatically assign the AQP4 residues important for the intermolecular binding of the monomer subunits (see figure 20).[376, 377]

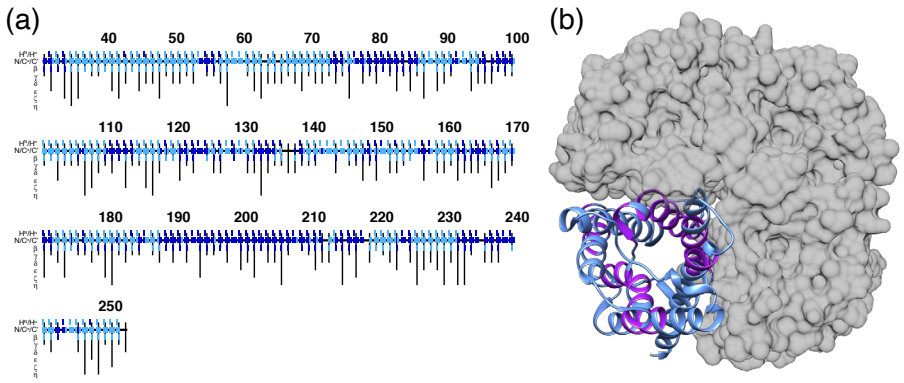

Figure 20: Automated resonance assignment of hAQP4. (a) Results of the CYANA calculations. Nuclei for which a signal could be assigned with strong confidence are depicted in dark blue. (b) Residues with assigned NMR resonances are depicted on a monomeric unit of hAQP4 3D structure (pdb code: 3GD8). Surfaces of the three remaining monomers are shown in grey. Spectra were obtained and evaluated by Tanguy Le Marchand, Centre de RMN à Très Hauts Champs.

The assignment of aquaporin interactions via NMR has been previously done with AQPZ from *E. coli*, which has a high similarity with its human counterpart AQP1, and the C-terminal peptide of AQP4 to CaM.[378-380]
The presented experimental setup provides a powerful platform to study the physiological role of aquaporin tetramerization. Non-tetrameric AQP4 mutants are unable to relocalize into the plasma membrane, and the tetramer formation of the monomeric subunits might be an important factor for regulatory protein interactions.[381]
Once established, studies with potential AQP4 interaction partner can be carried out with MAS NMR measurements, as well as the effects of OAPs formation.[382]

4.2. NEW AQUAPORIN STRUCTURES

X-ray crystallography as a tool has helped to transform our understanding of molecular mechanisms of biological processes in the last six decades.[383] New technologies such as cryo-electron microscopy are emerging, for the time being we are still depending on high-resolution structural determinations based on crystallography to explain the derived function of proteins.[384]

In **Paper II** we present the novel structure of AQP1 from *Anabas testudineus*, climbing perch, which plays a significant role in the variable osmoregulation of the fish species.

In **Paper III** we have a closer look at the structures of plant aquaporins AtPIP2;4 and SoPIP2;1, and the presence of cadmium cations for conformational changes in the different species will be discussed.

4.2.1. A NOVEL STRUCTURE OF A FISH AQUAPORIN (PAPER II)

In contrast to vertebrates living on land, aquatic vertebrates are surrounded by a medium, which is constantly changing in osmolarity. Teleosts, such as the climbing persh fish *Anabas testudineus*, adapted their osmoregulation to the external environment by the development of ionocytes in the gills, facilitating the ion- and water flux across the gills.[385, 386] Aquaporins are not only expressed in ionocytes, but also in a wide array of fish tissues, where they facilitate the homeostasis of the cells.[387] We chose AQP1 (cpAQP1aa) from climbing persh as target, since the diversity of the habitat of this fish should be reflected in the regulation and transport specificity of its aquaporins. Aquaporins in fish are known since the year 2000, and the basic components of an aquaporin structure (ar/R-region, NPA motifs etc.) are also present in the cpAQP1aa structure, but very little is known about its transport specificities and regulation.[388] The main factor for successful high-resolution structural determination of cpAQP1aa were the design of a truncated construct of the protein, missing flexible parts in the C-terminus which could interfere with crystal formation, and high production yields *P. pastoris* as expression host were achieved.

Insights into molecular mechanisms were obtained by comparing the cpAQP1aa to other (distant) species, both sequence alignment and high-resolution structures, highlighting variations in loop A and C, respectively. Especially Tyrosine 107 in loop C supports the formation of an extracellular hydrophobic constriction region, which could possibly act as an extracellular gate for water flux control. The open extracellular entrance of cpAQP1aa might be “capped” by loop C with Leucine 117 being pushed into the pore, resulting in a semi-gated entrance. The channel capping can be compared to the one observed in plant plasma membrane aquaporins, exemplified by SoPIP2;1, but is apparently less efficient since Leucine 117 is pushed further into the channel by the conformational change in loop C without fully plugging it.[389]

Intracellular gating as a mechanism for water flux control of aquaporins among yeast, plant and mammalian has been described previously, and can be affected by phosphorylation, pH, pressure, solute gradients, temperature and membrane tension among others.[390]
The high-resolution structure of cpAQP1aa is determined at pH 7.8 and pH 6.5, respectively, and no structural determinant related to pH was observed, which suggests that the conformational gating regulation of the extracellular loop C is not pH dependent. Instead, we found support for an extracellular phosphorylation influence on the efficiency of cpAQP1aa gating, supported by mutational studies and MD simulation (see chapter 4.3.2).
From the crystal structure alone, it is difficult to validate substrate specificities for aquaporins. The pore dimensions of cpAQP1aa were compared, via HOLE simulation, with aquaporins from other species, having different substrate specificities, and potential transport specificities for ammonia and glycerol could be excluded for the fish aquaporin. These simulations based on the high-resolution structure gave a hint for the unique extracellular regulation site and water transport specificity, nevertheless we examined the protein in functional assays to validate the proposed findings (see chapter 4.3.1).
The evaluation of molecular mechanisms with structural analysis is a valuable tool for getting insight into the function and regulation of cellular processes. This knowledge can then be used to influence various processes in a positive direction. An example of an application is the production of fish eggs in marine fish, where the proper function of aquaporins is essential.[391] In this context, the understanding of the intracellular pathways of oocyte hydration, could possibly improve egg viability and embryo survival in the aquaculture industry.[392]

4.2.2. A NOVEL STRUCTURE OF A PLANT AQUPAORIN (PAPER III)

Hydrogen peroxide transport is vital in plants as part of the recognition of pathogen infection.[114, 393] To shed further light on the structural determinants of hydrogen peroxide transport, we solved the structure of an aquaporin homologue from *Arabidopsis thaliana*, AtPIP2;4, for which hydrogen peroxide transport had been suggested. Initially, we compared the structure of AtPIP2;4 with its plant homologue from spinach, SoPIP2;1 (see figure 21).

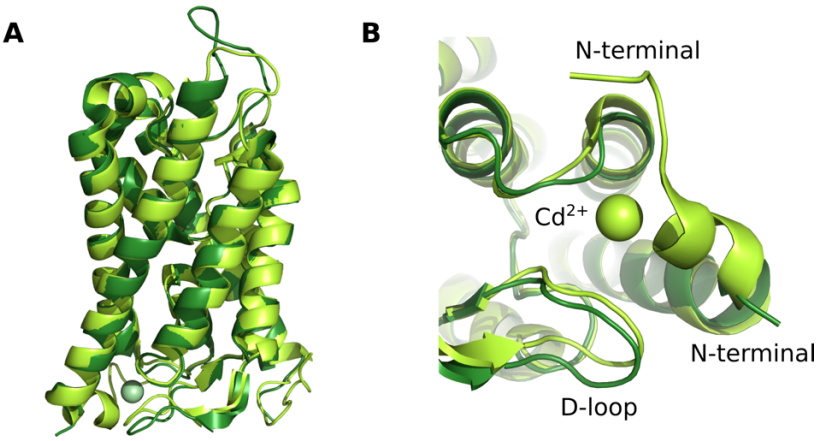

Figure 21: A) Superimposed high-resolution structure of SoPIP2;1 (PDB: 1Z98, light green) on the high-resolution structure of AtPIP2;4 (dark green). B) View on the N-terminal side of the superimposed proteins shows a Cd^{2+}, necessary for the closed conformation of SoPIP2;1.

The two plant homologues show a high structural similarity in the monomeric pore when superimposed to each other (see figure 21, A). An important difference was determined in extracellular loop D, where the closed conformation of SoPIP2;1 is depending on a divalent cation (Cd^{2+} in the crystal structure). This is not the case in AtPIP2;4, as a consequence we extended our study for indications of the importance of the loop regions for contribution to the transport specificities.

In hAQP1, the structural confirmation of loop D has been identified as an important factor for channel gating.[71] Indeed, in comparison to the plant aquaporins, loop D in human AQP1 is not only shorter, but also lacks Leu197, which plays a vital role in closing the cytoplasmic entrance for water passage in SoPIP2;1.[44]

A variation in transport specificities between the species can possibly also be explained by differences in loop A. The amino acid alignment of the three AQPs shows a divergence in the quantity of residues, which could have implications on the functionality of the aquaporin, especially regarding H_2O_2 transport. Loop B and C, on the other hand, do not show a comparable amino acid deviation, indicating a less profound impact on the transport specificities. This reasoning illustrates the importance of complementing functional verification of structural investigations, since a pore diameter comparison is not a dependable indicator for transport efficiencies.

Both, plant aquaporin SoPIP2;1 and hAQP1 share a similar diameter of the pore, but their specificities are not fully elucidated. By using structural information and functional characterization in concert, molecular mechanisms of water transport in aquaporins could be specified.

4.3. EVALUATION OF AQUAPORIN FUNCTION

The knowledge about the structure of proteins opens up opportunities to understand the derived functions. In **Paper II** the functionality of cpAQP1aa is verified, together with the evaluation of transport specificities for this specific aquaporin homologue. In addition, functional mutants were created to explain the possible regulatory mechanism for AQP1 from *Anabas testudineus*, being a critical player in the osmoregulation of the whole fish.

Plant aquaporins show a large diversity in transport function in comparison to other species[112], in **Paper III** and **IV** the H2O2 transport versatility of aquaporins from the species *Arabidopsis thaliana*, *Spinacia oleracea* and their human homologue are compared. To achieve this, a novel fluorescence-based transport assay for hydrogen peroxide transport has been developed.

4.3.1. EVALUATION OF WATER TRANSPORT (PAPER II, III, IV)

Stopped-flow assays are used in our studies to verify production of functional aquaporins and also for the validation of retained function for truncated versions of aquaporins aimed for crystallization.
In **Paper II**, the truncated version of cpAQP1aa used for structural determinations was tested against its full-length version and hAQP4. The orthodox AQP4 is used as a positive control in our lab, setting the standard for efficient water transport. All aquaporins are reconstituted into liposomes (see chapter 2.7), as a consequence empty liposome samples are included in the experiments as negative controls, representing the passive water transport through the membrane. As a result, the functional analysis showed comparable initial rate constants for cpAQP1aa and the truncated version, indicating their functionality. Both fish aquaporin variants are less efficient water transporter in comparison with hAQP4, a result of the unique structure regulation features of *Anabas testudineus*, and discussed in more detail in the next chapter.

These initial experiments were the basis for more advanced mutational studies based on the full length cpAQP1aa construct.

In **Paper III** functional H_2O transport rate comparisons via stopped-flow measurements were conducted to verify the truncated AtPIP2;4 variant (chapter 4.2.2) for structural determination. Initially, we compared the water transport capabilities of full length AtPIP2;4 to its close plan homologue, SoPIP2;1 and human AQP1. The human orthodox aquaporin got included in the measurements as a positive control, with the benefit of being inhibited by mercury. By the induced abolishment of transport function, the water transport effect seen in the assay are protein-related and not experimental artefacts. The previously used hAQP4 (**Paper II**) is less sensitive for the heavy metal, and the inhibition effect is based on a modification of a cysteine residue in cytoplasmic loop D rather than a plugging effect seen in AQP1.[394]
All three aquaporins isoforms, AtPIP2;4, SoPIP2;1 and hAQP, show comparable water transport rates, and a mercury inhibition comparison limited the transport effect to the presence of incorporated hAQP1 in the liposomes. Finally, the full length AtPIP2;4 and its truncated version, used for crystallization setups, were compared regarding their water transport ability. The water transport efficiency of AtPIP2;4(28-279) was lower in comparison to AtPIP2;4, but still higher than mercury inhibited AQP1. Nevertheless, the water transport seen for AtPIP2;4(28-279) is protein specific and this variant was chosen for structural determination.

The evaluation of the functional data is extremely depending on a sufficient number of reproducible experiments with a certain quality. In our analysis, we differentiate between biological replicates (= distinct experiment preparations) and technical replicates (= repetitions of experiments) to obtain a statistically relevant number of stopped-flow experiments. The intrinsic variation of a single stopped-flow measurement is averaged by technical repeats, additionally we use dual controls to identify eventual effects of different sample incubation times and the influence of temperature effects.
For measurements, every biological sample is split up into three technical experimental specimen which is used up in the actual experiment, resulting in average five to six scattering curves, which get averaged. The number of biological repeats used for data evaluation depends on the sample species and their reconstitution quality. Naturally, more liposome control samples were generated than protein samples, and the reconstitution ability between the protein samples differed between the used species. The reconstitution factor has to be considered for the evaluation of transport specificities.

For the preparation of samples, equal amounts of protein are used initially for the preparation of the reconstitution samples. That does not necessarily mean that the protein gets fully incorporated into liposomes.
This process depends on different criteria, such as protein concentration and quality, choice of detergent and how these are removed in the end.[395]
In **Paper II**, the protein reconstitution into proteolipsomes between the different constructs were compared, and mutant cpAQP1aa-Y107A and cpAQP1aa-L117A showed a fraction of protein incorporated into liposomes.
To evaluate the reconstitution efficiency of the used proteins, the immunoblot intensities for each sample got analysed and the specific initial transport rate was factorized related to the protein amount quantitated from the immunoblots. This approach is not ideal, since there is not necessarily a linear relationship between the amount of protein incorporated into liposomes and the resulting water transport activity. Nevertheless, the adjusted activity is closer to reality as those not taking protein amount into account, and also an established way of presenting data of this kind. It is however wise to apply a critical mind set and reflect on the intrinsic parameters in retrieved data.

4.3.2. A NOVEL EXTRACELLULAR GATE REGULATED BY PHOSPHORYLATION (PAPER II)

In the last two chapters we investigated the structure of cpAQP1aa and verified the water transport function of the full-length aquaporin, as well as the truncated version used for crystallization setups. The obtained high-resolution structure shows a static picture of the peptide chain, with a unique structural fold at the extracellular side. In summary, the putative influence of phosphorylation of the extracellular Tyrosine 107 residue on the conformation of loop C was investigated as a possible key component in the regulatory mechanism, as was suggested from the high-resolution structure of cpAQP1aa (see chapter 4.2.1). Mimicking the phosphorylation of a protein, and as result, activation and deactivation of the protein function by the disruption of intramolecular binding, cannot be directly done by adding a phosphate group to an amino acid. Instead, point mutations with similar characteristics are used to simulate the related effect.[396]
Based on the high-resolution structure and comparison to related structures, five different mutants were made to the mimic or abolish phosphorylation sites; T38A, T38E and Y107A, to mimic the sequence of AQP1; Y107S, or to take away the putative hydrophobic block; L117A.

To study the functional effects of amino acid aberration, the single mutant constructs cpAQPaa were transformed in *P. pastoris*, overexepressed, purified and reconstituted into proteoliposomes to evaluate water transport using stopped flow and compared to controls, wild type protein and empty liposomes, respectively.

Initially, we studied the noticeable structural extracellular loop C region, possibly responsible for the semi-open gating mechanism. The hydrophobic block characteristic of Leucine 117 was abolished by inserting an alanine at that specific position. The functional effect of the mutation was not easy to evaluate, since the reconstitution of the protein into the liposomes was low in comparison to wild type protein. That abnormality was also noticeable in mutant Y107A, created to examine the influence of phosphorylation on the assumed stabilization network around L117. Both mutants were produced to low yields in *P. pastoris*, and hence difficult to purify, only 0.5-1 mg of the proteins could be obtained per purification, which failed several times due to low membrane yields and poor binding to the affinity column. In comparison, it was easy to obtain 26 mg of the mutant cpAQP1aa-T39E per purification, resulting in a higher concentration of the protein in the final pool. The low concentration of cpAQP1aa-Y107A and cpAQP1aa-L117A had an impact on the sample preparation for the reconstitution experiments, since a larger volume of a less concentrated protein solution had a lower ratio between protein and detergent, which could possibly influence the efficiency of reconstitution. Even though the incorporation of L117A and Y107A protein into the liposomes was not efficient, we compensated that effect by virtually balancing the lower protein amount related to full length cpAQP1aa. Taken the compensation into account, it turned out, that the side chain containing L117A is not the primary reason for waterflow control, indicated by a wildtype like initial rate. At the same time, the “non-phosphorylated“ mutant Y107A indicated an open-pore like water transport in the compensated functional assays, supporting its importance for stabilizing the network around L117. An additional mutant was made at this position to mimic AQP1, Y107S. This mutant also showed wild-type like water transport rates, but in line with the increased compensated transport of the Y107A mutant, lacking the phosphorylation motif, we found a first indication for the importance of a phosphorylation site at Tyrosine 107.

Since phosphorylation is an important mechanism for aquaporin regulation[61], we focused our efforts on additional influence of phosphorylation on the regulatory mechanism of cpAQP1aa involving Threonine 38 in loop A, where putative impact of phosphorylation was examined with the mutants T38A and T38E to abolish and mimic phosphorylation, respectively. A mimicking effect of phosphorylation at T38 showed an increase of the water flow in comparison to the wild-type protein, indicating a regulatory effect of the modification, either on its own or in combination with Y107 from loop C.

The versatile osmoregulation of the cpAQP1aa could not be verified with the high-resolution structure alone or in combination with functional studies and results from phosphorylation evaluations.

With support of molecular dynamics (MD) simulations, the molecular puzzle of the cooperating effects for gating control finally fit together, giving a first osmoregulation model for a fish aquaporin. According to the simulations Y107 is indeed effected by phosphorylation, resulting in a pore closure. Functional studies of the mutant T38E on the other hand, are an indication for the involvement of phosphorylation for an opening of the channel, but this has to be further investigated.
The combination of different experimental methods in combination with theoretical support facilitated the development of an initial model for the osmoregulation mechanism in fish by an extracellular gate. These findings have implications on our understanding of aquaporin regulation, where the semi-open pore allows a more fine-tuned regulation of the water channel.

4.3.3. EVALUATION OF HYDROGEN PEROXIDE TRANSPORT IN PLANT HOMOLOGUES (PAPER III, IV)

The comparison of transport rates for aquaporins with different transport specificities and distinct origin can shed light on the molecular regulation of the observed effects. In **Paper III**, we compared the transport efficiencies of three AQPs, two with plant origin, and a human homologue regarding hydrogen peroxide as a substrate. We developed a novel assay, which allows the comparison of H_2O_2 transport efficiencies between these AQP homologues, and membrane proteins in general, based on standardized protein quantities reconstituted in proteoliposomes. Previous studies on facilitated hydrogen peroxide transport of aquaporins were depending on cell assays, where the expression level of the proteins could not be controlled and background reactions could interfere with the analysis.[397, 398] By using purified aquaporin homologues in a functional proteolipsome environment, we were able to quantify the differences in transport specificity related to protein amounts, rather than correlating growth of cells with protein appearance.
Initially, we compared the H_2O_2 transport of AtPIP2;4, selected based on its proposed specificity for hydrogen peroxide, with its plant homologue from spinach, SoPIP2;1.

The same amount of protein was reconstituted into the liposomes, and a comparable hydrogen peroxide transport rate was observed where the protein specific transport was verified by mercury inhibition. Beside human AQP3 and AQP8 (known "peroxiporins"), AQP1 has recently been suggested to transport hydrogen peroxide in whole cells.[399, 400]
Therefore, we included hAQP1 in our study, to compare its H_2O_2 transport specificity with the two plant aquaporins on protein level. In the proteoliposome assay, the human aquaporin showed a significant overall lower initial transport rate than AtPIP2;4 and SoPIP2;1. The hAQP1 derived transport of H_2O_2 was protein specific, since mercury addition showed an inhibition on the hydrogen peroxide transport in proteolipsomes.
The novel assay presented in the study addressed the problem of unspecific measurements of H_2O_2 transport. Concentration measurements of H_2O_2 as transport verification in tissues evaluated by microscopy have been extensively criticized.[401] Our established assay is cell-independent and allows the quantification of the H_2O_2 transport rate based on the amount of protein incorporated into the liposomes and therefore allows proper comparison of membrane proteins in general and their mutants. Furthermore, related to these results, the development of alternative transport assays is possible, by adapting the reporter system to the desired probe conditions.

4.4. ANALYSIS OF AQUAPORIN INTERACTIONS

Chapter 4.4 focuses on the development of methods for screening PPIs, including membrane proteins. In **Paper V**, BiFC complementation of AQP0 and CaM is used in combination with flow cytometry to enable future HTS screening of novel protein interactions *in vivo* in eukaryotic cells.
Potential interaction partner of AQP4, found in the screening process, can be evaluated via NMR experiments presented in chapter 4.1.2.

4.4.1. SCREENING AQUAPORIN COMPLEXES USING FLOW CYTOMETRY (PAPER V)

The detection and verification of protein-protein interactions contribute to the knowledge about the fundamental networks (interactomes) in which they are integrated. Understanding these networks can provide new insights into their regulation and the pathways involved, thus pointing the way forward for drug development.[402]
Various PPI detection methods and their characteristics have already been discussed (see chapter 2.8), and the intrinsic advantages of a technique must be evaluated with regard to the presumed application.

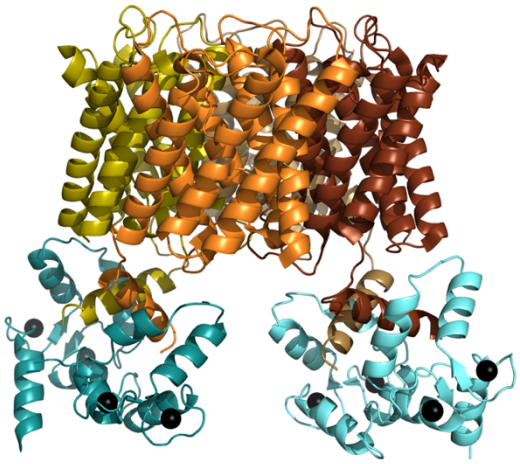

Figure 22: Ca^{2+} (black spheres) mediated binding of calmodulin (cyan) to the C-termini of AQP0 (PDB: 3J41). ITC studies have suggested the binding of a single CaM to two copies of AQP0.[65]

In **Paper V** we expand the capabilities of the well-established BiFC assay for *in vivo* HTS evaluation and screening of aquaporin interactions in *S. cerevisiae*. The well-investigated binding from AQP0 to CaM is used for high-throughput verification of yeast populations in this study.[63-65, 313, 403]

Physiologically, the interaction between AQP0 and CaM is crucial for the modulation of the water permeability in the eye lens.[404] The Ca^{2+} mediated binding of CaM to a cytoplasmic helix in the C-terminus of AQP0 results in a conformational change and finally in the pore closure (see figure 22).[63]

The BiFC assay meets our requirements for method development and evaluation, because our interacting proteins AQP0 and CaM are confirmed interaction partners with an initial binding affinity of Kd=71 nM and the detected fluorescence signals show a correct molecular interaction between these proteins, as indicated by the YFP complementation.[63, 313]

Different constructs of AQP0 and CaM were generated and evaluated by flow cytometric readout. By fusion of non-fluorescent cleavage fractions of YFP (YFP_C and YFP_N) to the target proteins, different interaction combinations were tested.

A negative control of unconstructive complex formation recommended in the literature was included in the experiments, a C-terminal truncated mutant of AQP0, co-transformed with CaM and both fused to their respective YFP halves.[405-407]

In a previous study, the evaluation of BiFC formation was performed manually. This includes both, the manual collection of brightfield and fluorescence images of the various construct samples and the manual counting of the fluorescent cells.[313] This labour-intensive work is not only time-consuming, but also prone to readout errors.

Flow cytometry was used to automate the counting and intensity evaluation of the fluorescent cells and to statistically analyse entire construct populations.

The exemplary comparison of the constructive BiFC pair Y_N-Aqp0 and Y_C-CaM regarding YFP intensity and frequency in the screened population revealed the importance of standardized pre-growth conditions.

The pre-selection of transformants associated with a fluorescent phenotype saves time in the subsequent evaluation in the downstream process, as there is no need to prepare cell samples that do not exhibit YFP complementation intensities.

Another factor for an optimal YFP intensity yield in the fluorescent cell fraction (frequency of fluorescing cells) is the growth of the pre-selected cells in liquid media up to the log phase prior to cytometric analysis. In comparison, cells pre-cultured on SC agar plates before analysis showed a lower sub-fraction of fluorescent cells in combination with low YFP intensities.

The reliability and comparability of a high-throughput readout of intensities is based on a reliable preparation of the cells before analysis. From our observations we could determine a significant effect from the sample preparation to the final readout of the cells. Since the presence of fluorescence in the cells is a direct indication for the interaction of the transformed protein partner, the presented standardization scheme for sample preparation was important to control the intrinsic fluorescence fluctuations of the cells.

In addition, iterations of biological repeats of the experiments provided a solid statistical fundament for the analysis of the different screened constructs, where the biological variation due to the transformation step could be controlled.
We used the rationalized cell preparation scheme for the screening of different constructive BiFC complexes, initially with a special interest in the median fluorescence intensities (see figure 23, A).

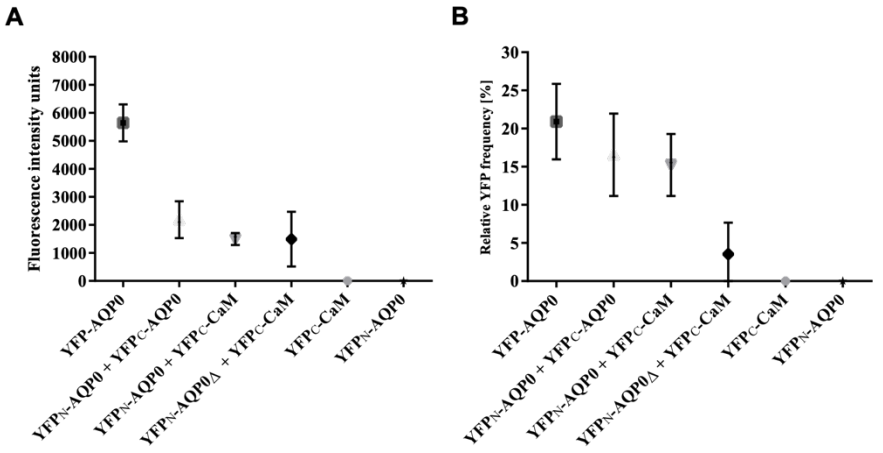

Figure 23: A) Average YFP fluorescence intensity readouts from different BiFC complexes. B) Average fraction of YFP fluorescent cells in percentage for the BiFC complexes.

We noticed, that focusing on fluorescence intensity readouts is not sufficient to distinguish between random and constructive BiFC interactions, but could well be used as the initial parameter for a pre-selection procedure. This was evident in all constructive BiFC pairs that showed average mean fluorescence intensities in the same range, although YFP_N-AQP0Δ + YFP_C-CaM has a higher standard deviation, indicating a larger non-fluorescent cell fraction (see figure 23, A).
The focus on intensity levels to screen for authentic PPIs can be misleading, as rare and random protein interactions occasionally could lead to above average fluorescence intensities, which was the case for the interaction-deficient construct.
In order to distinguish between authentic and random protein interactions, which leads to a higher signal-to-noise ratio, the inclusion of the fluorescence frequency (proportion of fluorescent cells) in the cell population was included as a second quantitative selection criterion in the analysis, and used as the determinant for formation of constructive membrane protein complexes (see figure 23, B).

This procedure required a reduced transformation variation, which was achieved by a consistent cell preparation prior to the measurement. As a result, the relative frequency allows the distinction of the interaction-deficient YFP_N-AQP0Δ + YFP_C-CaM pair from the other complementation constructs.

By considering the fluorescence fraction of the cells for the analysis of potential interaction partner, a threshold value can be derived from non-interaction constructs to separate authentic complex formation from random interaction events. Worth noting, though, is that this only serves as in indicator, and proper references should be evaluated for each protein complex.

A challenge for PPI interaction methods is the differentiation between authentic interactions and background signal (signal-to-noise ratio). This ratio has been be improved over the years, either by using improved fluorescent proteins or by combining BiFC with other methods.[311, 312, 318, 408-411]

By the addition of flow cytometry to the available methods for protein complex evaluation, the BiFC complementation can be read-out objectively on a large scale in less time. The results of this thesis show, that an improvement regarding background reduction can be implemented in a method without additional complexity. The required statistics of the readout are recorded by default and available for analysis.

5. CONCLUDING REMARKS AND FUTURE PERSPECTIVES

Nearly 20 years ago, the first high-resolution aquaporin structure was reported and it turned out, that the primary function as water transporter is accompanied by a huge variety in specificity and regulation as well as involvement in a broad range of human diseases. This thesis tried to elucidate different aspects of aquaporin research, providing insight into different levels of protein complexity in the fascination of the larger context of biochemistry and related fields.

A basic bottleneck emphasised in membrane protein research, is the availability of sufficient amounts of the protein of interest in a reliable quality, most pronounced for structural analysis where large amounts are typically required, but also a relevant aspect for functional evaluation.

In **Paper I**, my specific contribution was the production of reliable amounts of the soluble protein hSIRT2 in *P. pastoris*, an indirect regulator of AQP4, in its active form and a homogenous sample was obtained for future structural and inhibition studies. hSIRT2 is involved in a variety of human diseases, and the beneficial expression of this potential drug target in an eukaryotic host will be useful for the development of hSIRT2 modulators.

I also expanded my knowledge in overproduction of membrane proteins, focusing on hAQP4, the aquaporin homologue dominating in the brain, to facilitate the development of new research applications, as well as the understanding of the intermolecular binding of the protein. I also lay the fundament for future interaction studies between hAQP4 and potential interaction partner by solid-state NMR. A fundamental prerequisite for these applications is a highly pure protein sample, which I produced for various purposes; direct applications in the diagnosis of neurodegenerative diseases such as NMO, development of water filters and isotopic labelling. Manuscripts based on this work are in preparation or submitted.

Working with membrane proteins is challenging, and the main aim in biochemical projects is commonly structural analysis which requires a substantial effort all the way from genetic design to reliable production and systemic work in the crystallization trials. In this thesis, two novel aquaporin structures are described, the cpAPQ1aa and AtPIP2,4. The first structure were valuable to get a deeper understanding of the variable osmoregulation in the fish *A. testudineus*, showing a novel aquaporin regulation mechanism on the extracellular side (**Paper II)**. Based on the structure we derived several mutants to verify, by functional studies, the molecular mechanism, which helps the fish to survive in variable environments.

The method repertoire was also broadened by establishing a novel method for testing the transport functionality of aquaporins regarding hydrogen peroxide, **Paper III** and **IV**. Based on the H_2O_2 correlated readout linked to a fluorescence signal, a larger screening setup was established. Available methods of H_2O_2 transport evaluation are commonly based on cell growth assays, and the correlation between protein amount and transport function is therefore not trivial to evaluate. Hence, the contribution of a protein-based assay will assist further evaluation of specificity for membrane protein targets. Furthermore, by varying the probe system, the application of this assay could be extended to other specificities. The detection of ammonia transport could possibly be measured by the incorporation of substances into the (proteo-) liposomes, which either directly react with ammonia in solution, or indicate a pH change.[412-415]

Finally, a closer look on aquaporin interactions were done in **Paper V**, by evaluating the established AQP0-CaM fluorescence complementation by a high-throughput read-out using flow cytometry. Noteworthy, the detected fluorescence signals itself did not give enough information to discriminate constructive complexes from background, but establishing the fraction of fluorescing cells as a crucial quality strengthened the method substantially. Working with signals in living cells required the standardization of sample preparation before the actual measurements, being an important outcome for the method on the whole. In addition, I recognized a critical requirement of proper design for controls as well as controlling the intrinsic transformation variation of the cells. The quality of a method for PPI evaluation depends on its signal to noise ratio, and the contribution of **Paper V** is a way to increase it by recognizing and neglecting invalid signals. My contribution with this work is thereby providing a fundament for future screening of potential interaction partners to aquaporins or membrane proteins in general. By transferring a cDNA library into the YFP plasmids, used in the thesis work, the interaction partner of any protein of interest can be screened and evaluated based on the same principles as those established for the AQP0-CaM complex. Initial experiments with hAQP4 as a bait, and a brain cDNA library as a target, have been successful in the sense that initial hits have been identified. The benefit of using FACS analysis is not limited to the speed of the procedure as such, but cells showing a fluorescence signal can be isolated, and the target gene, and the protein responsible for the interaction signal, can be identified. In conclusion, my contribution to the method development in the field of membrane protein complex screening and analysis provides fundament for increased understanding of molecular mechanisms of importance for biochemical and medical questions.

6. ACKNOWLEDGEMENTS

Indeed, time is relative! It seems just like yesterday, when I sat on the plane for the last PhD candidate interview in Sweden. It was my final chance to fulfil my dream: Living in Sweden and doing fantastic science. I am blessed, that I had the opportunity to meet and share remarkable (MEGA!) moments with you!

I can say, that everything in life is about chances. You can have talent and passion, but there are these moments, when you just need someone who is believing in you.

Kristina, you believed in me, when I started here and whatever it was, I knew that we can find a solution together. Over the years, your "lagom" diffused into me, and I can clearly say, that I have developed. Not only from a professional perspective, but also as a human being. I think, this is something that makes a good supervisor a great mentor. I know, that I sometimes had my paranoid phases (we get scooped!), but hopefully I could give something back from your trust in me. I really hope, that you reach the goal you deserve!

Richard, my co-supervisor and the only singing professor in the world. I can clearly remember our interview. To be more precise, I can remember, that I heard someone singing in the corridor and suddenly this super happy kiwi is sitting in front of me ☺ I learned two lessons from the years listening to 1970s songs in the corridor (and the wisdom of the singer): There is always a solution, and there is always a smile.

Leif, thank you for being my examiner. You are a great teacher and the first professor I saw in my life, sitting next to his students explaining the chemistry material. I became a better teacher in our joined teaching lessons, thank you!

Team Hedfalk: This thesis was only possible, because I had great colleagues around me, who I can call my friends now. **Jessica**, I am glad, that you came to Gothenburg! Together we ruled "Heidi", and I am thankful to have a friend in my office dark-zone. Make my Swedish dream become true with el Pablo! And sorry, there is any second **Adina**…

Piero and **Lorena**, two reasons why I survived my start phase in the lab. I have learned the fermenter business the hard way from the yeast god (Piero), will never forget your courage. Lorena, you were a friend, when I needed it the most. **Stefan S**., so much fun and progress when you started here. Hope, you have a great real life!! **Hao**, I still feel bad for shocking you at Chalmers, but the obtained data was worth it. **Jiao**, just a short description: you are a diamond in a billion. **Vijay**, there is a great Swedish life in front of you and your family. My former students **Kener**, **Jana** and **Rasmus**: You have all the skills needed to succeed. In every setback, there is the seed for a greater return. Our collaborators around the world: It directly felt like home, when I arrived in Lund. Thank you, **Susanna**, for taking time for doing the experiments.

You are my second beacon for orientation, when I need help with our tetrameric friends. Our Texas connection, **Greg**, **Esther** and the others. I am glad, that science overcomes all (bureaucratic) borders. I am especially thankful for the help of **Ulf** and his team, notably **Rebecca** and **Samuel**. Without you, we would still count fluorescent cells manually! **Simon**, what can I say? Our collaboration was always fruitful, and the meetings were the most efficient scientific gatherings I have ever had. I appreciate your professionality and your attitude in balancing life and business. Greetings to **Jenny**! Team **Göran**, I am looking forward to hear great news about aquaporin NMR science. And thank you, for sending **Tanguy** in our lab. Was a pleasure to work with you, I expect a magnificent career with a magic angle (sorry for NMR related jokes!).
Team Westenhoff: **Elin C.**, there is only one Swedish princess, and she does not live in Stockholm. Even cleaning-day became fun with you. **Leo**, cannot believe, that mainstream parties could be so much fun. I guess, it depends on the right people to party with! Miss both of you! **Matthijs**, I am so glad that you are able to translate biology → informatics. Thanks for handling the annoying python in my computer ;-D We definitely need more metalheads in the lab. Without you, I would still analyse my curves. **Weixiao**, finally even my journey ends. Thank you for listening to my complaints and giving useful advices. **Linnea**, you always had an open ear. I was quite jealous on your fantastic chair, now I can confess. **Petra E.**, don`t mess with THAT roller girl. Keep your power mode! **Joachim**, isn`t it fantastic that I worked alongside a real ultimate (frisbee) champion? **Stephan N.**, soon I will be member of the anonymous swedoholics. You are one of the kindest persons I have ever met. **Ann**, combining the best of all cultures. I am so jealous on your Swedish skills! **Amke**, you are the good soul of the institute, and the reason I have to do sport again. **Andrea**, I thought, I was working like crazy when I started, Haha. Such a thoughtful human being. **Michal**, good luck building up your own legacy. **Manoop**, a man of silence ;-) Since we meet and greet, the day is so much better. **Lidija**, another power woman. I still have the opinion, that your straightforward characteristic is useful on faculty level. **Laras**, I know of your secret piano hobby ☺ Would be nice to listen to it one day! **Jenny and Emil**: I guess it is OK to bold the "and" now! I am very happy for you and glad, that we became friends. Fantastic, that you do the next step together. I am ready now for every relaxing technique! **Oskar**, the golden boy. Hopefully, I am able to stay at least half as cool, as you did, on my defence day. Neutze group: **Petra B.**, the human philosophers stone. Thanks for the best engagement of all times and, yes, it will happen. **Rebecka**, since you have left, half of the fun is lost! How do I learn about new rumours now? **Sarabi**, a man of taste. With whom can I talk an hour about watch faces? I need your style on my party! **Cecilia W.**, what has the lab become without you? You were never too busy to help me, when I started my journey. I tried to be as helpful to others, as you have

been to me. **Rajiv**, we shared everything together. I. mean. everything. I miss our epic table-tennis tournaments. Cannot wait to hear your Stockholm stories. You might notice, that I copy the order of names from Elin`s thesis, since I forgot my name list. **Professor Greger** is a name I would never forget ;-D
I like your taste of quality and your new outlaw look. Still, you are allowed to wear leather elbow patches on your tweed jacket ;-) **Rob B.**, such a British humour. Was already funny while only understanding half of it, Haha. Good luck in Oxford. **Rob D.**, let us be clear about it: I need you on my party! Everything just gets better with you on board. **Giorgia**: I am so happy, that you settle down with your cutie in Sweden. Sir **Per**, such a dry Swedish humour. I am glad, that we have you around. **Swaggie**, good luck with your business, and maybe our ways will cross at the venture centre. **Analia**, we are both cat lovers in our hearts. **Adams**, such a cool guy. You saved my python life, when I needed the last figure. **Lucija**, thought the whole time you are a student, ahhh. Sorry, and welcome on board. Another metalhead! Bränden group: **Cecilia S.**, I had the best party of my life with you, and most likely I am deaf in ten years. But, it was worth it! Thanks for the fantastic times together, always cheering me up. Eurodance **Dunge**, we both do not have to be ashamed for our great music taste. After all, rhythm is a dancer. I would directly go to Ecuadooor with you, think about the way. **Jonathan**, please keep supporting the Indian roll guy. You are a team player, keep on going. **Doris**, you have the fighting spirit. Try, to not end like me (nearly losing parts of your body). **Owens**, OK, where should I start? Always in a good mood, a fantastic style. Officially Flo-approved by wearing his trousers Swedish-like AND looking great at the same time. And even your breakfast is great. Something is going on here… **Elin D.**, I was blessed to share the office with a positive energy source. I promised, to leave the path of darkness behind me. I guess, for the outcome you have to talk to Jessy. I miss our shared time. **Rhawnie**, your positive energy is also missed every day. Katonians: **Majo**, I think, you were the only true biologist in the lab when I started. We experienced the good and bad times of lab life. I will be always there, if you need support! **Maja**, another cat lover! It was time, that you come back. **Viktor**, I know, that bromance is real! So much fun with The Offspring, and near-death experiences in the USA. There will be a after PhD life, and it feels like… **Julia**, I am ready for worm world domination. **Tinna**, I cannot express, how fortunate we are to have you in the lab. Basically, we should clean the floor on our knees (only on the last Friday of the month! Risk Assessment!). Would be amazing to see these mysterious Icelandic ponies ;-D
Team Burmann: The best dungeon master! Keep control of **Ylber**, spending far too much time in middle-earth with laser eyes. **Jens**, welcome to the Boys ;-) **Darius**, I just want to say in public, that I was once able to defeat you in a tabletop game. One day, I will tell it to my grandchildren. **Laura**, I wish you only the best for your new start in France! **Emilie**, I realised, that you are now alone with the guys. They have a good heart! Keep your style.

Ashish, I am so happy that you have a family now. Good luck with your future plans, wherever they will guide you. **Damasus**, keep on rocking the Äkta! Darius will happily repair it, Haha. **Yosh and Lisa**, science is not everything. You got the greatest gift, nature has to offer! The Höög cryo-team: **Katharina**, sorry for leaving the council so fast, had a book to write. You are doing a great job. Annoy the bosses! **Davide**, you are courtesy in perfection. Never heard a single bad word from you. With you as a role model, this planet would be a better place to live. **Jake**, when I look at your muscles, I sometimes believe you carried the cryo-EM inside the building by yourself. You fit so well into the team. **Dimitra**, every time I see photos of you with the baby, I believe you have found the purpose of life.
We have a great **PI** network at Lundberg lab, a constructive environment where we support each other. As a PhD student I am thankful, that we can always ask other group leader for help, which is, from my perspective, one of the reasons for the positive collaboration behaviour.
Bruno, **Lars** and **Valida**: I am not able to recap all the times you bailed me out of misery situations. I guess, I can speak for the whole lab here. Without you, the lab would crash within a day.
My path through life was not really straightforward, but I always had the support from **my parents**. Basically, it is a little miracle, that I am able to write these words. I belong to the 1% of working-class kids attaining a PhD degree, which is ten times more likely to achieve for kids with academical parents. It makes me angry, that the social origin still has so much influence on the future of kids. I am grateful for the chances I got in life from different supporters, but these words belong to my parents, who did not accept my negative educational selection and supported my desire for knowledge. I will not take it for granted, others were not as lucky as me. The reason I write this down, is my request to you to be supportive for other human beings. Education is not a question of origin or privilege, it is a chance everyone should get. Has the right to get.
For 16 years, I have the privilege (a good one) to call a few special souls my second family. I am thankful, to know you on my side **Gisela**, **Katja** and **Amelie**. You supported me in all life situations, and showed me the beauty of art. A passion I share with my love **Anne**, and I thought about writing cheesy words here, which cannot represent my feelings for you anyway. You were one of the pillars for my success, giving me support in all these years. You never questioned my decisions, even if they turned out to be unsuccessful (such as a company called Waterflo), or quite hopeless (studying nano-engineering). You took the risk of a Swedish adventure with me, and we have been richly rewarded with new friendships and perspectives.

I would wish, to have you on my side for many more years to come.

And I promise to find more challenging adventures for us.

7. REFERENCES

[1] Smart, O. S., Neduvelil, J. G., Wang, X., Wallace, B. A., and Sansom, M. S. (1996) HOLE: a program for the analysis of the pore dimensions of ion channel structural models, *J Mol Graph 14*, 354-360, 376.

[2] Koch, A. L., and Silver, S. (2005) The first cell, *Adv Microb Physiol 50*, 227-259.

[3] Schrum, J. P., Zhu, T. F., and Szostak, J. W. (2010) The origins of cellular life, *Cold Spring Harb Perspect Biol 2*, a002212.

[4] Tanford, C. (1980) *The hydrophobic effect: formation of micelles and biological membranes 2d ed*, J. Wiley.

[5] Yang, N. J., and Hinner, M. J. (2015) Getting across the cell membrane: an overview for small molecules, peptides, and proteins, *Methods Mol Biol 1266*, 29-53.

[6] Rosenberg, T. (1948) On accumulation and active transport in biological systems. 1. Thermodynamic considerations, *Acta Chemica Scandinavica 2*, 14-33.

[7] Nicolson, G. L. (2014) The Fluid-Mosaic Model of Membrane Structure: still relevant to understanding the structure, function and dynamics of biological membranes after more than 40 years, *Biochim Biophys Acta 1838*, 1451-1466.

[8] Nicolson, G. L. (2013) Update of the 1972 Singer-Nicolson Fluid-Mosaic Model of Membrane Structure, *Discoveries (Craiova) 1*, e3.

[9] Alberts, B. (2002) *Molecular biology of the cell*, Garland, New York.

[10] Spector, A. A., and Yorek, M. A. (1985) Membrane lipid composition and cellular function, *J Lipid Res 26*, 1015-1035.

[11] Gupta, K., Donlan, J. A. C., Hopper, J. T. S., Uzdavinys, P., Landreh, M., Struwe, W. B., Drew, D., Baldwin, A. J., Stansfeld, P. J., and Robinson, C. V. (2017) The role of interfacial lipids in stabilizing membrane protein oligomers, *Nature 541*, 421-424.

[12] Dawaliby, R., Trubbia, C., Delporte, C., Masureel, M., Van Antwerpen, P., Kobilka, B. K., and Govaerts, C. (2016) Allosteric regulation of G protein-coupled receptor activity by phospholipids, *Nat Chem Biol 12*, 35-39.

[13] Cho, I., Jackson, M. R., and Swift, J. (2016) Roles of Cross-Membrane Transport and Signaling in the Maintenance of Cellular Homeostasis, *Cellular and Molecular Bioengineering 9*, 234-246.

[14] Szymanski, D., and Staiger, C. J. (2018) The Actin Cytoskeleton: Functional Arrays for Cytoplasmic Organization and Cell Shape Control, *Plant Physiol 176*, 106-118.

[15] Zik, J. B., and Roberts, D. L. (2015) The many faces of oxytocin: implications for psychiatry, *Psychiatry Res 226*, 31-37.

[16] Ślesak, I., Ślesak, H., and Kruk, J. (2017) RubisCO Early Oxygenase Activity: A Kinetic and Evolutionary Perspective, *Bioessays 39*.
[17] Pandey, A., Shin, K., Patterson, R. E., Liu, X. Q., and Rainey, J. K. (2016) Current strategies for protein production and purification enabling membrane protein structural biology, *Biochem Cell Biol 94*, 507-527.
[18] Gunner, M. R., Amin, M., Zhu, X., and Lu, J. (2013) Molecular mechanisms for generating transmembrane proton gradients, *Biochim Biophys Acta 1827*, 892-913.
[19] Djokic, T., Van Kranendonk, M. J., Campbell, K. A., Walter, M. R., and Ward, C. R. (2017) Earliest signs of life on land preserved in ca. 3.5 Ga hot spring deposits, *Nat Commun 8*, 15263.
[20] Hacke, U. G., and Laur, J. (2016) Aquaporins: channels for the molecule of life, *eLS*, 1-6.
[21] Sidel, V. W., and Solomon, A. K. (1957) Entrance of water into human red cells under an osmotic pressure gradient, *J Gen Physiol 41*, 243-257.
[22] Paganelli, C. V., and Solomon, A. K. (1957) The rate of exchange of tritiated water across the human red cell membrane, *J Gen Physiol 41*, 259-277.
[23] Macey, R. I., and Farmer, R. E. (1970) Inhibition of water and solute permeability in human red cells, *Biochim Biophys Acta 211*, 104-106.
[24] Preston, G. M., Jung, J. S., Guggino, W. B., and Agre, P. (1993) The mercury-sensitive residue at cysteine 189 in the CHIP28 water channel, *J Biol Chem 268*, 17-20.
[25] Denker, B. M., Smith, B. L., Kuhajda, F. P., and Agre, P. (1988) Identification, purification, and partial characterization of a novel Mr 28,000 integral membrane protein from erythrocytes and renal tubules, *J Biol Chem 263*, 15634-15642.
[26] Zeidel, M. L., Ambudkar, S. V., Smith, B. L., and Agre, P. (1992) Reconstitution of functional water channels in liposomes containing purified red cell CHIP28 protein, *Biochemistry 31*, 7436-7440.
[27] Neumann, S., Fuchs, A., Mulkidjanian, A., and Frishman, D. (2010) Current status of membrane protein structure classification, *Proteins 78*, 1760-1773.
[28] Ishibashi, K., Morishita, Y., and Tanaka, Y. (2017) The Evolutionary Aspects of Aquaporin Family, *Adv Exp Med Biol 969*, 35-50.
[29] Zardoya, R. (2005) Phylogeny and evolution of the major intrinsic protein family, *Biol Cell 97*, 397-414.
[30] Calvanese, L., Pellegrini-Calace, M., and Oliva, R. (2013) In silico study of human aquaporin AQP11 and AQP12 channels, *Protein Sci 22*, 455-466.
[31] Ishibashi, K., Tanaka, Y., and Morishita, Y. (2014) The role of mammalian superaquaporins inside the cell, *Biochim Biophys Acta 1840*, 1507-1512.

[32] Murata, K., Mitsuoka, K., Hirai, T., Walz, T., Agre, P., Heymann, J. B., Engel, A., and Fujiyoshi, Y. (2000) Structural determinants of water permeation through aquaporin-1, *Nature 407*, 599-605.
[33] Jung, J. S., Preston, G. M., Smith, B. L., Guggino, W. B., and Agre, P. (1994) Molecular structure of the water channel through aquaporin CHIP. The hourglass model, *J Biol Chem 269*, 14648-14654.
[34] Mathai, J. C., and Agre, P. (1999) Hourglass pore-forming domains restrict aquaporin-1 tetramer assembly, *Biochemistry 38*, 923-928.
[35] Borgnia, M., Nielsen, S., Engel, A., and Agre, P. (1999) Cellular and molecular biology of the aquaporin water channels, *Annu Rev Biochem 68*, 425-458.
[36] Nielsen, S., Marples, D., Frokiaer, J., Knepper, M., and Agre, P. (1996) The aquaporin family of water channels in kidney: an update on physiology and pathophysiology of aquaporin-2, *Kidney Int 49*, 1718-1723.
[37] Alishahi, M., and Kamali, R. (2019) A novel molecular dynamics study of CO2 permeation through aquaporin-5, *Eur Phys J E Soft Matter 42*, 151.
[38] Kaldenhoff, R., Kai, L., and Uehlein, N. (2014) Aquaporins and membrane diffusion of CO2 in living organisms, *Biochim Biophys Acta 1840*, 1592-1595.
[39] Kruse, E., Uehlein, N., and Kaldenhoff, R. (2006) The aquaporins, *Genome Biol 7*, 206.
[40] Yool, A. J., and Campbell, E. M. (2012) Structure, function and translational relevance of aquaporin dual water and ion channels, *Mol Aspects Med 33*, 553-561.
[41] Sutka, M., Amodeo, G., and Ozu, M. (2017) Plant and animal aquaporins crosstalk: what can be revealed from distinct perspectives, *Biophys Rev 9*, 545-562.
[42] Kitchen, P., Salman, M. M., Pickel, S. U., Jennings, J., Tornroth-Horsefield, S., Conner, M. T., Bill, R. M., and Conner, A. C. (2019) Water channel pore size determines exclusion properties but not solute selectivity, *Sci Rep 9*, 20369.
[43] Gomes, D., Agasse, A., Thiebaud, P., Delrot, S., Geros, H., and Chaumont, F. (2009) Aquaporins are multifunctional water and solute transporters highly divergent in living organisms, *Biochim Biophys Acta 1788*, 1213-1228.
[44] Kreida, S., and Tornroth-Horsefield, S. (2015) Structural insights into aquaporin selectivity and regulation, *Curr Opin Struct Biol 33*, 126-134.
[45] Jensen, M. O., Tajkhorshid, E., and Schulten, K. (2003) Electrostatic tuning of permeation and selectivity in aquaporin water channels, *Biophys J 85*, 2884-2899.

[46] Fu, D., Libson, A., Miercke, L. J., Weitzman, C., Nollert, P., Krucinski, J., and Stroud, R. M. (2000) Structure of a glycerol-conducting channel and the basis for its selectivity, *Science 290*, 481-486.
[47] Hub, J. S., and de Groot, B. L. (2008) Mechanism of selectivity in aquaporins and aquaglyceroporins, *Proc Natl Acad Sci U S A 105*, 1198-1203.
[48] Law, R. J., and Sansom, M. S. (2002) Water transporters: how so fast yet so selective?, *Curr Biol 12*, R250-252.
[49] Kozono, D., Yasui, M., King, L. S., and Agre, P. (2002) Aquaporin water channels: atomic structure molecular dynamics meet clinical medicine, *J Clin Invest 109*, 1395-1399.
[50] Kapilan, R., Vaziri, M., and Zwiazek, J. J. (2018) Regulation of aquaporins in plants under stress, *Biol Res 51*, 4.
[51] Hsu, Y., Tran, M., and Linninger, A. A. (2015) Dynamic regulation of aquaporin-4 water channels in neurological disorders, *Croatian medical journal 56*, 401.
[52] Hedfalk, K., Tornroth-Horsefield, S., Nyblom, M., Johanson, U., Kjellbom, P., and Neutze, R. (2006) Aquaporin gating, *Curr Opin Struct Biol 16*, 447-456.
[53] Luu, D. T., and Maurel, C. (2013) Aquaporin trafficking in plant cells: an emerging membrane-protein model, *Traffic 14*, 629-635.
[54] Adnan, M., Islam, W., Zhang, J., Zheng, W., and Lu, G. D. (2019) Diverse Role of SNARE Protein Sec22 in Vesicle Trafficking, Membrane Fusion, and Autophagy, *Cells 8*.
[55] Daniotti, J. L., Pedro, M. P., and Valdez Taubas, J. (2017) The role of S-acylation in protein trafficking, *Traffic 18*, 699-710.
[56] Rice, W. L., Li, W., Mamuya, F., McKee, M., Paunescu, T. G., and Lu, H. A. (2015) Polarized Trafficking of AQP2 Revealed in Three Dimensional Epithelial Culture, *PLoS One 10*, e0131719.
[57] Wang, X., Huang, T., Bu, G., and Xu, H. (2014) Dysregulation of protein trafficking in neurodegeneration, *Mol Neurodegener 9*, 31.
[58] Frick, A., Eriksson, U. K., de Mattia, F., Oberg, F., Hedfalk, K., Neutze, R., de Grip, W. J., Deen, P. M., and Tornroth-Horsefield, S. (2014) X-ray structure of human aquaporin 2 and its implications for nephrogenic diabetes insipidus and trafficking, *Proc Natl Acad Sci U S A 111*, 6305-6310.
[59] Maurel, C., Boursiac, Y., Luu, D. T., Santoni, V., Shahzad, Z., and Verdoucq, L. (2015) Aquaporins in Plants, *Physiol Rev 95*, 1321-1358.
[60] Sachdeva, R., and Singh, B. (2014) Insights into structural mechanisms of gating induced regulation of aquaporins, *Prog Biophys Mol Biol 114*, 69-79.
[61] Nesverova, V., and Tornroth-Horsefield, S. (2019) Phosphorylation-Dependent Regulation of Mammalian Aquaporins, *Cells 8*.
[62] Frick, A., Jarva, M., Ekvall, M., Uzdavinys, P., Nyblom, M., and Tornroth-Horsefield, S. (2013) Mercury increases water permeability

of a plant aquaporin through a non-cysteine-related mechanism, *Biochem J 454*, 491-499.
[63] Kreida, S., Roche, J. V., Olsson, C., Linse, S., and Tornroth-Horsefield, S. (2018) Protein-protein interactions in AQP regulation - biophysical characterization of AQP0-CaM and AQP2-LIP5 complex formation, *Faraday Discuss 209*, 35-54.
[64] Fields, J. B., Nemeth-Cahalan, K. L., Freites, J. A., Vorontsova, I., Hall, J. E., and Tobias, D. J. (2017) Calmodulin Gates Aquaporin 0 Permeability through a Positively Charged Cytoplasmic Loop, *J Biol Chem 292*, 185-195.
[65] Reichow, S. L., Clemens, D. M., Freites, J. A., Nemeth-Cahalan, K. L., Heyden, M., Tobias, D. J., Hall, J. E., and Gonen, T. (2013) Allosteric mechanism of water-channel gating by Ca2+-calmodulin, *Nat Struct Mol Biol 20*, 1085-1092.
[66] Assentoft, M., Larsen, B. R., and MacAulay, N. (2015) Regulation and Function of AQP4 in the Central Nervous System, *Neurochem Res 40*, 2615-2627.
[67] de Almeida, A., Martins, A. P., Mosca, A. F., Wijma, H. J., Prista, C., Soveral, G., and Casini, A. (2016) Exploring the gating mechanisms of aquaporin-3: new clues for the design of inhibitors?, *Mol Biosyst 12*, 1564-1573.
[68] Rodrigues, C., Mosca, A. F., Martins, A. P., Nobre, T., Prista, C., Antunes, F., Cipak Gasparovic, A., and Soveral, G. (2016) Rat Aquaporin-5 Is pH-Gated Induced by Phosphorylation and Is Implicated in Oxidative Stress, *Int J Mol Sci 17*.
[69] Janosi, L., and Ceccarelli, M. (2013) The gating mechanism of the human aquaporin 5 revealed by molecular dynamics simulations, *PLoS One 8*, e59897.
[70] Gotfryd, K., Mosca, A. F., Missel, J. W., Truelsen, S. F., Wang, K., Spulber, M., Krabbe, S., Helix-Nielsen, C., Laforenza, U., Soveral, G., Pedersen, P. A., and Gourdon, P. (2018) Human adipose glycerol flux is regulated by a pH gate in AQP10, *Nat Commun 9*, 4749.
[71] Kourghi, M., De Ieso, M. L., Nourmohammadi, S., Pei, J. V., and Yool, A. J. (2018) Identification of Loop D Domain Amino Acids in the Human Aquaporin-1 Channel Involved in Activation of the Ionic Conductance and Inhibition by AqB011, *Front Chem 6*, 142.
[72] Ozu, M., Dorr, R. A., Gutierrez, F., Politi, M. T., and Toriano, R. (2013) Human AQP1 is a constitutively open channel that closes by a membrane-tension-mediated mechanism, *Biophys J 104*, 85-95.
[73] Kuzmanov, U., and Emili, A. (2013) Protein-protein interaction networks: probing disease mechanisms using model systems, *Genome Medicine 5*, 37.
[74] Sin, O., and Nollen, E. A. A. (2015) Regulation of protein homeostasis in neurodegenerative diseases: the role of coding and non-coding genes, *Cellular and Molecular Life Sciences 72*, 4027-4047.

[75] Roche, J. V., and Tornroth-Horsefield, S. (2017) Aquaporin Protein-Protein Interactions, *Int J Mol Sci 18*.
[76] Abir-Awan, M., Kitchen, P., Salman, M. M., Conner, M. T., Conner, A. C., and Bill, R. M. (2019) Inhibitors of Mammalian Aquaporin Water Channels, *Int J Mol Sci 20*.
[77] Tradtrantip, L., Jin, B. J., Yao, X., Anderson, M. O., and Verkman, A. S. (2017) Aquaporin-Targeted Therapeutics: State-of-the-Field, *Adv Exp Med Biol 969*, 239-250.
[78] Day, R. E., Kitchen, P., Owen, D. S., Bland, C., Marshall, L., Conner, A. C., Bill, R. M., and Conner, M. T. (2014) Human aquaporins: regulators of transcellular water flow, *Biochim Biophys Acta 1840*, 1492-1506.
[79] Harvengt, P., Vlerick, A., Fuks, B., Wattiez, R., Ruysschaert, J. M., and Homble, F. (2000) Lentil seed aquaporins form a hetero-oligomer which is phosphorylated by a Mg(2+)-dependent and Ca(2+)-regulated kinase, *Biochem J 352 Pt 1*, 183-190.
[80] Yaneff, A., Vitali, V., and Amodeo, G. (2015) PIP1 aquaporins: Intrinsic water channels or PIP2 aquaporin modulators?, *FEBS Lett 589*, 3508-3515.
[81] Yaneff, A., Sigaut, L., Marquez, M., Alleva, K., Pietrasanta, L. I., and Amodeo, G. (2014) Heteromerization of PIP aquaporins affects their intrinsic permeability, *Proc Natl Acad Sci U S A 111*, 231-236.
[82] Engel, A., Fujiyoshi, Y., Gonen, T., and Walz, T. (2008) Junction-forming aquaporins, *Curr Opin Struct Biol 18*, 229-235.
[83] Ozu, M., Galizia, L., Acuna, C., and Amodeo, G. (2018) Aquaporins: More Than Functional Monomers in a Tetrameric Arrangement, *Cells 7*.
[84] Li, C., and Wang, W. (2017) Molecular Biology of Aquaporins, *Adv Exp Med Biol 969*, 1-34.
[85] Li, S., Li, C., and Wang, W. (2020) Molecular aspects of aquaporins, *Vitam Horm 113*, 129-181.
[86] Sjohamn, J., and Hedfalk, K. (2014) Unraveling aquaporin interaction partners, *Biochim Biophys Acta 1840*, 1614-1623.
[87] Roche, J. V., and Törnroth-Horsefield, S. (2017) Aquaporin Protein-Protein Interactions, *Int J Mol Sci 18*.
[88] Mendes, K. L., Lelis, D. F., and Santos, S. H. S. (2017) Nuclear sirtuins and inflammatory signaling pathways, *Cytokine Growth Factor Rev 38*, 98-105.
[89] Yuan, F., Xu, Z. M., Lu, L. Y., Nie, H., Ding, J., Ying, W. H., and Tian, H. L. (2016) SIRT2 inhibition exacerbates neuroinflammation and blood-brain barrier disruption in experimental traumatic brain injury by enhancing NF-kappaB p65 acetylation and activation, *J Neurochem 136*, 581-593.
[90] Lin, Q., Geng, Y., Lin, S., and Tian, Z. (2016) Sirtuin1 (SIRT1) Regulates Tumor Necrosis Factor-alpha (TNF-alpha-Induced) Aquaporin-2

(AQP2) Expression in Renal Medullary Collecting Duct Cells Through Inhibiting the NF-kappaB Pathway, *Med Sci Monit Basic Res 22*, 165-174.

[91] Yang, S. Y., Lin, S. L., Chen, Y. M., Wu, V. C., Yang, W. S., and Wu, K. D. (2016) A low-salt diet increases the expression of renal sirtuin 1 through activation of the ghrelin receptor in rats, *Sci Rep 6*, 32787.

[92] Wu, Z., Uchi, H., Morino-Koga, S., Shi, W., and Furue, M. (2014) Resveratrol inhibition of human keratinocyte proliferation via SIRT1/ARNT/ERK dependent downregulation of aquaporin 3, *J Dermatol Sci 75*, 16-23.

[93] (2019) Sirtuins as Drug Targets, In *Epigenetic Drug Discovery*, pp 185-200.

[94] Zwergel, C., Rotili, D., Valente, S., and Mai, A. (2019) Sirtuins as Drug Targets, *Epigenetic Drug Discovery*, 185-200.

[95] Dai, H., Sinclair, D. A., Ellis, J. L., and Steegborn, C. (2018) Sirtuin activators and inhibitors: Promises, achievements, and challenges, *Pharmacol Ther 188*, 140-154.

[96] Wang, Y., Yang, J., Hong, T., Chen, X., and Cui, L. (2019) SIRT2: Controversy and multiple roles in disease and physiology, *Ageing Res Rev 55*, 100961.

[97] Wang, T., Xu, Z., Lu, Y., Shi, J., Liu, W., Zhang, C., Jiang, Z., Qi, B., and Bai, L. (2019) Recent Progress on the Discovery of Sirt2 Inhibitors for the Treatment of Various Cancers, *Curr Top Med Chem 19*, 1051-1058.

[98] Chen, G., Huang, P., and Hu, C. (2020) The role of SIRT2 in cancer: A novel therapeutic target, *Int J Cancer*.

[99] Zhang, Y., Anoopkumar-Dukie, S., Arora, D., and Davey, A. K. (2020) Review of the anti-inflammatory effect of SIRT1 and SIRT2 modulators on neurodegenerative diseases, *Eur J Pharmacol 867*, 172847.

[100] Jing, H., Hu, J., He, B., Negron Abril, Y. L., Stupinski, J., Weiser, K., Carbonaro, M., Chiang, Y. L., Southard, T., Giannakakou, P., Weiss, R. S., and Lin, H. (2016) A SIRT2-Selective Inhibitor Promotes c-Myc Oncoprotein Degradation and Exhibits Broad Anticancer Activity, *Cancer Cell 29*, 767-768.

[101] Bohm, J. (1893) Capillaritat und Saftsteigen, *Ber. Dtsch. Bot. Ges. 11*, 203-212.

[102] Bentrup, F. W. (2017) Water ascent in trees and lianas: the cohesion-tension theory revisited in the wake of Otto Renner, *Protoplasma 254*, 627-633.

[103] Zimmermann, U., Schneider, H., Wegner, L. H., Wagner, H. J., Szimtenings, M., Haase, A., and Bentrup, F. W. (2002) What are the driving forces for water lifting in the xylem conduit?, *Physiol Plant 114*, 327-335.

[104] Steudle, E. (2001) The Cohesion-Tension Mechanism and the Acquisition of Water by Plant Roots, *Annu Rev Plant Physiol Plant Mol Biol 52*, 847-875.
[105] Thoday, D. (1918) On turgescence and the absorption of water by the cells of plants, *New Phytologist 17*, 108-113.
[106] Prado, K., Cotelle, V., Li, G., Bellati, J., Tang, N., Tournaire-Roux, C., Martiniere, A., Santoni, V., and Maurel, C. (2019) Oscillating Aquaporin Phosphorylation and 14-3-3 Proteins Mediate the Circadian Regulation of Leaf Hydraulics, *Plant Cell 31*, 417-429.
[107] Maurel, C., Verdoucq, L., and Rodrigues, O. (2016) Aquaporins and plant transpiration, *Plant Cell Environ 39*, 2580-2587.
[108] Scharwies, J. D., and Dinneny, J. R. (2019) Water transport, perception, and response in plants, *J Plant Res 132*, 311-324.
[109] Vandeleur, R. K., Sullivan, W., Athman, A., Jordans, C., Gilliham, M., Kaiser, B. N., and Tyerman, S. D. (2014) Rapid shoot-to-root signalling regulates root hydraulic conductance via aquaporins, *Plant Cell Environ 37*, 520-538.
[110] Abascal, F., Irisarri, I., and Zardoya, R. (2014) Diversity and evolution of membrane intrinsic proteins, *Biochim Biophys Acta 1840*, 1468-1481.
[111] Wang, L., Liu, Y., Feng, S., Yang, J., Li, D., and Zhang, J. (2017) Roles of Plasmalemma Aquaporin Gene StPIP1 in Enhancing Drought Tolerance in Potato, *Front Plant Sci 8*, 616.
[112] Singh, R. K., Deshmukh, R., Muthamilarasan, M., Rani, R., and Prasad, M. (2020) Versatile roles of aquaporin in physiological processes and stress tolerance in plants, *Plant Physiol Biochem 149*, 178-189.
[113] Tian, S., Wang, X., Li, P., Wang, H., Ji, H., Xie, J., Qiu, Q., Shen, D., and Dong, H. (2016) Plant Aquaporin AtPIP1;4 Links Apoplastic H2O2 Induction to Disease Immunity Pathways, *Plant Physiol 171*, 1635-1650.
[114] Rodrigues, O., Reshetnyak, G., Grondin, A., Saijo, Y., Leonhardt, N., Maurel, C., and Verdoucq, L. (2017) Aquaporins facilitate hydrogen peroxide entry into guard cells to mediate ABA- and pathogen-triggered stomatal closure, *Proc Natl Acad Sci U S A 114*, 9200-9205.
[115] Jang, J. Y., Rhee, J. Y., Chung, G. C., and Kang, H. (2012) Aquaporin as a membrane transporter of hydrogen peroxide in plant response to stresses, *Plant Signal Behav 7*, 1180-1181.
[116] Watanabe, S., Moniaga, C. S., Nielsen, S., and Hara-Chikuma, M. (2016) Aquaporin-9 facilitates membrane transport of hydrogen peroxide in mammalian cells, *Biochemical and biophysical research communications 471*, 191-197.
[117] Laforenza, U., Pellavio, G., Marchetti, A. L., Omes, C., Todaro, F., and Gastaldi, G. (2017) Aquaporin-mediated water and hydrogen peroxide transport is involved in normal human spermatozoa functioning, *International Journal of Molecular Sciences 18*, 66.

[118] Hooijmaijers, C., Rhee, J. Y., Kwak, K. J., Chung, G. C., Horie, T., Katsuhara, M., and Kang, H. (2012) Hydrogen peroxide permeability of plasma membrane aquaporins of Arabidopsis thaliana, *Journal of Plant Research 125*, 147-153.
[119] Michalek, K. (2016) Aquaglyceroporins in the kidney: present state of knowledge and prospects, *J Physiol Pharmacol 67*, 185-193.
[120] Mendez-Gimenez, L., Rodriguez, A., Balaguer, I., and Fruhbeck, G. (2014) Role of aquaglyceroporins and caveolins in energy and metabolic homeostasis, *Mol Cell Endocrinol 397*, 78-92.
[121] Mendez-Gimenez, L., Ezquerro, S., da Silva, I. V., Soveral, G., Fruhbeck, G., and Rodriguez, A. (2018) Pancreatic Aquaporin-7: A Novel Target for Anti-diabetic Drugs?, *Front Chem 6*, 99.
[122] Hirako, S., Wakayama, Y., Kim, H., Iizuka, Y., Matsumoto, A., Wada, N., Kimura, A., Okabe, M., Sakagami, J., Suzuki, M., Takenoya, F., and Shioda, S. (2016) The relationship between aquaglyceroporin expression and development of fatty liver in diet-induced obesity and ob/ob mice, *Obes Res Clin Pract 10*, 710-718.
[123] Hara-Chikuma, M., and Verkman, A. S. (2008) Prevention of skin tumorigenesis and impairment of epidermal cell proliferation by targeted aquaporin-3 gene disruption, *Mol Cell Biol 28*, 326-332.
[124] Rutzler, M., Rojek, A., Damgaard, M. V., Andreasen, A., Fenton, R. A., and Nielsen, S. (2017) Temporal deletion of Aqp11 in mice is linked to the severity of cyst-like disease, *Am J Physiol Renal Physiol 312*, F343-F351.
[125] da Silva, I. V., Cardoso, C., Mendez-Gimenez, L., Camoes, S. P., Fruhbeck, G., Rodriguez, A., Miranda, J. P., and Soveral, G. (2020) Aquaporin-7 and aquaporin-12 modulate the inflammatory phenotype of endocrine pancreatic beta-cells, *Arch Biochem Biophys 691*, 108481.
[126] Vandebroek, A., and Yasui, M. (2020) Regulation of AQP4 in the Central Nervous System, *Int J Mol Sci 21*.
[127] Pirici, I., Balsanu, T. A., Bogdan, C., Margaritescu, C., Divan, T., Vitalie, V., Mogoanta, L., Pirici, D., Carare, R. O., and Muresanu, D. F. (2017) Inhibition of Aquaporin-4 Improves the Outcome of Ischaemic Stroke and Modulates Brain Paravascular Drainage Pathways, *Int J Mol Sci 19*.
[128] Selmaj, K., and Selmaj, I. (2019) Novel emerging treatments for NMOSD, *Neurol Neurochir Pol 53*, 317-326.
[129] Alam, J., Koh, J. H., Kim, N., Kwok, S. K., Park, S. H., Song, Y. W., Park, K., and Choi, Y. (2016) Detection of autoantibodies against aquaporin-5 in the sera of patients with primary Sjogren's syndrome, *Immunol Res 64*, 848-856.
[130] Amiry-Moghaddam, M. (2019) AQP4 and the Fate of Gliomas, *Cancer Res 79*, 2810-2811.

[131] Yang, C., Huang, X., Huang, X., Mai, H., Li, J., Jiang, T., Wang, X., and Lu, T. (2016) Aquaporin-4 and Alzheimer's Disease, *J Alzheimers Dis 52*, 391-402.
[132] Itoh, T., Rai, T., Kuwahara, M., Ko, S. B., Uchida, S., Sasaki, S., and Ishibashi, K. (2005) Identification of a novel aquaporin, AQP12, expressed in pancreatic acinar cells, *Biochem Biophys Res Commun 330*, 832-838.
[133] Finn, R. N., and Cerda, J. (2015) Evolution and functional diversity of aquaporins, *Biol Bull 229*, 6-23.
[134] Varadaraj, K., Kumari, S. S., Patil, R., Wax, M. B., and Mathias, R. T. (2008) Functional characterization of a human aquaporin 0 mutation that leads to a congenital dominant lens cataract, *Exp Eye Res 87*, 9-21.
[135] Verkman, A. S. (2012) Aquaporins in clinical medicine, *Annu Rev Med 63*, 303-316.
[136] Meli, R., Pirozzi, C., and Pelagalli, A. (2018) New Perspectives on the Potential Role of Aquaporins (AQPs) in the Physiology of Inflammation, *Front Physiol 9*, 101.
[137] Noda, Y. (2014) Dynamic regulation and dysregulation of the water channel aquaporin-2: a common cause of and promising therapeutic target for water balance disorders, *Clin Exp Nephrol 18*, 558-570.
[138] Li, Z., Li, B., Zhang, L., Chen, L., Sun, G., Zhang, Q., Wang, J., Zhi, X., Wang, L., Xu, Z., and Xu, H. (2016) The proliferation impairment induced by AQP3 deficiency is the result of glycerol uptake and metabolism inhibition in gastric cancer cells, *Tumour Biol 37*, 9169-9179.
[139] Hara-Chikuma, M., and Verkman, A. S. (2008) Roles of aquaporin-3 in the epidermis, *J Invest Dermatol 128*, 2145-2151.
[140] Maeda, N., Funahashi, T., and Shimomura, I. (2013) Cardiovascular-metabolic impact of adiponectin and aquaporin, *Endocr J 60*, 251-259.
[141] Prudente, S., Flex, E., Morini, E., Turchi, F., Capponi, D., De Cosmo, S., Tassi, V., Guida, V., Avogaro, A., Folli, F., Maiani, F., Frittitta, L., Dallapiccola, B., and Trischitta, V. (2007) A functional variant of the adipocyte glycerol channel aquaporin 7 gene is associated with obesity and related metabolic abnormalities, *Diabetes 56*, 1468-1474.
[142] Iena, F. M., and Lebeck, J. (2018) Implications of Aquaglyceroporin 7 in Energy Metabolism, *Int J Mol Sci 19*.
[143] Chao, G., and Zhang, S. (2017) Aquaporins 1, 3 and 8 expression in irritable bowel syndrome rats' colon via NF-kappaB pathway, *Oncotarget 8*, 47175-47183.
[144] Xiong, Z., Li, B., Wang, L., Zeng, X., Li, B., Sha, X., and Liu, H. (2019) AQP8 and AQP9 expression in patients with polycystic ovary syndrome and its association with in vitro fertilization-embryo transfer outcomes, *Exp Ther Med 18*, 755-760.

[145] Bertolotti, M., Farinelli, G., Galli, M., Aiuti, A., and Sitia, R. (2016) AQP8 transports NOX2-generated H2O2 across the plasma membrane to promote signaling in B cells, *J Leukoc Biol 100*, 1071-1079.
[146] Rodriguez, A., Gena, P., Mendez-Gimenez, L., Rosito, A., Valenti, V., Rotellar, F., Sola, I., Moncada, R., Silva, C., Svelto, M., Salvador, J., Calamita, G., and Fruhbeck, G. (2014) Reduced hepatic aquaporin-9 and glycerol permeability are related to insulin resistance in non-alcoholic fatty liver disease, *Int J Obes (Lond) 38*, 1213-1220.
[147] Liu, J. Y., Chen, X. X., Chen, H. Y., Shi, J., Leung, G. P., Tang, S. C., Lao, L. X., Yip, H. K., Lee, K. F., Sze, S. C., Zhang, Z. J., and Zhang, K. Y. (2018) Downregulation of Aquaporin 9 Exacerbates Beta-amyloid-induced Neurotoxicity in Alzheimer's Disease Models In vitro and In vivo, *Neuroscience 394*, 72-82.
[148] Verkman, A. S., Anderson, M. O., and Papadopoulos, M. C. (2014) Aquaporins: important but elusive drug targets, *Nat Rev Drug Discov 13*, 259-277.
[149] Soler, D. C., Bai, X., Ortega, L., Pethukova, T., Nedorost, S. T., Popkin, D. L., Cooper, K. D., and McCormick, T. S. (2015) The key role of aquaporin 3 and aquaporin 10 in the pathogenesis of pompholyx, *Med Hypotheses 84*, 498-503.
[150] Soler, D. C., Young, A. E., Griffith, A. D., Fu, P. F., Cooper, K. D., McCormick, T. S., and Popkin, D. L. (2017) Overexpression of AQP3 and AQP10 in the skin exacerbates psoriasiform acanthosis, *Exp Dermatol 26*, 949-951.
[151] Morishita, Y., Matsuzaki, T., Hara-chikuma, M., Andoo, A., Shimono, M., Matsuki, A., Kobayashi, K., Ikeda, M., Yamamoto, T., Verkman, A., Kusano, E., Ookawara, S., Takata, K., Sasaki, S., and Ishibashi, K. (2005) Disruption of aquaporin-11 produces polycystic kidneys following vacuolization of the proximal tubule, *Mol Cell Biol 25*, 7770-7779.
[152] Tait, M. J., Saadoun, S., Bell, B. A., and Papadopoulos, M. C. (2008) Water movements in the brain: role of aquaporins, *Trends Neurosci 31*, 37-43.
[153] Amiry-Moghaddam, M., and Ottersen, O. P. (2003) The molecular basis of water transport in the brain, *Nat Rev Neurosci 4*, 991-1001.
[154] Rash, J. E., Yasumura, T., Hudson, C. S., Agre, P., and Nielsen, S. (1998) Direct immunogold labeling of aquaporin-4 in square arrays of astrocyte and ependymocyte plasma membranes in rat brain and spinal cord, *Proc Natl Acad Sci U S A 95*, 11981-11986.
[155] Smith, A. J., Jin, B. J., Ratelade, J., and Verkman, A. S. (2014) Aggregation state determines the localization and function of M1- and M23-aquaporin-4 in astrocytes, *J Cell Biol 204*, 559-573.
[156] Pisani, F., Sparaneo, A., Tortorella, C., Ruggieri, M., Trojano, M., Mola, M. G., Nicchia, G. P., Frigeri, A., and Svelto, M. (2013) Aquaporin-4

autoantibodies in Neuromyelitis Optica: AQP4 isoform-dependent sensitivity and specificity, *PLoS One 8*, e79185.
[157] Verkman, A. S., Rossi, A., and Crane, J. M. (2012) Live-cell imaging of aquaporin-4 supramolecular assembly and diffusion, *Methods Enzymol 504*, 341-354.
[158] Van Hoek, A. N., Bouley, R., Lu, Y., Silberstein, C., Brown, D., Wax, M. B., and Patil, R. V. (2009) Vasopressin-induced differential stimulation of AQP4 splice variants regulates the in-membrane assembly of orthogonal arrays, *Am J Physiol Renal Physiol 296*, F1396-1404.
[159] Furman, C. S., Gorelick-Feldman, D. A., Davidson, K. G., Yasumura, T., Neely, J. D., Agre, P., and Rash, J. E. (2003) Aquaporin-4 square array assembly: opposing actions of M1 and M23 isoforms, *Proc Natl Acad Sci U S A 100*, 13609-13614.
[160] Nicchia, G. P., Mastrototaro, M., Rossi, A., Pisani, F., Tortorella, C., Ruggieri, M., Lia, A., Trojano, M., Frigeri, A., and Svelto, M. (2009) Aquaporin-4 orthogonal arrays of particles are the target for neuromyelitis optica autoantibodies, *Glia 57*, 1363-1373.
[161] Palazzo, C., Buccoliero, C., Mola, M. G., Abbrescia, P., Nicchia, G. P., Trojano, M., and Frigeri, A. (2019) AQP4ex is crucial for the anchoring of AQP4 at the astrocyte end-feet and for neuromyelitis optica antibody binding, *Acta Neuropathol Commun 7*, 51.
[162] Palazzo, C., Abbrescia, P., Valente, O., Nicchia, G. P., Banitalebi, S., Amiry-Moghaddam, M., Trojano, M., and Frigeri, A. (2020) Tissue Distribution of the Readthrough Isoform of AQP4 Reveals a Dual Role of AQP4ex Limited to CNS, *Int J Mol Sci 21*.
[163] Mader, S., and Brimberg, L. (2019) Aquaporin-4 Water Channel in the Brain and Its Implication for Health and Disease, *Cells 8*.
[164] Assefa, B. T., Gebre, A. K., and Altaye, B. M. (2018) Reactive Astrocytes as Drug Target in Alzheimer's Disease, *Biomed Res Int 2018*, 4160247.
[165] Verkman, A. S., Smith, A. J., Phuan, P. W., Tradtrantip, L., and Anderson, M. O. (2017) The aquaporin-4 water channel as a potential drug target in neurological disorders, *Expert Opin Ther Targets 21*, 1161-1170.
[166] Filippidis, A. S., Carozza, R. B., and Rekate, H. L. (2016) Aquaporins in Brain Edema and Neuropathological Conditions, *Int J Mol Sci 18*.
[167] Lana-Peixoto, M. A., and Talim, N. (2019) Neuromyelitis Optica Spectrum Disorder and Anti-MOG Syndromes, *Biomedicines 7*.
[168] Patterson, S. L., and Goglin, S. E. (2017) Neuromyelitis Optica, *Rheum Dis Clin North Am 43*, 579-591.
[169] Hinson, S. R., Lennon, V. A., and Pittock, S. J. (2016) Autoimmune AQP4 channelopathies and neuromyelitis optica spectrum disorders, *Handb Clin Neurol 133*, 377-403.

[170] Funato, K., Hayashi, T., Echizen, K., Negishi, L., Shimizu, N., Koyama-Nasu, R., Nasu-Nishimura, Y., Morishita, Y., Tabar, V., Todo, T., Ino, Y., Mukasa, A., Saito, N., and Akiyama, T. (2018) SIRT2-mediated inactivation of p73 is required for glioblastoma tumorigenicity, *EMBO Rep 19*.

[171] Hubbard, J. A., Szu, J. I., and Binder, D. K. (2018) The role of aquaporin-4 in synaptic plasticity, memory and disease, *Brain Res Bull 136*, 118-129.

[172] Ikeshima-Kataoka, H. (2016) Neuroimmunological Implications of AQP4 in Astrocytes, *Int J Mol Sci 17*.

[173] Stokum, J. A., Kwon, M. S., Woo, S. K., Tsymbalyuk, O., Vennekens, R., Gerzanich, V., and Simard, J. M. (2018) SUR1-TRPM4 and AQP4 form a heteromultimeric complex that amplifies ion/water osmotic coupling and drives astrocyte swelling, *Glia 66*, 108-125.

[174] Neely, J. D., Amiry-Moghaddam, M., Ottersen, O. P., Froehner, S. C., Agre, P., and Adams, M. E. (2001) Syntrophin-dependent expression and localization of Aquaporin-4 water channel protein, *Proc Natl Acad Sci U S A 98*, 14108-14113.

[175] Jesus, T. T., Bernardino, R. L., Martins, A. D., Sa, R., Sousa, M., Alves, M. G., and Oliveira, P. F. (2014) Aquaporin-4 as a molecular partner of cystic fibrosis transmembrane conductance regulator in rat Sertoli cells, *Biochem Biophys Res Commun 446*, 1017-1021.

[176] Glas, E. (1999) The Evolution of a Scientific Concept, *Journal for General Philosophy of Science / Zeitschrift für allgemeine Wissenschaftstheorie 30*, 37-58.

[177] Institute of Medicine (U.S.). Committee on Military Nutrition Research. (1999) *The role of protein and amino acids in sustaining and enhancing performance*, National Academy Press, Washington, DC.

[178] Hedin, S. G. (1906) Trypsin and Antitrypsin, *Biochem J 1*, 474-483.

[179] Szent-Gyorgyi, A. G. (2004) The early history of the biochemistry of muscle contraction, *J Gen Physiol 123*, 631-641.

[180] Braun, P., and Gingras, A. C. (2012) History of protein-protein interactions: from egg-white to complex networks, *Proteomics 12*, 1478-1498.

[181] Piutti, A. (1886) Ein neues Asparagin, *Berichte der deutschen chemischen Gesellschaft 19*, 1691-1695.

[182] Gopal, G. J., and Kumar, A. (2013) Strategies for the production of recombinant protein in Escherichia coli, *Protein J 32*, 419-425.

[183] Snijder, H. J., and Hakulinen, J. (2016) Membrane Protein Production in E. coli for Applications in Drug Discovery, *Adv Exp Med Biol 896*, 59-77.

[184] Kuipers, G., Peschke, M., Ismail, N. B., Hjelm, A., Schlegel, S., Vikstrom, D., Luirink, J., and de Gier, J. W. (2017) Optimizing E. coli-Based Membrane Protein Production Using Lemo21(DE3) or pReX and GFP-Fusions, *Methods Mol Biol 1586*, 109-126.

[185] Baumgarten, T., Schlegel, S., Wagner, S., Low, M., Eriksson, J., Bonde, I., Herrgard, M. J., Heipieper, H. J., Norholm, M. H., Slotboom, D. J., and de Gier, J. W. (2017) Isolation and characterization of the E. coli membrane protein production strain Mutant56(DE3), *Sci Rep 7*, 45089.

[186] Kesidis, A., Depping, P., Lodé, A., Vaitsopoulou, A., Bill, R. M., Goddard, A. D., and Rothnie, A. J. (2020) Expression of eukaryotic membrane proteins in eukaryotic and prokaryotic hosts, *Methods*.

[187] Pandey, A., Shin, K., Patterson, R. E., Liu, X.-Q., and Rainey, J. K. (2016) Current strategies for protein production and purification enabling membrane protein structural biology, *Biochemistry and Cell Biology 94*, 507-527.

[188] Nielsen, J. (2013) Production of biopharmaceutical proteins by yeast: advances through metabolic engineering, *Bioengineered 4*, 207-211.

[189] Berger, M., Kaup, M., and Blanchard, V. (2012) Protein glycosylation and its impact on biotechnology, *Adv Biochem Eng Biotechnol 127*, 165-185.

[190] Poljak, K., Selevsek, N., Ngwa, E., Grossmann, J., Losfeld, M. E., and Aebi, M. (2018) Quantitative Profiling of N-linked Glycosylation Machinery in Yeast Saccharomyces cerevisiae, *Mol Cell Proteomics 17*, 18-30.

[191] Vieira Gomes, A. M., Souza Carmo, T., Silva Carvalho, L., Mendonca Bahia, F., and Parachin, N. S. (2018) Comparison of Yeasts as Hosts for Recombinant Protein Production, *Microorganisms 6*.

[192] Wang, S., Rong, Y., Wang, Y., Kong, D., Wang, P. G., Chen, M., and Kong, Y. (2020) Homogeneous production and characterization of recombinant N-GlcNAc-protein in Pichia pastoris, *Microb Cell Fact 19*, 7.

[193] Werten, M. W. T., Eggink, G., Cohen Stuart, M. A., and de Wolf, F. A. (2019) Production of protein-based polymers in Pichia pastoris, *Biotechnol Adv 37*, 642-666.

[194] Gonzalez, M. W., and Kann, M. G. (2012) Chapter 4: Protein interactions and disease, *PLoS Comput Biol 8*, e1002819.

[195] Poverennaya, E., Kiseleva, O., Romanova, A., and Pyatnitskiy, M. (2020) Predicting Functions of Uncharacterized Human Proteins: From Canonical to Proteoforms, *Genes (Basel) 11*.

[196] Stephen, S. L., Beales, L., Peyret, H., Roe, A., Stonehouse, N. J., and Rowlands, D. J. (2018) Recombinant Expression of Tandem-HBc Virus-Like Particles (VLPs), In *Virus-Derived Nanoparticles for Advanced Technologies: Methods and Protocols* (Wege, C., and Lomonossoff, G. P., Eds.), pp 97-123, Springer New York, New York, NY.

[197] He, H., Zhai, C., Mei, M., Rao, Y., Liu, Y., Wang, F., Ma, L., Jiang, Z., Zhang, G., and Yi, L. (2019) Functional expression of porcine

interferon-α using a combinational strategy in Pichia pastoris GS115, *Enzyme Microb Technol 122*, 55-63.
[198] Zhu, W., Gong, G., Pan, J., Han, S., Zhang, W., Hu, Y., and Xie, L. (2018) High level expression and purification of recombinant human serum albumin in Pichia pastoris, *Protein Expr Purif 147*, 61-68.
[199] Ahmad, M., Hirz, M., Pichler, H., and Schwab, H. (2014) Protein expression in Pichia pastoris: recent achievements and perspectives for heterologous protein production, *Appl Microbiol Biotechnol 98*, 5301-5317.
[200] Karbalaei, M., Rezaee, S. A., and Farsiani, H. (2020) Pichia pastoris: A highly successful expression system for optimal synthesis of heterologous proteins, *J Cell Physiol 235*, 5867-5881.
[201] Barrero, J. J., Casler, J. C., Valero, F., Ferrer, P., and Glick, B. S. (2018) An improved secretion signal enhances the secretion of model proteins from Pichia pastoris, *Microb Cell Fact 17*, 161.
[202] Khan, K. H. (2013) Gene expression in Mammalian cells and its applications, *Adv Pharm Bull 3*, 257-263.
[203] Hunter, M., Yuan, P., Vavilala, D., and Fox, M. (2019) Optimization of Protein Expression in Mammalian Cells, *Curr Protoc Protein Sci 95*, e77.
[204] Byrne, B. (2015) Pichia pastoris as an expression host for membrane protein structural biology, *Curr Opin Struct Biol 32*, 9-17.
[205] Wang, J., Wang, X., Shi, L., Qi, F., Zhang, P., Zhang, Y., Zhou, X., Song, Z., and Cai, M. (2017) Methanol-Independent Protein Expression by AOX1 Promoter with trans-Acting Elements Engineering and Glucose-Glycerol-Shift Induction in Pichia pastoris, *Sci Rep 7*, 41850.
[206] Koch, C., Neumann, P., Valerius, O., Feussner, I., and Ficner, R. (2016) Crystal Structure of Alcohol Oxidase from Pichia pastoris, *PLoS One 11*, e0149846.
[207] Yang, Z., and Zhang, Z. (2018) Engineering strategies for enhanced production of protein and bio-products in Pichia pastoris: A review, *Biotechnol Adv 36*, 182-195.
[208] Liu, W. C., Inwood, S., Gong, T., Sharma, A., Yu, L. Y., and Zhu, P. (2019) Fed-batch high-cell-density fermentation strategies for Pichia pastoris growth and production, *Crit Rev Biotechnol 39*, 258-271.
[209] Holmes, W. J., Darby, R. A., Wilks, M. D., Smith, R., and Bill, R. M. (2009) Developing a scalable model of recombinant protein yield from Pichia pastoris: the influence of culture conditions, biomass and induction regime, *Microb Cell Fact 8*, 35.
[210] Bawa, Z., Routledge, S. J., Jamshad, M., Clare, M., Sarkar, D., Dickerson, I., Ganzlin, M., Poyner, D. R., and Bill, R. M. (2014) Functional recombinant protein is present in the pre-induction phases of Pichia pastoris cultures when grown in bioreactors, but not shake-flasks, *Microb Cell Fact 13*, 127.

[211] Daly, R., and Hearn, M. T. (2005) Expression of heterologous proteins in Pichia pastoris: a useful experimental tool in protein engineering and production, *J Mol Recognit 18*, 119-138.
[212] Gomes, A. M. V., Carmo, T. S., Carvalho, L. S., Bahia, F. M., and Parachin, N. S. (2018) Comparison of Yeasts as Hosts for Recombinant Protein Production, *Microorganisms 6*.
[213] Schwarzhans, J. P., Wibberg, D., Winkler, A., Luttermann, T., Kalinowski, J., and Friehs, K. (2016) Non-canonical integration events in Pichia pastoris encountered during standard transformation analysed with genome sequencing, *Sci Rep-Uk 6*.
[214] Zhu, T., Guo, M., Tang, Z., Zhang, M., Zhuang, Y., Chu, J., and Zhang, S. (2009) Efficient generation of multi-copy strains for optimizing secretory expression of porcine insulin precursor in yeast Pichia pastoris, *J Appl Microbiol 107*, 954-963.
[215] Naseem, M. U., Ahmed, N., Khan, M. A., Tahir, S., and Zafar, A. U. (2020) Production of potent long-lasting consensus interferon using albumin fusion technology in Pichia pastoris expression system, *Protein Expr Purif 166*, 105509.
[216] Wu, D., Chu, J., Hao, Y. Y., Wang, Y. H., Zhuang, Y. P., and Zhang, S. L. (2012) Incomplete protein disulphide bond conformation and decreased protein expression result from high cell growth during heterologous protein expression in Pichia pastoris, *J Biotechnol 157*, 107-112.
[217] Ponomarenko, E. A., Poverennaya, E. V., Ilgisonis, E. V., Pyatnitskiy, M. A., Kopylov, A. T., Zgoda, V. G., Lisitsa, A. V., and Archakov, A. I. (2016) The Size of the Human Proteome: The Width and Depth, *Int J Anal Chem 2016*, 7436849.
[218] Manzoni, C., Kia, D. A., Vandrovcova, J., Hardy, J., Wood, N. W., Lewis, P. A., and Ferrari, R. (2018) Genome, transcriptome and proteome: the rise of omics data and their integration in biomedical sciences, *Brief Bioinform 19*, 286-302.
[219] Smith, L. M., Kelleher, N. L., and Consortium for Top Down, P. (2013) Proteoform: a single term describing protein complexity, *Nat Methods 10*, 186-187.
[220] Hyun, K., Jeon, J., Park, K., and Kim, J. (2017) Writing, erasing and reading histone lysine methylations, *Exp Mol Med 49*, e324.
[221] Gillette, T. G., and Hill, J. A. (2015) Readers, writers, and erasers: chromatin as the whiteboard of heart disease, *Circ Res 116*, 1245-1253.
[222] Esteve-Puig, R., Bueno-Costa, A., and Esteller, M. (2020) Writers, readers and erasers of RNA modifications in cancer, *Cancer Lett 474*, 127-137.
[223] Lee, S., Chen, Z., and Zhang, G. (2017) Catching Sirtuin-2 intermediates one structure at the time, *Cell Chemical Biology 24*, 248-249.

[224] Drazic, A., Myklebust, L. M., Ree, R., and Arnesen, T. (2016) The world of protein acetylation, *Biochim Biophys Acta 1864*, 1372-1401.
[225] Gil, J., Ramirez-Torres, A., and Encarnacion-Guevara, S. (2017) Lysine acetylation and cancer: A proteomics perspective, *J Proteomics 150*, 297-309.
[226] Gertz, M., and Steegborn, C. (2016) Using mitochondrial sirtuins as drug targets: disease implications and available compounds, *Cell Mol Life Sci 73*, 2871-2896.
[227] Xu, H., Yu, X., Wang, B., Zhang, H., Li, J., Gao, H., and Wang, Y. (2020) The clinical significance of the SIRT2 expression level in the early stage of sepsis patients, *Ann Palliat Med 9*, 1413-1419.
[228] Zhang, L., Kim, S., and Ren, X. (2020) The Clinical Significance of SIRT2 in Malignancies: A Tumor Suppressor or an Oncogene?, *Frontiers in Oncology 10*.
[229] Chen, J., Chan, A. W., To, K. F., Chen, W., Zhang, Z., Ren, J., Song, C., Cheung, Y. S., Lai, P. B., Cheng, S. H., Ng, M. H., Huang, A., and Ko, B. C. (2013) SIRT2 overexpression in hepatocellular carcinoma mediates epithelial to mesenchymal transition by protein kinase B/glycogen synthase kinase-3beta/beta-catenin signaling, *Hepatology 57*, 2287-2298.
[230] Wang, B., Zhang, Y., Cao, W., Wei, X., Chen, J., and Ying, W. (2016) SIRT2 Plays Significant Roles in Lipopolysaccharides-Induced Neuroinflammation and Brain Injury in Mice, *Neurochem Res 41*, 2490-2500.
[231] Choi, B. K., Warburton, S., Lin, H., Patel, R., Boldogh, I., Meehl, M., d'Anjou, M., Pon, L., Stadheim, T. A., and Sethuraman, N. (2012) Improvement of N-glycan site occupancy of therapeutic glycoproteins produced in Pichia pastoris, *Appl Microbiol Biotechnol 95*, 671-682.
[232] Lorber, B., Skouri, M., Munch, J. P., and Giege, R. (1993) The Influence of Impurities on Protein Crystallization - the Case of Lysozyme, *J Cryst Growth 128*, 1203-1211.
[233] Niedzialkowska, E., Gasiorowska, O., Handing, K. B., Majorek, K. A., Porebski, P. J., Shabalin, I. G., Zasadzinska, E., Cymborowski, M., and Minor, W. (2016) Protein purification and crystallization artifacts: The tale usually not told, *Protein Science 25*, 720-733.
[234] Grabski, A. C. (2009) Advances in preparation of biological extracts for protein purification, *Methods Enzymol 463*, 285-303.
[235] Fido, R. J., Mills, E. N., Rigby, N. M., and Shewry, P. R. (2004) Protein extraction from plant tissues, *Methods Mol Biol 244*, 21-27.
[236] Tan, S. C., and Yiap, B. C. (2009) DNA, RNA, and protein extraction: the past and the present, *J Biomed Biotechnol 2009*, 574398.
[237] Gomes, T. A., Zanette, C. M., and Spier, M. R. (2020) An overview of cell disruption methods for intracellular biomolecules recovery, *Prep Biochem Biotech 50*, 635-654.

[238] Rolland, N., Ferro, M., Ephritikhine, G., Marmagne, A., Ramus, C., Brugiere, S., Salvi, D., Seigneurin-Berny, D., Bourguignon, J., Barbier-Brygoo, H., Joyard, J., and Garin, J. (2006) A versatile method for deciphering plant membrane proteomes, *Journal of Experimental Botany 57*, 1579-1589.

[239] Desuzinges Mandon, E., Agez, M., Pellegrin, R., Igonet, S., and Jawhari, A. (2017) Novel systematic detergent screening method for membrane proteins solubilization, *Anal Biochem 517*, 40-49.

[240] Kang, H. J., Lee, C., and Drew, D. (2013) Breaking the barriers in membrane protein crystallography, *Int J Biochem Cell Biol 45*, 636-644.

[241] Seidel, S. A., Dijkman, P. M., Lea, W. A., van den Bogaart, G., Jerabek-Willemsen, M., Lazic, A., Joseph, J. S., Srinivasan, P., Baaske, P., Simeonov, A., Katritch, I., Melo, F. A., Ladbury, J. E., Schreiber, G., Watts, A., Braun, D., and Duhr, S. (2013) Microscale thermophoresis quantifies biomolecular interactions under previously challenging conditions, *Methods 59*, 301-315.

[242] Labrou, N. E. (2014) Protein purification: an overview, *Methods Mol Biol 1129*, 3-10.

[243] Oliveira, C., and Domingues, L. (2018) Guidelines to reach high-quality purified recombinant proteins, *Appl Microbiol Biotechnol 102*, 81-92.

[244] Fekete, S., Beck, A., Veuthey, J. L., and Guillarme, D. (2014) Theory and practice of size exclusion chromatography for the analysis of protein aggregates, *J Pharm Biomed Anal 101*, 161-173.

[245] Brusotti, G., Calleri, E., Colombo, R., Massolini, G., Rinaldi, F., and Temporini, C. (2018) Advances on Size Exclusion Chromatography and Applications on the Analysis of Protein Biopharmaceuticals and Protein Aggregates: A Mini Review, *Chromatographia 81*, 3-23.

[246] Kimple, M. E., Brill, A. L., and Pasker, R. L. (2013) Overview of affinity tags for protein purification, *Curr Protoc Protein Sci 73*, 9 9 1-9 9 23.

[247] Wood, D. W. (2014) New trends and affinity tag designs for recombinant protein purification, *Curr Opin Struct Biol 26*, 54-61.

[248] Wingfield, P. T. (2015) Overview of the purification of recombinant proteins, *Curr Protoc Protein Sci 80*, 6 1 1-6 1 35.

[249] Renzi, F., Panetta, G., Vallone, B., Brunori, M., Arceci, M., Bozzoni, I., Laneve, P., and Caffarelli, E. (2006) Large-scale purification and crystallization of the endoribonuclease XendoU: troubleshooting with His-tagged proteins, *Acta Crystallogr Sect F Struct Biol Cryst Commun 62*, 298-301.

[250] Mohanty, A. K., and Wiener, M. C. (2004) Membrane protein expression and production: effects of polyhistidine tag length and position, *Protein Expr Purif 33*, 311-325.

[251] Routzahn, K. M., and Waugh, D. S. (2002) Differential effects of supplementary affinity tags on the solubility of MBP fusion proteins, *J Struct Funct Genomics 2*, 83-92.

[252] Su, X. D., Zhang, H., Terwilliger, T. C., Liljas, A., Xiao, J., and Dong, Y. (2015) Protein Crystallography from the Perspective of Technology Developments, *Crystallogr Rev 21*, 122-153.
[253] Egli, M. (2016) Diffraction Techniques in Structural Biology, *Curr Protoc Nucleic Acid Chem 65*, 7 13 11-17 13 41.
[254] Bragg, W. L. (1912) The Specular Reflection of X-rays, *Nature 90*, 410-410.
[255] Eisenberg, D. (1994) Max Perutz's achievements: how did he do it?, *Protein Sci 3*, 1625-1628.
[256] Taylor, G. L. (2010) Introduction to phasing, *Acta Crystallogr D Biol Crystallogr 66*, 325-338.
[257] Hendrickson, W. A. (2014) Anomalous diffraction in crystallographic phase evaluation, *Q Rev Biophys 47*, 49-93.
[258] Evans, P., and McCoy, A. (2008) An introduction to molecular replacement, *Acta Crystallogr D Biol Crystallogr 64*, 1-10.
[259] Scapin, G. (2013) Molecular replacement then and now, *Acta Crystallogr D Biol Crystallogr 69*, 2266-2275.
[260] Abergel, C. (2013) Molecular replacement: tricks and treats, *Acta Crystallogr D Biol Crystallogr 69*, 2167-2173.
[261] Shimizu, K., Cao, W., Saad, G., Shoji, M., and Terada, T. (2018) Comparative analysis of membrane protein structure databases, *Biochim Biophys Acta Biomembr 1860*, 1077-1091.
[262] Callaway, E. (2020) Revolutionary cryo-EM is taking over structural biology, *Nature 578*, 201.
[263] Brooks-Bartlett, J., and Garman, E. (2015) The Nobel Science: One Hundred Years of Crystallography (vol 40, pg 244, 2015), *Interdiscipl Sci Rev 40*, I-I.
[264] Almeida, J. G., Preto, A. J., Koukos, P. I., Bonvin, A., and Moreira, I. S. (2017) Membrane proteins structures: A review on computational modeling tools, *Biochim Biophys Acta Biomembr 1859*, 2021-2039.
[265] Birch, J., Axford, D., Foadi, J., Meyer, A., Eckhardt, A., Thielmann, Y., and Moraes, I. (2018) The fine art of integral membrane protein crystallisation, *Methods 147*, 150-162.
[266] Moraes, I., Evans, G., Sanchez-Weatherby, J., Newstead, S., and Stewart, P. D. (2014) Membrane protein structure determination - the next generation, *Biochim Biophys Acta 1838*, 78-87.
[267] Hünefeld, F. L. (1840) *Der Chemismus in der thierischen Organisation: Physiologisch-chemische Untersuchungen der materiellen Veränderungen, oder des Bildungslebens im thierischen Organismus; insbesondere des Blutbildungsprocesses, der Natur der Blut körperchen und ihrer Kernchen. Ein Beitrag zur Physiologie und Heilmittellehre*, Brockhaus.
[268] Giege, R. (2013) A historical perspective on protein crystallization from 1840 to the present day, *FEBS J 280*, 6456-6497.

[269] McPherson, A., and Gavira, J. A. (2014) Introduction to protein crystallization, *Acta Crystallogr F Struct Biol Commun 70*, 2-20.
[270] Obata, T., Kershaw, J., Tachibana, Y., Miyauchi, T., Abe, Y., Shibata, S., Kawaguchi, H., Ikoma, Y., Takuwa, H., Aoki, I., and Yasui, M. (2018) Comparison of diffusion-weighted MRI and anti-Stokes Raman scattering (CARS) measurements of the inter-compartmental exchange-time of water in expression-controlled aquaporin-4 cells, *Sci Rep 8*, 17954.
[271] Eriksson, S., Elbing, K., Soderman, O., Lindkvist-Petersson, K., Topgaard, D., and Lasic, S. (2017) NMR quantification of diffusional exchange in cell suspensions with relaxation rate differences between intra and extracellular compartments, *PLoS One 12*, e0177273.
[272] Mukherjee, A., Wu, D., Davis, H. C., and Shapiro, M. G. (2016) Non-invasive imaging using reporter genes altering cellular water permeability, *Nat Commun 7*, 13891.
[273] Hartridge, H., and Roughton, F. (1923) The Measurement of the Rates of Oxidation and Reduction of Hæmoglobin, *Nature 111*, 325-326.
[274] Gierusz, L. A., and Pinheiro, T. J. T. (2013) Continuous Flow, In *Encyclopedia of Biophysics* (Roberts, G. C. K., Ed.), pp 366-371, Springer Berlin Heidelberg, Berlin, Heidelberg.
[275] Chance, B. (1943) The kinetics of the enzyme-substrate compound of peroxidase, *Journal of Biological Chemistry 151*, 553-577.
[276] Bagshaw, C. R. (2013) Stopped-Flow Techniques, In *Encyclopedia of Biophysics* (Roberts, G. C. K., Ed.), pp 2460-2466, Springer Berlin Heidelberg, Berlin, Heidelberg.
[277] Skrzypek, R., Iqbal, S., and Callaghan, R. (2018) Methods of reconstitution to investigate membrane protein function, *Methods 147*, 126-141.
[278] Wang, L., and Tonggu, L. (2015) Membrane protein reconstitution for functional and structural studies, *Sci China Life Sci 58*, 66-74.
[279] Posson, D. J., Rusinova, R., Andersen, O. S., and Nimigean, C. M. (2018) Stopped-Flow Fluorometric Ion Flux Assay for Ligand-Gated Ion Channel Studies, In *Potassium Channels: Methods and Protocols* (Shyng, S.-L., Valiyaveetil, F. I., and Whorton, M., Eds.), pp 223-235, Springer New York, New York, NY.
[280] Brower, V. (2001) Proteomics: biology in the post-genomic era. Companies all over the world rush to lead the way in the new post-genomics race, *EMBO Rep 2*, 558-560.
[281] Uetz, P., Giot, L., Cagney, G., Mansfield, T. A., Judson, R. S., Knight, J. R., Lockshon, D., Narayan, V., Srinivasan, M., Pochart, P., Qureshi-Emili, A., Li, Y., Godwin, B., Conover, D., Kalbfleisch, T., Vijayadamodar, G., Yang, M., Johnston, M., Fields, S., and Rothberg, J. M. (2000) A comprehensive analysis of protein-protein interactions in Saccharomyces cerevisiae, *Nature 403*, 623-627.

[282] Hao, T., Peng, W., Wang, Q., Wang, B., and Sun, J. (2016) Reconstruction and Application of Protein-Protein Interaction Network, *Int J Mol Sci 17*.
[283] Oughtred, R., Chatr-aryamontri, A., Breitkreutz, B. J., Chang, C. S., Rust, J. M., Theesfeld, C. L., Heinicke, S., Breitkreutz, A., Chen, D., Hirschman, J., Kolas, N., Livstone, M. S., Nixon, J., O'Donnell, L., Ramage, L., Winter, A., Reguly, T., Sellam, A., Stark, C., Boucher, L., Dolinski, K., and Tyers, M. (2016) BioGRID: A Resource for Studying Biological Interactions in Yeast, *Cold Spring Harb Protoc 2016*, pdb top080754.
[284] Szklarczyk, D., Franceschini, A., Wyder, S., Forslund, K., Heller, D., Huerta-Cepas, J., Simonovic, M., Roth, A., Santos, A., Tsafou, K. P., Kuhn, M., Bork, P., Jensen, L. J., and von Mering, C. (2015) STRING v10: protein-protein interaction networks, integrated over the tree of life, *Nucleic Acids Res 43*, D447-452.
[285] Chen, C., Huang, H., and Wu, C. H. (2017) Protein Bioinformatics Databases and Resources, *Methods Mol Biol 1558*, 3-39.
[286] Bartoschik, T., Galinec, S., Kleusch, C., Walkiewicz, K., Breitsprecher, D., Weigert, S., Muller, Y. A., You, C., Piehler, J., Vercruysse, T., Daelemans, D., and Tschammer, N. (2018) Near-native, site-specific and purification-free protein labeling for quantitative protein interaction analysis by MicroScale Thermophoresis, *Sci Rep 8*, 4977.
[287] Rainard, J. M., Pandarakalam, G. C., and McElroy, S. P. (2018) Using Microscale Thermophoresis to Characterize Hits from High-Throughput Screening: A European Lead Factory Perspective, *SLAS Discov 23*, 225-241.
[288] Miernyk, J. A., and Thelen, J. J. (2008) Biochemical approaches for discovering protein-protein interactions, *Plant J 53*, 597-609.
[289] Piston, D. W., and Kremers, G. J. (2007) Fluorescent protein FRET: the good, the bad and the ugly, *Trends Biochem Sci 32*, 407-414.
[290] Wu, Y., Li, Q., and Chen, X. Z. (2007) Detecting protein-protein interactions by Far western blotting, *Nat Protoc 2*, 3278-3284.
[291] Sakamoto, S., Putalun, W., Vimolmangkang, S., Phoolcharoen, W., Shoyama, Y., Tanaka, H., and Morimoto, S. (2018) Enzyme-linked immunosorbent assay for the quantitative/qualitative analysis of plant secondary metabolites, *J Nat Med 72*, 32-42.
[292] Bruckner, A., Polge, C., Lentze, N., Auerbach, D., and Schlattner, U. (2009) Yeast two-hybrid, a powerful tool for systems biology, *Int J Mol Sci 10*, 2763-2788.
[293] Yin, H., and Flynn, A. D. (2016) Drugging Membrane Protein Interactions, *Annu Rev Biomed Eng 18*, 51-76.
[294] Liu, P., Yang, L., Shi, D., and Tang, X. (2015) Prediction of protein-protein interactions related to protein complexes based on protein interaction networks, *Biomed Res Int 2015*, 259157.

[295] Hamp, T., and Rost, B. (2015) Evolutionary profiles improve protein-protein interaction prediction from sequence, *Bioinformatics 31*, 1945-1950.
[296] Zhang, J., Zhong, C., Lin, H. X., and Wang, M. (2019) Identifying Protein Complexes from Dynamic Temporal Interval Protein-Protein Interaction Networks, *Biomed Res Int 2019*, 3726721.
[297] Massoud, T. F., Paulmurugan, R., De, A., Ray, P., and Gambhir, S. S. (2007) Reporter gene imaging of protein-protein interactions in living subjects, *Curr Opin Biotechnol 18*, 31-37.
[298] Erffelinck, M. L., Ribeiro, B., Perassolo, M., Pauwels, L., Pollier, J., Storme, V., and Goossens, A. (2018) A user-friendly platform for yeast two-hybrid library screening using next generation sequencing, *PLoS One 13*, e0201270.
[299] Huang, H., Jedynak, B. M., and Bader, J. S. (2007) Where have all the interactions gone? Estimating the coverage of two-hybrid protein interaction maps, *PLoS Comput Biol 3*, e214.
[300] Gagarinova, A., Babu, M., Greenblatt, J., and Emili, A. (2012) Mapping bacterial functional networks and pathways in Escherichia Coli using synthetic genetic arrays, *J Vis Exp*.
[301] Xing, S., Wallmeroth, N., Berendzen, K. W., and Grefen, C. (2016) Techniques for the Analysis of Protein-Protein Interactions in Vivo, *Plant Physiol 171*, 727-758.
[302] Richards, F. M. (1958) On the enzymic activity of subtilisin-modified ribonuclease, *Proceedings of the National Academy of Sciences of the United States of America 44*, 162.
[303] Johnsson, N., and Varshavsky, A. (1994) Split ubiquitin as a sensor of protein interactions in vivo, *Proc Natl Acad Sci U S A 91*, 10340-10344.
[304] Ghosh, I., Hamilton, A. D., and Regan, L. (2000) Antiparallel Leucine Zipper-Directed Protein Reassembly: Application to the Green Fluorescent Protein, *Journal of the American Chemical Society 122*, 5658-5659.
[305] Shimomura, O. (2005) The discovery of aequorin and green fluorescent protein, *J Microsc 217*, 1-15.
[306] Lowder, M. A., Appelbaum, J. S., Hobert, E. M., and Schepartz, A. (2011) Visualizing protein partnerships in living cells and organisms, *Curr Opin Chem Biol 15*, 781-788.
[307] Day, R. N., and Davidson, M. W. (2009) The fluorescent protein palette: tools for cellular imaging, *Chem Soc Rev 38*, 2887-2921.
[308] Kudla, J., and Bock, R. (2016) Lighting the Way to Protein-Protein Interactions: Recommendations on Best Practices for Bimolecular Fluorescence Complementation Analyses, *Plant Cell 28*, 1002-1008.
[309] Rodriguez, E. A., Campbell, R. E., Lin, J. Y., Lin, M. Z., Miyawaki, A., Palmer, A. E., Shu, X., Zhang, J., and Tsien, R. Y. (2017) The Growing

and Glowing Toolbox of Fluorescent and Photoactive Proteins, *Trends Biochem Sci 42*, 111-129.
[310] Lu, K., Vu, C. Q., Matsuda, T., and Nagai, T. (2019) Fluorescent Protein-Based Indicators for Functional Super-Resolution Imaging of Biomolecular Activities in Living Cells, *Int J Mol Sci 20*.
[311] Wang, S., Ding, M., Xue, B., Hou, Y., and Sun, Y. (2018) Live Cell Visualization of Multiple Protein-Protein Interactions with BiFC Rainbow, *ACS Chem Biol 13*, 1180-1188.
[312] Nickerson, A., Huang, T., Lin, L. J., and Nan, X. (2014) Photoactivated localization microscopy with bimolecular fluorescence complementation (BiFC-PALM) for nanoscale imaging of protein-protein interactions in cells, *PLoS One 9*, e100589.
[313] Sjohamn, J., Bath, P., Neutze, R., and Hedfalk, K. (2016) Applying bimolecular fluorescence complementation to screen and purify aquaporin protein:protein complexes, *Protein Sci 25*, 2196-2208.
[314] Tebo, A. G., and Gautier, A. (2019) A split fluorescent reporter with rapid and reversible complementation, *Nat Commun 10*, 2822.
[315] Li, P., Wang, L., and Di, L. J. (2019) Applications of Protein Fragment Complementation Assays for Analyzing Biomolecular Interactions and Biochemical Networks in Living Cells, *J Proteome Res 18*, 2987-2998.
[316] Kaufholdt, D., Baillie, C. K., Meinen, R., Mendel, R. R., and Hansch, R. (2017) The Molybdenum Cofactor Biosynthesis Network: In vivo Protein-Protein Interactions of an Actin Associated Multi-Protein Complex, *Front Plant Sci 8*, 1946.
[317] Zhang, X. E., Cui, Z., and Wang, D. (2016) Sensing of biomolecular interactions using fluorescence complementing systems in living cells, *Biosens Bioelectron 76*, 243-250.
[318] Miller, K. E., Kim, Y., Huh, W. K., and Park, H. O. (2015) Bimolecular Fluorescence Complementation (BiFC) Analysis: Advances and Recent Applications for Genome-Wide Interaction Studies, *J Mol Biol 427*, 2039-2055.
[319] Bischof, J., Duffraisse, M., Furger, E., Ajuria, L., Giraud, G., Vanderperre, S., Paul, R., Bjorklund, M., Ahr, D., Ahmed, A. W., Spinelli, L., Brun, C., Basler, K., and Merabet, S. (2018) Generation of a versatile BiFC ORFeome library for analyzing protein-protein interactions in live Drosophila, *Elife 7*.
[320] Moldavan, A. (1934) Photo-Electric Technique for the Counting of Microscopical Cells, *Science 80*, 188-189.
[321] Fulwyler, M. J. (1965) Electronic separation of biological cells by volume, *Science 150*, 910-911.
[322] Hulett, H. R., Bonner, W. A., Barrett, J., and Herzenberg, L. A. (1969) Cell sorting: automated separation of mammalian cells as a function of intracellular fluorescence, *Science 166*, 747-749.

[323] Bonner, W. A., Hulett, H. R., Sweet, R. G., and Herzenberg, L. A. (1972) Fluorescence activated cell sorting, *Rev Sci Instrum 43*, 404-409.
[324] Silveira, G. (2015) Evolution of flow cytometry technology, *J Microb Biochem Technol 7*, 213-216.
[325] Torres, J., Stevens, T. J., and Samso, M. (2003) Membrane proteins: the 'Wild West' of structural biology, *Trends Biochem Sci 28*, 137-144.
[326] Seifert, T., Malo, M., Lengqvist, J., Sihlbom, C., Jarho, E. M., and Luthman, K. (2016) Identification of the Binding Site of Chroman-4-one-Based Sirtuin 2-Selective Inhibitors using Photoaffinity Labeling in Combination with Tandem Mass Spectrometry, *J Med Chem 59*, 10794-10799.
[327] Yang, S. R., Wright, J., Bauter, M., Seweryniak, K., Kode, A., and Rahman, I. (2007) Sirtuin regulates cigarette smoke-induced proinflammatory mediator release via RelA/p65 NF-kappaB in macrophages in vitro and in rat lungs in vivo: implications for chronic inflammation and aging, *Am J Physiol Lung Cell Mol Physiol 292*, L567-576.
[328] Grimley, R., Polyakova, O., Vamathevan, J., McKenary, J., Hayes, B., Patel, C., Smith, J., Bridges, A., Fosberry, A., Bhardwaja, A., Mouzon, B., Chung, C. W., Barrett, N., Richmond, N., Modha, S., and Solari, R. (2012) Over expression of wild type or a catalytically dead mutant of Sirtuin 6 does not influence NFkappaB responses, *PLoS One 7*, e39847.
[329] Lee, H. S., Ka, S. O., Lee, S. M., Lee, S. I., Park, J. W., and Park, B. H. (2013) Overexpression of sirtuin 6 suppresses inflammatory responses and bone destruction in mice with collagen-induced arthritis, *Arthritis Rheum 65*, 1776-1785.
[330] Sinha, S., Patel, S., Athar, M., Vora, J., Chhabria, M. T., Jha, P. C., and Shrivastava, N. (2019) Structure-based identification of novel sirtuin inhibitors against triple negative breast cancer: An in silico and in vitro study, *Int J Biol Macromol 140*, 454-468.
[331] Laurent, G., German, N. J., Saha, A. K., de Boer, V. C., Davies, M., Koves, T. R., Dephoure, N., Fischer, F., Boanca, G., Vaitheesvaran, B., Lovitch, S. B., Sharpe, A. H., Kurland, I. J., Steegborn, C., Gygi, S. P., Muoio, D. M., Ruderman, N. B., and Haigis, M. C. (2013) SIRT4 coordinates the balance between lipid synthesis and catabolism by repressing malonyl CoA decarboxylase, *Mol Cell 50*, 686-698.
[332] Rahnasto-Rilla, M., Tyni, J., Huovinen, M., Jarho, E., Kulikowicz, T., Ravichandran, S., V, A. B., Ferrucci, L., Lahtela-Kakkonen, M., and Moaddel, R. (2018) Natural polyphenols as sirtuin 6 modulators, *Sci Rep 8*, 4163.
[333] Schuetz, A., Min, J., Antoshenko, T., Wang, C. L., Allali-Hassani, A., Dong, A., Loppnau, P., Vedadi, M., Bochkarev, A., Sternglanz, R., and Plotnikov, A. N. (2007) Structural basis of inhibition of the human

NAD+-dependent deacetylase SIRT5 by suramin, *Structure 15*, 377-389.

[334] Huang, Z., Zhao, J., Deng, W., Chen, Y., Shang, J., Song, K., Zhang, L., Wang, C., Lu, S., Yang, X., He, B., Min, J., Hu, H., Tan, M., Xu, J., Zhang, Q., Zhong, J., Sun, X., Mao, Z., Lin, H., Xiao, M., Chin, Y. E., Jiang, H., Xu, Y., Chen, G., and Zhang, J. (2018) Identification of a cellularly active SIRT6 allosteric activator, *Nat Chem Biol 14*, 1118-1126.

[335] Finnin, M. S., Donigian, J. R., and Pavletich, N. P. (2001) Structure of the histone deacetylase SIRT2, *Nat Struct Biol 8*, 621-625.

[336] Rumpf, T., Schiedel, M., Karaman, B., Roessler, C., North, B. J., Lehotzky, A., Olah, J., Ladwein, K. I., Schmidtkunz, K., Gajer, M., Pannek, M., Steegborn, C., Sinclair, D. A., Gerhardt, S., Ovadi, J., Schutkowski, M., Sippl, W., Einsle, O., and Jung, M. (2015) Selective Sirt2 inhibition by ligand-induced rearrangement of the active site, *Nat Commun 6*, 6263.

[337] Wang, Y., Fung, Y. M. E., Zhang, W., He, B., Chung, M. W. H., Jin, J., Hu, J., Lin, H., and Hao, Q. (2017) Deacylation Mechanism by SIRT2 Revealed in the 1'-SH-2'-O-Myristoyl Intermediate Structure, *Cell Chem Biol 24*, 339-345.

[338] Teng, Y. B., Jing, H., Aramsangtienchai, P., He, B., Khan, S., Hu, J., Lin, H., and Hao, Q. (2015) Efficient demyristoylase activity of SIRT2 revealed by kinetic and structural studies, *Sci Rep 5*, 8529.

[339] Hong, J. Y., Price, I. R., Bai, J. J., and Lin, H. (2019) A Glycoconjugated SIRT2 Inhibitor with Aqueous Solubility Allows Structure-Based Design of SIRT2 Inhibitors, *ACS Chem Biol 14*, 1802-1810.

[340] Pirrie, L., McCarthy, A. R., Major, L. L., Morkunaite, V., Zubriene, A., Matulis, D., Lain, S., Lebl, T., and Westwood, N. J. (2012) Discovery and validation of SIRT2 inhibitors based on tenovin-6: use of a (1)H-NMR method to assess deacetylase activity, *Molecules 17*, 12206-12224.

[341] Buler, M., Andersson, U., and Hakkola, J. (2016) Who watches the watchmen? Regulation of the expression and activity of sirtuins, *FASEB J 30*, 3942-3960.

[342] Revollo, J. R., and Li, X. (2013) The ways and means that fine tune Sirt1 activity, *Trends Biochem Sci 38*, 160-167.

[343] Santos, L., Escande, C., and Denicola, A. (2016) Potential Modulation of Sirtuins by Oxidative Stress, *Oxid Med Cell Longev 2016*, 9831825.

[344] Sun, C., Song, D., Marcotte, P. A., Richardson, P. L., and Hajduk, P. J. (2006) High-level bacterial expression and purification of human SirT2 protein for NMR studies, *Protein Expr Purif 48*, 56-60.

[345] Swyter, S. (2017) Identifizierung und Charakterisierung neuer Modulatoren der humanen Sirtuine 1, 2 und 3, Albert-Ludwigs-Universität Freiburg im Breisgau.

[346] Shen, W., Xue, Y., Liu, Y., Kong, C., Wang, X., Huang, M., Cai, M., Zhou, X., Zhang, Y., and Zhou, M. (2016) A novel methanol-free Pichia pastoris system for recombinant protein expression, *Microb Cell Fact 15*, 178.

[347] Deller, M. C., Kong, L., and Rupp, B. (2016) Protein stability: a crystallographer's perspective, *Acta Crystallogr F Struct Biol Commun 72*, 72-95.

[348] Julien, O., Graether, S. P., and Sykes, B. D. (2009) Monitoring prion protein stability by NMR, *J Toxicol Environ Health A 72*, 1069-1074.

[349] Puglisi, R., Brylski, O., Alfano, C., Martin, S. R., Pastore, A., and Temussi, P. A. (2020) Quantifying the thermodynamics of protein unfolding using 2D NMR spectroscopy, *Communications Chemistry 3*, 100.

[350] Boivin, S., Kozak, S., and Meijers, R. (2013) Optimization of protein purification and characterization using Thermofluor screens, *Protein Expr Purif 91*, 192-206.

[351] Oberg, F., Ekvall, M., Nyblom, M., Backmark, A., Neutze, R., and Hedfalk, K. (2009) Insight into factors directing high production of eukaryotic membrane proteins; production of 13 human AQPs in Pichia pastoris, *Mol Membr Biol 26*, 215-227.

[352] Oberg, F., Sjohamn, J., Conner, M. T., Bill, R. M., and Hedfalk, K. (2011) Improving recombinant eukaryotic membrane protein yields in Pichia pastoris: the importance of codon optimization and clone selection, *Mol Membr Biol 28*, 398-411.

[353] Shahmohammadi, S., Doosti, R., Shahmohammadi, A., Mohammadianinejad, S. E., Sahraian, M. A., Azimi, A. R., Harirchian, M. H., Asgari, N., and Naser Moghadasi, A. (2019) Autoimmune diseases associated with Neuromyelitis Optica Spectrum Disorders: A literature review, *Mult Scler Relat Disord 27*, 350-363.

[354] Wingerchuk, D. M., Banwell, B., Bennett, J. L., Cabre, P., Carroll, W., Chitnis, T., de Seze, J., Fujihara, K., Greenberg, B., Jacob, A., Jarius, S., Lana-Peixoto, M., Levy, M., Simon, J. H., Tenembaum, S., Traboulsee, A. L., Waters, P., Wellik, K. E., Weinshenker, B. G., and International Panel for, N. M. O. D. (2015) International consensus diagnostic criteria for neuromyelitis optica spectrum disorders, *Neurology 85*, 177-189.

[355] Wu, Y., Zhong, L., and Geng, J. (2019) Neuromyelitis optica spectrum disorder: Pathogenesis, treatment, and experimental models, *Mult Scler Relat Disord 27*, 412-418.

[356] Jiao, Y., Fryer, J. P., Lennon, V. A., Jenkins, S. M., Quek, A. M., Smith, C. Y., McKeon, A., Costanzi, C., Iorio, R., Weinshenker, B. G., Wingerchuk, D. M., Shuster, E. A., Lucchinetti, C. F., and Pittock, S. J. (2013) Updated estimate of AQP4-IgG serostatus and disability outcome in neuromyelitis optica, *Neurology 81*, 1197-1204.

[357] DeKosky, B. J., Kojima, T., Rodin, A., Charab, W., Ippolito, G. C., Ellington, A. D., and Georgiou, G. (2015) In-depth determination and analysis of the human paired heavy- and light-chain antibody repertoire, *Nat Med 21*, 86-91.
[358] Lavinder, J. J., Horton, A. P., Georgiou, G., and Ippolito, G. C. (2015) Next-generation sequencing and protein mass spectrometry for the comprehensive analysis of human cellular and serum antibody repertoires, *Curr Opin Chem Biol 24*, 112-120.
[359] Kim, D., and Park, D. (2019) Deep sequencing of B cell receptor repertoire, *BMB Rep 52*, 540-547.
[360] Georgiou, G., Ippolito, G. C., Beausang, J., Busse, C. E., Wardemann, H., and Quake, S. R. (2014) The promise and challenge of high-throughput sequencing of the antibody repertoire, *Nat Biotechnol 32*, 158-168.
[361] Lopez-Santibanez-Jacome, L., Avendano-Vazquez, S. E., and Flores-Jasso, C. F. (2019) The Pipeline Repertoire for Ig-Seq Analysis, *Front Immunol 10*, 899.
[362] Greenlee, L. F., Lawler, D. F., Freeman, B. D., Marrot, B., and Moulin, P. (2009) Reverse osmosis desalination: Water sources, technology, and today's challenges, *Water Research 43*, 2317-2348.
[363] Elimelech, M., and Phillip, W. A. (2011) The Future of Seawater Desalination: Energy, Technology, and the Environment, *Science 333*, 712-717.
[364] Zhu, A., Christofides, P. D., and Cohen, Y. (2009) Effect of thermodynamic restriction on energy cost optimization of RO membrane water desalination, *Industrial & Engineering Chemistry Research 48*, 6010-6021.
[365] Wan, C. F., and Chung, T.-S. (2016) Maximize the operating profit of a SWRO-PRO integrated process for optimal water production and energy recovery, *Renewable Energy 94*, 304-313.
[366] Lohrasebi, A., and Koslowski, T. (2019) Modeling water purification by an aquaporin-inspired graphene-based nano-channel, *Journal of Molecular Modeling 25*, 280.
[367] Amy, G., Ghaffour, N., Li, Z., Francis, L., Linares, R. V., Missimer, T., and Lattemann, S. (2017) Membrane-based seawater desalination: Present and future prospects, *Desalination 401*, 16-21.
[368] Xie, W., He, F., Wang, B., Chung, T.-S., Jeyaseelan, K., Armugam, A., and Tong, Y. W. (2013) An aquaporin-based vesicle-embedded polymeric membrane for low energy water filtration, *Journal of Materials Chemistry A 1*, 7592-7600.
[369] Duong, P. H., Chung, T.-S., Jeyaseelan, K., Armugam, A., Chen, Z., Yang, J., and Hong, M. (2012) Planar biomimetic aquaporin-incorporated triblock copolymer membranes on porous alumina supports for nanofiltration, *Journal of Membrane Science 409*, 34-43.

[370] Kumar, M., Grzelakowski, M., Zilles, J., Clark, M., and Meier, W. (2007) Highly permeable polymeric membranes based on the incorporation of the functional water channel protein Aquaporin Z, *Proceedings of the National Academy of Sciences 104*, 20719-20724.
[371] Li, Y., and Yip, W. T. (2005) Liposomes as Protective Capsules for Active Silica Sol− Gel Biocomposite Synthesis, *Journal of the American Chemical Society 127*, 12756-12757.
[372] Lin, Y. (2018) What's happened over the last five years with high-throughput protein crystallization screening?, *Expert Opin Drug Discov 13*, 691-695.
[373] Burley, S. K., Berman, H. M., Kleywegt, G. J., Markley, J. L., Nakamura, H., and Velankar, S. (2017) Protein Data Bank (PDB): The Single Global Macromolecular Structure Archive, *Methods Mol Biol 1607*, 627-641.
[374] Schanda, P., and Ernst, M. (2016) Studying Dynamics by Magic-Angle Spinning Solid-State NMR Spectroscopy: Principles and Applications to Biomolecules, *Prog Nucl Magn Reson Spectrosc 96*, 1-46.
[375] Lalli, D., Idso, M. N., Andreas, L. B., Hussain, S., Baxter, N., Han, S., Chmelka, B. F., and Pintacuda, G. (2017) Proton-Based Structural Analysis of a Heptahelical Transmembrane Protein in Lipid Bilayers, *J Am Chem Soc 139*, 13006-13012.
[376] Barbet-Massin, E., Pell, A. J., Retel, J. S., Andreas, L. B., Jaudzems, K., Franks, W. T., Nieuwkoop, A. J., Hiller, M., Higman, V., Guerry, P., Bertarello, A., Knight, M. J., Felletti, M., Le Marchand, T., Kotelovica, S., Akopjana, I., Tars, K., Stoppini, M., Bellotti, V., Bolognesi, M., Ricagno, S., Chou, J. J., Griffin, R. G., Oschkinat, H., Lesage, A., Emsley, L., Herrmann, T., and Pintacuda, G. (2014) Rapid proton-detected NMR assignment for proteins with fast magic angle spinning, *J Am Chem Soc 136*, 12489-12497.
[377] Schmidt, E., and Guntert, P. (2012) A new algorithm for reliable and general NMR resonance assignment, *J Am Chem Soc 134*, 12817-12829.
[378] Xie, H., Zhao, Y., Wang, J., Zhang, Z., and Yang, J. (2018) Solid-state NMR chemical shift assignments of aquaporin Z in lipid bilayers, *Biomol NMR Assign 12*, 323-328.
[379] Kitchen, P., Salman, M. M., Halsey, A. M., Clarke-Bland, C., MacDonald, J. A., Ishida, H., Vogel, H. J., Almutiri, S., Logan, A., Kreida, S., Al-Jubair, T., Winkel Missel, J., Gourdon, P., Tornroth-Horsefield, S., Conner, M. T., Ahmed, Z., Conner, A. C., and Bill, R. M. (2020) Targeting Aquaporin-4 Subcellular Localization to Treat Central Nervous System Edema, *Cell 181*, 784-799 e719.
[380] Calamita, G. (2000) The Escherichia coli aquaporin-Z water channel, *Mol Microbiol 37*, 254-262.

[381] Kitchen, P., Conner, M. T., Bill, R. M., and Conner, A. C. (2016) Structural Determinants of Oligomerization of the Aquaporin-4 Channel, *J Biol Chem 291*, 6858-6871.
[382] Crane, J. M., Rossi, A., Gupta, T., Bennett, J. L., and Verkman, A. S. (2011) Orthogonal array formation by human aquaporin-4: examination of neuromyelitis optica-associated aquaporin-4 polymorphisms, *J Neuroimmunol 236*, 93-98.
[383] Shi, Y. (2014) A glimpse of structural biology through X-ray crystallography, *Cell 159*, 995-1014.
[384] Bai, X. C., McMullan, G., and Scheres, S. H. (2015) How cryo-EM is revolutionizing structural biology, *Trends Biochem Sci 40*, 49-57.
[385] Dymowska, A. K., Hwang, P. P., and Goss, G. G. (2012) Structure and function of ionocytes in the freshwater fish gill, *Respir Physiol Neurobiol 184*, 282-292.
[386] Conte, F. P. (2012) Origin and differentiation of ionocytes in gill epithelium of teleost fish, *Int Rev Cell Mol Biol 299*, 1-25.
[387] Tingaud-Sequeira, A., Calusinska, M., Finn, R. N., Chauvigne, F., Lozano, J., and Cerda, J. (2010) The zebrafish genome encodes the largest vertebrate repertoire of functional aquaporins with dual paralogy and substrate specificities similar to mammals, *BMC Evol Biol 10*, 38.
[388] Cutler, C. P., and Cramb, G. (2000) Water transport and aquaporin expression in fish, In *Molecular biology and physiology of water and solute transport*, pp 433-441, Springer.
[389] Canessa Fortuna, A., Zerbetto De Palma, G., Aliperti Car, L., Armentia, L., Vitali, V., Zeida, A., Estrin, D. A., and Alleva, K. (2019) Gating in plant plasma membrane aquaporins: the involvement of leucine in the formation of a pore constriction in the closed state, *The FEBS journal 286*, 3473-3487.
[390] Madeira, A., Moura, T. F., and Soveral, G. (2016) Detecting Aquaporin Function and Regulation, *Front Chem 4*, 3.
[391] Cerda, J. (2009) Molecular pathways during marine fish egg hydration: the role of aquaporins, *J Fish Biol 75*, 2175-2196.
[392] Lubzens, E., Young, G., Bobe, J., and Cerda, J. (2010) Oogenesis in teleosts: how eggs are formed, *Gen Comp Endocrinol 165*, 367-389.
[393] Torres, M. A. (2010) ROS in biotic interactions, *Physiol Plant 138*, 414-429.
[394] Yukutake, Y., Tsuji, S., Hirano, Y., Adachi, T., Takahashi, T., Fujihara, K., Agre, P., Yasui, M., and Suematsu, M. (2008) Mercury chloride decreases the water permeability of aquaporin-4-reconstituted proteoliposomes, *Biol Cell 100*, 355-363.
[395] Lambert, O., Levy, D., Ranck, J. L., Leblanc, G., and Rigaud, J. L. (1998) A new "gel-like" phase in dodecyl maltoside-lipid mixtures: implications in solubilization and reconstitution studies, *Biophys J 74*, 918-930.

[396] McReynolds, A. C., Karra, A. S., Li, Y., Lopez, E. D., Turjanski, A. G., Dioum, E., Lorenz, K., Zaganjor, E., Stippec, S., McGlynn, K., Earnest, S., and Cobb, M. H. (2016) Phosphorylation or Mutation of the ERK2 Activation Loop Alters Oligonucleotide Binding, *Biochemistry 55*, 1909-1917.

[397] Bienert, G. P., and Chaumont, F. (2014) Aquaporin-facilitated transmembrane diffusion of hydrogen peroxide, *Biochim Biophys Acta 1840*, 1596-1604.

[398] Almasalmeh, A., Krenc, D., Wu, B., and Beitz, E. (2014) Structural determinants of the hydrogen peroxide permeability of aquaporins, *FEBS J 281*, 647-656.

[399] Montiel, V., Bella, R., Michel, L. Y. M., Esfahani, H., De Mulder, D., Robinson, E. L., Deglasse, J. P., Tiburcy, M., Chow, P. H., Jonas, J. C., Gilon, P., Steinhorn, B., Michel, T., Beauloye, C., Bertrand, L., Farah, C., Dei Zotti, F., Debaix, H., Bouzin, C., Brusa, D., Horman, S., Vanoverschelde, J. L., Bergmann, O., Gilis, D., Rooman, M., Ghigo, A., Geninatti-Crich, S., Yool, A., Zimmermann, W. H., Roderick, H. L., Devuyst, O., and Balligand, J. L. (2020) Inhibition of aquaporin-1 prevents myocardial remodeling by blocking the transmembrane transport of hydrogen peroxide, *Sci Transl Med 12*.

[400] Vieceli Dalla Sega, F., Zambonin, L., Fiorentini, D., Rizzo, B., Caliceti, C., Landi, L., Hrelia, S., and Prata, C. (2014) Specific aquaporins facilitate Nox-produced hydrogen peroxide transport through plasma membrane in leukaemia cells, *Biochim Biophys Acta 1843*, 806-814.

[401] Smirnoff, N., and Arnaud, D. (2019) Hydrogen peroxide metabolism and functions in plants, *New Phytol 221*, 1197-1214.

[402] Maccarrone, G., Bonfiglio, J. J., Silberstein, S., Turck, C. W., and Martins-de-Souza, D. (2017) Characterization of a Protein Interactome by Co-Immunoprecipitation and Shotgun Mass Spectrometry, *Methods Mol Biol 1546*, 223-234.

[403] Freites, J. A., Nemeth-Cahalan, K. L., Hall, J. E., and Tobias, D. J. (2019) Cooperativity and allostery in aquaporin 0 regulation by Ca(2), *Biochim Biophys Acta Biomembr 1861*, 988-996.

[404] Kalman, K., Nemeth-Cahalan, K. L., Froger, A., and Hall, J. E. (2008) Phosphorylation determines the calmodulin-mediated Ca2+ response and water permeability of AQP0, *J Biol Chem 283*, 21278-21283.

[405] Horstman, A., Tonaco, I. A., Boutilier, K., and Immink, R. G. (2014) A cautionary note on the use of split-YFP/BiFC in plant protein-protein interaction studies, *Int J Mol Sci 15*, 9628-9643.

[406] Kerppola, T. K. (2006) Design and implementation of bimolecular fluorescence complementation (BiFC) assays for the visualization of protein interactions in living cells, *Nat Protoc 1*, 1278-1286.

[407] Kodama, Y., and Hu, C. D. (2012) Bimolecular fluorescence complementation (BiFC): a 5-year update and future perspectives, *Biotechniques 53*, 285-298.

[408] Shyu, Y. J., Suarez, C. D., and Hu, C. D. (2008) Visualization of ternary complexes in living cells by using a BiFC-based FRET assay, *Nat Protoc 3*, 1693-1702.
[409] Hu, H., Zhang, H., Wang, S., Ding, M., An, H., Hou, Y., Yang, X., Wei, W., Sun, Y., and Tang, C. (2017) Live visualization of genomic loci with BiFC-TALE, *Sci Rep 7*, 40192.
[410] Kwaaitaal, M., Keinath, N. F., Pajonk, S., Biskup, C., and Panstruga, R. (2010) Combined bimolecular fluorescence complementation and Forster resonance energy transfer reveals ternary SNARE complex formation in living plant cells, *Plant Physiol 152*, 1135-1147.
[411] Bagher, A. M., Kelly, M. E. M., and Denovan-Wright, E. M. (2019) Combining SRET(2) and BiFC to Study GPCR Heteromerization and Protein-Protein Interactions, *Methods Mol Biol 1947*, 199-215.
[412] Waich, K., Mayr, T., and Klimant, I. (2008) Fluorescence sensors for trace monitoring of dissolved ammonia, *Talanta 77*, 66-72.
[413] Timmer, B., Olthuis, W., and Berg, A. v. d. (2005) Ammonia sensors and their applications—a review, *Sensors and Actuators B: Chemical 107*, 666-677.
[414] Das, T., Pramanik, A., and Haldar, D. (2017) On-line Ammonia Sensor and Invisible Security Ink by Fluorescent Zwitterionic Spirocyclic Meisenheimer Complex, *Sci Rep 7*, 40465.
[415] Mroz, E. A., Roman, R. J., and Lechene, C. (1982) Fluorescence assay for picomole quantities of ammonia, *Kidney Int 21*, 524-527.

I

PAPER I

Efficient production of pure and catalytically active SIRT2 in *Pichia pastoris*

Florian Schmitz,[†] Kristina Luthman,[ǂ] Elina M. Jarho,[‡] Kristina Hedfalk,[†*] Tina Seifert[ǂ*]

[†]Department of Chemistry and Molecular Biology, Biochemistry, University of Gothenburg, P.O. Box 462, 405 30 Göteborg, Sweden

[ǂ]Department of Chemistry and Molecular Biology, Medicinal Chemistry, University of Gothenburg, Kemivägen 10, 412 96 Göteborg, Sweden

[‡]School of Pharmacy, University of Eastern Finland, P.O. Box 1627, 70211 Kuopio, Finland

Correspondence to: Tina Seifert, tina.seifert@gu.se; Kristina Hedfalk, kristina.hedfalk@gu.se

Sirtuin 2 (SIRT2) is an enzyme that catalyzes the removal of acyl groups from the side chain of the amino acid lysine, and, having that activity, this target has a putative involvement in cancer and neurodegenerative diseases. Being an interesting drug target, we looked for a suitable eukaryotic protein production system for further medicinal chemistry and biochemical applications, and the yeast *P. pastoris* was selected. In this study we report a high yield of catalytically active protein, more than 40 mg/L, after a three step purification procedure. Furthermore, we show that the recombinant SIRT2 is thermostable, able to catalyse lysine deacylation reactions and amendable for photoaffinity labelling studies. All together, we hereby present a protocol for monodisperse SIRT2 highly suitable for structural attempts and further characterization of the inhibitor binding site using a MS supported approach.

Sirtuins (SIRTs) are a conserved family of enzymes catalyzing the removal of different acyl groups from the side chain amino moiety of lysine residues in numerous protein substrates. Thereby various key biological processes related to gene silencing, cell cycle regulation, inflammation, stress, DNA damage and repair responses can be controlled. Thus SIRTs have received attention as potential therapeutic targets.[1] In particular SIRT2 has been considered as a disease modifying protein target due to its potential involvement in the development of cancer and neurodegenerative disorders.[2-5]

We have previously reported potent chroman-4-one based SIRT2 selective inhibitors which have shown to possess anti-proliferative effects.[6, 7] In order to gain knowledge about the binding mode and to support our continued compound design process we have carried out docking studies which have provided a binding mode which is in line with our acquired structure-activity relationship (SAR) data. Now, we are interested to put further efforts into the experimental verification of the suggested binding mode of the chroman-4-one based SIRT2 inhibitors by continuation of our photoaffinity labeling (PAL) strategy[8] and initiation of co-crystallization experiments.

To investigate the biological effects of sirtuin activity and their downstream events in cell based studies, sirtuin isoforms are commonly overexpressed in mammalian cell lines.[9, 10] However, for biomedical characterization, such as structural characterization, a robust protein production method needs to be developed which gives access to high yields of a stable protein product. hSIRT2 and truncated versions[11] have previously been produced for structural or interaction analysis as well as inhibition studies, where the dominating host has been *Escherichia coli*.[12-16] As it seems, the highest reported yield of a hSIRT2 construct (AA 50–356) is more than 10 mg IMAC purified protein per L culture of *E. coli* grown on minimal media, where the protein sample was used for NMR studies.[16] However, commonly it is non-trivial to compare the final yield of the recombinant protein since that is apparently not the main scope of most studies.

Producing a human target in a prokaryotic host has its limitations, especially when it comes to post-translational modifications (PTMs) which are often connected to protein activity. For sirtuins, specifically, there are many reports on the importance of PTMs for proper regulation.[17-19] For our PAL experiments and co-crystallization trials we therefore looked for a suitable eukaryotic host for producing $hSIRT2_{56-356}$, a truncate that has been shown suitable for application in *in vitro* assays and crystallization trials.[11] The yeast *Pichia pastoris* is a unicellular eukaryote that combines high-production levels with functional recombinant protein product and is capable of performing most of the PTMs from higher eukaryotes.[20-22] To our knowledge, only SIRT4 has been produced using this eukaryotic host.[23] Based on our previous successes, mainly producing complex membrane proteins in *P. pastoris*, we also included SIRT2 in our repertoire.[24-27] In conclusion, we achieved a highly pure and homogenous sample of $hSIRT2_{56-356}$ with a yield of at least 40 mg/L, which is about four times higher than previously reported. Notably, the protein has been shown to be both stable and catalytically active in enzyme inhibition studies.

Materials and Methods

Cloning of recombinant $hSIRT2_{56-356}$ for expression in *P. pastoris*

The gene optimized $hSIRT2_{56-356}$ plasmid was purchased from GeneScript, cloned in the pPICZB vector (Invitrogen) with the consensus sequence AAA ATG G around the start methionine and a *C*-terminal 8x His-tag. Before transformation by electroporation (BioRad GenePulser Xcell, *P. pastoris* pre-settings) into the wild type *P. pastoris* strain X-33 (Invitrogen), the

plasmid was linearized using the restriction enzyme *Pme*I.

Production screening for high yielding clones

After transformation, *P. pastoris* cells were grown on YPD agara plates containing a high Zeocin concentration (2000 µg/mL) in order to screen for transformants having the expression cassette with SIRT2 inserted multiple times in the genome. Six transformants of X33/pPIZB-hSIRT2$_{56-356}$-His$_8$ were screened for initial protein production (Invitrogen EasySelect Pichia) in order to find a high yielding clone suitable for final expression in the fermenter system. The small-scale production was performed in duplicates with two non-target samples and cells without transformed plasmid as controls. Cells were incubated overnight, 180 rpm and 30 °C, and the precultures were diluted in 5 mL BMGY the next day to OD_{600}=1. At OD_{600} =3.5-4.5, the cells were harvested and tested for hSIRT2 production. Cell samples were mixed in 2x SDS loading buffer (46 µL 4x Laemmli sample buffer (BioRad), 20 mM DTT, 50 µL mq H_2O) and heated up to 100 °C for 10 min. Cell debris and unbroken cells were collected by centrifugation at 13,000 g for 3 min. The final supernatant, 10 µL, was loaded on an SDS-PAGE gel (Mini-PROTEAN TGX, 4-20 % polyacrylamide, BioRad; 300V, 16 min). The protein signal was detected by using immunoblot using ECL substrate (Pierce Fast Western Blot Kit, Thermo Fisher) and chemiluminescence was analyzed via an imager system (ChemiDoc MP, BioRad).

Large scale growth of hSIRT2$_{56-356}$-His$_8$

To ensure and optimize recombinant hSIRT2 production, a high expression clone of *P. pastoris* producing hSIRT2$_{56-356}$-His$_8$ was grown at 30 °C in a 3 L fermenter (Minifors 2, INFORS HT) containing initial basal salts medium volume, 1.5 L with PTM1 trace salts (Sunrise Science), 7 mL.[28] The initial fermentation volume was inoculated by a pre-culture; 50 mL and OD_{600} = 4-7. After 24 h, the initial glycerol carbon source was consumed, and glycerol was feeded with a 50% solution (v/v in water) for another 24 h to increase biomass; 282 mL was consumed. Overexpression of recombinant hSIRT2$_{56-356}$ was induced by feeding the culture with 100% methanol solution for 48 h, approximately 250 mL was consumed, and a total cell mass of 342 g cells was harvested.

Purification of recombinant hSIRT2$_{56-356}$

The purification process was carried out according to the protocol for bacterial expression of hSIRT2.[16] In brief, the frozen cell pellet, 100 g, was thawn in 200 mL lysis buffer (20 mM Tris–HCl, pH 8.0, 200 mM NaCl, 10 mM imidazole, 2 mM β-mercaptoethanol, 0.1 % v/v Triton X-100, Roche Diagnostics Complete EDTA-free anti-proteases cocktail) and cells were broken using a beadbeater with 0.5 mm glass beads for breakage (5x30 s, 1 min pause in between, 4 °C, Bead-Beater, Biospec Products). Unbroken cells and debris were collected by centrifugation, 500xg for 30 min. For purification of hSIRT2$_{56-356}$-His$_8$, the supernatant was loaded on a pre-equilibrated 5 mL Ni-NTA HisTrap HP column (GE Healthcare), pre-equilibrated with three CV lysis buffer, and cycled for at least 12 h at 4 °C. Non-specifically bound proteins were removed by washing the column matrix with 3 CV wash buffer (20 mM Tris–HCl, pH 8.0, containing 200 mM NaCl, 10 mM imidazole, and 2 mM β-mercaptoethanol, 0.1% v/v Triton X-100) and loosely attached proteins were removed by a step gradient using three CV wash buffer containing 50 mM imidazole. Protein, hSIRT2$_{56-356}$-His$_8$, was eluted with five CV elution buffer (20 mM Tris–HCl, pH 8.0, containing 200 mM NaCl, 300 mM imidazole, and 2 mM β-mercaptoethanol, 0.1 % v/v Triton X-100) and collected in fractions. Protein fractions were analyzed using SDS-PAGE and hSIRT2 containing fractions were pooled together and

concentrated (30 kDa cut-off, Sartorius). The homogeneity of the of hSIRT2$_{56-356}$-His$_8$, target was verified using size exclusion chromatography (Superdex200 increased, GE Healthcare), with a buffer containing 50 mM Tris pH 7.5, 100 mM NaCl, 5% glycerol, and 5 mM DTT. To increase the purity of the protein, a subsequent gel filtration step was performed with the concentrated sample of the main peak.

Protein stability measurements

To evaluate the stability of purified hSIRT2$_{56-356}$, samples from each SEC step were analyzed on a Prometheus instrument (NanoTemper Technologies) using a sample volume of 10 µL per capillary. The capillaries were filled directly from the respective solution without laborious sample loading or sealing steps. Data analysis was performed using the Prometheus software packages PR.ThermControl, PR.ChemControl and PR.TimeControl. The initial fluorescence scan of loaded capillaries was performed at 20 °C. The emission at 330 nm and 350 nm showed that all samples were within the optimal concentration range. For evaluation of the thermostability, samples were subjected to a temperature ramp of 2 °C/min from 20 °C to 90 °C and fluorescence was constantly monitored. Data was analysed with the PR.ThermControl software.

In Vitro Fluor de Lys Assay for SIRT2 Activities

The Fluor de Lys fluorescence assays were based on the method described in the BioMol product sheet (Enzo Life Sciences) using the peptide substrate Gln-Pro-Lys-Lys(ε-acetyl)-AMC. The determined K_m values of SIRT2 for the peptide substrate was 103 µM and for NAD^+ 350 µM. Briefly, assays were carried out using the Fluor de Lys acetylated peptide substrate at a concentration corresponding to 0.7 K_m and NAD^+ (KI282) at a concentration corresponding to 0.9 K_m, recombinant SIRT2$_{56-356}$-His$_8$ enzyme and SIRT assay buffer (KI286). The buffer, Fluor de Lys acetylated peptide substrate, NAD^+ and DMSO/compounds in DMSO (2.5 µL in 50 µL total reaction volume) and the reaction was started by adding the enzyme. The reaction mixture was incubated for 1 h at 37 °C. After that, Fluor de Lys developer (KI176) and nicotinamide (KI283) were added, and the incubation was continued for 45 min at 37 °C. Fluorescence readings were obtained using a Safire^2 Multi-mode plate reader (Tecan) with excitation wavelength 370 nm and emission 460 nm.

The IC_{50} values were determined as two or three independent determinations with 8−10 different inhibitor concentrations in each determination. The collected data points were included in the calculation of the best-fit value for nonlinear curve fitting with GraphPad Prism8 (GraphPad Software, Inc.).

Synthesis of the bifunctional chroman-4-one based PAL probe 11

The synthetic pathway towards PAL probe **11** is illustrated in **Scheme 1** (see the **Supplementary** for more detailed information). 1,12-Dodecanediol was mono-protected using TBDMSCl and imidazole in DMF and the remaining unprotected hydroxyl group was oxidized using a Swern oxidation. The formed aldehyde was reacted with 5-bromo-2-hydroxyacetopheone in a base-promoted one-pot reaction to form the desired chroman-4-one derivative which after isolation was directly used in a subsequent reduction step with $NaBH_4$ to obtain the 4-chromanol **3** in 64% yield over two steps. The newly formed alcohol group was protected with TBDMSCl. For the installation of the light-sensitive diazirine moiety, compound **4** was treated with *n*-BuLi and ethyl trifluoroacetate to introduce a trifluoroacetyl group. A reaction of the ketone with *N*-hydroxylamine in pyridine at 70 °C provided oxime **6** in a 1:1 isomeric mixture. Tosylation of **6** with TsCl in the presence of Et_3N and DMAP in CH_2Cl_2 yielded intermediate **7** which was reacted

with liquid ammonia, the following oxidation step with iodine furnished the photoreactive diazirine moiety. Deprotection of the two alcohols was achieved using TBAF in THF followed by selective oxidation of the benzylic alcohol using MnO_2 as oxidant. The desired PAL probe **11** was obtained in 86% yield after amide coupling of **10** with biotin applying EDC-HCl as coupling agent in the presence of DMAP.

Scheme 1. Synthesis of biotin-functionalized diazirine-based chroman-4-one probe.[a]

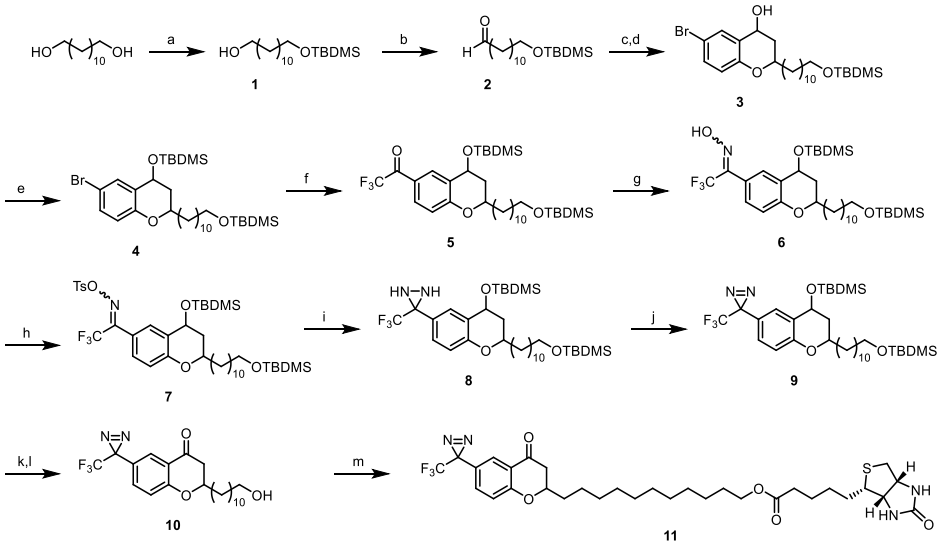

[a]Reagents and conditions: (a) TBDMSCl, imidazole, DMF, rt, 45 min, 45%; (b) $(COCl)_2$, DMSO, Et_3N, THF, -78 °C→rt, 98%; (c) 5'-Bromo-2-hydroxyacetophenone, DIPA, EtOH, MW, 170 °C, 2 h; (d) $NaBH_4$, MeOH, rt, 5 min, 64% over 2 steps; (e) TBDMSCl, imidazole, CH_2Cl_2, rt, 7 h, 98%; (f) *n*-BuLi, ethyl trifluoroacetate, THF, –78 °C→rt, 18 h, 79%; (g) $NH_2OH{\cdot}HCl$, py, 70 °C, 16 h, 94%; (h) TsCl, Et_3N, DMAP, CH_2Cl_2, rt, 5 h; (i) NH_3(l), CH_2Cl_2, -78 °C→rt, 17h; (j) I_2, Et_3N, CH_2Cl_2, rt, 2 h, 67% over 3 steps; (k) TBAF, THF, rt, 6 h; (l) MnO_2, CH_2Cl_2, rt, 44 h, 77% over 2 steps; (m) biotin, EDC · HCl, DMAP, DMF, rt, 6h, 86%.

Photoaffinity labeling experiment

The hSIRT2$_{56-356}$ protein expressed in *P. pastoris* was used in the experiments. For the labeling reactions, the photoprobe **11** in DMSO (final concentration of 0−600 µM, 2.5 µL in 50 µL total volume) and recombinant SIRT2$_{56-356}$ enzyme (10 µL, 3.8 mg/mL) were mixed in buffer (HDAC buffer) at room temperature in the dark, and the mixture was incubated for 5 min at 22 °C protected from light. After incubation, the samples were irradiated with a high-power UV LED (λ = 365 nm, 2 cm from the LED, light flux: 23 mW/cm^2) for 3 x 15 s and a resting period of 10 s. For the competition experiments, **KE-091** in DMSO (final concentration of 0−200 µM, 2.5 µL in 50 µL total volume) and photoprobe **11** in DMSO (final concentration of 200 µM, 2.5 µL in 50 µL total volume) were added to the buffer (HDAC buffer) prior to the addition of SIRT2$_{56-356}$. The samples were subjected to SDS Page and Western blotting to detect labelled protein using a streptavidin-HRP conjugate.

Results

High expression levels of recombinant hSIRT2$_{56-356}$ is achieved in *P. pastoris*

P. pastoris provides a eukaryotic host suitable for producing protein targets from human origin with a potential for high protein yields as well as correct post translational modifications. To make use of these attributes, target protein hSIRT2$_{56-356}$ was cloned into the pPIZB-His$_8$ vector, which was linearized and transformed into the wild-type X33 *P. pastoris* strain. After Zeocin selection, six fast growing colonies were tested for a small-scale protein production. The clone with the highest hSIRT2$_{56-356}$ production, as verified by immunoblot (data not shown), was selected for large scale growth using a 3 L fermenter. Under tightly controlled conditions, a total cell mass of 342 g wet weight could be obtained from 1.5 L initial basal salt medium, resulting in approximately 2 L of final culture volume. The production of hSIRT2$_{56-356}$ resulted in a stable protein product with the expected molecular weight of 35 kDa. The overall expression level was approximately 5% of hSIRT2$_{56-356}$ of the total protein content. A three step purification procedure consisting of one IMAC step and two following gel filtrations resulted in a highly pure and homogenous sample for further analysis. The whole purification process resulted in a 20-fold concentration of the targeted protein in comparison to the lysate and a final protein yield of 0.17 mg hSIRT2$_{56-356}$ per gram cells (**Table 1**). The additional size exclusion chromatography (SEC) step was accompanied with an 89% protein loss, resulting in 39 mg hSIRT2$_{56-356}$ per litre initial fermentation volume in comparison to 415 mg after the first SEC step. In conclusion, the target hSIRT2$_{56-356}$ was produced in high levels in *P. pastoris* and could be purified to homogeneity providing samples for crystallography or enzymatic assays.

Table 1. Overview of the purification of hSIRT2$_{56-356}$. Total protein content and the amount of hSIRT2$_{56-356}$, respectively, are given for 100 g of wet cells. Purity, recovery and fold of purification are also stated in the lysate as well as after the full purification procedure, after the second SEC.

Purification Step	Total protein (mg)	hSIRT2 (mg)	Purity (%)	Recovery (%)	Fold of purification
Lysate	46151	2146	5	1	1
2. SEC	17	17	100	0.8	20

A three-step purification process results in highly pure and homogenous hSIRT2$_{56-356}$

P. pastoris cells were mechanically lysed using a bead beater and the His-tag (His_8) fused to hSIRT2$_{56-356}$ was captured from the background cell proteins by Ni^{2+} IMAC purification. After elution, hSIRT2$_{56-356}$ was detected at the expected molecular weight (35 kDa) on an SDS-PAGE gel, together with a band at 50 kDa (**Fig. 1A**), being a protein contamination of serine hydroxymethyl transferase in the purification process, as verified by mass spectrometry (see **Supplementary Fig. 1** and **Table 1**). An immunoblot confirmed the overexpression of hSIRT2$_{56-356}$ in the cells and the importance of using affinity chromatography to achieve high purity (**Fig. 1B**). The highly specific immunoblot analysis also revealed the presence of a 70 kDa hSIRT2$_{56-356}$ fraction, not visible on SDS gel, being a putative dimeric form of the target protein.

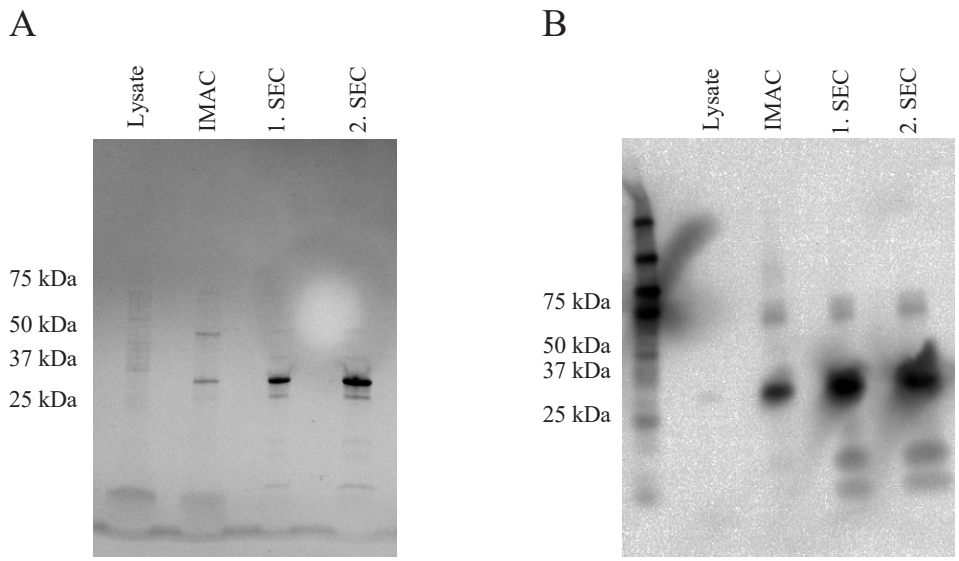

Figure 1. Purification of hSIRT2$_{56-356}$ from *P. pastoris*. (A) SDS-PAGE gel showing the pooled fractions after each purification step with the corresponding immunoblot shown in (B). A dominating band of the expected molecular weight of 35 kDa is observed in all purified fractions. The immunoblot also show a putative dimeric form of the target protein at 70 kDa as well as some putative degradation products.

A subsequent SEC showed a peak at 15 mL containing hSIRT2$_{56-356}$ with the correct size of 35 kDa, as verified by SDS-PAGE combined with immunoblot analysis. Notably, the main peak from the first SEC was accompanied by a shoulder peak. When analyzed by SDS-PAGE, the 50 kDa protein was the dominating protein in this peak (**Fig. 2A**), but this band was not pronounced for the pooled fraction on the immunoblot (**Fig. 1B**). Thus, the first SEC step provided a constructive purification step for hSIRT2$_{56-356}$ which was separated from the contaminating 50 kDa protein product. The purity of hSIRT2$_{56-356}$ after the first SEC can be sufficient for activity assays, but for crystallization approaches, a higher demand for a monodisperse peak is required. To fulfil this criterion and obtain hSIRT2$_{56-356}$ of highest purity and uniformity, a second SEC was performed with pooled fractions 11 and 12 from the previous gel filtration. The obtained hSIRT2$_{56-356}$ protein sample indeed showed monodisperse behaviour as well as high purity validated by SDS-PAGE.

Immunoblot analysis of concentrated hSIRT2$_{56-356}$ after the second gel filtration showed similar size and band pattern as after first SEC, indicating a similar purity. The 50 kDa impurity band seen on the SDS-PAGE after the first SEC was efficiently removed and a monomeric form of hSIRT$_{56-356}$ achieved (**Fig. 2B**). Worth noting is that hSIRT2$_{56-356}$ appears as a double band in the purified fraction (**Fig. 1A**) where both bands corresponds to full-lengths products of the protein target (**Supplementary Fig. 1** and **Table 1**), which opens up for the possibility that recombinant SIRT2 produced in *P. pastoris* has some PTMs.

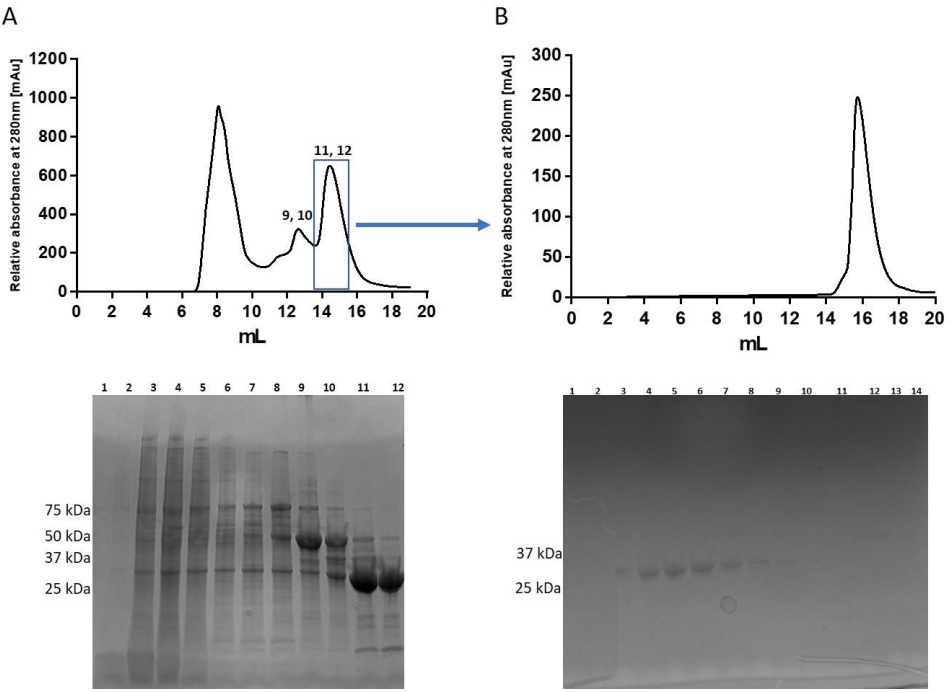

Figure 2. Purification of SIRT2$_{56-356}$ using SEC. (A) The chromatogram from the first SEC where samples covering all peaks are analysed using SDS-PAGE, as shown below. The last peak (lanes 11 and 12) mainly contains the monomeric form of the protein while the peak before (lanes 9 and 10) contains more of the contaminating protein at 50 kDa. (B) Chromatogram showing the second SEC where the last peak from the first SEC is pooled and purified again to achieve a highly pure and homogenous hSIRT2$_{56-356}$ sample. Samples from the SEC peak were analysed using SDS-PAGE, shown below. Lanes 3-10 represent the elution peak from 14–20 mL.

Recombinantly produced hSIRT2$_{56-356}$ is thermostable

The size exclusion chromatogram showed that hSIRT2$_{56-356}$ can be produced with high quality indicated by monodispersity and supported by SDS-PAGE showing a monomeric form of the protein. In order to evaluate the stability of the recombinant protein product, hSIRT2 samples from both gel filtration runs were tested for thermostability (**Fig. 3**) using microscale thermophoresis. In general, higher thermal denaturation temperatures indicate a more stable protein. The measurements for each SEC run were performed in triplicates and the average first derivative of the melting scans fluorescence ratios (350 nm / 330 nm) was evaluated. After the first SEC, the average was 42.97 °C and after the second SEC it was 45.33 °C. Thus, the second SEC

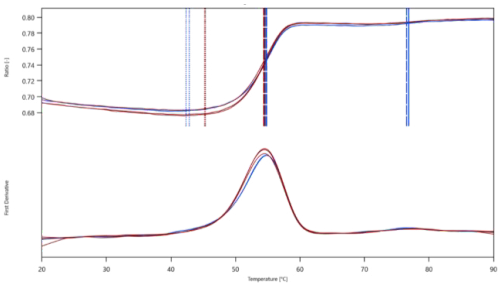

Figure 3. Microscale thermophoresis measurements of hSIRT2. Upper part: Melting Scan of samples SIRT2-1.SEC (blue) and SIRT2-2.SEC (red), showing the fluorescence ratio (350 nm/330 nm) in the top panel and the first derivative in the lower panel. Thermal unfolding onsets (ON) and unfolding transitions (Tm) are indicated by vertical lines in the graph. Lower Picture: Time control profile of samples SIRT2-1.SEC (blue) and SIRT2-2.SEC (red).

run had a positive effect on the thermostability of hSIRT2$_{56-356}$, as the stability was improved by 2.36 °C in average. This improvement went along with a 90% loss in protein yield between the purification steps, which might be negligible if homogeneity of the sample is crucial. However, since the overall production level of hSIRT2$_{56-356}$ was very high in *P. pastoris* (**Table 1**) a three step purification procedure could be afforded, still giving a high final yield of the desired protein.

Biochemical evaluation of SIRT2

The production of hSIRT2$_{56-356}$ in *P. pastoris* yields a catalytically active enzyme that effectively catalyzes lysine deacetylation reactions. The K_m values of NAD^+ and the acetylated peptide substrate Gln-Pro-Lys-Lys(ε-acetyl)-AMC used in the assay has been determined to be 350 µM and 103 µM, respectively. The enzyme has been successfully applied in the assessment of SIRT2 inhibitors for which the protein from the first SEC step shows sufficient purity and stability. The obtained inhibitory values and IC_{50} data are in line with our previously determined data; also two compounds reported in the literature (**Table 2**) gave similar results.[29]

The evaluation of the inhibitory activity of the bifunctional PAL probe **11** has identified an IC_{50} value of 100 µM (see **Supplementary**, **Fig. 2**). Efforts in developing more potent PAL probes were unfortunately unsuccessful.

Table 2. Results from inhibition of SIRT2$_{56-356}$ using various known inhibitors[a]

Entry	Structure	Inh.% at 200 µM	IC_{50}
1[b]	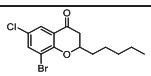	83% ± 1.2	2.26 µM ± 0.13
2[c]	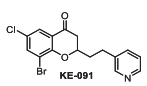 KE-091	79% ± 1.8	-
3[d]	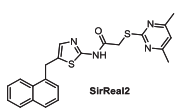 SirReal2	-	0.47 µM ± 0.12
4[e]	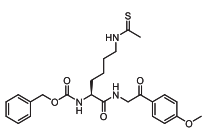	-	4.3 µM ± 2.5

[a]Literature values given as footnotes; [b]88%, IC_{50} 4.3 µM[6]; [c]82%, IC_{50} 5,5 µM[7]; [d]IC_{50} 0.4 µM[11]; [e]IC_{50} 2.53 µM[29]

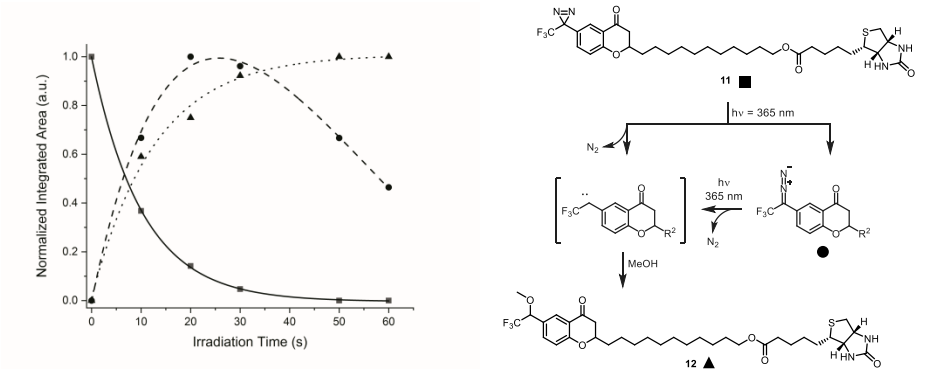

Figure 4. HPLC analysis of photolysis solution of diazirine **11** in MeOH upon irradiation with 365 nm light. Samples taken after t = 0, 10, 20, 30, 50, 60 s of UV irradiation were injected on the column (reversed-phase, C18). Integration of the absorption peaks in the chromatogram (UV detection at 254 nm) shows the rapid photo-conversion of **11** (squares) directly into the insertion product **12** (triangles) or partially via formation of a diazo isomer (circles).

Evaluation of photochemical properties and labelling capability of 11 with hSIRT2$_{56-356}$

The photochemical decomposition of the bifunctional PAL probe **11** was evaluated using HPLC analysis (**Fig. 4**). Aliquots from a solution of **11** in methanol were taken at defined time points during irradiation with 365 nm delivered by a high-power LED. The HPLC analysis shows the expected formation of the insertion product **12** over time concurrent with the decay of **11** and build-up and decline of the diazo by-product.

In subsequent experiments, we have performed labeling experiments of our produced hSIRT2$_{56–356}$ with varying concentrations of **11** (**Fig. 5**). For the detection of a successful cross-linking of the probe with SIRT2, the biotin moiety is utilized as a detection handle in Western blot analysis applying a streptavidin-horseradish peroxidase (HRP) conjugate. The Western blot showed clearly a dose-depended incorporation of the probe into hSIRT2$_{56-356}$. Also, a competition experiment (**Fig. 6**) with the known chroman-4-one-based inhibitor **KE-091** showed a decrease in labeling efficacy of **11** with increasing concentration of **KE-091**.

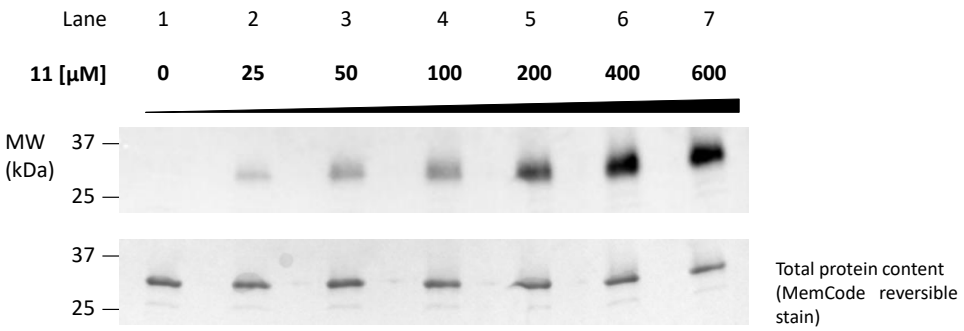

Figure 5. Dose-depended labeling of SIRT2$_{56-356}$ with **11.**

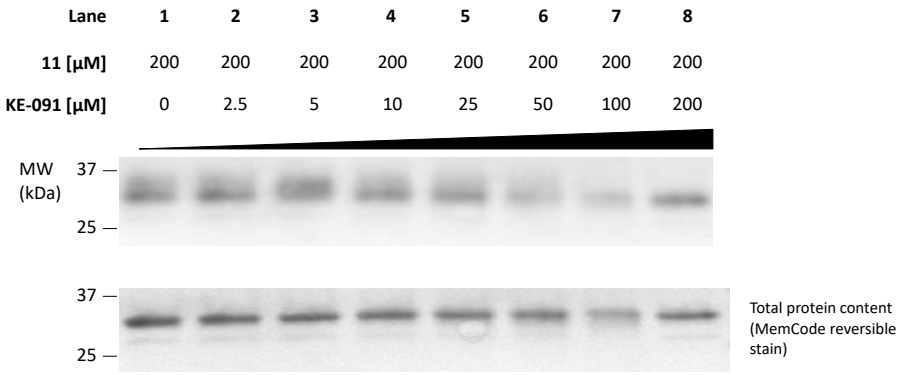

Figure 6. Competition experiment of **11** with the known chroman-4-one based SIRT2 inhibitor **KE-091**.

Base-promoted hydrolysis of the ether adduct 12

To investigate the binding site of the chroman-4-ones we are planning to follow a similar approach as previously published where the labelled $hSIRT_{56-356}$ was treated with trypsin and then subjected to MS-MS analysis to identity the incorporation site of **11**.[8] However, in contrast to our previous report, an enrichment step using an affinity resin utilizing the biotin moiety in **11** as a tag will be included to remove non-labelled protein prior to the tyrosination. The release of captured biotinylated compounds from the typically used avidin beads requires harsh conditions, therefore it was planned perform an on-bead ester hydrolysis to release the cross-linked protein fraction. To test this hypothesis, the ether adduct **12** formed after photolysis of diazirine **11** in MeOH was subjected to base-promoted hydrolysis in a Na_2HPO_4/NaOH buffer (pH 12) at 37 °C. The reaction was monitored by HPLC. The hydrolysis was proceeding slowly, after 48 h the main part was hydrolyzed (**Fig. 7**), no other products were formed. The experiment indicates that the ester can be successfully hydrolyzed using basic conditions and after filtering off the beads the labelled protein could then be analyzed further.

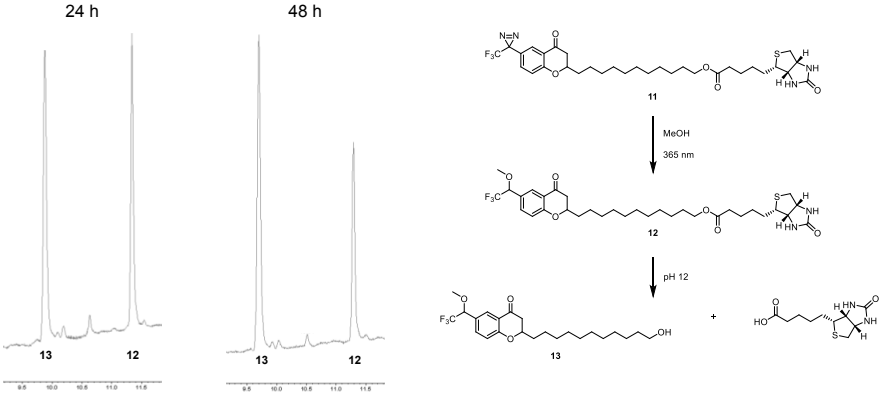

Figure 7. The hydrolysis of **12** was run in a Na_2HPO_4/NaOH buffer, pH 12.

Discussion

For a successful medicinal chemistry project, it is of utmost importance to have a protein of high quality as well as purity and, especially for structural approaches, a high production yield is required. The high quality aspects in consideration, is a mainly correctly folded protein product that is biologically active. Especially for human targets, a suitable protein production host has to be selected to assure proper PTMs as well as folding processes. For this particular study, we are interested in SIRT2, a putative target for cancer and neurodegenerative disorders. Being a human target, we aimed for a eukaryotic host system and found *P. pastoris* to be highly suitable for high level production of fully functional hSIRT2$_{56\text{-}356}$, which apparently is the first example of recombinant production of this specific sirtuin isoform in a eukaryotic host. As mentioned above, hSIRT4 is the only sirtuin isoform that has been produced in *P. pastoris* before,[23, 30] supporting the suitability of this yeast as host system for sirtuins. Worth noting, however, is that the yields of hSIRT4 were not clearly stated, hence, a proper comparison of the productions cannot easily be made.

It is not only the high yield that is of major importance for the structural approach, especially valid for crystallization involving many trial and error attempts consuming a lot of purified protein. In order to succeed with the actual crystal formation, a highly homogenous population of the protein is required and to tolerate the high concentration of the protein sample, a high protein stability is desired. The standardized way to evaluate the homogeneity of a sample is a qualitative evaluation of the elution peak in the SEC purification step. As seen for hSIRT2$_{56\text{-}356}$, a second SEC step was needed to achieve this monodisperse peak (**Fig. 2B**). This additional step was accompanied with a major loss of the protein of interest, which could be tolerated due to the high initial enrichment of hSIRT2 in the yeast cells (**Table 1**). Even though the combination of SDS gels and homogeneity from SEC are good indicators of a well-produced protein, they do not necessarily guarantee the desired biophysical properties. A complementing evaluation is therefore thermostability, which provides a key indicator for protein degradation, aggregation, precipitation, and folding instability [31, 32] Noteworthy, the stability of hSIRT2$_{56\text{-}356}$ was positively affected by the additional purification step, as verified by the thermostability evaluation (**Fig. 3**). Altogether, the purification procedure and the evaluation of the final product support a production of hSIRT2 in *P*. pastoris in high yields as well as high quality.

Already the protein fractions of hSIRT2$_{56\text{-}356}$ from the 1st SEC have shown to be catalytically active and are suitable for the application in the fluorescence based *in vitro* assay to assess the biological activity of SIRT2 inhibitors. The read out of the *in vitro* assay also allows the use of fractions with less homogeneity. However, in order to perform photoaffinity labeling studies, a protein of high purity is necessary to avoid off-target labeling with impurities, and to suppress the background noise in tandem mass spectrometric analyses originating from contaminations if affinity enrichment is omitted. We have also investigated the potential of the bifunctional probe **11** to be applied in PAL studies. Investigation of the photodecomposition of **11** in MeOH showed a complete photodecomposition of **11** within 60 s after exposure to UV-light and the expected MeOH insertion product **12** was formed which was accompanied by the undesired diazo pathway. We have shown that the bifunctional PAL probe **11** is binding covalently to hSIRT2$_{56\text{-}356}$. A competition experiment with the known chroman-4-one based SIRT2 inhibitor **KE-091** demonstrated that both compounds share the same binding site which verifies the suitability of **11** to elucidate the binding

site of the chroman-4-ones. In addition, the ester moiety in **11** can serve as a cleavable linker which allows the release of labeled proteins from affinity resin.

In conclusion, we present a successful protein production procedure in *P. pastoris* providing a highly pure and catalytically active hSIRT2 truncate. The high yielding production of a stable protein enables crystallization approaches and further characterization of SIRT2 with bound inhibitor, which is an ongoing research activity in our laboratories.

Acknowledgements

We thank Vinko Misetic at Nanotempertech, Germany, for the thermostability measurement of purified SIRT2 and Dr Annette Almgren, Food science, Chalmers University of Technology for the use of the fluorescent plate reader. We thank the Department of Chemistry and Molecular Biology, University of Gothenburg, for financial support. T.S. and K.L. thank the Swedish Research Council for project grant #2017-3984.

References

[1] Wang, Y., He, J., Liao, M., Hu, M., Li, W., Ouyang, H., Wang, X., Ye, T., Zhang, Y., and Ouyang, L. (2019) An overview of Sirtuins as potential therapeutic target: Structure, function and modulators, *Eur J Med Chem 161*, 48-77.

[2] de Oliveira, R. M., Vicente Miranda, H., Francelle, L., Pinho, R., Szego, E. M., Martinho, R., Munari, F., Lazaro, D. F., Moniot, S., Guerreiro, P., Fonseca-Ornelas, L., Marijanovic, Z., Antas, P., Gerhardt, E., Enguita, F. J., Fauvet, B., Penque, D., Pais, T. F., Tong, Q., Becker, S., Kugler, S., Lashuel, H. A., Steegborn, C., Zweckstetter, M., and Outeiro, T. F. (2017) The mechanism of sirtuin 2-mediated exacerbation of alpha-synuclein toxicity in models of Parkinson disease, *PLoS Biol 15*, e2000374.

[3] Outeiro, T. F., Kontopoulos, E., Altmann, S. M., Kufareva, I., Strathearn, K. E., Amore, A. M., Volk, C. B., Maxwell, M. M., Rochet, J. C., McLean, P. J., Young, A. B., Abagyan, R., Feany, M. B., Hyman, B. T., and Kazantsev, A. G. (2007) Sirtuin 2 inhibitors rescue alpha-synuclein-mediated toxicity in models of Parkinson's disease, *Science 317*, 516-519.

[4] Liu, Y., Zhang, Y., Zhu, K., Chi, S., Wang, C., and Xie, A. (2019) Emerging Role of Sirtuin 2 in Parkinson's Disease, *Front Aging Neurosci 11*, 372.

[5] Chopra, V., Quinti, L., Kim, J., Vollor, L., Narayanan, K. L., Edgerly, C., Cipicchio, P. M., Lauver, M. A., Choi, S. H., Silverman, R. B., Ferrante, R. J., Hersch, S., and Kazantsev, A. G. (2012) The sirtuin 2 inhibitor AK-7 is neuroprotective in Huntington's disease mouse models, *Cell Rep 2*, 1492-1497.

[6] Friden-Saxin, M., Seifert, T., Landergren, M. R., Suuronen, T., Lahtela-Kakkonen, M., Jarho, E. M., and Luthman, K. (2012) Synthesis and evaluation of substituted chroman-4-one and chromone derivatives as sirtuin 2-selective inhibitors, *J Med Chem 55*, 7104-7113.

[7] Seifert, T., Malo, M., Kokkola, T., Engen, K., Friden-Saxin, M., Wallen, E. A., Lahtela-Kakkonen, M., Jarho, E. M., and Luthman, K. (2014) Chroman-4-one- and chromone-based sirtuin 2 inhibitors with antiproliferative properties in cancer cells, *J Med Chem 57*, 9870-9888.

[8] Seifert, T., Malo, M., Lengqvist, J., Sihlbom, C., Jarho, E. M., and Luthman, K. (2016) Identification of the Binding Site of Chroman-4-one-Based Sirtuin 2-Selective Inhibitors using Photoaffinity Labeling in Combination with Tandem Mass

Spectrometry, *J Med Chem 59*, 10794-10799.
[9] Sinha, S., Patel, S., Athar, M., Vora, J., Chhabria, M. T., Jha, P. C., and Shrivastava, N. (2019) Structure-based identification of novel sirtuin inhibitors against triple negative breast cancer: An in silico and in vitro study, *Int J Biol Macromol 140*, 454-468.
[10] Laurent, G., German, N. J., Saha, A. K., de Boer, V. C. J., Davies, M., Koves, T. R., Dephoure, N., Fischer, F., Boanca, G., Vaitheesvaran, B., Lovitch, S. B., Sharpe, A. H., Kurland, I. J., Steegborn, C., Gygi, S. P., Muoio, D. M., Ruderman, N. B., and Haigis, M. C. (2013) SIRT4 coordinates the balance between lipid synthesis and catabolism by repressing malonyl CoA decarboxylase, *Mol Cell 50*, 686-698.
[11] Rumpf, T., Schiedel, M., Karaman, B., Roessler, C., North, B. J., Lehotzky, A., Olah, J., Ladwein, K. I., Schmidtkunz, K., Gajer, M., Pannek, M., Steegborn, C., Sinclair, D. A., Gerhardt, S., Ovadi, J., Schutkowski, M., Sippl, W., Einsle, O., and Jung, M. (2015) Selective Sirt2 inhibition by ligand-induced rearrangement of the active site, *Nat Commun 6*, 6263.
[12] Wang, Y., Fung, Y. M. E., Zhang, W., He, B., Chung, M. W. H., Jin, J., Hu, J., Lin, H., and Hao, Q. (2017) Deacylation Mechanism by SIRT2 Revealed in the 1'-SH-2'-O-Myristoyl Intermediate Structure, *Cell Chem Biol 24*, 339-345.
[13] Teng, Y. B., Jing, H., Aramsangtienchai, P., He, B., Khan, S., Hu, J., Lin, H., and Hao, Q. (2015) Efficient demyristoylase activity of SIRT2 revealed by kinetic and structural studies, *Sci Rep 5*, 8529.
[14] Hong, J. Y., Price, I. R., Bai, J. J., and Lin, H. (2019) A Glycoconjugated SIRT2 Inhibitor with Aqueous Solubility Allows Structure-Based Design of SIRT2 Inhibitors, *ACS Chem Biol 14*, 1802-1810.
[15] Pirrie, L., McCarthy, A. R., Major, L. L., Morkunaite, V., Zubriene, A., Matulis, D., Lain, S., Lebl, T., and Westwood, N. J. (2012) Discovery and validation of SIRT2 inhibitors based on tenovin-6: use of a (1)H-NMR method to assess deacetylase activity, *Molecules 17*, 12206-12224.
[16] Sun, C., Song, D., Marcotte, P. A., Richardson, P. L., and Hajduk, P. J. (2006) High-level bacterial expression and purification of human SirT2 protein for NMR studies, *Protein Expr Purif 48*, 56-60.
[17] Buler, M., Andersson, U., and Hakkola, J. (2016) Who watches the watchmen? Regulation of the expression and activity of sirtuins, *FASEB J 30*, 3942-3960.
[18] Revollo, J. R., and Li, X. (2013) The ways and means that fine tune Sirt1 activity, *Trends Biochem Sci 38*, 160-167.
[19] Santos, L., Escande, C., and Denicola, A. (2016) Potential Modulation of Sirtuins by Oxidative Stress, *Oxid Med Cell Longev 2016*, 9831825.
[20] Karbalaei, M., Rezaee, S. A., and Farsiani, H. (2020) Pichia pastoris: A highly successful expression system for optimal synthesis of heterologous proteins, *J Cell Physiol 235*, 5867-5881.
[21] Nieto-Taype, M. A., Garcia-Ortega, X., Albiol, J., Montesinos-Seguí, J. L., and Valero, F. (2020) Continuous Cultivation as a Tool Toward the Rational Bioprocess Development With Pichia Pastoris Cell Factory, *Front Bioeng Biotechnol 8*.
[22] Werten, M. W. T., Eggink, G., Cohen Stuart, M. A., and de Wolf, F. A. (2019) Production of protein-based polymers in Pichia pastoris, *Biotechnol Adv 37*, 642-666.
[23] Tan, Y., Xu, Z., Tao, J., Ni, J., Zhao, W., Lu, J., and Yao, Y. F. (2016) A SIRT4-like auto ADP-ribosyltransferase is essential for the environmental growth of Mycobacterium smegmatis, *Acta Biochim Biophys Sin (Shanghai) 48*, 145-152.
[24] Oberg, F., and Hedfalk, K. (2013) Recombinant production of the human aquaporins in the yeast Pichia pastoris (Invited Review), *Mol Membr Biol 30*, 15-31.
[25] Pingitore, P., Pochini, L., Scalise, M., Galluccio, M., Hedfalk, K., and

Indiveri, C. (2013) Large scale production of the active human ASCT2 (SLC1A5) transporter in Pichia pastoris--functional and kinetic asymmetry revealed in proteoliposomes, *Biochim Biophys Acta 1828*, 2238-2246.
[26] Pingitore, P., Pirazzi, C., Mancina, R. M., Motta, B. M., Indiveri, C., Pujia, A., Montalcini, T., Hedfalk, K., and Romeo, S. (2014) Recombinant PNPLA3 protein shows triglyceride hydrolase activity and its I148M mutation results in loss of function, *Biochim Biophys Acta 1841*, 574-580.
[27] Fantoni, A., Bill, R. M., Gustafsson, L., and Hedfalk, K. (2007) Improved yields of full-length functional human FGF1 can be achieved using the methylotrophic yeast Pichia pastoris, *Protein Expr Purif 52*, 31-39.
[28] Stratton, J., Chiruvolu, V., and Meagher, M. (1998) High cell-density fermentation, *Methods Mol Biol 103*, 107-120.
[29] Mellini, P., Kokkola, T., Suuronen, T., Salo, H. S., Tolvanen, L., Mai, A., Lahtela-Kakkonen, M., and Jarho, E. M. (2013) Screen of pseudopeptidic inhibitors of human sirtuins 1-3: two lead compounds with antiproliferative effects in cancer cells, *J Med Chem 56*, 6681-6695.
[30] Haigis, M. C., Mostoslavsky, R., Haigis, K. M., Fahie, K., Christodoulou, D. C., Murphy, A. J., Valenzuela, D. M., Yancopoulos, G. D., Karow, M., Blander, G., Wolberger, C., Prolla, T. A., Weindruch, R., Alt, F. W., and Guarente, L. (2006) SIRT4 inhibits glutamate dehydrogenase and opposes the effects of calorie restriction in pancreatic beta cells, *Cell 126*, 941-954.
[31] Vandecaetsbeek, I., and Vangheluwe, P. (2016) Time-Dependent Protein Thermostability Assay, *Methods Mol Biol 1377*, 79-85.
[32] Mancusso, R., Karpowich, N. K., Czyzewski, B. K., and Wang, D. N. (2011) Simple screening method for improving membrane protein thermostability, *Methods 55*, 324-329.

II

PAPER II

Novel structural mechanism of extracellular gating of aquaporin from the fish climbing perch (*Anabas testudineus*)

Short title: High resolution structure of a fish aquaporin

Jiao Zeng[1], Florian Schmitz[2], Simon Isaksson[3], Olivia Arbab[2], Martin Andersson[3], Kristina Sundell[4], Leif A. Eriksson[2], Kunchithapadam Swaminathan[1*], Susanna Törnroth-Horsefield[5*], Kristina Hedfalk[2**]

***Corresponding authors:** Susanna Törnroth-Horsefield, Department of Biochemistry and Structural Biology, Lund University, Box 118, 221 00 Lund, Sweden, +46 46 222 4584, Susanna.Horsefield@biochemistry.lu.se, Kunchithapadam Swaminathan, Department of Biological Sciences, National University of Singapore, 117543 Singapore, +1 856 270 9141, ksntan99@gmail.com
****Correspondence to:** Kristina Hedfalk, Department of Chemistry and Molecular Biology, Gothenburg University, Box 463, 405 30 Göteborg, +46-31-7863923, kristina.hedfalk@gu.se

[1] Department of Biological Sciences, National University of Singapore, 117543 Singapore
[2] Department and Chemistry and Molecular Biology, Gothenburg University, Box 462, 405 30 Göteborg, Sweden
[3] Chemistry and Chemical Engineering, Applied Surface Chemistry, Chalmers University of Technology, 412 96 Gothenburg, Sweden
[4] Department of Biology and Environmental Sciences, Gothenburg University, Box 463, 405 30 Göteborg, Sweden
[5] Department of Biochemistry and Structural Biology, Lund University, Box 118, 221 00 Lund, Sweden

Abstract

Aquaporins are protein channels embedded in the lipid bilayer in cells from all organisms on earth. These channels are mainly transporters of water and thereby they are crucial for the water homeostasis at the cellular or tissue level. The water transport can be regulated which is fine tuned by conformational changes in the actual peptide chain. In this study we have investigated the water channel from climbing perch (cpAQP1aa), an air breathing fresh water fish (*Anabas testudineus*) that can spend time in brakish and full strength seawater as well as up to a week on land, providing an interesting species for studies on osmoregulation. Remarkably, from the high-resolution structures, a novel structural fold is seen on the extracellular side of the aquaporin providing a semi open channel. Combining functional analysis and Molecular Dynamic simulations suggest that phosphorylation of Tyrosine 107 gives rise to a closed conformation of the aquaporin.

Keywords

Aquaporin, fish, *Anabas testudineus, Pichia pastoris*

Osmoregulation is a major challenge for fish species in general since they are in direct contact with water and continuously need to compensate for passive water loss or uptake, depending on the envoironment. The ionic mechanisms and the structural organization of both gill and the intestinal epithelia are very well understood [1,2] [3], but the presence and regulation of aquaporins in various fish tissues and organs are not so well studied [2,4]. Partial air breathing fish species, spending long times in terrestrial conditions, are even more challenged with respect to osmoregulation due to evaporation and risk of drying out. Of particular interest among the various fish species is the climbing perch fish *Anabas testudineus*, a fresh water (FW) teleost which is extremely adaptable to environmental changes: (1) it can acclimate to higher salinity and acclimate from FW to seawater (SW) over seven days in a progressive manner [5], (2) it can live on land for up to six days and utilize air via breathing through a special accessory respiratory organ (ABO), the "labyrinth organ", located in the upper part of the gill chambers [6], and (3) it is capable of active ammonia excretion during emersion [7,8] (**Fig. 1a**). In conclusion, among the fish species, *A. testudineus* provides an attractive model organism for studying the mechanisms of water homeostasis as well as ammonia excretion.

Aquaporins in fish were first identified in 2000 [9] and most of our current understanding concerns the involvement of aquaporins in fish intestine where they are essential for keeping water homeostasis in SW. Aquaporin isoforms are localized in both the apical and basolateral membranes (**Fig. 1b**) where they provide a transcellular water flow [4,10]. Investigation of numerous fish species reveals that aquaporins are up-regulated in the intestine as a response to transfer to SW, indirectly supporting a general mechanism for osmoregulation and water absorption [2,4]. Furthermore, skin and gills are of major interest for fish osmoregulation and, potentially, aquaporins are also involved in a regulated water flow in these organs. As compared to the consensus for aquaporin mRNA levels in the intestine, less is understood for the organs being in direct contact with the surrounding [4]. AQP homologues are present in all organisms where their primary function is passive transport of water as a direct response to the osmotic pressure. Some AQPs could also transport other small neutral solutes, such as glycerol, urea, ammonia and carbon dioxide, across plasma membrane. In mammals, 13 AQPs (AQP0-12) have been identified and they are classified into three subgroups: orthodox AQPs (AQP0, 1, 2, 4, 5, 6 and 8), which could transport only water; aquaglyceroporins (AQP3, 7, 9 and 10), which could transport glycerol, urea, ammonia and carbon dioxide; and superaquaporins (AQP11 and 12), whose details are to be further elucidated [11] A selection of the aquaporin isoforms are also peroxiporins transporting hydrogen peroxide, being part of the cellular redox signaling [12]. Compared to human, fish is phylogenetically distant and at the opposite end of the vertebrate taxon. Not surprisingly, highly efficient mechanisms for osmoregulation has been developed in all life stages of fish in order to maintain water and ion balance in an organism constantly surrounded by water. Those mechanisms are even more crucial for euryhaline teleosts which can survive in extreme conditions and acclimatize to sudden changes in osmolality presented by fresh water (FW), seawater (SW) and brakish water (BW) environments [13]. The osmoregulation in fish is complex and involves many organs, including gill, skin, esophagus, gastrointestinal tract, kidney and bladder. Comparably, a large variety of AQPs have also been identified from fish, implicating their essential roles for maintaining water balance. Interestingly, there seems to be a connection between the complexity of the organism and the diversity of AQPs produced, reflecting the trends of evolution, as illustrated by 18

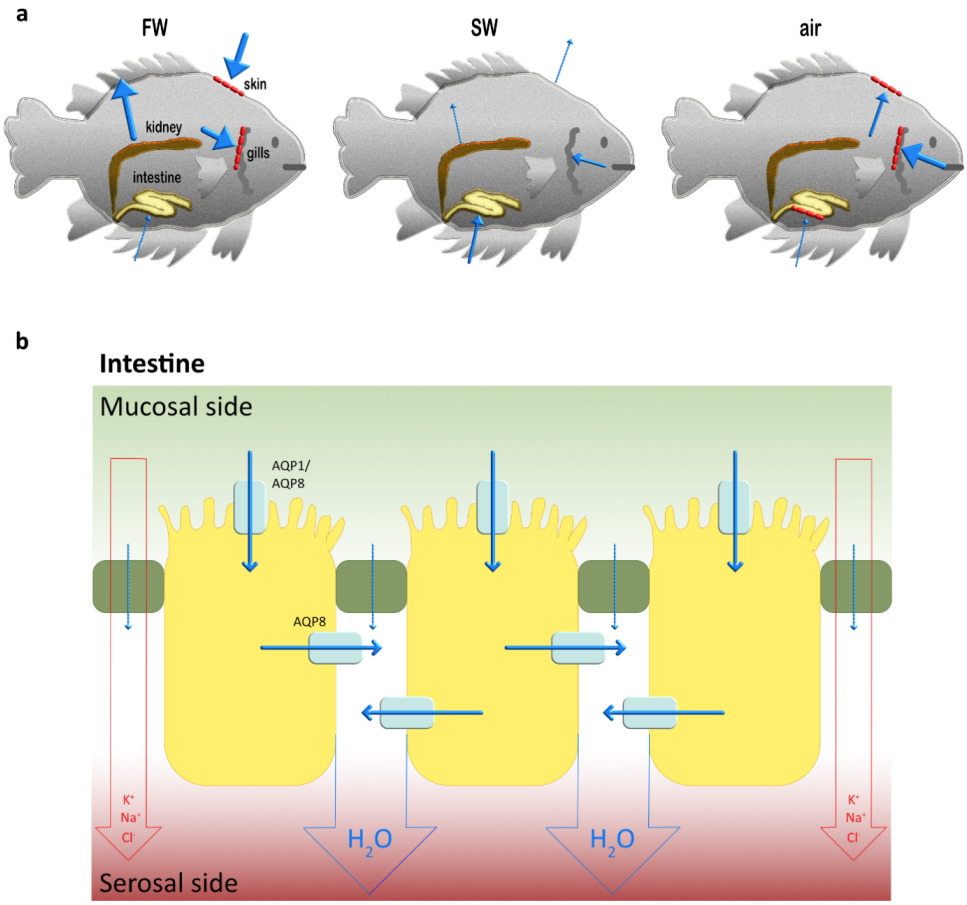

hyperosmotic osmoregulator trying to minimize the diffusional inflow of water across the gills and producing a dilute urine to get rid of excess water. In SW, on the other hand, *A. testudineus* will acclimate and become a hypoosmotic osmoregulator with the revers problem with water diffusing out across all epithelia which is counteracted by an ion-coupled water uptake acorss the intestine and a decreased glomerular filtration rate and thus urine production. During terrestrial exposure, it will be critical for *A. testudineus* to reduce water loss from the large surface areas constituted especially by the gills, but also by the skin. The intestinal water absorption is also supposed to be reduced as that is dependent on drinking, which ceases in air. (b) During SW acclimation a total water flow is directed from the mucosal to the serosal side of the intestine driven by an ionic gradient of mainly K^+, Na^+ and Cl^-. In SW trout the increased intestinal water absorption is facilitated by aquaporin isoforms in the apical (Aqp1a and Aqp8ab) and basolateral (Aqp8ab) membranes, respectively (reviewed in Madsen 2015).

AQP members identified in the model organism zebrafish *Danio rerio* [14] and the Atlantic salmon genome comprises 42 paralogs, possibly resulting from a whole genome duplication event [4]. The aquaporins in fish are expressed in osmoregulatory organs and tissues, where homologues are distributed in skin, gill, intestine and kidney. Furthermore, expression levels vary with changes in salinity supporting the involvement of aquaporins in fish osmoregulation [15].

The structure of AQPs is highly similar, also though some homologues share low sequence identity, indicating a

history of conservation [16]. High resolution structures of various AQP homologues are available to date, including AQP1 from human [17]. AQPs share a common topology of six transmembrane helices with five connecting loops and two half helices containing one highly conserved NPA motif each forming the functional pore, as established in the hourglass model [18]. Furthermore, biochemical studies support that AQPs have a tetrameric assembly with each monomer being a functional unit [19]. High resolution structural studies have explained the mechanism for proton exclusion of the water channels, where the highly conserved AQP signature NPA motifs provide a marco-dipole positive electrostatic barrier in the middle of the channel [20]. Further, in the super high resolution for the Aqy1 channel, a pair-wise movement of water was proposed which would prevent proton conduction via the Grotthuss mechanism [21]. Structural studies have also highlighted a site near the extracellular vestibule, the ar/R motif with a highly conserved arginine residue. The diameter, ~3 Å in water-specific AQPs and one Ångström wider in a typical aquaglyceroporins such as the glycerol transporter GlpF from *E. coli* [22,23], and the polarity of this site direct the substrate specificity of the AQP channel.

In this study we have focused on a homologue to AQP1 from *A. testudineus* (cpAQP1aa), the only characterized AQP from this species to date [7] (**Supplementary Fig. 1**). Studies of cpAQP1aa expression reveal that it is mainly produced in gills and skin which implies that this AQP might have a more pronounced physiological role in ammonia excretion as compared to osmoregulation [7]. To shed more light on the specificity of this specific AQP homologue from fish we have produced the target to high yields in *P. pastoris*, isolated the protein to homogeneity and solved the structure to high resolution. To get an even deeper understanding of the regulatory mechanism, we pursued a mutational analysis of key residues in cpAQP1aa where molecular dynamic simulations complement the functional analysis. This study thereby provides the first atomic structure of a fish AQP together with some insight into the mechanism of regulation at the extracellular side of the pore also contributing to increased understanding of the variation in the molecular mechanisms of the AQP family of proteins.

Results

High-resolution structure of cpAQP1aa reveals a novel fold on the extracellular side

Since flexible termini are known to hamper crystallization of AQPs [11,12], a construct of cpAQP1aa that had been truncated after residue 243 was made. The protein was recombinantly produced in the methylotropic yeast Pichia pastoris, purified and crystallized. The structure was solved to 1.9 Å resolution by molecular replacement using a homology model of cpAQP1aa that had been based the crystal structure of bovine AQP1 [13] (**Supplementary Table 1**). The overall structure of cpAQP1aa shares most of the common AQP structural features; each protomer consists of six transmembrane α-helices (1-6) and five connecting loops (A-E). A seventh pseudo-transmembrane α-helix is formed by the insertion of two half-helices in loops B and E into the pore which each contain the AQP signature NPA motif (**Fig. 2a**). Furthermore, cpAQP1aa assembles as a tetramer with each protomer possessing a functional pore and a fifth pore is formed at the center (**Fig. 2b**). A single file of water molecules is aligned within the water conducting pore of each protomer, indicating that cpAQP1aa is in a functional state. Loops A (residues 33-42) and C (residues 108-126) are partly disordered, wherefore residues 34-37 and 108-112 lack electron density and have been omitted from the structure. The visible parts of the loops have well-defined electron density and reasonable B-factors, supporting their modelling. Since the last residue that could be unambiguously modeled for cpAQP1aa

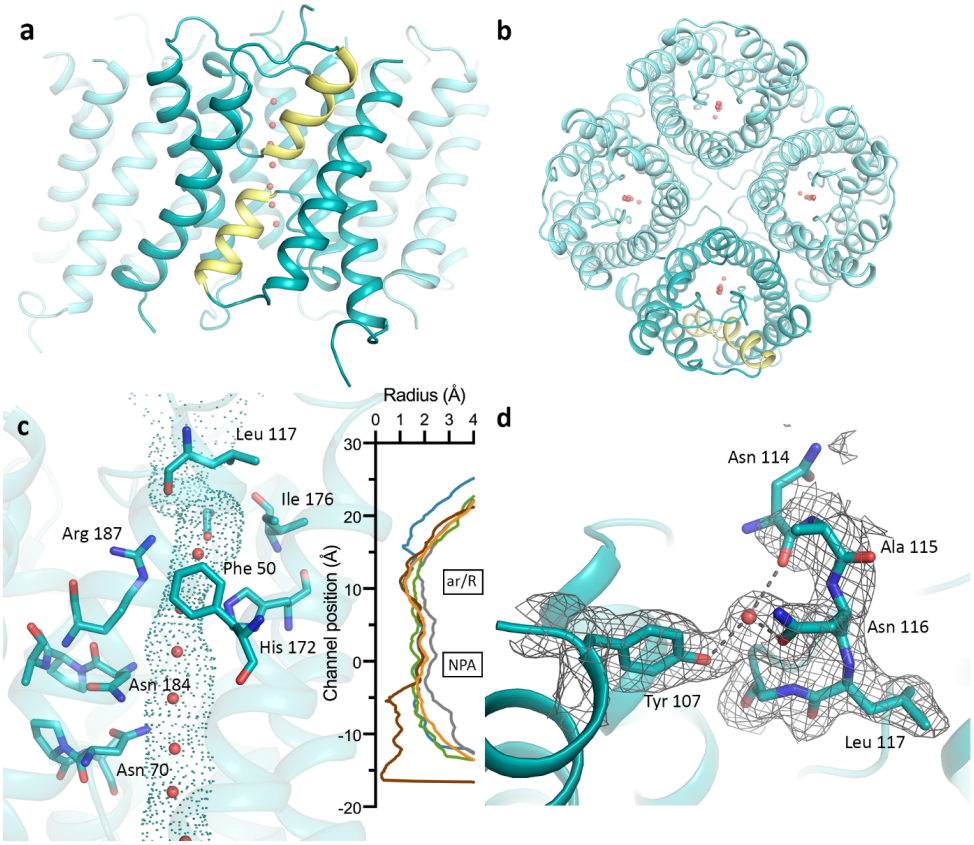

Figure 2. Crystal structure of cpAQP1aa. The cpAQP1aa tetramer viewed (a) parallel to the membrane and (b) from the extracellular side. The two half-helices forming the seventh pseudo-transmembrane segment are coloured yellow in the frontmost monomer. Water molecules inside the channel are showed as red spheres. (c) HOLE analysis of the water-conducting channel with the channel dimensions visualized as dots. Residues in the aromatic-arginine (ar/R) and NPA regions as well as the extracellular gate are shown in stick representation. The graph shows a comparison between the channel profiles of cpAQP1aa (teal), human AQP4 (orange, PDB code 3GD8), human AQP7 (grey, PDB code 6QZI), Arabidopsis TIP2;1 (green, PDB code 5I32) and spinach PIP2;1 (brown, PDB code 1Z98). For cpAQP1aa, the channel is significantly narrower on the extracellular side of the ar/R-region with a channel radius of 1.1 Å around Leu 117. The zero channel position corresponds to the midpoint between the two NPA motifs. (d) Close-up view of the interaction between Tyr 107 and Asn 114 and 116 that stabilizes the conformation of loop C that allows to extracellular gate to form. Electron density shown as grey mesh represents the 2fofc-map contoured at 1.0 σ. Hydrogen bonds are depicted as dotted lines.

is Lys226, its C-terminus is deemed to be disordered beyond this residue.

In order to explore the features of cpAQP1aa water-conducting channel, its shape and dimensions was calculated using the program HOLE [14] (**Fig 2c**). Similar to other AQPs, the channel of cpAQP1aa is dumbbell-shaped, consisting of open vestibules at both intracellular and extracellular sides, and an elongated narrow pore in between. The pore constricts to a radius of ~1.2 Å at the ar/R-region, formed by residues Arg187, His172, Cys181 and Phe50, a width and residue composition that is typical for water-specific AQPs[13]. However, when comparing the channel profile of cpAQP1aa with those of the water specific channels human AQP4 [15] and spinach PIP2;1 [16], the aquaglyceroporin human AQP7 [17] and the ammonia-

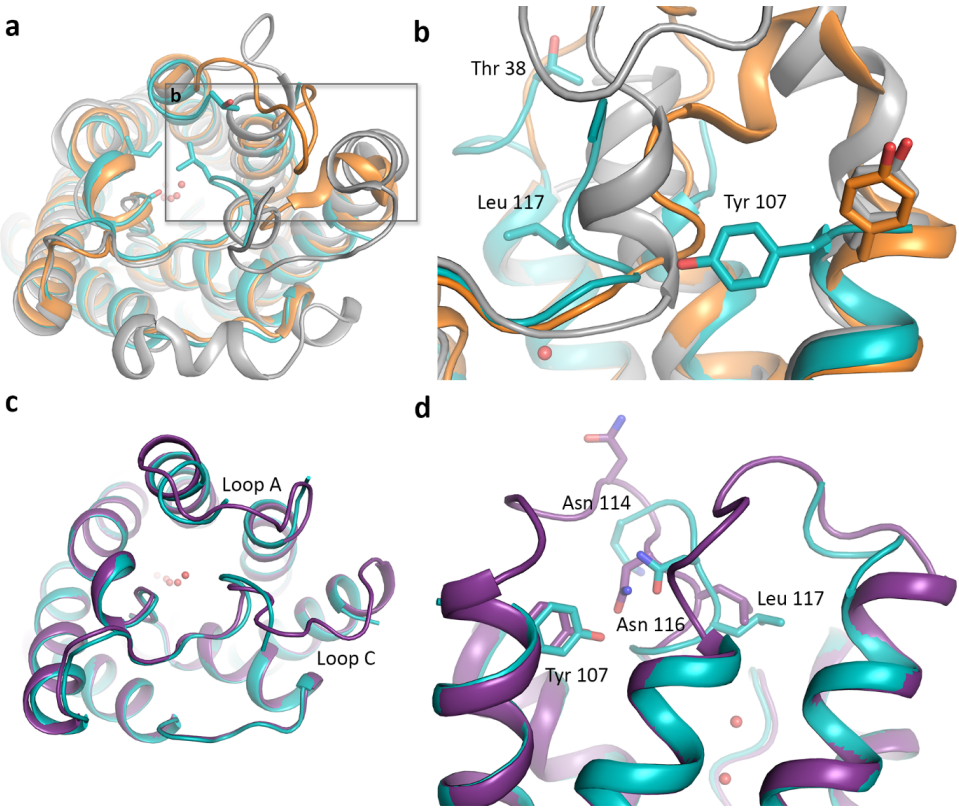

Figure 3. Structural comparison of cpAQP1aa with other AQPs and at different pH. Structural overlay of cpAQP1aa (teal), human AQP4 (orange) and human AQP7 (grey), viewed from the extracellular side. Residues in the cpAQP1aa extracellular gate and the suggested phosphorylation site at Thr 38 are shown in stick representation. Waters in the channel are shown as red spheres. (a) View from the extracellular side showint that the main structural differences are found in loops A and C (b) Zoom-in on loop C showing significant structural differences between the three overlaid structures. In cpAQP1aa, the side-chain of Tyr 107 has flipped compared to AQP4 and AQP7, pushing loop C further into the extracellular vestibule. closer to the channel opening. (c) Structural overlay of the cpAQP1aa structures at pH 7.8 (teal) and 6.5 (purple). The two structures are highly similar, but differ in loops A and C. In the structure at pH 6.5, these two loops could be built in full in two monomers, whereas they were mostly dsordered in all monomers in the structure at 7.8. (d) Zoom-in on the extracellular part of the overlay, showing that, despite the structural differences in loops A and C, Tyr 107, Asn 116 and Leu 117 occupy similar positions in both structures.

permeable TIP2;1 from Arabidopsis thaliana[18], a unique constriction region at the extracellular side of the ar/R-region can be found. This region is defined by loop C adopting a conformation which places residues 114-117 closer to the centre of the extracellular vestibule, with Leu 117, Ile 176 and Gly 180 forming a hydrophobic constriction region with a radius of 1.1 Å, approximately 8 Å away from the ar/R-region. The conformation of loop C is stabilized by hydrogen bonds between Tyr 107 in transmembrane helix three and the carbonyl oxygen and side chain of Asn 114 and 116 respectively, via a water molecule (**Fig 3d**). The formation of a hydrophobic constriction region is reminiscent of what is seen in the gated spinach aquaporin SoPIP2;1, where a conformational change of cytoplasmic loop D results in the insertion of a Leucine side chain into the opening of the channel from the

cytoplasmic side, albeit on the opposite side of the membrane. In SoPIP2;1 this severely constricts the channel to a radius of less than 0.5 Å (**Fig 2c**), efficiently blocking water transport. Although the radius of the hydrophobic constriction region in the cpAQP1aa structure may not small enough to completely rule out the passage of water molecules, it is possible that even minor structural changes in this region could narrow it down further suggesting it may function as a hydrophobic gate and that the structure could represent a semi-open state. Such structural changes could be triggered by phosphorylation and/or pH as has been shown for SoPIP2;1. It is therefore interesting to note that two putative phosphorylation sites, as suggested by the high-resolution structure, are located in this region, Thr 38 and Tyr 107 (**Figure 3a and b**).

A structural comparison between cpAQP1aa, human AQP4 (water-specific) and human AQP7 (glycerol-permeable) show structural variability in extracellular loops A and C, (**Figure 3a**) and an extended comparison with several other eukaryotic AQPs reveal that loops A and C are able to adopt a number of unique conformations, specific for each homologue/isoform (**Supplementary Figure 2**). Interestingly, although Tyr 107 is conserved in all three AQPs, its side chain is pointing away from the channel in AQP4 and AQP7 and as a result loop C and remains further away from the channel opening (**Fig 3b**). Furthermore, Leu 117 is highly conserved in vertebrate AQPs, including fish and human (albeit not in human AQP7) (**Supplementary Figure 1**), indicating that the extracellular constriction is not directly related to this residue being present in not. Taken together, the structural differences in loop C and its dependence on the side chain conformation of Tyr 107 supports the extracellular constriction region functioning as a hydrophobic gate.

The extracellular constriction region in cpAQP1aa is not dependent on pH

To investigate if the conformation of loop C is dependent on pH, we crystallized and solved the structure of cpAQP1aa at a lower pH; pH 6.5 instead of 7.8 which was used for the cpAQP1aa structure above. The crystals at the lower pH belonged to a different space group, $C222_1$ instead of $P42_12$ as seen for the crystals grown at higher pH and diffracted to significantly lower resolution (3.5 Å). The lower diffraction quality is consistent with the differences in crystal packing; the crystals grown at pH 6.5 has considerably weaker crystal contacts and higher solvent content (**Supplementary Figure 4**). Furthermore, in the structure at lower pH, there are four cpAQP1aa protomers in the asymmetric unit compared to one in the structure at pH 7.8. Due to this, structural differences can be observed between the protomers, most notably the fact that loops A and C could be built in its entirety in one of the protomers (protomer C) (**Supplementary Figure 4a and b**).

As seen in **Figure 3c and d** the two structures at different pH are very similar although some minor differences can be seen in loops A and C. Nevertheless, the residues responsible for narrowing the channel on the extracellular side, in particular Tyr 107, Asn 116 and Leu 117 line up well and seem to be able to involved in the same interactions (hydrogen bonds can not be reliably assigned due to the low resolution of the structure at low pH). This is supported by the fact that the channel profiles as calculated by HOLE are very similar in both structures (**Supplementary Figure 5c and d**), suggesting that the extracellular hydrophobic constriction region is unaffected by pH.

cpAQP1aa is a channel for water but not glycerol

To verify that the cpAQP1aa, recombinantly produced in *P. pastoris* and purified to homogeneity, is a functional water channel both the full length protein (cpAQP1aa-FL) and the truncated variant used for crystallization (cpAQP1aa-243)

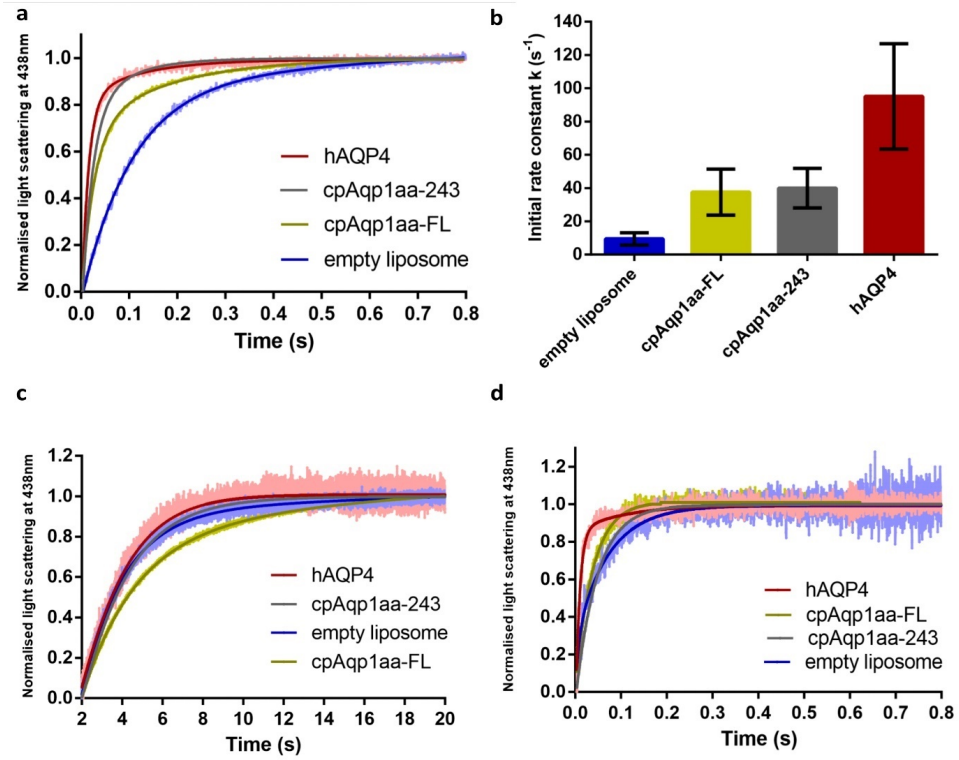

protein of both cpAQP1aa-FL and cpAQP1aa-243 are functional. (b) Initial rate (i.r.) of the water transport of hAQP4 (positive control), cpAQP1aa-243, cpAQP1aa-FL and empty liposome (negative control) showing that purified protein of both cpAQP1aa-FL and cpAQP1aa-243 are functiona,l n = 9-25 +/- SD. (c) Representative curves for glycerol transport of cpAQP1aa-FL, cpAQP1aa-243, hAQP4 and empty liposome (negative control) n=3 . (d) Representative curves for water transport of cpAQP1aa-FL, cpAQP1aa-243, hAQP4 and empty liposome (negative control) at pH 6.5.

were reconstituted in liposome and tested for water transport by stopped flow (**Fig. 4a**). The water transport was compared to the efficient water transport of human AQP4 (hAQP4) as well as empty liposome. The initial rates were 37.59 ± 13.84 s^{-1} and 39.97 ± 11.92 s^{-1} for cpAQP1aa-FL and cpAQP1aa-243, respectively. Comparably, the initial rates of the controls were 9.49 ± 3.68 s^{-1} and 95.13 ± 31.67 s^{-1} for empty liposome and hAQP4, respectively. Thus, both full length and truncated cpAQP1aa are equally efficient in their water transporting activities. As seen in **Fig. 4b**, however, the efficiency for the cpAQP1aa water transport is substantially lower than for hAQP4, being in agreement with a semi open conformation of the aqueous pore (**Fig. 3a, b**). Notably, the measured water transport is due to similar levels of protein in the liposome (**Supplementary Figure 6a**).

Since many aquaporins have broader transport specificity than water and commonly also transport glycerol, glycerol transport was also evaluated for cpAQP1aa. Neither of the reconstituted aquaporins, cpAQP1aa-FL, cpAQP1aa-243 or hAQP4, showed any transport of glycerol (**Fig. 4c**). The immunoblot analysis supports that the aquaporins are properly reconstituted, the cpAQP1aa even slightly better than hAQP4

(**Supplementary Figure 5b**), which could possibly result in more tightly sealed liposomes and a slower transport than empty liposome. The specificity of water observed for the cpAQP1aa is well related to the observed diameter and structure of the actual water pore which is much more narrow than the one of the glycerol transporter human AQP7 (**Fig. 3a**). Furthermore, to confirm that the transport function for cpAQP1aa is not affected by a lower pH, as indicated by the comparison of the two structures at pH 7.8 and 6.5 (**Fig 3c and d**), respectively, water transport was also evaluated at the lower pH. Even though the liposome preparation was a somewhat less stable under this condition, it could indeed be concluded that cpAQP1aa was much less efficient in its water transport as compared to hAQP4 (**Fig. 4d**). This observation is valid for full length as well as for truncated protein supporting that the extracellular hydrophobic constriction region is unaffected by pH **(Supplementary Figure 5)**.

Possible regulatory mechanism for the cpAQP1aa involves the conformation of loop C and phosphorylation

The semi open structure of cpAQP1aa reveals that loop C forms a unique 'capping' conformation on the top of the channel where Leu117 has a central role plugging the entrance from the extracellular side (**Fig. 3a, b**). In order to evaluate the importance of Leu117 for channel regulation, it was mutated to alanine (L117A) to possibly take away the hydrophobic block (**Fig. 3a, b**). The water transport of this specific mutant was very low and the initial rate very similar to the one of the empty liposome, 7.49 ± 0.73 s^{-1} as compared to 9.49 ± 3.68 s^{-1} (**Fig. 5a**). Noteworthy, this specific mutant did not reconstitute very well and the amount of protein in the proteoliposome was very low (**Supplementary Fig. 6c**). Taking the protein amount into account, it cannot be excluded that that L117A is as efficient as the wild type cpAQP1aa (**Fig. 5a**), suggesting that it is not the side chain of L117 in itself that is critical for the restricted water flow of cpAQP1aa but rather the overall fold of loop C.

Taking a closer look in the structure, the location around the critical residue L117 is stabilized by the hydrogen bonding network between the residues Tyr107, Asn114 and Asn116 (**Fig.3d**). In order to investigate the role of this network and a possible influence of phosphorylation on the closure of the extracellular gate, Tyr107 was mutated to Alanine to abolish phosphorylation (Y107A) and Serine (Y107S) to mimic this position in human AQP1 (**Supplementary Fig. 1**), and tested for water transport (**Fig. 5a**). Both mutants showed wild type characteristics, where more accurate comparison of the initial rate showed that Y107S was very similar to wild type, 39.36 ± 6.68 s^{-1} as compared to 37.59 ± 13,84 s^{-1}, while Y107A was slightly slower, 23.26 ± 8.14 s^{-1}. Comparing the protein amounts (**Supplementary Fig. 6c**), however, wild type and Y107S both reconstitute efficiently while a much lower amount was found in the proteoliposome for Y107A. Taking this into account, the transport of Y107A is substantially more efficient than wild type, potentially giving rise to a fully open water pore with transport capacity in the range of hAQP4 (**Fig. 5a**), supporting that the tyrosine side chain is important in forming the network that stabilizes the unique fold of loop C seen in cpAQP1aa and that phosphorylation of this specific site could be involved in channel regulation.

To further investigate if phosphorylation could be a regulatory mechanism for cpAQP1aa, an additional putative phosphorylation site was investigated, Thr38. Based on the structure, this residue is located in loop A and its putative phosphorylation status could possibly influence the conformation of loop C and closure of the channel. Again, two mutants were produced, one to abolish (T38A) and one to mimic (T38E)

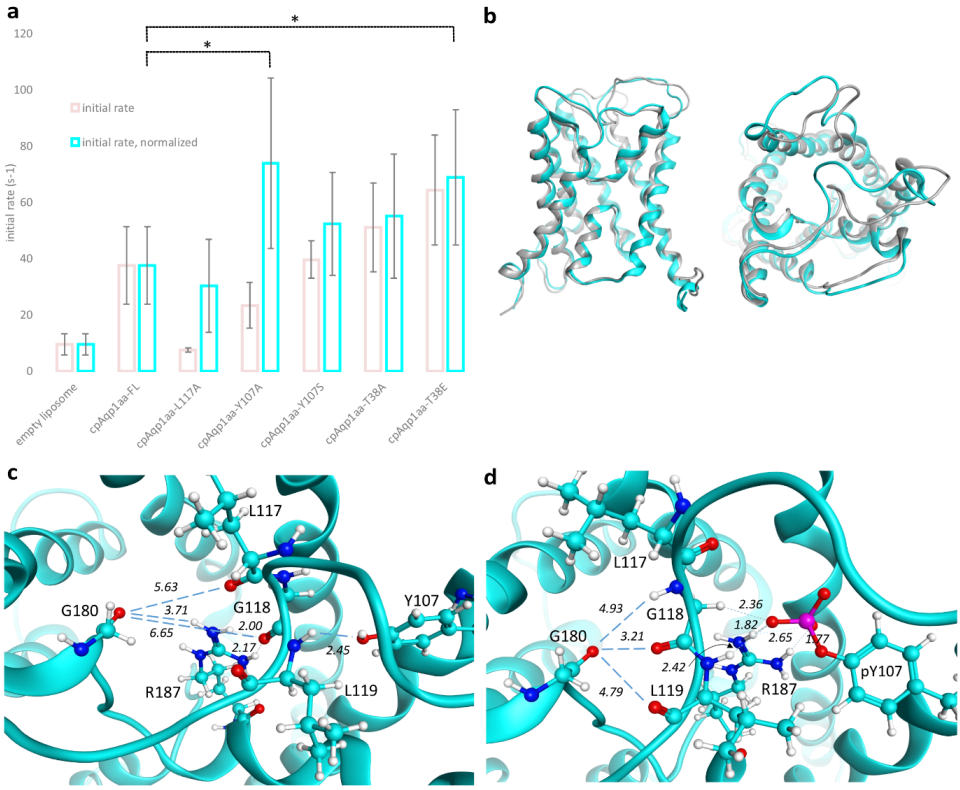

Figure 5. Phosphorylation-dependent regulation of cpAQP1aa. (a) The initial rates, measured and normalized taking the protein amount into account, respectively, n=2-25 +/- standard deviation. The intensity of the immunoblot signal was quantified for each protein target (n=2), wild type cpAQP1aa and mutants, and related to the measured k-values for each. The relationship between protein amount in the protein liposome and initial rate is not necessarily linear, but the correlation gives an indication of the real effect for each target, highlighting that the Y107A mutant is clearly more efficient than the wild type protein, up to three times and in the range of hAQP4, the L117A mutant is in the range of wild type cpAQP1aa and T38E is slightly higher. (b) Superposition of the energy minimized structures of the final snapshots after 100 ns MD simulation of the wild type AQP (grey) and the pY107 system (turquoise); side view (left) and view from extracellular side (right). The differences in orientation of the two loops connecting transmembrane helices 1 and 2 (top) and helices 3 and 4 (across) are clearly visible. (c) Zoom-in of the wild type system, with residues L117, G118, L119 and G180 forming the pore opening, R187 located just beneath this, and Y107 to the right. (c) Energy minimized final snapshot from the 100 ns MD simulation. Same as (b), but for the pY107 system. The extracellular loop has shifted to the left, closing the pore opening, and is held in place by the interactions from R187 – pY107.

phosphorylation, which were both tested for water transport. (**Fig. 5a**). Interestingly, T38A had wild type like transport, with an initial rate of 51.01 ± 15.76 s^{-1} as compared to 37.59 ± 13,84 s^{-1}, while the transport of T38E was significantly more efficient, k_{init} = 64.38 ± 19.50 s^{-1} (**Fig. 5a**). In this comparison, the protein amounts were equal in the proteoliposome supporting the actual differences in transport capacity (**Fig. 5a**). Hence, it seems that phosphorylation of Thr 38 is important for channel regulation of cpAQP1aa, either on its own or in addition to phosphorylation of Tyr 107, leading to channel opening.

To investigate phosphorylation of cpAQP1aa, the protein (cpAQP1aa-243) was analyzed by phosphostaining after separation of protein samples by SDS-PAGE confirming that it indeed is

phosphorylated (**Supplementary Figure 7**) From the structure it can be seen that Y107 is not phosphorylated while T38 is more difficult to evaluate due to less clear electron density. In order to get further insight into the phosphorylation status of cpAQP1aa, this modification was looked for in the masspectrometry analysis. Phosphorylation was confirmed at three C-terminal residues, S239, T254 and T255 (**Supplementary Figure 1**), but despite multiple efforts, no phosphorylation was found on residue 38 and 107, respectively, supporting that the recombinant crystallized cpAQP1aa was not phosphorylated at Thr38 nor at Tyr107 (data not shown). These findings are consistent with the fact that the T38A mutant exhibited a water transport rate similar to wild-type (**Fig. 5A**).

MD reveals that phosphorylation of cpAQP1aa influences channel regulation

To further examine whether phosphorylation could influence a putative gating of cpAQP1aa, Molecular Dynamic (MD) was applied to investigate whether the side chain of Y107 could stabilize the conformation of the loop that blocks the channel from the extracellular side, where the main chain is more important than blockage by the L117 residue itself. Noteworthy, the simulated structures; pT38, L117A, Y107A, Y107S and pY107, are highly stable in the time frame of the current simulations, and show, with the exception of pY107, very close overlap in the pore entry and restriction point. For pY107 larger changes are noted in the extracellular loop regions (**Fig 5b**). The overall heavy atom RMSD of the two models is 1.24 Å, with essentially all the difference localized to the terminal part of membrane spanning helix 1 (having a larger tilt angle in pY107) and the extracellular loops connecting helices 1 and 2, and helices 3 and 4, respectively.

In the structure of the wild type aquaporin, Y107 displays a clear stabilizing role for the loop between membrane spanning helices 3 and 4 by establishing a hydrogen bonding between the phenolic oxygen of Y107 and the backbone NH of G118 (2.45 Å in the minimized structure after 100 ns MD simulation). The distances between backbone carbonyl oxygen of G180 and those of L117, G118 and L119, representing the pore opening, are also very stable through the simulation (5.63, 6.65 and 6.82 Å in the minimized final snapshot, (**Fig 5c**), and highly similar to the values obtained for pT38, L117A, Y107A and Y107S. We also note the role of R187 located just below the pore opening, forming two stable hydrogen bonds to the carbonyl oxygen of G118 (distances 2.00 and 2.17 Å), and a stable interaction to the carbonyl of G180 (O - - HN distance 3.71 Å); **Fig 5c**.

In the pY107 system, however, the system gradually adjusts to the bulkier side chain and altered electrostatics and hydrogen bonding conditions. During the initial stages of the simulation, G118 of the loop connecting helix 3 and 4 is pushed towards G180 by the bulky phosphate group of pY107, narrowing the pore opening, also resulting in a rotation of the backbone of L117 such that its carbonyl points away from the pore opening and the amine group of G118 instead orients towards G180. After about 50 ns of the production run, there is a rotation of the phosphate group which in turn is accompanied by a motion of R187 from its position near the pore opening, to instead form two strong hydrogen bonds to the phosphate of pY107. The phosphate group also forms strong interactions to the backbone NH of L119 and a hydrogen of G118. Due to the shift in loop orientation, which is then kept in place by the strong interactions to the pY107 – R187 pair, the diameter of the pore opening is drastically reduced with distances between the carbonyl oxygen of G180 an G118 being 3.21 Å (and 4.8-4.9 Å to the CO of L119 and NH of L117, respectively), **Fig 5d**, i.e., markedly smaller than the 5.6 – 6.9 Å noted for both the wild type system.

Discussion

The role of aquaporin in climbing perch

Our understanding of the relevance of aquaporins in fish is mainly based on gene identification and phylogenetic analysis, indicating that AQPs are involved in many physiological functions. Besides water, many aquaporins also transport glycerol [19] and fish aquaporins, specifically, have been reported to be involved in gas transport, especially ammonia and CO_2 [20,21]. This study provides the first structural and biochemical analysis of a pure aquaporin homologue from a fish of utmost interest regarding osmoregulation. Climbing perch is able to live in different environments and it is superior in acclimation to different conditions connected to tight regulation of ion-transporters and ion and water channels in the osmoregulatory organs and tissues. cpAQP1aa is expressed in multiple tissues with high expression in gills and skin, tissues that are in direct contact with the surrounding of the fish [7], implying a possible role of cpAQP1aa in transport of both water and gas. mRNA analysis showing an increase in cpAQP1aa gene expression in gills following terrestrial exposure have suggested that it may have a greater physiological role in ammonia excretion rather than osmoregulation[7].

When the structure of cpAQP1aa is compared to aquaporins with different substrate specificities; the aquaglyceroporin human AQP7 and the ammonia transporting channel from *A. thaliana* (AtTIP2;1), it is evident that cpAQP1aa is less uniform throughout the channel and has an channel radius and residue composition at the ar/R-region that is much more consistent with water-specific AQPs (**Fig 3a and b, Supplementary Figure 2**). Moreover, the additional narrowing on the extracellular side is completely unique for cpAQP1aa, regardless of the substrate specificity of the AQPs that are used in the comparison. Based on the analysis by HOLE, cpAQP1aa significantly differs from the glycerol and ammonia transporting aquaporins, providing support that it is unlikely that cpAQP1aa transports these compounds. The transport data for glycerol indeed support this where cpAQP1aa is as inefficient in glycerol transport as the human water channel AQP4 (**Fig. 4c**).

The ammonia channel AtPIP2;1, has been described as comprising an extended specificity filter which together with a deprotonation mechanism provided by His131 are believed to contribute to ammonia transport, in addition to water [22]. The presence of a histidine in position 131 forces the side chain of the arginine in the ar/R-region of AtTIP2;1 adopts a novel conformation that has not been seen in other AQPs (**Fig 6**). Furthermore, the ammonia-transporting capability of AtTIP2;1 is also believed to correlate with the position of the carbonyl of Gly 194 which is located in a position typically assigned with non-specific AQPs as well as the hydrogen bonding pattern. When comparing this region in AtTIP2;1 and cpAQP1aa it is evident that the structure of cpAQP1aa strongly resembles those of water-specific AQPs, specifically the presence of an asparagine (Asn 120) in the equivalent position to His 131, the position of the carbonyl of Cys 181 and the hydrogen bonding pattern between residues and water molecules. In conclusion, contradicting to previous analysis of mRNA indicating a greater physiological role for the cpAQP1aa in ammonia excretion than in osmoregulation [7], structural evaluation suggests that it is rather unlikely that this aquaporin is involved in ammonia transport. Possibly, in the acclimation of climbing perch to seawater, it is instead a Na^+/H^+ exchanger that provide the route for passive ammonia transport along with acid-base balance [23].

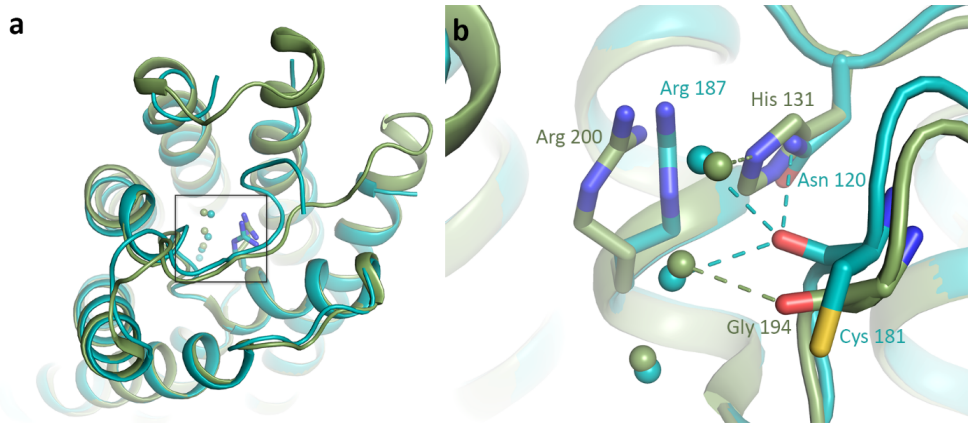

Figure 6. Structural comparison between cpAQP1aa and the ammonia-transporting aquaporin AtTIP2;1. (a) Overlay of cpAQP1aa (teal) and AtTIP2;1 (green) viewed from the extracellular side. The arginine in the ar/R-region is shown in stick representation. Water molecules in the channel are shown as spheres of the respective protein colour. (b) Zoom-in on the boxed area in (a), showing the different side-chain orientation of the arginine in the ar/R-region and the hydrogen bonding pattern between water molecules and residues within the channel. Hydrogen bonds are shown as dotted lines in the respective protein colour. In cpAQP1aa, the carbonyl position of Cys 181 and its hydrogen bonds to Asn 120 and two water molecules correspond to what is typically seen in water-specific AQPs. In contrast, the carbonyl of Gly 194 in AtTIP2;1 occupies a different position, observed mainly in non-water specific AQPs, and shows a different hydrogen bonding pattern.

Combining all the results, the current study supports that cpAQP1aa is mainly a transporter for water and thus is primarily involved in osmoregulation. The special character of the climbing perch is its ability to both be truly euryhaline and able to spend time on land, in air. Under these conditions it is likely that the presence of regulated aquaporins is beneficial in order for the fish to be able to finely regulate the water flow across its epithelia. When residing in FW or air, it is advantageous for the fish that the channel can be efficiently closed. This will, in FW, minimize diffusional inflow of water across the epithelia while in air it will instead avoid evaporative water loss, mainly from gills and skin. When residing in SW on the other hand, the ability to rapidly change between open and closed conformations in a tissue-dependent manner is a favorable scenario, since in epithelia facing the outer environment, diffusional water loss should be counteracted, whereas in the intestine the fish needs to have an active fluid uptake to compensate for the water loss [1,2] (**Fig. 1**).

The high-resolution structure of cpAQP1aa reveals a novel extracellular gating mechanism that is controlled by phosphorylation

The unique constriction region in the high-resolution structure of cpAQP1aa suggests that a novel extracellular gating mechanism amongst AQPs (**Fig. 2**). Based on the HOLE analysis of the channel dimensions (**Fig 2c**) and the functional evaluation that shows that the water transport via cpAQP1aa is less efficient than the one via hAQP4 (**Fig. 4a, b**), cpAQP1aa is likely to be a gated channel that is captured in a semi open state. Known regulatory mechanisms for aquaporins are influenced by pH, phosphorylation and mechanosensitivity. For the cpAQP1aa specifically, we have looked more closely into the impact by pH and phosphorylation on the regulation of the water transporting function of the channel. While a decrease in

pH did not have any apparent effect on the cpAQP1aa water transport (**Fig. 4d**) or the protein structure (**Figure 3c and d and Supplementary Figure 5**), there are two critical positions on the extracellular side of the protein where phosphorylation possibly affects the efficiency in water flow, Y107 and T38 (**Fig 3a and b**). The high-resolution structure of cpAQP1aa reveals that Tyr 107 is important for the unique conformation of loop C that results in the formation of the extracellular gate, via a hydrogen bonding network involving Asn 114 and 116 and a water molecule (**Fig 2d**). As suggested by MD simulations, phosphorylation of Tyr107 influences channel closure by interacting with the highly conserved arginine R187 (**Fig. 5d**). Looking at the other putative phosphorylation site, T38, the phosphomimicking mutant T38E shows significantly higher water transport than the wild type protein (**Fig. 5a**), suggesting that phosphorylation of this residue provides a more open channel, an observation that could not be supported by MD simulations. However, it should be noted that the position and conformation of this residue is more uncertain due to less well-defined density than for Tyr 107, and that there may be phosphorylation-dependent structural changes that could not be captured during the time-scale of the MD simulation. Interestingly, T38 is not a conserved residue among fish species (**Supplementary Fig. 1**), but appears in frog, which opens up for speculations on a general osmoregulatory mechanism for an organisms living both on land and in water.

In conclusion, the structural and functional analysis together with the results from MD support a model where non-phosphorylated cpAQP1aa is a semi open pore, which is less efficient for water transport than for example hAQP4, and it can adapt a closed conformation upon phosphorylation of Y107 (**Fig. 7**). A structural mechanism for a possible involvement of phosphorylation of T38 in creating a fully open pore, as suggested by functional analysis, remains to be shown.

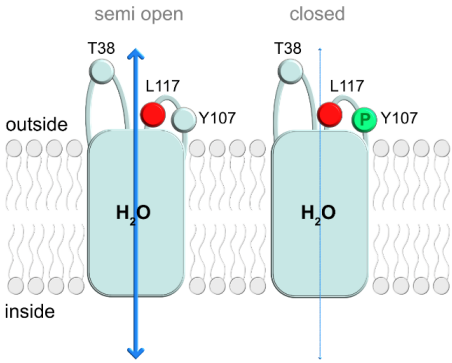

Fig
mechanism of cpAQP1aa. Model of the regulation of the extracellular gate of cpAQP1aa where phosphorylation of Y107 gives rise to a closed water channel.

Gating as a regulatory mechanism has been proposed for several eukaryotic aquaporin homologues where regulation by capping (larger conformational changes) or pinching (small side-chain movements) have been presented [24]. Structural studies have resulted in detailed gating mechanisms to be proposed for AQP0 from mammals [25], SoPIP2;1 from plant [16] and Aqy1 [26] from yeast, all of which involves restriction of the channel radius on the cytoplasmic side and triggers such as as pH (AQP0 and SoPIP2;1), phosphorylation (SoPIP2;1 and Aqy1) and mechanosensitivity (Aqy1). In addition, a gating mechanism for mammalian AQP0 involving an extracellular gate has also been suggested, whereby channel closures is triggered by AQP0-mediated cell-cell contacts during the formation of junctions in the eye lens [25]. This involves a pinching-type mechanism in which, in the junctional (closed) form, the side chain of Met176 protrudes into the channel while it points away from the channel in the non-junctional form (open), allowing additional water molecules to pass through (**Fig. 8**). As seen in **Supplementary Figure 1**, Met176 in AQP0 is a unique residue at this position

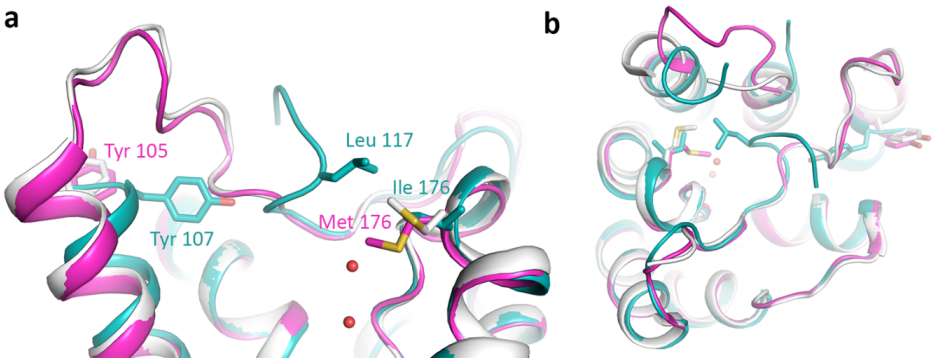

PDB code 1YMG) form. mammalian AQP0 and cpAQP1aa (teal) viewed (a) parallel to the membrane and (b) from the extracellular side. In junctional (closed, magenta) AQP0, the side chain of Met 176 points into the channel, causing restriction, whereas in non-junctional AQP0 (open, white) it points away from the channel. In cpAQP1aa, this position corresponds to Ile 176 which, together with Leu 117 and Gly 180 constitutes an extracellular constriction site. The cpAQP1aa constriction site is a result of a unique conformation of loop C whereby the side chain of Tyr 107 pushes it towards the center of the channel. In AQP0, the corresponding residue, Tyr 105, points in the opposite direction, as seen for other AQPs (Figure 3b).

among the aquaporins, most isoforms have isoleucine at this site. In cpAQP1aa, this residue corresponds to Ile176, which together with Leu117 and Gly180 forms the extracellular hydrophobic constriction region that is involved in the proposed phosphorylation-dependent gating mechanism. However, in comparison to mammalian AQP0, the cpAQP1aa structure demonstrates a novel mechanism consistent with capping whereby a conformational of change of loop C which puts Leu117 further into the channel. Moreover, whereas the ability to rapidly regulate water flow through cpAQP1aa in this manner seems plausible for osmoregulation in the fish, the physiological relevance of extracellular gating of AQP0 via junction-formation is not obvious since in this form it has its main function as an adhesion protein.

Amongst to established aquaporin regulatory mechanisms, gating of cpAQP1aa mostly resembles the one of SoPIP2;1; in both cases conformational change of a loop results in the insertion of a leucine residue into the channel opening, albeit from opposite sides of the membrane (**Figure 3 and Supplementary Figure 3**). A leucine residue in the position equivalent to 117 in cpAQP1aa is highly conserved among the aquaporins. It is therefore not obvious why Leu117 adopts a specific conformation in cpAQP1aa, different from the other aquaporin homologues. A possible explanation lies in the hydrogen bonding network surrounding Leu117 which is stabilized by the neighboring residues Tyr107, Asn114 and Asn116, where none of these are conserved among the aquaporins. Tyr107 is rather well-conserved among fish species, as well as present in several mammalian AQP homologues, including AQP0, AQP4 and AQP7 (**Supplementary Figure 1**), Asn116 is present at this site in AQP0 and Asn114 is only present in a few fish species.

Taken together, this study suggests a novel gating mechanism for aquaporin regulation where phosphorylation on the extracellular side of the protein determines the size of the aqueous pore. Compared to known aquaporin gating mechanisms involving phosphorylation, these sites are localized on the cytoplasmic side of the protein [27]. Nevertheless, extracellular phosphorylation has been suggested for a long time and the conserved pattern *in vivo* is further understood by the characterization

of specific kinases [28]; for example, a Tyrosine kinase has been suggested to influence the localization and regulation of a synaptic receptor [29]. Furthermore, according to the mRNA expression of *A. testudineus* cpAQP1aa regulated by environmental conditions, it is mainly localized in the epithelial cell layers of the osmoregulatory organs like gill, skin, kidney and intestine [7]. If localized on the basolateral (mucosal) side of the polarized epithelia cells the extracellular part of the protein will actually be phasing the circulation (see **Fig. 1b**), which may influence the variants of kinases present.

Based on our studies of purified cpAQP1aa, recombinantly produced in *P. pastoris*, we have confirmed that this aquaporin homologue is a specific transporter of water, supporting that this protein is involved in osmoregulation *in vivo*. Furthermore, key residues for the molecular mechanism of regulation have been identified supporting that phosphorylation Y107, and possibly also T38, fine-tunes the extracellular gate of the channel. This is the first structure of a fish AQP and provides unique new insights into the adaptation mechanisms that allows them to tackle osmolarity changes in changing water conditions.

Online Methods

Cloning and protein overproduction

The full-length gene for *Anabas testudineus*, climbing perch, aquaporin 1aa (cpAQP1aa-FL, residues 1-261) (Genbank accession code JX645188.1) was codon optimized for protein production in *P. pastoris* (Genscript) and sub-cloned into the pPICZA vector (Invitrogen), fused with a C-terminal 8xHis-tag (cpAQP1aa-FL). Two truncated constructs, untagged-cpAQP1aa-243 (residues 1-243) and C-terminal 8×His-tagged-cpAQP1aa-244 were prepared for crystallization. The genes were ligated into the pPICZA vector between the EcoRI and XhoI or NotI restriction sites, respectively. The plasmids were linearized by the restriction enzyme MssI (Thermo Scientific) and transformed into an aquaporin deficient Δ33 strain of *P. pastoris* by electroporation [26]. For all the constructs of cpAQP1aa used in this study, extra nucleotides 'GCT' encoding an alanine were intentionally added after the start codon 'ATG' to meet the Kozak consensus sequence [30,31] and the first methionine is numbered as Met0.

Yeast clone selection was performed on YPD plates containing 2,000 μg/mL Zeocin [30] and small-scale protein production was tested for selected strains. Membrane fractions were analyzed by SDS-PAGE and western blot. Strains with the highest production of His-tagged proteins were picked for large scale production in 3 L fermentors. For untagged-cpAQP1aa-243, the strain corresponding to the largest colony on the high-Zeocin plate was used for fermentation directly. Protein production was induced by methanol fed-batch, typically lasting between 24 and 48 h, resulting in a yield of more than 250 g wet cells per liter culture. Cells were harvested by centrifugation (6000 g, 45 min, 4 °C) and stored at -20°C.

Membrane preparation, solubilization and protein purification

For cpAQP1aa-FL, 60 g of cells were thawed at room temperature and resuspended in 200 mL breaking buffer [50 mM KH_2PO_4 (pH 7.5) and 5% (w/v) glycerol], supplemented with Complete EDTA-free protease inhibitor (Roche). A Bead Beater (Bio Spec) was used to break the cells with 0.5 mm glass beads (Scientific industries) grinding for 12×30 s, with 30 s cooling between runs. Cell debris was separated by a first centrifugation (10000 g, 30 min, 4 °C) followed by a second centrifugation (15000 g, 30 min, 4 °C). Crude membrane was harvested from the supernatant by ultracentrifugation (100000 g, 90 min, 4 °C). The resultant membrane was washed with urea buffer [4 M urea, 5 mM Tris-HCl (pH 9.5), 2 mM EDTA and 2 mM EGTA] and ultracentrifuged again at 158000 g for 90 min at 4 °C. A final wash

was performed to remove traces of urea by homogenizing the membrane in membrane resuspension buffer [20 mM Tris-HCl (pH 8.3), 300 mM NaCl, 10% glycerol and 2 mM β-mercaptoethanol (β-MeOH)] and centrifuging at 158000 g for 1 h at 4 °C. Finally, the membrane was homogenized in the membrane resuspension buffer and stored at -80 °C. For untagged-cpAQP1aa-243 and His-tagged-cpAQP1aa-243, the same procedure was used except that the pH of the membrane resuspension buffer was adjusted to 8.

Membrane solubilization of cpAQP1aa-FL was carried out by mixing the membrane with solubilization buffer [20 mM Tris-HCl (pH 8.3), 300 mM NaCl, 10% glycerol, 4% (w/v) n-nonyl-β-D-glucopyranoside (NG, Anatrace) and 2 mM β-MeOH] in a 1:1 volume ratio supplemented with Complete EDTA-free protease inhibitor (Roche). The mixture was gently rocked for 1 h in a cold room. Unsolubilized material was removed by ultracentrifugation (149000 g, 30 min, 4 °C) and the supernatant was transferred to a falcon tube containing pre-equilibrated Ni-NTA agarose beads (Qiagen) and rocked for 3 h or overnight. 5 mM imidazole was added 20 min before centrifugation to avoid non-specific binding. The supernatant containing unbound proteins was discarded after centrifugation at 3000 g for 3 min at 4 °C. Non-specifically bound proteins were removed by washing the matrix in 15 mL wash buffer [20 mM Tris-HCl (pH 8.3), 300 mM NaCl, 10% glycerol, 0.4% NG], 50 mM imidazole and 2 mM β-MeOH] for three times, with centrifugation between washes (3000 g, 3 min, 4 °C). Thereafter the resin with bound protein was transferred to a 6-mL gravity-flow column (Qiagen). Protein was eluted with 10 mL elution buffer [20 mM Tris-HCl (pH 8.3), 300 mM NaCl, 10% glycerol, 0.4% NG, 350 mM imidazole and 2 mM β-MeOH]. Protein fractions were analyzed using SDS-PAGE. Protein containing fractions were pooled together and buffer was exchanged to gel filtration buffer [20 mM Tris-HCl (pH 8.3), 100 mM NaCl, 10% glycerol, 0.4% NG and 2 mM β-MeOH] immediately using a PD-10 column (GE Healthcare). The protein eluted from the column was concentrated to 500 µL using a 50 kDa cut-off concentrator (Merck Millipore), filtered through a 0.2 µm centrifugal filter (VWR) and injected to a Superdex 200 increase gel filtration column (GE Healthcare), pre-equilibrated with gel filtration buffer. Fractions were analyzed using SDS-PAGE and the protein-containing fractions were pooled together. For crystallization, the protein was concentrated to ~18 mg/mL and stored at -80°C. For His-tagged-cpAQP1aa-243, the protocols were same except that the pH of all the buffers was 8.

For the untagged protein, the solubilization buffer contained 20 mM Tris-HCl (pH 8), 10% glycerol, 4% NG and 2 mM β-MeOH. After solubilization and centrifugation, the solubilized material was diluted in a 1:3 (v/v) ratio with drop-wise addition of pre-chilled dilution buffer [20 mM MES (pH 6), 10% glycerol, 0.4% NG and 2 mM β-MeOH]. The diluted sample was filtered using a 0.2 µm bottle top filter (Thermo Fisher Scientific) and applied to a Resource S cation exchange column (GE Healthcare) pre-equilibrated with buffer A [20 mM MES (pH 6), 37.5 mM NaCl, 10% glycerol, 0.4% NG and 2 mM β-MeOH] at a flow rate of 0.5 mL/min. After washing the column with 10 column volume of buffer A, protein was eluted with the gradient 0-40% of buffer B [20 mM MES (pH 6), 1 M NaCl, 10% glycerol, 0.4% NG and 2 mM β-MeOH]. Fractions were analyzed using SDS-PAGE and the protein containing fractions were pooled together and concentrated to 500 µL and injected to a Superdex 200 increase column (GE Healthcare) pre-equilibrated with gel filtration buffer [20 mM Tris-HCl (pH 8), 100 mM NaCl, 10% glycerol, 0.4% NG and 2 mM β-MeOH]. The untagged protein was analyzed, concentrated and saved as described above. The identity of all proteins was verified by mass-spectrometry.

Phosphostain

The aquaporin form climbing perch, cpAQP1aa-243, was analysed for phosphorylation together with a positive and negative control, lysozyme and the periplasmic chaperone spy), respectively, by using a selective phosphate-binding tag molecule (BTL-111), with streptavidin-conjugated HRP bound to it (prepared according the manual from Fujifilm Wako Pure Chemical Corporation). An SDS-PAGE is performed by loading 7.5 µg of each protein species and operated at 300 V for 15 minutes. After transferring the proteins to a PVDF membrane, the instruction manual is followed, which briefly consists of a soaking step with 1 x TBS-T for at least one hour, 30 minutes of incubation with the tag molecule and consecutive washing steps. The blot was developed by using 4 mL of Genescript LumiSensor chemiluminescent HRP substrate.

X-ray crystallography

Crystallization trials were carried out for all the constructs and best crystals were obtained for untagged-cpAQP1aa-243 by the hanging drop vapour diffusion method at 4 °C. The reservoir solution contained 100 mM Tris-HCl (pH 7.8), 5% poly-γ-glutamic acid low molecular weight polymer (γ-PGA, Na+ form, LM) and 30% (w/v) PEG400. 4 µL of the reservoir solution was mixed with 1 µL 30% (w/v) D-Sorbitol. Crystallization drops were then set up by mixing the mixture with protein at 1:1 or 2:1 ratio, against 0.5 mL reservoir. Crystals with different shapes appeared after a few days. Crystals were mounted in cryo-loops, flash frozen in liquid nitrogen and stored for data collection.

Complete data sets were collected at beam line P13 (wavelength 0.8 Å) at the PETRA III storage ring (DESY, Hamburg, Germany) [32]. Data sets were processed using MOSFLM [33] and scaled using SCALA of the CCP4 program suite [34]. Molecular replacement was carried out using the program Phaser from the CCP4 program suite [34] with a homology model of cpAQP1aa generated using the SWISS-MODEL web server [35] based on the structure of bovine AQP1 (PDB: 1J4N) [13]. The model was examined and adjusted manually in COOT [36] and subsequent refinement was carried out with Phenix-refine [37].

Transport studies

Water transport studies were carried out using similar protocols described in [38,39]. Liposome stock (25 mg/mL) was prepared by homogenizing *E. coli* polar lipid extract (Avanti Polar Lipids) in reconstitution buffer [50 mM NaCl and 50 mM Tris-HCl (pH 8.3) for cpAQP1aa-FL and pH 8.0 for His-tagged-cpAQP1aa-243]. An n-Octyl-β-D-Glucoside (β-OG, Anatrace) stock solution [50 mM Tris-HCl (pH 8.0), 50 mM NaCl and 10% β-OG (w/v)] was added to the liposome solution to a final concentration of 1%. Purified protein was added into the mixture with a theoretical lipid-to-protein ratio of 50. Samples were gently mixed and incubated for 10 min. Subsequently, Biobeads (Bio-Rad laboratories) was added to the mixture to remove the detergents by incubation (and rocking) at room temperature in dark overnight. The resulting proteoliposome was pelleted (100000 g, 1 h, 10 °C) and gently resuspended in reconstitution (same as described before) buffer to a final lipid concentration of 2 mg/mL. Samples were filtered using a 0.2 µm spin column filter (VWR) by centrifugation (10000 g, 3 min, 20 °C) before measurements. Control liposomes were prepared using the same protocol but with addition of corresponding gel filtration buffer instead of purified protein.

Water transport experiments were conducted on an SFM 2000 (BioLogic Science Instruments). In brief, 88 µL of sample was rapidly mixed with the same amount of hyperosmolar solution (reconstitution buffer with 300 mM sucrose). Change in light scattering intensity at the wavelength of 438 nm was

monitored at the fixed angle of 90°. Two independent proteoliposome preparations were made for each target protein and three samples were measured for each. For each sample, three measurements were averaged for each curve providing the raw data for the calculation of the initial rate. The light scattering data was normalized and fitted to a two exponential equation:

$$I = A_1 e^{-k_1(t-t_0)} + A_2\, e^{-k_2(t-t_0)} + A_3 \quad \text{Eq. 1}$$

where I is the intensity corresponding to the time point t; A_1, A_2 and A_3 are coefficients; k_1, k_2 are the rate constants of water transport and t_0 is the dead time of the measurements.

Vesicle size for one third of randomly picked liposome and proteoliposome samples was measured using a Malvern Zetasizer Nano ZS instrument (Malvern). The osmotic permeability coefficient (P_f, cm/s) was calculated using the following equation:

$$P_f = \frac{k}{\left(\frac{S}{V_0}\right) * V_w * C_{out}} \quad \text{Eq. 2}$$

where k (s^{-1}) is the fitted rate constant; (S/V_o) is the external surface to internal volume ratio of the vesicles; V_w is the partial molar volume of water and C_{out} is the external osmolality [40].

Averaged curves (n = 6-25 (2-9)), were the number of individual preparations are given in parenthesis, were used to calculate initial rate. Average plus standard deviation was calculated for each target. Figures were made using Graphpad Prism version 6.0 and the error bars represent standard deviation.

Glycerol transport measurements were performed using the same setup with the difference that the liposomes were preloaded with glycerol buffer (300 mM glycerol, 50 mM Tris pH 8.3, 50 mM NaCl) and the transport of glycerol out of the proteoliposome was measured via light scattering at 90° and a wavelength of 438 nm. For each measurement, 88 µL glycerol buffer and 88 µL sucrose buffer (300 mM sucrose, 50 mM Tris pH 8.3, 50 mM NaCl) assuring that the osmolarity of 528 mOsm was applied. For each experiment, minimum three traces of single stopped-flow performances were averaged and fitted to a two-exponential function using R^2 values of minimum 0.95.

Molecular Dynamics Simulations

All molecular dynamics (MD) simulations were conducted using the MD engine [41] in the YASARA program [42], with the AMBER14 force field [43]. The crystal structure of the aquaporin was first protonated assuming a pH of 7, and energy minimized. The different mutants or phosphorylated variants (pY107, pT38, Y107A, L117A) were generated by modifying the corresponding residue of the minimized structure *in silico*, followed by additional energy minimization. Each system was placed in a cubic water box extending 10Å away from nearest protein atom in each direction, water molecules were randomly replaced by Na^+ or Cl^- ions to ensure charge neutrality and assuming a physiological salt concentration of 0.9% NaCl.

Following a stepwise sequence of equilibration, the 100 ns production runs were performed on wild type crystal structure and the five modified proteins, assuming T=298 kelvin, as maintained through velocity rescaling, and simulation box rescaling to ensure water density of 0.997 for pressure control. Each simulation box contained in the order of 55000 atoms. All simulations were performed using the default macro md.run in the YASARA program. Analyses were performed with the macro md_analyze in the YASARA program, to which analysis of the bond distances were added.

Acknowledgements

The work presented in this study was supported from research grants from the Swedish research Council (VR-M, Structural studies of aquaporin:protein complexes) to Kristina Hedfalk as well as from Academic Research Grant, Ministry of Education, Singapore (R154-000-632-112)

and Environment and Water Industry Development Council, Singapore (R706-000-041-279) to Kunchithapadam Swaminathan. We thank Zhengjun Li and Siew Hong Lam of Department of Biological Sciences, National University of Singapore for providing the cpAQP1 plasmid, which we later modified and recloned. Matthijs Panman has been of crucial help in improving the quality of the script for analysing the stopped-flow data and Darius Sulskis provided the SPY protein. The atomic coordinates and structure factors (PDB ID: 7D5H) have been deposited in the Protein Data Bank (http://wwpdb.org/).

Author Contributions

The project presented in this manuscript is result of collaboration between University of Gothenburg, Sweden, National University of Singapore, Singapore, Lund University, Sweden and Chalmers University of Technology, Sweden.

Jiao Zeng conducted the majority of the experiments on protein design, protein production, crystallization and structural evaluation. JZ also made a major contribution writing the initial draft of the manuscript (Data curation, Formal analysis, Methodology, Supervision, Visualization, Writing - original draft).

Florian Schmitz produced and purified all mutated variants of cpAQPaa from *P. pastoris* and made all the functional experiments on water and glycerol transport (Data curation, Formal analysis, Methodology, Visualization).

Simon Isaksson has contributed to data analysis of the functional experiments (Data curation, Formal analysis, Methodology).

Olivia Arbab, master student supervised by KH and JZ, assisted in the optimization of crystallization and structural determination (Data curation, Formal analysis, Methodology).

Martin Andersson, main supervisor of SI, assisted in finalizing the manuscript (Conceptualization, Funding acquisition, Writing - review & editing).

Leif Eriksson has contributed with the MD simulations of cpAQP1aa (Conceptualization, Methodology, Validation, Visualization, Resources, Writing - review & editing)

Swaminathan Kunchithapadam is the initiator of the project and main supervisor of JZ (Conceptualization, Funding acquisition, Investigation, Project administration, Resources, Supervision, Writing - review & editing).

Susanna Törnroth-Horsefield contributed with expertise in membrane protein crystallography and solved the structure of cpAQPaa together with JZ (Conceptualization, Funding acquisition, Methodology, Supervision, Validation, Visualization, Resources, Writing - review & editing).

Kristina Hedfalk is the main supervisor of FS, mentor to JZ, project leader of the path from protein production to characterization and she wrote the paper where all co-authors contributed to the writing process (Conceptualization, Data curation, Formal analysis, Funding acquisition, Investigation, Project administration, Resources, Supervision, Validation, Writing - review & editing).

Competing Interests Statement

The authors declare that they have no conflicts of interest with the contents of this article.

References

1 Grosell, M. The role of the gastrointestinal tract in salt and water balance *in Fish Physiology,edsM. Grosell, A. P. Farrell, and J. B. Colin (San Diego, CA: Academic Press)*, 135–164. (2010).

2 Sundell, K. S. & Sundh, H. Intestinal fluid absorption in anadromous salmonids: importance of tight junctions and aquaporins. *Front Physiol* **3**, 388, doi:10.3389/fphys.2012.00388 (2012).

3 Lema, S. C., Carvalho, P. G., Egelston, J. N., Kelly, J. T. & McCormick, S. D. Dynamics of Gene Expression Responses for Ion Transport Proteins and Aquaporins in the Gill of a Euryhaline Pupfish during Freshwater and High-Salinity Acclimation. *Physiol Biochem Zool* **91**, 1148-1171, doi:10.1086/700432 (2018).

4 Madsen, S. S., Engelund, M. B. & Cutler, C. P. Water transport and functional dynamics of aquaporins in osmoregulatory organs of fishes. *Biol Bull* **229**, 70-92, doi:10.1086/BBLv229n1p70 (2015).

5 Chang, E. W. *et al.* Changes in tissue free amino acid contents, branchial Na+/K+ -ATPase activity and bimodal breathing pattern in the freshwater climbing perch, Anabas testudineus (Bloch), during seawater acclimation. *J Exp Zool A Ecol Genet Physiol* **307**, 708-723, doi:10.1002/jez.a.424 (2007).

6 Davenport, J. & Abdulmatin, A. K. M. Terrestrial Locomotion in the Climbing Perch, Anabas-Testudineus (Bloch) (Anabantidea, Pisces). *J Fish Biol* **37**, 175-184, doi:DOI 10.1111/j.1095-8649.1990.tb05938.x (1990).

7 Ip, Y. K. *et al.* Molecular characterization of branchial aquaporin 1aa and effects of seawater acclimation, emersion or ammonia exposure on its mRNA expression in the gills, gut, kidney and skin of the freshwater climbing perch, Anabas testudineus. *PLoS One* **8**, e61163, doi:10.1371/journal.pone.0061163 (2013).

8 Tay, Y. L. *et al.* Active ammonia transport and excretory nitrogen metabolism in the climbing perch, Anabas testudineus, during 4 days of emersion or 10 minutes of forced exercise on land. *J Exp Biol* **209**, 4475-4489, doi:10.1242/jeb.02557 (2006).

9 Cutler, C. P., and G. Cramb. 2000. . Pp. 431–441 Water transport and aquaporin expression in fish. *in Molecular Biology and Physiology of Water and Solute Transport, S. Hohmann, and S. Nielsen, eds. Kluwer Academic Press, London.* , 431–441 (2000).

10 Fischbarg, J. Fluid transport across leaky epithelia: central role of the tight junction and supporting role of aquaporins. *Physiol Rev* **90**, 1271-1290, doi:10.1152/physrev.00025.2009 (2010).

11 Frick, A. *et al.* X-ray structure of human aquaporin 2 and its implications for nephrogenic diabetes insipidus and trafficking. *Proceedings of the National Academy of Sciences of the United States of America* **111**, 6305-6310, doi:10.1073/pnas.1321406111 (2014).

12 Horsefield, R. *et al.* High-resolution x-ray structure of human aquaporin 5. *Proceedings of the National Academy of Sciences of the United States of America* **105**, 13327-13332, doi:10.1073/pnas.0801466105 (2008).

13 Sui, H., Han, B. G., Lee, J. K., Walian, P. & Jap, B. K. Structural basis of water-specific transport through the AQP1 water channel. *Nature* **414**, 872-878, doi:10.1038/414872a (2001).

14 Smart, O. S., Goodfellow, J. M. & Wallace, B. A. The pore dimensions of gramicidin A. *Biophys J* **65**, 2455-2460, doi:10.1016/S0006-3495(93)81293-1 (1993).

15 Ho, J. D. *et al.* Crystal structure of human aquaporin 4 at 1.8 A and its mechanism of conductance. *Proc Natl Acad Sci U S A* **106**, 7437-7442, doi:10.1073/pnas.0902725106 (2009).

16 Tornroth-Horsefield, S. *et al.* Structural mechanism of plant aquaporin gating. *Nature* **439**, 688-694, doi:10.1038/nature04316 (2006).

17 de Mare, S. W., Venskutonyte, R., Eltschkner, S., de Groot, B. L. & Lindkvist-Petersson, K. Structural Basis for Glycerol Efflux and Selectivity of Human Aquaporin 7. *Structure* **28**, 215-222 e213, doi:10.1016/j.str.2019.11.011 (2020).

18 Kirscht, A. *et al.* Crystal Structure of an Ammonia-Permeable Aquaporin. *PLOS Biology* **14**, e1002411, doi:10.1371/journal.pbio.1002411 (2016).

19 Ishibashi, K., Hara, S. & Kondo, S. Aquaporin water channels in mammals. *Clin Exp Nephrol* **13**, 107-117, doi:10.1007/s10157-008-0118-6 (2009).

20 Horng, J. L., Chao, P. L., Chen, P. Y., Shih, T. H. & Lin, L. Y. Aquaporin 1 Is Involved in Acid Secretion by Ionocytes of Zebrafish Embryos through Facilitating CO2 Transport. *PLoS One* **10**, e0136440, doi:10.1371/journal.pone.0136440 (2015).

21 Talbot, K., Kwong, R. W., Gilmour, K. M. & Perry, S. F. The water channel aquaporin-1a1 facilitates movement of CO(2) and ammonia in zebrafish (Danio rerio) larvae. *J Exp Biol* **218**, 3931-3940, doi:10.1242/jeb.129759 (2015).

22 Kirscht, A. *et al.* Crystal Structure of an Ammonia-Permeable Aquaporin. *PLoS Biol* **14**, e1002411, doi:10.1371/journal.pbio.1002411 (2016).

23 Chen, X. L. *et al.* Na(+)/H(+) Exchanger 3 Is Expressed in Two Distinct Types of Ionocyte, and Probably Augments Ammonia Excretion in One of Them, in the Gills of the Climbing Perch Exposed to

Seawater. *Front Physiol* **8**, 880, doi:10.3389/fphys.2017.00880 (2017).
24 Hedfalk, K. *et al.* Aquaporin gating. *Current opinion in structural biology* **16**, 447-456, doi:10.1016/j.sbi.2006.06.009 (2006).
25 Gonen, T. *et al.* Lipid-protein interactions in double-layered two-dimensional AQP0 crystals. *Nature* **438**, 633-638, doi:10.1038/nature04321 (2005).
26 Fischer, G. *et al.* Crystal structure of a yeast aquaporin at 1.15 angstrom reveals a novel gating mechanism. *PLoS biology* **7**, e1000130, doi:10.1371/journal.pbio.1000130 (2009).
27 Nesverova, V. & Tornroth-Horsefield, S. Phosphorylation-Dependent Regulation of Mammalian Aquaporins. *Cells* **8**, doi:10.3390/cells8020082 (2019).
28 Bordoli, M. R. *et al.* A secreted tyrosine kinase acts in the extracellular environment. *Cell* **158**, 1033-1044, doi:10.1016/j.cell.2014.06.048 (2014).
29 Hanamura, K. *et al.* Extracellular phosphorylation of a receptor tyrosine kinase controls synaptic localization of NMDA receptors and regulates pathological pain. *PLoS Biol* **15**, e2002457, doi:10.1371/journal.pbio.2002457 (2017).
30 Oberg, F., Sjohamn, J., Conner, M. T., Bill, R. M. & Hedfalk, K. Improving recombinant eukaryotic membrane protein yields in Pichia pastoris: the importance of codon optimization and clone selection. *Mol Membr Biol* **28**, 398-411, doi:10.3109/09687688.2011.602219 (2011).
31 Romanos, M. A., Scorer, C. A. & Clare, J. J. Foreign gene expression in yeast: a review. *Yeast* **8**, 423-488, doi:10.1002/yea.320080602 (1992).
32 Cianci, M. *et al.* P13, the EMBL macromolecular crystallography beamline at the low-emittance PETRA III ring for high- and low-energy phasing with variable beam focusing. *J Synchrotron Radiat* **24**, 323-332, doi:10.1107/S1600577516016465 (2017).
33 Leslie, A. G. W. Recent changes to the MOSFLM package for processing film and image plate data. *oint CCP4 + ESF-EAMCB Newsletter on Protein Crystallography* **26**, doi:citeulike-article-id:7955322 (1992).
34 Collaborative Computational Project, N. The CCP4 suite: programs for protein crystallography. *Acta Crystallogr D Biol Crystallogr* **50**, 760-763, doi:10.1107/S0907444994003112 (1994).
35 Biasini, M. *et al.* SWISS-MODEL: modelling protein tertiary and quaternary structure using evolutionary information. *Nucleic Acids Res* **42**, W252-258, doi:10.1093/nar/gku340 (2014).
36 Emsley, P. & Cowtan, K. Coot: model-building tools for molecular graphics. *Acta Crystallogr D Biol Crystallogr* **60**, 2126-2132, doi:10.1107/S0907444904019158 (2004).
37 Afonine, P. V. *et al.* Towards automated crystallographic structure refinement with phenix.refine. *Acta Crystallogr D Biol Crystallogr* **68**, 352-367, doi:10.1107/S0907444912001308 (2012).
38 Isaksson, S. *et al.* Protein-Containing Lipid Bilayers Intercalated with Size-Matched Mesoporous Silica Thin Films. *Nano Lett* **17**, 476-485, doi:10.1021/acs.nanolett.6b04493 (2017).
39 Oberg, F. *et al.* Glycosylation increases the thermostability of human aquaporin 10 protein. *The Journal of biological chemistry* **286**, 31915-31923, doi:10.1074/jbc.M111.242677 (2011).
40 van Heeswijk, M. P. & van Os, C. H. Osmotic water permeabilities of brush border and basolateral membrane vesicles from rat renal cortex and small intestine. *J Membr Biol* **92**, 183-193 (1986).
41 Krieger, E. & Vriend, G. New ways to boost molecular dynamics simulations. *J Comput Chem* **36**, 996-1007, doi:10.1002/jcc.23899 (2015).
42 Krieger, E. & Vriend, G. YASARA View - molecular graphics for all devices - from smartphones to workstations. *Bioinformatics* **30**, 2981-2982, doi:10.1093/bioinformatics/btu426 (2014).
43 Maier, J. A. *et al.* ff14SB: Improving the Accuracy of Protein Side Chain and Backbone Parameters from ff99SB. *J Chem Theory Comput* **11**, 3696-3713, doi:10.1021/acs.jctc.5b00255 (2015).

Supplementary Material

Optimization of the production of cpAQP1 in Pichia pastoris

The full length cpAQP1aa was successfully produced to high yields in the *P. pastoris* membranes, with an estimated yield of 63 mg highly pure protein per liter culture after a two-step purification procedure. This protein was used for functional characterization after reconstitution into liposome using stopped flow. Crystallization attempts were also pursued, but no crystals were achieved. In the optimization of the crystallization approach for cpAQP1aa, truncated versions of the protein were evaluated, where truncations were based on the alignment with vertebrate AQPs with available structures. The N-terminus of cpAQPaa is very short and the focus for truncations leaned on the C-terminus of the protein which specifically aligned with the C-terminal domain of mammalian AQP0, 1, 2 and 5 (**Supplementary Figure 1**). Based on this alignment, six different C-terminal truncations were made from cpAQP1aa residue 228 to 243, where the shortest truncation showed the highest production level (38 mg/L) and it was therefore taken further to large scale production and crystallization. Resolution down to 7 Å was achieved for this truncated version of cpAQP1aa, and based on inhomogeneity and instability during purification three additional versions of the same construct were evaluated including an untagged variant, since it was suspected that the His-tag had a negative influence on the crystallization event. This hypothesis turned out to be valid; a monodisperse peak appeared after size-exclusion chromatography indicating a homogenous population of stable protein. Importantly, highly ordered crystals were achieved for this version and a diffraction at 1.9 Å was achieved (**Supplementary Table 1**).

Supplementary Table 1. Data collection and refinement statistics of cpAQP1aa. Values in parentheses are for the highest resolution shell.

Crystal	**Form A (pH 7.8)**	**Form B (pH 6.5)**
Condition	0.1 M Tris-HCl (pH 7.8), 5% (w/v) γ-PGA (Na+ form, LM), 30% (v/v) PEG400 and 3% (w/v) D-Sorbitol	0.3 M Lithium sulfate, 0.1 M ADA (pH 6.5), 30% (v/v) PEG400 and 3% (w/v) Dextran sulfate sodium salt (Mr 5,000)
Data collection		
Space group	$P42_12$	$C222_1$
Unit Cell parameters		
a, b, c (Å)	80.06 80.06 95.28	113.670 178.100 177.900
Resolution (Å)	95.28-1.90 (2.00-1.90)	95.82-3.46 (3.65-3.46)
R_{merge}	0.108 (0.657)	0.177 (0.832)
Mean I/σ(I)	15.1 (4.0)	4.5 (1.3)
Completeness (%)	100 (100)	98.8 (97.9)
Redundancy	12.2 (12.1)	4.5 (4.3)
Number of unique reflections	25108 (3588)	23598 (3367)
Wilson B-factor ($Å^2$)	25.19	89.59
Refinement		
Resolution (Å)	56.61-1.9 (1.968-1.9)	84.36-3.46 (3.584-3.46)
R_{work}/R_{free}	0.1779/0.2017	0.2707/0.2991
Number of protein atoms	1594	6438
Average B-factors($Å^2$)	36.39	119.41
Ramachandran plot statistics (%)		
Favored region	95.28	90.4
Allowed region	3.77	8.1
Disallowed region	0.94	1.5
RMSD bond lengths (Å)	0.014	0.003
RMSD bond angles(°)	1.171	0.704

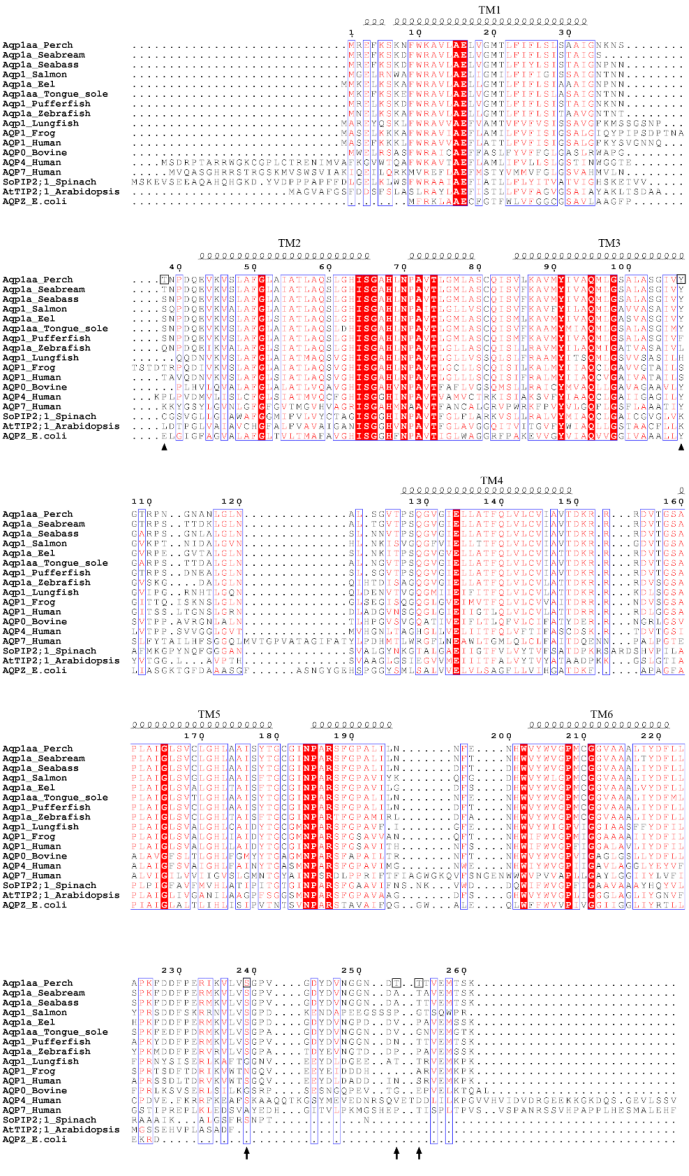

Supplementary Figure 1. Sequence alignment of selected aquaporin homologues from various species. Strictly conserved residues are rendered with white characters on a red background in the column. Well-conserved residues (>70% similarity) are rendered as red characters in the column. Specific amino acids of importance for cpAQP1aa regulation or modification are marked by black boxes and highlighted by arrows; namely T38 and Y107 involved in channel gating and the three confirmed C-terminal phosphorylation sites. Sequence alignment was performed using Clustal Omega, EMBL-EBI (https://www.ebi.ac.uk/Tools/msa/clustalo/), and the figure was made with ESPript 3.0 (http://espript.ibcp.fr/ESPript/ESPript/).

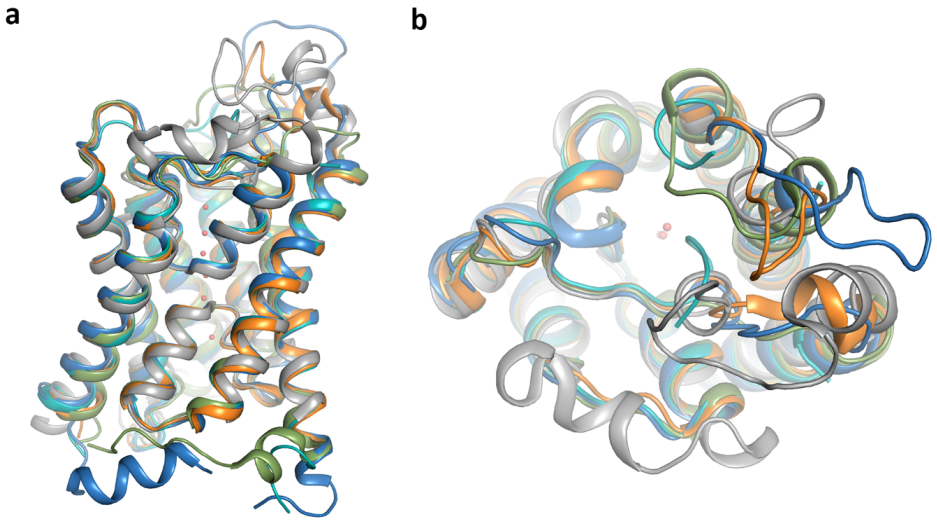

Supplementary Figure 2. Structural comparison of eukaryotic AQPs. Overlay of crystal structures of cpAQP1aa (teal), bovine AQP1 (blue), human AQP4 (orange), human AQP7 (grey) and Arabidopsis TIP2;1 (green) viewed (a) parallel to the membrane and (b) from the extracellular side. Water molecules are shown as red spheres.

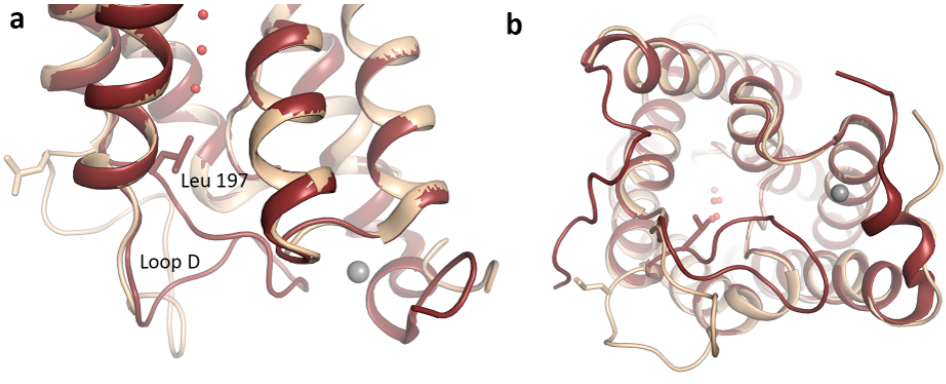

Supplementary Figure 3. Gating mechanism of SoPIP2;1. Crystal structures of SoPIP2;1 in closed (brown, PDB code 1Z98) and open (beige, PDB code 2B5F) conformations viewed (a) parallel to the membrane and (b) from the cytoplasmic side. Channel closure is achieved through a conformational change of loop D, resulting in the insertion of Leu 197 into the channel opening. A Ca^{2+}-binding site at the N-terminus, occupied by Cd^{2+} in the crystal structure, that is involved in stabilizing loop D in the closed conformation is indicated by a grey sphere.

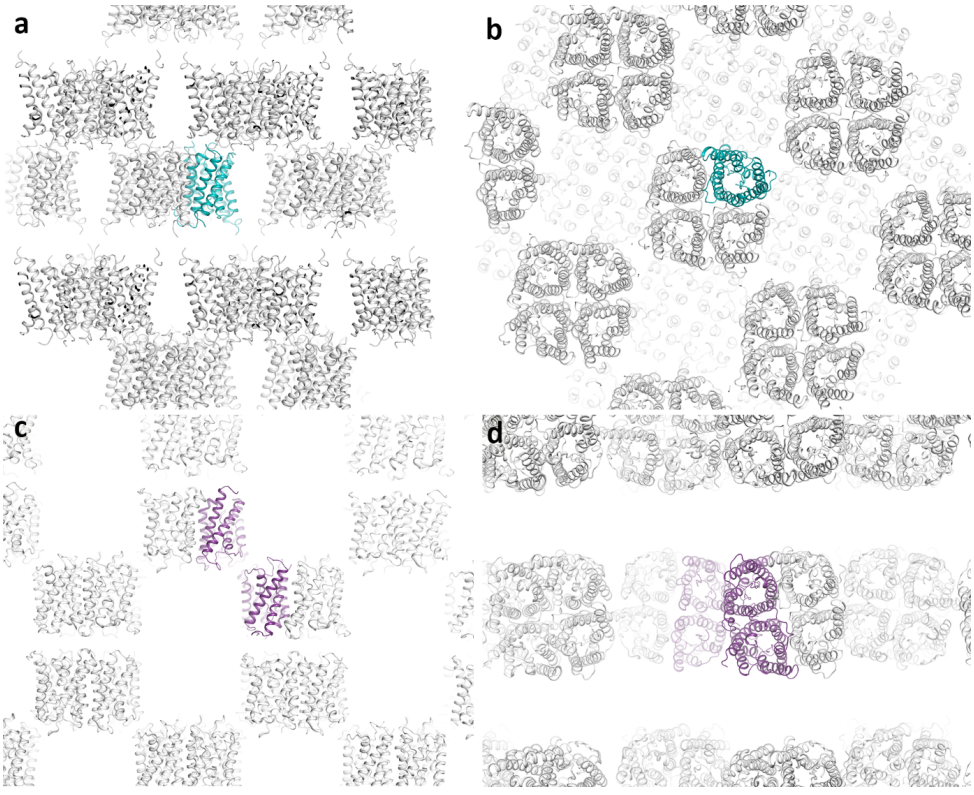

Supplementary Figure 4. Crystal packing for cpAQP1aa at different pH. Cartoon representation of crystal packing in cpAQP1aa crystals grown at (a) pH 7.8 and (b) pH 6.5. The protein molecules corresponding to the asymmetric unit are coloured teal and purple respectively.

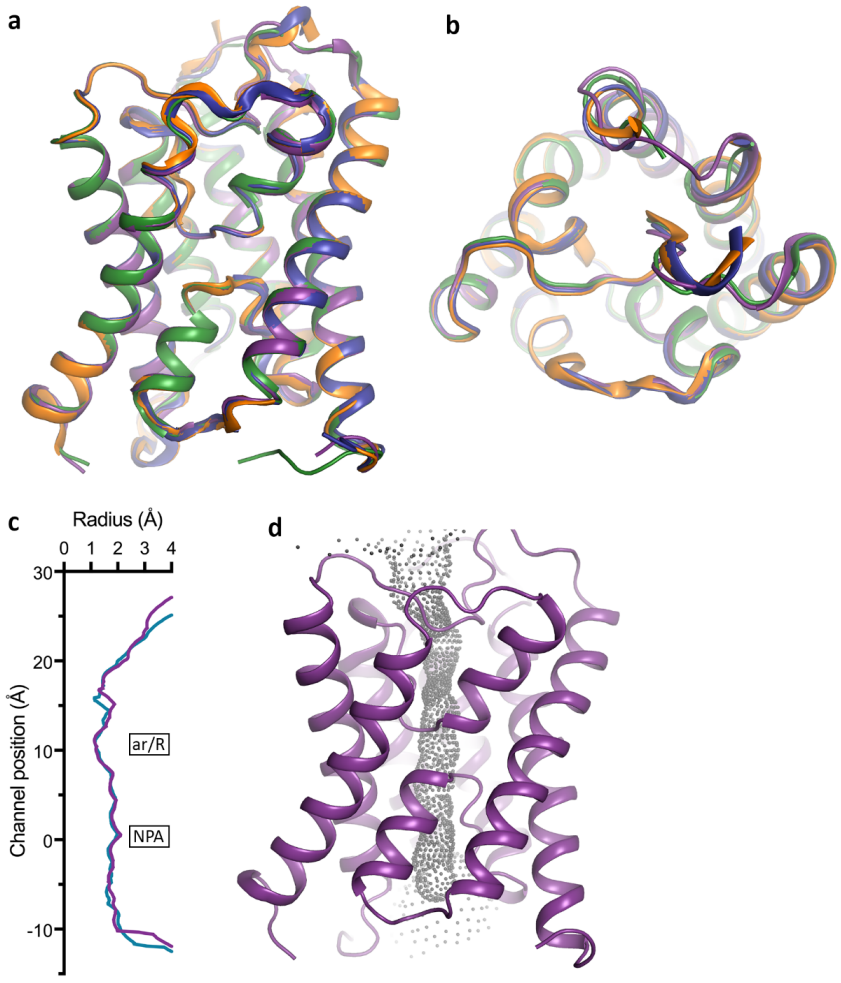

Supplementary Figure 5. Structure of cpAQP1aa at pH 6.5. Overlay of the four monomers in the cpAQP1aa tetramer viewed (a) parallel to the membrane and (b) from the extracellular side, displaying only minor structural differences between the monomers. In one monomer only, monomer C (purple), loops A and C could be built in full. (c) Graph comparing the channel profiles of cpAQP1aa structures at pH 6.5 (monomer C, purple) and 7.8 (teal), as calculated by HOLE. In both structures, a similar constriction can be seen on the extracellular side of the ar/R-region. The zero channel position corresponds to the midpoint between the two NPA motifs. (d) Structure of cpAQP1aa at pH 6.5 (monomer C) with the channel dimensions represented by grey dots.

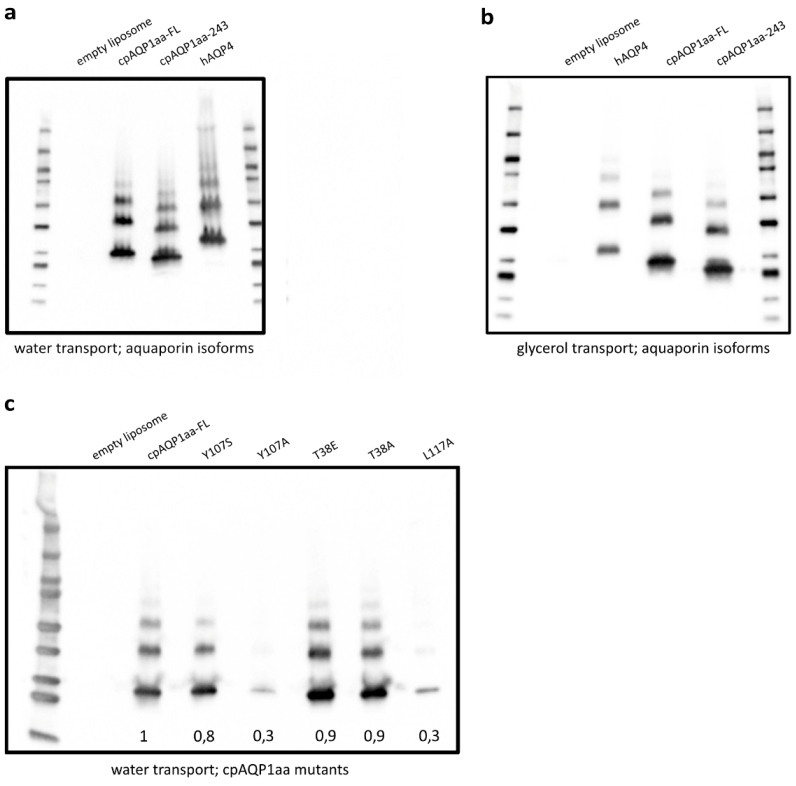

Supplementary Figure 6. Immunoblots showing liposome reconstitution. (a) Immunoblot using the 6x His monoclonal antibody (Takara Clontech) showing typical proteoliposome preps for empty liposome (negative control), cpAQP1aa-FL, cpAQP1-243 and hAQP4 (positive control) for the functional analysis of the water transport. (b) Immunoblot using the 6x His monoclonal antibody (Takara Clontech) showing typical proteoliposome preps for empty liposome (negative control), hAQP4 (positive control), cpAQP1aa-FL and cpAQP1-243 for the functional analysis of the glycerol transport. (c) Immunoblot using the 6x His monoclonal antibody (Takara Clontech) showing the liposome preps for empty liposome (negative control), cpAQP1aa-FL, cpAQP1aa-Y107S, cpAQP1aa-Y107A, cpAQP1aa-T38E, cpAQP1aa-T38A and cpAQP1aa-L117A. The relative protein fractions are averages from two immunoblots.

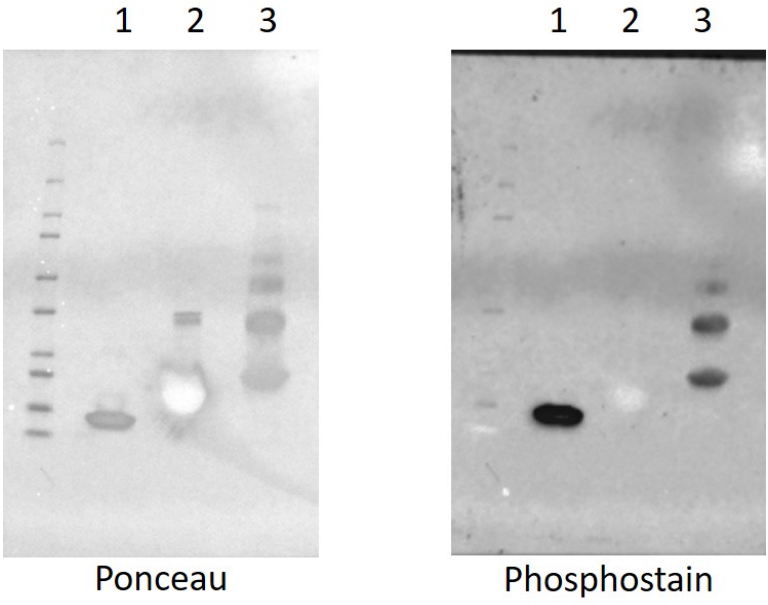

Supplementary Figure 7. Confirmation of phosphorylation and cpAQP1aa structure showing putative phosphorylation sites. SDS-PAGE and phosphostain for (1) positive control (lysozyme), (2) negative control (SPY) and (3) cpAQP1aa-243.

PAPER III

III

BBA - Biomembranes 1862 (2020) 183065

Contents lists available at ScienceDirect

BBA - Biomembranes

journal homepage: www.elsevier.com/locate/bbamem

Characterization of aquaporin-driven hydrogen peroxide transport

Hao Wang[a,b], Stefan Schoebel[b], Florian Schmitz[b], Hansong Dong[a,*], Kristina Hedfalk[b,**]

[a] Department of Plant Pathology, Nanjing Agricultural University, 1 Weigang, Nanjing 210095, China
[b] Department of Chemistry and Molecular Biology, Gothenburg University, Box 462, 405 30 Göteborg, Sweden

ARTICLE INFO

Keywords:
Aquaporin
Arabidopsis thaliana
Hydrogen peroxide
Membrane transporter reconstitution
Proteoliposomes
Water channel
X-ray crystallography
Yeast

ABSTRACT

Aquaporins are membrane-intrinsic proteins initially defined as water (H_2O) channels in all organisms and subsequently found to have multiple substrate specificities, such as hydrogen peroxide (H_2O_2). H_2O_2 is a signaling molecule that partakes in immune responses where its transport is mediated by aquaporins. To shed further light on the molecular basis of the aquaporin function in H_2O_2 transport, we have characterized an *Arabidopsis thaliana* aquaporin, AtPIP2;4, recombinantly produced to high yields in *Pichia pastoris*. Here, we present a newly established assay that allows detection of H_2O_2 transport by purified aquaporins reconstituted into liposomes, enabling us to compare aquaporin homologues with respect to substrate specificity. To get additional insight into the structural determinants for aquaporin-mediated H_2O_2 transport, we solved the 3D-structure of AtPIP2;4 to 3.7 Å resolution and found structural identity to the water channel from spinach (SoPIP2;1), with the difference that Cd^{2+} cation is not required to retain the closed conformation. The transport specificities of the two plant aquaporins were compared to a human homologue, AQP1. Overall, we conclude that AtPIP2;4, SoPIP2;1 and hAQP1 are all transporters of both H_2O and H_2O_2, but have different efficiencies for various specificities. Notably, all three homologues expedite H_2O transport equally well while the plant aquaporins are more permeable to H_2O_2 than hAQP1. Comparison of the structures indicates that the observed variations in H_2O and H_2O_2 transport cannot be explained by differences in the monomeric pore. Possibly, the determinants for transport specificities reside in the flexible domains outside the membrane core of these channels.

1. Introduction

Aquaporins (AQPs) are present in all organisms where they have the primary function to mediate the transport of water under osmotic pressure. Some AQPs could also transport other small neutral solutes, such as glycerol, urea, ammonia, as well as gases, like carbon dioxide, across the plasma membrane. In mammals, 13 AQPs (AQP0-12) have been identified and they are traditionally classified into three subgroups: orthodox AQPs (AQP0, 1, 2, 4, 5, 6 and 8), which have been viewed as mainly transporting water; aquaglyceroporins (AQP3, 7, 9 and 10), which in addition to water can transport glycerol, urea, ammonia, carbon dioxide and metalloids; and superaquaporins (AQP11 and 12), whose details are to be further elucidated [1,2]. AQPs share a common topology of six transmembrane helices with five connecting loops and two half helices containing one highly conserved NPA motif each forming the functional pore, as established in the hourglass model [3]. Even though some homologues share low sequence identity, the three-dimensional fold of AQPs is highly similar, indicating a history of conservation originating two to three billion years back in time [4]. Biochemical studies support that AQPs have a tetrameric assembly with each protomer being a functional unit [5]. High resolution structural studies have explained the mechanism for proton exclusion of the water channels, where two highly conserved AQP signature motifs, constituted of an amino acid triplet each (NPA), provide a macro-dipole positive electrostatic barrier in the middle of the channel [6]. Further, in the super high resolution study of the Aqy1 channel, a pair-wise movement of water was proposed which would prevent proton conduction via the Grotthuss mechanism [7]. Structural studies have also highlighted a site near the extracellular vestibule, the ar/R motif with a highly conserved arginine residue, constituting a specificity filter of the aquaporin channel. The diameter, ~3 Å (Å) in water-specific AQPs and 1 Å wider in a typical aquaglyceroporins such as the glycerol transporter GlpF from *E. coli* [8,9], and the polarity of this site is suggested to constrict and define the substrate specificity of the aquaporin channel. Based on the similarity in the chemical properties of water (H_2O) and hydrogen peroxide (H_2O_2), it is likely that a transporter of H_2O is also a

* Corresponding author.
** Correspondence to: K. Hedfalk, Department of Chemistry and Molecular Biology, Gothenburg University, Box 463, 405 30 Göteborg, Sweden.
E-mail addresses: hsdong@njau.edu.cn (H. Dong), kristina.hedfalk@gu.se (K. Hedfalk).

https://doi.org/10.1016/j.bbamem.2019.183065
Received 14 May 2019; Received in revised form 20 August 2019; Accepted 10 September 2019
Available online 12 September 2019

transporter of H_2O_2.

Indeed, several studies support that selected aquaporins from mammals and plants transport hydrogen peroxide, as evaluated in various cell based systems [10–13]. Further, the insight of a broader function for the water transporting channels has recently been recognized as a subclass of the aquaporin family, the peroxiporins, including AQP3, AQP8, AQP9 and AQP11 [14]. Interestingly, also AQP5 has been noted as a transporter of hydrogen peroxide having a putative role in tumor growth [15]. In plant genomes, there are more AQPs encoded as compared to any other organism. In the plant *A. thaliana*, specifically, 38 sequences with homology to aquaporin have been identified and these are divided into four subfamilies based on their localization: Plasma membrane Intrinsic Proteins (PIP), Tonoplast Intrinsic Proteins (TIP), Nodulin26-like Intrinsic Proteins (NIP) and Small basic Intrinsic Proteins (SIP). Focusing on the aquaporins located to the plasma membrane, the PIPs, there are 13 isoforms in *A. thaliana*, the same number as there are aquaporin isoforms encoded in the human genome [16]. The PIPs in *A. thaliana* are divided into two groups, AtPIP1 and AtPIP2. There are eight AtPIP2 which localize to the plasma membrane as homotetramers while the five AtPIP1s form heterotetramers with AtPIP2s in order to properly localize to the plasma membrane [17,18]. Based on assays testing the viability of yeast cells, five isoforms from *A. thaliana* were suggested to increase the sensitivity to hydrogen peroxide; AtPIP2;1, AtPIP2;2, AtPIP2;4, AtPIP2;5 and AtPIP2;7 [13] where AtPIP2;1 is the only PIP2 ortholog for which an increase of hydrogen peroxide into yeast has been demonstrated previously [19].

Transport of hydrogen peroxide also means that aquaporins contribute to the signaling in living cells [20]. Hydrogen peroxide is a relatively stable Reactive Oxygen Species (ROS) that acts as an extracellular and intracellular signal molecule that mediates pleiotropic effects in animals and plants. In animals, it has been shown that hydrogen peroxide plays an important role in the recruitment of immune cells to damaged areas [21]. Further, in plants the production of ROS is a consequence of a successful recognition of pathogen infection leading to an activation of the defense but it is also involved in other beneficial biotic interactions [22]. The hydrogen peroxide generating system is supposed to be similar in mammals and plants, leading to a rapid production of extracellular hydrogen peroxide after a microbial pathogen infection [23]. The general mechanism for hydrogen peroxide production utilizes the NADPH oxidase complex (NOX) to transfer electrons from NADH or NADPH to O_2 to form superoxide [24–26]. Recent studies have indeed suggested an involvement of aquaporins in the migration of cancer cells as well as a role in inflammation [27,28]. Further, aquaporins have been shown to contribute to the signaling pathway of the immune system in plants [29]. In *A. thaliana*, specifically, it has been shown that AtPIP1;4 and the extracellular hydrogen peroxide play a fundamental role in the intracellular immunity pathways critical to build resistance to pathogens, such as the systemic acquired resistance (SAR) and the immunity triggered by the Pathogen-associated molecular pattern (PAMP) [29]. In plants, aquaporins also provide the hydrogen peroxide export from the chloroplast assisting the clearance of byproducts of photosynthetic activities [30].

Notably, transport studies for hydrogen peroxide have so far been performed in whole cells and characterization of this aspect on pure protein has been lacking. To shed more light on the specificity for hydrogen peroxide for certain AQP homologues, we have identified a target from plant, AtPIP2;4 from *A. thaliana*, produced it to high yields in *P. pastoris* and isolated the protein to homogeneity, enabling functional studies using proteoliposomes. Further, we have evaluated the transport of water and hydrogen peroxide, respectively, between homologues from plant and human. Structure determination of AtPIP2;4 by protein crystallography and detailed analysis enabled the comparison to SoPIP2;1 from spinach and AQP1 from human. By this study, we thereby provide a new proteoliposome assay for the characterization of hydrogen peroxide transport mediated by aquaporin and we also present the first structure of a PIP aquaporin from *A. thaliana*. Both these results contribute to an increased understanding of the aquaporin function and its physiological role.

2. Material and methods

2.1. Cloning

For yeast growth complementation assay, yeast expression plasmids based on the pYES2 vector were constructed with cDNAs of the various AtPIP isoforms using *Eco*RI, *Hind*III and *Kpn*I (TAKARA), respectively. Yeast cells from the NMY51 strain, *Saccharomyces cerevisiae*, were transformed with the expression plasmids and positive transformants were selected and maintained using SC-URA$^-$ medium (0.17% yeast nitrogen base, 2% glucose, 0.5% $(NH_4)_2SO_4$, 0,002% histidine, 0,0023% lysine and 0.01% leucine, with 2% w/v agar for solid plates) at a temperature of 30 °C.

For overproduction of AtPIP2;4 (NM_125459) in *Pichia pastoris*, full-length (FL) and truncated version (28-279), the genes were codon optimized and purchased from GenScript. The truncated version of AtPIP2;4 was based on analysis using the protein prediction website topcons.cbr.su.se, giving that AtPIP2;4(1–27) and AtPIP2;4(280-291) are disordered or not well folded, and therefore considered to be not essential for the protein function. In the design of a truncated version of the protein aiming towards a more efficient crystal packing for structural determination, we designed the truncated variant AtPIP2;4(28-279) leaving out flexible parts of the protein. Both targets were fused to Tobacco Etch Virus (TEV) protease digestion site followed by an 8xHis-tag at the C-terminus and sub-cloned into the pPICZB vector (Invitrogen) using the restriction sites *Eco*RI and *Kpn*I (Thermo Scientific), resulting in AtPIP2;4 (FL) and AtPIP2;4 (28-279), respectively. The plasmids were linearized by the restriction enzyme *Mss*I (Thermo Scientific) and transformed into an aquaporin deficient wild type strain of *P. pastoris,* X-33Δ, by electroporation [31]. For all the constructs used in overproduction, AtPIP2;4 was cloned to mimic the Kozak consensus sequence around the start ATG [32].

2.2. Measurement of H_2O_2 transport in vivo

For the yeast growth assay using *S. cerevisiae*, overnight cultures were prepared from fresh NMY51 transformants by inoculating single colonies in SC-URA medium. The cell pellets were washed with sterile water and diluted to a normalized cell density of OD_{600} = 1. Three 10-fold serial dilutions were prepared from each normalized suspension. Five dilutions, 10 µL of each, from each transformant were spotted on YPD agar plates with or without 3 mM H_2O_2. The plates were incubated for 3–4 days at 30 °C.

To confirm the uptake of H_2O_2 in yeast, a DCF fluorescence assay was applied where intracellular hydrogen peroxide was detected by staining with the ROS-probing dye H2DCFDA (Sigma-Aldrich). *S. cerevisiae*, the NMY51 strain, transformed with AtPIP2;4 was cultured in liquid YPD [33] for 16 to 18 h in a shaker at 200 rpm and 30 °C, spun down using 800*g* and washed twice with phosphate buffer solution (PBS, 0.2 mM, pH 7.4). Cells were suspended with PBS containing H2DCFDA at a final concentration of 10 µM, incubated for 30 min, and then supplied with 3 mM H_2O_2. Yeast cells were observed at 15 min after the addition of H_2O_2 using a confocal microscope (Zeiss).

2.3. Recombinant protein overproduction in Pichia pastoris

In order to identify *P. pastoris* transformants producing high-yields of AtPIP2;4, a high-zeocin (2000 µg/mL Zeocin) growth screen was performed followed by a small-scale production screen, as previously described [32]. To optimize the production level of strains with the highest production of His-tagged AtPIP2;4 s, culturing in a 2 L fermenter was pursued [34], applying methanol induction for three days

continuously assuring that dissolved oxygen was available keeping the carbon source as the limitation for growth. Cells were harvested by centrifugation (6000*g*, 45 min, 4 °C) and stored at −20 °C.

2.4. Membrane preparation, solubilization and protein purification

For AtPIP2;4-FL and AtPI2;4 (28-279), cells were thawed at room temperature, diluted 1:2 with breaking buffer (50 mM potassium phosphate, pH 7.5, 5% (v/v) glycerol, 2 mM EDTA, 1 mM PMSF). Glass beads (0.5 mm) were added and cells broken by grinding in a bead beater (Bio Spec) for 12 × 30 s, with 30 s cooling between runs. Cell debris and unbroken cells were spun down at 10,000*g* for 2 × 20 min at 4 °C. Isolation of the total membrane fraction was performed as previously described [35]. In brief, the membrane was collected by centrifugation (200,000*g* for 90 min at 4 °C) and washed with urea buffer (4 M urea, 5 mM Tris·HCl pH 9.5, 2 mM EDTA, 2 mM EGTA) followed by a wash in membrane wash buffer (20 mM Tris pH 8, 20 mM NaCl, 10% glycerol, 2 mM EDTA, 1 mM PMSF). Finally, the membrane was resuspended in buffer (20 mM Tris pH 8, 20 mM NaCl, 10% glycerol, 1 mM PMSF) and stored at −80 °C.

To find a suitable detergent for AtPIP2;4, a solubilization screen was performed using the following detergents: 3-[(3-cholamidopropyl) dimethylammonio]-1-propanesulfonate (CHAPS), n-Dodecyl-β-D-Maltopyranoside (DDM), n-Decyl-β-D-Maltopyranoside (DM), Fos-Choline-12 (fc12), n-Dodecyl-*N*,*N*-Dimethylamine-N-Oxide (LDAO), Lauryl Maltose Neopentyl Glycol (MNG), Decyl Glucose Neopentyl Glycol (NG) and n-Octyl-β-D-Glucopyranoside (β-OG). Solubilization buffer (4% detergent, 20 mM Tris pH 8, 20 mM NaCl, 1 mM PMSF). Each detergent was added drop-wise into thawed membranes with the end ratio of 1:1 and incubated at 4 °C for 2 h with rotation. Non-solubilized membranes were was spun down at 160,000*g* for 30 min at 4 °C, supernatant and pellet were collected for immunoblot analysis, respectively. Based on the screen for a suitable detergent, LDAO with a final concentration of 2% (w/v) was chosen for large scale solubilization of AtPIP2;4.

For purification of AtPIP2;4, the membranes were solubilized in buffer A (2% LDAO, 200 mM Tris pH 8, 200 mM NaCl), supplemented with Complete EDTA-free protease inhibitor (Roche) for 2 h. Solubilized material was collected by ultracentrifugation (200,000 ×*g*, 30 min, 4 °C) and the supernatant was collected for subsequent purification. Imidazole, to a final concentration of 10 mM, was added to the supernatant which was then incubated with Ni-NTA agarose (Qiagen), pre-equilibrated with buffer (20 mM Tris-HCl pH 8.0, 200 mM NaCl, 10% glycerol, 0.4% LDAO, 10 mM Imidazole), in a 50 mL Falcon tube for 3 h at 4 °C. The Ni-NTA resin was washed two times in Ni-wash buffer (20 mM Tris-HCl pH 8.0, 200 mM NaCl, 10% glycerol, 0.4% LDAO, 50 mM imidazole) and eluted with 5 × 5 mL Elution buffer (20 mM Tris-HCl pH 8.0, 200 mM NaCl, 10% glycerol, 0.4% LDAO, 300 mM imidazole). The protein containing fractions were pooled and concentrated (VivaSpin 100 kDa concentration tube, Sartorius Stedim Biotech GmbH) to a volume of 1 mL, diluted 10× with buffer lacking imidazole (20 mM Tris-HCl pH 8.0, 200 mM NaCl, 10% glycerol, 0.4% LDAO) and concentrated to a final protein concentration of to 10 mg/mL using a VivaSpin 100 kDa concentration tube (Sartorius Stedim Biotech GmbH). The final protein sample was aliquoted into fractions of 500 µL and stored at −80 °C or used immediately for further purification. In the second purification step, the buffer of the protein sample was exchanged to Gel filtration buffer (20 mM Tris-HCl pH 8.0, 200 mM NaCl and detergent (1% OG or 0.145% Octyl Glucose Neopentyl Glycol (OGNPG)) using Superdex200 increase 10/300 gl column (GE Healtcare). Fractions with target protein were collected and used for crystallization or functional assays.

2.5. Measurement of hydrogen peroxide transport in proteoliposomes

The method to measure transport of hydrogen peroxide by purified aquaporins reconstituted in proteoliposomes was developed from the method established by Piwonski et al using horseradish peroxidase (HRP) molecules trapped in lipid vesicles and the addition of externally added Amplex Red substrate [36].

Liposomes were prepared by homogenizing *E. coli* polar lipid extract (Avanti Polar Lipids) in Reconstitution buffer (50 mM NaCl, 50 mM Tris-HCl, pH 8.0) to a final concentration of 25 mg/mL. An n-Octyl-β-D-Glucoside (β-OG, Anatrace) stock solution (50 mM NaCl, 50 mM Tris-HCl, pH 8.0, 10% β-OG (w/v)) was added to the liposome solution to achieve a final concentration of 1% β-OG (w/v). Purified protein was then added to the liposome solution with a theoretical lipid-to-protein ratio of 50 (w/w) and incubated for 10 min with gently mixing. To remove the detergent, Biobeads (Bio-Rad laboratories) were added to the lipid-protein mixture which was then incubated overnight, in darkness with rocking at 4 °C. The resulting proteoliposomes were collected by centrifugation (100,000*g*, 1 h, 4 °C) and gently resuspended in Reconstitution buffer (see above) to a final lipid concentration of 2 mg/mL. Before measurements, samples were filtered by centrifugation (10,000*g*, 3 min, 4 °C) using a 0.2 µm spin column filter (VWR). Control liposomes were prepared using the same protocol but with addition of the corresponding volume of Gel filtration buffer instead of purified protein solution. HRP (0.5 µM) was added to the liposome or proteoliposomes after their formation.

To remove excess of non-encapsulated HRP liposomes were pelleted by centrifugation (100,000*g*, 4 °C for 30 min) and resuspended in Reconstitution buffer with EDTA (50 mM NaCl, 50 mM Tris pH 8.0, 1 mM EDTA). Residual HRP was removed using a MicroSpin S-400 HR Column (GE Healthcare). The aquaporin and control liposomes, respectively, with HRP trapped inside, were incubated in 10 µM Amplex Red (AR, ThermFisher) for 20 min at room temperature. For inhibition studies using mercury, mercury chloride was added to the liposomes and proteoliposomes to a final concentration of 300 µM and incubated for 20 min at room temperature. The resulting liposome mixture was distributed into black Matriplate 96 glass bottom plate (Brooks LIFE SCIENCE SYSTEMS), 150 µL in each well, and mixed with 50 µL H_2O_2 stock solution (200 µM H_2O_2, 50 mM NaCl, 50 mM Tris pH 8.0, 1 mM EDTA). The plate was immediately put into a POLARstar Omega plate reader (BMG TECH) to follow the fluorescent signal from the oxidation of Amplex by HRP and H_2O_2 inside the liposomes. Fluorescence signal was collected for 40 cycles with an interval of 2 min, using wavelength of 544 nm and 590 nm for excitation and emission, respectively. For each sample, triplicates were measured (technical replicates), and the experiment was repeated at least three times (n = 3–6 biological replicates). Each triplicate measurement was fitted to a quadratic equation and the initial rate was calculated for each of these where initial rate = dF/dt. To eliminate the possible experimental variations between different experiments performed in different plates, relative initial rate was determined by relating all proteoliposome experiments those of the empty liposomes. All data represented in the bar graph are provided as the average +/− standard deviation. For each sample, the experiment was repeated in at least three biological replicates consisting of averages of three technical replicates (measurements from the same 96-well plate). The significance of the relative initial rate was analyzed by ANOVA analysis by Fisher's LSD (least significant difference) test ($P < 0.05$) using the software of SPSS (Statistical Product and Service Solutions, USA). Significant differences are indicated by a, b, c. The liposomes and proteoliposomes were analyzed on SDS-PAGE and the band intensity was measured using the software of Image J (developed by National Institutes of Health, USA). The gel images were opened in the type of 8-bit and calibrated through the function of uncalibrated OD. The integrated density (Intden, indicating the quantity of corresponding protein) was measured after subtracting the background. The average +/− standard deviation is shown for three individual gels constituting three biological replicates.

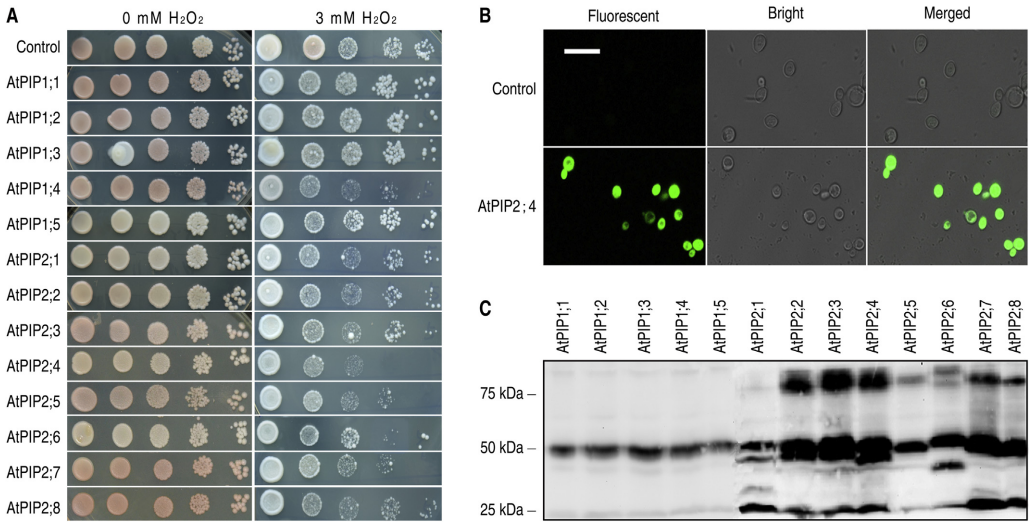

Fig. 1. In vivo hydrogen peroxide transport in yeast transformed with individual AtPIPs. (A) Toxicity of externally applied H_2O_2 on *S. cerevisiae* cells that were not transformed (control) or transformed with a single gene encoding AtPIP homologues fused with a 10× His-tag. Dilutions series, 10-fold, of yeast cells were spotted on YPD agar plates with and without 3 mM H_2O_2, respectively, and image taken after four days incubation. (B) The intracellular accumulation of ROS in yeast cells, not transformed or transformed with AtPIP2;4, the isoform showing the highest sensitivity to H_2O_2 when produced in yeast, grown on medium with H_2O_2 supply. ROS was visualized by staining suspensions of yeast cultures after 20 min with a green-fluorescent dye. (C) Confirmation of production of AtPIP isoforms in yeast cells, analyzed by immunoblot using primary antibody to the His-tag.

2.6. Measurement of water transport in proteoliposomes

Water transport studies were carried out using protocols similar to those previously described [37]. Liposomes were prepared as previously described for the hydrogen peroxide transport studies above, but excluding the addition of HRP to the liposomes or proteoliposomes after their formation.

Water transport experiments were conducted on an SFM 2000 (BioLogic Science Instruments). In brief, 88 µL of sample was rapidly mixed with the same amount of hyperosmolar solution (Reconstitution buffer with 300 mM sucrose). The change in light scattering intensity was monitored at the wavelength of 438 nm and the fixed angle of 90°. Two to four preparations of proteoliposomes (biological replicates) were made for each target and split into three technical replicates which were measured at least three times each to get average curves. For each proteoliposome preparation, the vesicle size was measured for one third of randomly picked liposome and proteoliposome samples, respectively, using a Malvern Zetasizer Nano ZS instrument (Malvern). The surface and volume calculations are based on the average sizes of the vesicles per species, determined via dynamic light scattering (DLS), where the autocorrelation function showed a single decline to zero and the count rates were stable throughout all measurements.

The light scattering data was normalized and fitted to a one exponential equation (Eq. (1)):

$$I = A_1 e^{-k_1(t-t_0)} + A_2 e^{-k_2(t-t_0)} + A_3 \quad (1)$$

where I is the intensity corresponding to the time point t; A_1, A_2 and A_3 are coefficients; k_1, k_2 are the rate constants of water transport and t_0 is the dead time of the measurements.

The osmotic permeability coefficient (P_f, cm/s) was calculated using the following equation (Eq. (2)):

$$P_f = \frac{k}{\left(\frac{S}{V_0}\right) * V_w * C_{out}} \quad (2)$$

where k (s^{-1}) is the fitted rate constant; (S/V_o) is the external surface to internal volume ratio of the vesicles; V_w is the partial molar volume of water and C_{out} is the external osmolality [38]. Averaged curves ($n = 3$) of technical replicates ($n = 5$–11) were used to calculated Pf values for each target, where only r^2 values above 0.9 were accepted. Average plus standard deviation was calculated for each target. The significance of the relative initial rate was analyzed by ANOVA analysis as described above. Significant differences are indicated by a, b, c, where ab is neither significantly different from a, nor b.

2.7. Crystallization, X-ray analysis and structural characterization

Crystallization trials were carried out for both constructs, AtPIP2;4-FL and AtPIP2;4(28-279), applying the hanging drop vapour diffusion method at 4 °C using commercial protein crystallization kits (Membrane Gold™HT-96, Membrane Gold2™HT-96, MemStart™, MemSys™ HT-96 and MemPlus™ HT-96 from Molecular Dimensions as well as HR2–130 from HAMPTON RESEARCH). For both targets, the protein sample was concentrated to 20 mg/mL and crystallization drops were set up by mixing the protein and the reservoir solution to a ratio of 1:1 or 2:1, respectively, using 0.5 mL of the reservoir solution in each case. Two different conditions, [0.1 M NaCl, 0.1 M $MgCl_2$, 0.1 M sodium citrate pH 5.5, 30% (v/v) PEG400] and [1.5 M sodium formate, 0.05 M sodium cacodylate pH 5.5, 30% (v/v) PEG400], respectively, resulted in promising crystallization leads. In the crystal optimization step, 3% w/v Trimethylamine N-oxide dihydrate or 3% w/v 6-Aminohexanoic acid was added to each condition. Crystals with different shapes appeared after a few days. Crystals were mounted in cryo-loops, flash frozen in liquid nitrogen and stored for data collection.

Complete data sets were automatically collected at the ESRF

beamline MASSIF-1 (ID30A-1, workflow: MXPressE) in Grenoble, France [39,40]. Data sets were processed using EDNA [41] and XDS [42]. Molecular replacement was carried out using the program Phaser from the Phenix program suite [43] with a model of SoPIP2;1 (pdb: 4jc6, Mercury activation of the plant aquaporin SoPIP2;1 - structural and functional characterization [44],). The model was then manually mutated, adjusted and examined in Coot [45,46]. Subsequent refinement was carried out with Phenix-refine [47].

3. Results

3.1. AtPIP2;4 is a transporter for hydrogen peroxide

Yeast growth assay were carried out to test H_2O_2 permeability in *Saccharomyces cerevisiae* cells overexpressing AtPIP homologues. Yeast cells transformed with AtPIP2;4 showed the most significant growth defect at 3 mM H_2O_2 as compared to the other twelve AtPIP homologues (Fig. 1A) and was hence selected for further studies. To confirm the transport of H_2O_2 in the yeast transformants, a DCF fluorescence assay was performed. As compared to untransformed cells, cells producing AtPIP2;4 had a much stronger accumulation of H_2O_2 supporting this transport specificity for this particular aquaporin homologue (Fig. 1B). To verify the production of AtPIP isoforms in the yeast cells, whole yeast extract was analyzed by immunoblot using the primary antibody to the His-tag, detecting the monomeric and dimeric form of the protein, respectively. As confirmed for AtPIP2;4, the sensitivity to hydrogen peroxide was connected to production of recombinant protein in the yeast cells (Fig. 1C).

3.2. Optimization of production of AtPIP2;4 in Pichia pastoris

To enable detailed characterization of AtPIP2;4, the protein was expressed in and purified from the methylotrophic yeast *P. pastoris*. Full length protein (AtPIP2;4-FL) and a truncated variant (AtPI2;4(28-279)) were transformed into *P. pastoris*, strain ΔX33 having endogenous AQY1 gene disrupted [31]. To screen for high yielding clones, three colonies for each construct were screened for growth on high-zeocin and further evaluated using the small-scale production screen evaluated by immunoblot [32] (Fig. 2A). The high-yielding clones were taken further to large scale production using fermenter growth. From the large scale culturing, using a volume of 1.5 L, 360 g and 340 g cells were achieved from AtPIP2;4-FL and AtPIP2;4(28-279), respectively. In the optimization of purification, eight of the common detergents for membrane protein solubilization (CHAPS, DDM, DM, FC12, LDAO, MNG, NG, β-OG) was evaluated by immunoblot analysis of the solubilized material from each detergent. LDAO turned out to be the most efficient detergent with respect AtPIP2;4-FL (Fig. 2B), and hence chosen for subsequent purification. The same analysis was also performed on the truncated version of the target, AtPIP2;4(28-279), with the same outcome (data not shown). After the first purification step, using Ni-NTA agarose purification, 50 mg AtPIP2;4-FL and 25 mg AtPIP2;4(28-279) were obtained from 90 g and 85 g *P. pastoris* cells, respectively, giving a total yield of 0.3–0.6 mg pure protein per gram cells. For the crystallization attempts, size-exclusion chromatography was conducted for further purification and detergent exchange, resulting in highly pure protein for the full-length as well as the truncated variant of the target (Fig. 2C). Also for the second purification step, several detergents (β-OG, OGNPG, DDM, DM, LDAO, NG) were evaluated for detergent exchange and the resulting elution peak was analyzed. For AtPIP2;4-FL, only β-OG and OGNPG gave monodisperse peaks (Fig. 2D). For the truncated variant of the target, AtPIP2;4(28-279), β-OG, DM and DDM gave monodisperse peaks indicating homogenous material amendable for crystallization.

3.3. A novel assay for hydrogen peroxide transport using proteoliposomes

Using the *S. cerevisiae* growth assay, AtPIP2;4 was shown to transport hydrogen peroxide, being a strong indication of this transport specificity for this aquaporin homologue from *A. thaliana* (Fig. 1). To analyze the transport specificity for hydrogen peroxide among aquaporin homologues, we have established a novel fluorescent proteoliposome assay relying on purified target protein and the HRP reaction inside the liposome. Empty liposomes or proteoliposomes with reconstituted aquaporin, both having HRP and Amplex Red (AR, Invitrogen) trapped inside, were mixed with a specific concentration of external H_2O_2. Hydrogen peroxide will pass the membrane by simple diffusion, but if aquaporins are specific H_2O_2 transporters, the transport will be faster. When H_2O_2 molecules reach the inside of the liposome HRP catalyzes the reaction of Amplex Red and H_2O_2 resulting in a product of highly fluorescent resorufin which can be quantified as secondary

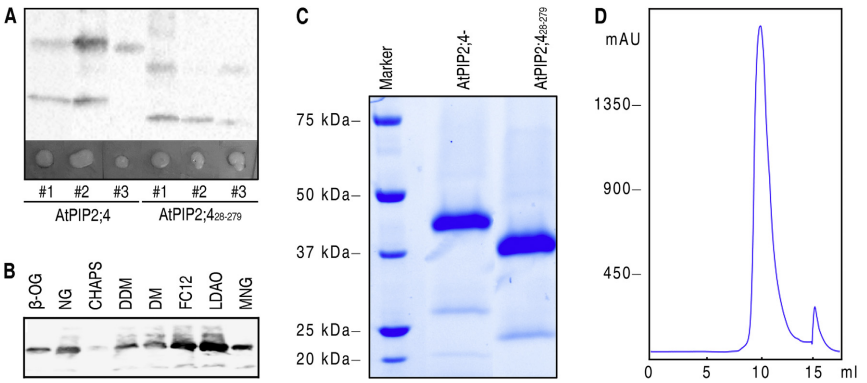

Fig. 2. Purification of AtPIP2;4 recombinantly produced in *Pichia pastoris*. (A) Initial production screening of *P. pastoris* transformed with AtPIP2;4, full-length gene and truncated variant shortened in the N- and C-terminus (residue 28-279), respectively, both equipped with an 8× His-tag. Three different transformants are shown together with the corresponding signal on the immunoblot using the antibody towards the His-tag. (B) Detergent screen using eight different detergents commonly used for membrane protein extraction. The supernatant after solubilization was investigated using immunoblot and the antibody directed towards the his-tag showing that LDAO was the most efficient detergent with respect to the AtPIP2;4-FL (C) SDS-PAGE gel showing purified AtPIP2;4, full-length and truncated, respectively, after a two-step purification scheme. (D) The final peak of homogenous AtPIP2;4-FL after the second purification step using SEC.

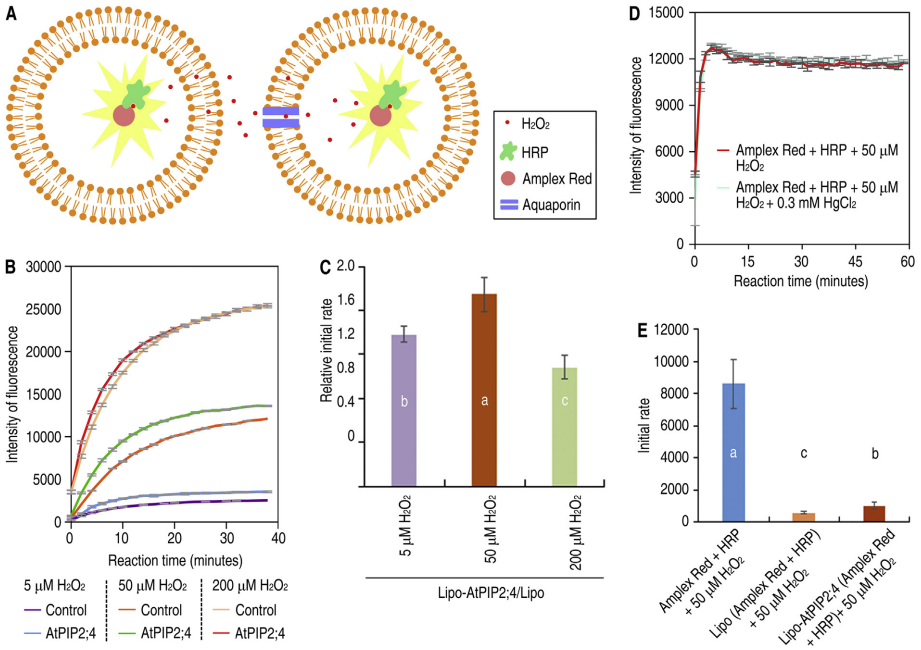

Fig. 3. Functional assay of hydrogen peroxide transport in proteoliposomes. (A) Schematic representation of the hydrogen peroxide transport measurements in proteoliposomes with the coupled reaction of HRP inside the liposomes where the reaction of Amplex Red and H_2O_2 gives rise to the fluorescent product resorufin The more efficient hydrogen peroxide transport that takes place via the aquaporin gives rise to a higher fluorescent read-out, as compared to the simple diffusion in the control liposomes. (B) In order to establish the assay, different H_2O_2 concentrations (5, 50 and 200 μM, respectively) were evaluated to find the concentration that gave a clear difference of the aquaporin mediated transport as compared to simple diffusion (average of technical replicates +/− standard deviation is shown, $n = 3$). (C) Bar graph showing the relative initial rates at different H_2O_2 concentrations where a, b and c illustrate the significance from the ANOVA analysis (average of technical replicates +/− standard deviation is shown, n = 3). (D) The control experiment for the detection system of hydrogen peroxide mixed with $HgCl_2$ showing that the conventional aquaporin inhibitor does not interfere with the enzymatic detection system encapsulated inside the liposomes (average of technical replicates +/− standard deviation is shown, n = 3–9). (E) Bar graph showing the initial rates for the reaction between HRP, AmplexRed and hydrogen peroxide, in resuspension or encapsulated in liposomes, also comparing control liposomes and liposomes having AtPIP2;4 integrated (average of technical replicates +/− standard deviation is shown, $n = 9$–24). The letters a, b and c illustrate the significance from the ANOVA analysis.

readout for the transport (Fig. 3A). A major advantage with this assay is that many samples can be evaluated simultaneously using a 96-well format and assessment of the reaction using a plate reader. The main principle for the method is that the stronger the fluorescent signal, the more efficient is the H_2O_2 transport. However, a critical parameter with the assay is that the internal reaction giving rise to fluorescence is the rate limiting step so if an excess of external hydrogen peroxide is added, no differences in transports efficiencies can be observed. Hence, in order to establish the assay, the key experiment was to evaluate the transport efficiencies for proteoliposomes having AtPIP2;4 reconstituted using various concentrations of external H_2O_2. As seen in Fig. 3B, a low concentration of external H_2O_2 (5 μM) resulted in low fluorescence intensity and only a minor difference between liposomes and proteoliposomes. Using a high concentration, 200 μM H_2O_2, also gave a high fluorescent signal, but again only a minor difference between liposomes and proteoliopsomes, indicating that the internal reaction is saturated. Noteworthy, using an intermediate concentration of H_2O_2 (50 μM) gave a clear fluorescent signal and importantly, a significant difference between the sample and control could be evaluated (Fig. 3C). Based on this evaluation, an external concentration of 50 μM H_2O_2 was established for investigation of hydrogen peroxide transport for various aquaporin targets. To further evaluate the suitability of this assay for aquaporins, we investigated a putative interference of mercury with the fluorescent reaction between Amplex Red (AR), horseradish peroxidase (HRP) and hydrogen peroxide. (Fig. 3D). By this test, it was concluded that the established hydrogen peroxide assay is compatible with the established aquaporin inhibitor. Finally, we compared the initial rate of the reaction between AmplexRed, HRP and hydrogen peroxide at the established concentration of 50 μM, having the reactants encapsulated or free in solution showing a huge difference in rate supporting that the measured reaction indeed is an outcome of protein based transport or simple diffusion of H_2O_2 (Fig. 3E).

3.4. Aquaporin isoforms transport hydrogen peroxide with different efficiencies

As confirmed with this novel assay, AtPIP2;4 efficiently transports hydrogen peroxide through the lipid bilayer, as compared to the control liposomes lacking protein (Fig. 3B). To further test our assay, we also included the highly related homologue from spinach, SoPIP2;1, in the experiment being equally efficient with respect to hydrogen peroxide transport. As confirmed with SDS-PAGE, the observed transport can be related to comparable amounts of protein reconstituted into the liposomes (Fig. 4A). To evaluate the specificity to hydrogen peroxide among aquaporin homologues, an aquaporin from human was also included in the assay, hAQP1. Notably, hAQP1 has a lower capacity of

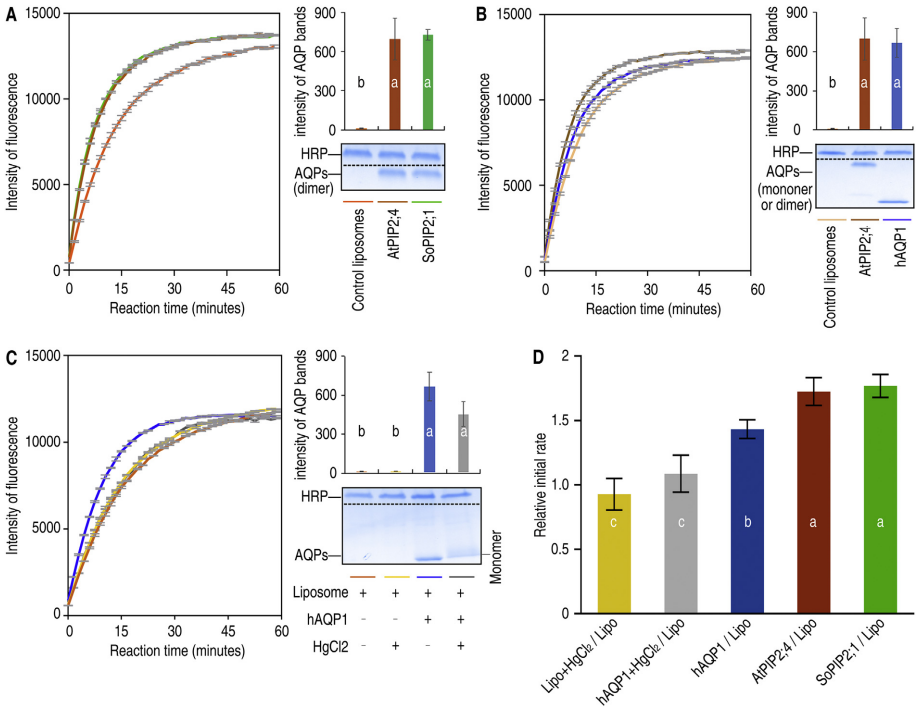

Fig. 4. Functional analysis of the hydrogen peroxide transport in aquaporins. (A) Hydrogen peroxide transport of AtPIP2;4 and SoPIP2;1 as compared to empty liposomes (negative control). The SDS-PAGE gel confirms comparable levels of protein in each sample. (B) Comparison of the hydrogen peroxide transport for AtPIP2;4 and hAQP1. The SDS-PAGE gel confirms comparable levels of protein in each sample, including the observation that AtPIP2;4 migrates as a dimer while hAQP1 migrates as a monomer. (C) Mercury inhibition of the hydrogen peroxide transport via hAQP1 confirming a protein specific transport. For the hydrogen peroxide measurements in A-C, the average of three individual curves (technical replicates) +/− standard deviation, n = 3, are shown together with an SDS-PAGE confirming equal protein content reconstituted in the liposomes, average of biological replicates +/− standard deviation is shown, *n* = 3. (D) The relative initial rate calculated for all tested targets (n = 3–6 biological replicates) showing that the two tested aquaporins from plant are significantly more efficient for hydrogen peroxide transport as compared to the human aquaporin, hAQP1. The letters a, b and c illustrate the significance from the ANOVA analysis.

hydrogen peroxide transport as compared to the homologues from plants, as shown for AtPIP2;4. As seen on the SDS-PAGE analysis, the protein amounts are comparable, even though AtPIP2;4 migrates as a dimer and hAQP1 as a monomer (Fig. 4B). To confirm that the observed transport of hydrogen peroxide is protein specific, it was inhibited by mercury, as tested for hAQP1. Indeed, a decrease in hydrogen peroxide transport was observed, comparable to the control with empty liposomes, which implied that the difference in fluorescent curves between aquaporin-liposomes and empty liposomes was due to H_2O_2 transport by hAQP1 (Fig. 4C). Since no background reaction was observed (Fig. 3D), we can conclude that mercury is an efficient inhibitor of hAQP1 also in this method.

For proper comparison of the transport efficiencies for different targets, the initial rate (min^{-1}) was estimated for each and related to the negative control (Fig. 4D). For this calculation, three to six biological replicates were summarized where each repeat represents an average of three curves (technical replicates). The overall conclusion is that the plant aquaporins are significantly more efficient with respect to hydrogen peroxide transport, as compared to hAQP1, as confirmed with an ANOVA statistical test.

3.5. AtPIP2;4 is an efficient channel for water

To further characterize the aquaporin channels, transport of water was also evaluated using stopped-flow. Water transport capacity of full length protein, AtPIP2;4-FL, as well as the truncated form used for crystallization, AtPIP2;4(28-279), were assayed by stopped-flow analysis. The average external surface of the liposome vesicles was $2.7 \times 10^{-14}\,m^2$, while the average internal volume of the vesicles is $4.17 \times 10^{-22}\,m^3$. The corresponding values for the average proteoliposome vesicles are $3.65 \times 10^{-14}\,m^2$ for the external surface and $6.56 \times 10^{-22}\,m^3$ for the internal volume. The average diameter for the liposomes vesicles is 92.72 nm and for the proteoliposome vesicles 107.82 nm.

Compared to control liposomes, AtPIP2;4-FL showed a high level of water transport, comparable to the positive controls of hAQP1 and SoPIP2;1, respectively (Fig. 5A). To confirm that the observed effect was due to protein specific transport, the hAQP1 containing liposomes were incubated with mercury giving the expected abolishment of the transport capacity (Fig. 5B). The truncated variant of AtPIP2;4 used for crystallization was shown to be a functional form of the protein, albeit the water transport was somewhat lower as compared to the full-length protein (Fig. 5C). The proteoliposome preparation was repeated at least twice and the Pf value was calculated for each sample based on average

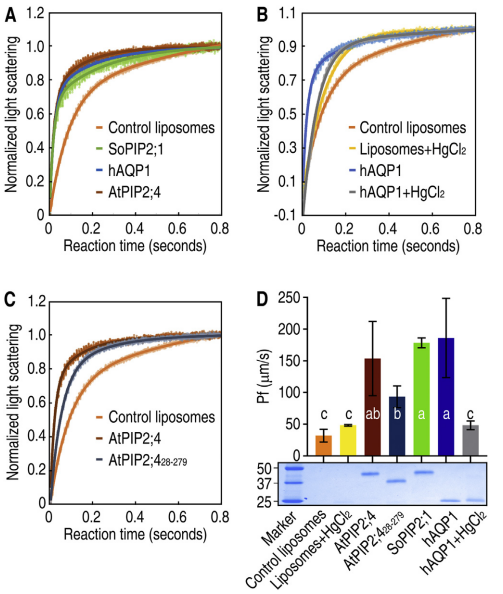

Fig. 5. Functional analysis of the aquaporin water transport. (A) Water transport of aquaporin homologues (SoPIP2;1, hAQP1 and AtPIP2;4,) together with control (empty liposomes). (B) Inhibition of the hAQP1 water transport by mercury. (C) The water transport of the AtPIP2;4 full-length protein as compared to the truncated variant used for crystallization, AtPIP2;4(28-279). In A-C, shaded curves show representative averages of three measurements of a technical replicate for each target, where the line is the fitted curve. (D) For each target, the Pf value was calculated. In the bar graph, the average of technical replicates (n = 5–11, based on 2–4 biological replicates) and the standard deviation are shown. SDS-PAGE gel is shown below, confirming comparable protein levels in each proteoliposome preparation. The letters a, b and c illustrate the significance from the ANOVA analysis.

curves (n = 5–11) in order to establish the observed differences in transport capacity of the various aquaporin isoforms. Further, to exclude the possibility that observed effects could be related to differences in protein levels reconstituted into the liposomes, an SDS-PAGE analysis was performed, indeed showing comparable amounts of proteins in the various proteoliposome preparations (Fig. 5D). Hence, the overall conclusion is that there is no significant difference in water transport between AtPIP2;4, SoPIP2;1 and hAQP1.

3.6. Structure of AtPIP2;4

Several conditions were tried out for crystallization of AtPIP2;4(28-279), and the best resolution was achieved from protein in 1% OG and the crystallization condition containing 1.5 M sodium formate, 0.05 M sodium cacodylate pH 5.5, 30% PEG400, 3% W/V 6-Aminohexanoic acid, 0.01 M Calcium chloride dehydrate (Fig. 6A). The structure was determined for the membrane core of the channel with the parameters defined in Table 1. The tetramer of AtPIP2;4 shows a typical aquaporin oligomer with four individual water pores (Fig. 6B). To illustrate the similarity between the known high-resolution PIP structure of aquaporin from plant, the AtPIP2;4 monomer was superimposed on the closed structure of SoPIPI2;1 (Fig. 6C). In this comparison, helices are fully aligned on top of each other. Loop D, being essential for the closing mechanism in SoPIP2;1, is resolved in only one of the two molecules found in the asymmetric unit of the AtPIP2;4 structure. Notably, when resolved, it also aligns with the corresponding loop D region in the SoPIP2;1 structure. The very high correlation between the structures is not surprising since both share a sequence similarity of 75%.

4. Discussion

The ability to accurately measure hydrogen peroxide transport through membrane protein targets is of interest for various targets, where peroxiporins have specific implications in cancer [48]. Diffusion of hydrogen peroxide through the plasma membrane of *S. cerevisiae* has been evaluated previously and suggested to not be mediated by aquaporins. This conclusion was based on the observation that the permeability constant, the first-order rate constant for the permeation of H_2O_2 into the cell, was not altered in the presence of mercuric chloride [49]. Producing aquaporin homologues from plants and mammals in yeast, on the other hand, has provided direct evidence for hydrogen peroxide transport across membranes mediated by selected isoforms [50]. However, current methods to evaluate the hydrogen peroxide permeability of aquaporins, including yeast growth and intracellular fluorescence dying assays, respectively, rely on expression of aquaporins in whole cells. An intrinsic difficulty with cell based assays like these is the variation in expression level between different targets in the same cells. Hence, it is problematic to standardize the quantity of the aquaporins and measure the transport efficiencies for different isoforms and mutants. Thus, proper comparison of transport specificities is thereby difficult. Indeed, the deficiency in performance of hydrogen peroxide transport among certain aquaporins, such as hAQP1, has been considered to be explained by a low production level in the cells under study [51]. The comparison of H_2O_2 permeability between aquaporins is therefore meaningless without having equal amount of functional proteins. Here, we have established a new quantitative method to compare purified and functional aquaporins. We have adapted a fluorescent liposome assay [36] to reconstitute purified aquaporins into liposomes and measure hydrogen peroxide transport specifically. As seen in Fig. 4, the hydrogen peroxide transport is equally efficient for both plant aquaporins (AtPIP2;4 and SoPIP2;1) while it is clearly less efficient for hAQP1. Notably, the amount of protein responsible for the transport in the proteoliposomes is comparable, even though hAQP1 is a monomer while the AtPIP2;4 and SoPIP2;1 are dimeric when analyzed by SDS-PAGE. Further, since the measured hydrogen peroxide transport can be inhibited by mercury it is proved to be protein specific and occur via the monomeric pore (Fig. 4C). This effect of inhibition can only be evaluated for hAQP1 for which mercury is a very efficient inhibitor, blocking the channel entrance by binding to Cys189 [52]. In the corresponding position in the selectivity filter, the plant aquaporins have a threonine residue which does not interact with mercury (Fig. 7A). While the hydrogen peroxide transport was clearly different for hAQP1 and the plant aquaporins, all three aquaporin isoforms transport water with comparable efficiencies. Again, the observed transport was due to similar amounts of protein reconstituted in the liposomes and the water permeability of hAQP1 could be efficiently inhibited by mercury (Fig. 5). Taken together, our transport measurements using purified protein support different transport efficiencies for different aquaporin isoforms, when comparing water and hydrogen peroxide, respectively.

Based on our functional evaluation of transport specificities for proteins reconstituted in proteoliposomes, we conclude that the H_2O_2 transport by an aquaporin is not correlated with the aquaporin specific transport efficiency for H_2O. To shed further light on the differences in transport observed for aquaporin homologues, and the efficient transport of H_2O_2 for the aquaporin isoform from *A. thaliana*, we determined the structure of AtPIP2;4 (Fig. 6). The sequence- and structural alignments show that the pore-lining residues of hAqp1, SoPIP2;1 and AtPIP2;4 are almost identical (Fig. 7A and B). The comparison of specificity filter residues [9] (F87, H216, T225 and R231 in ATPIP2;4)

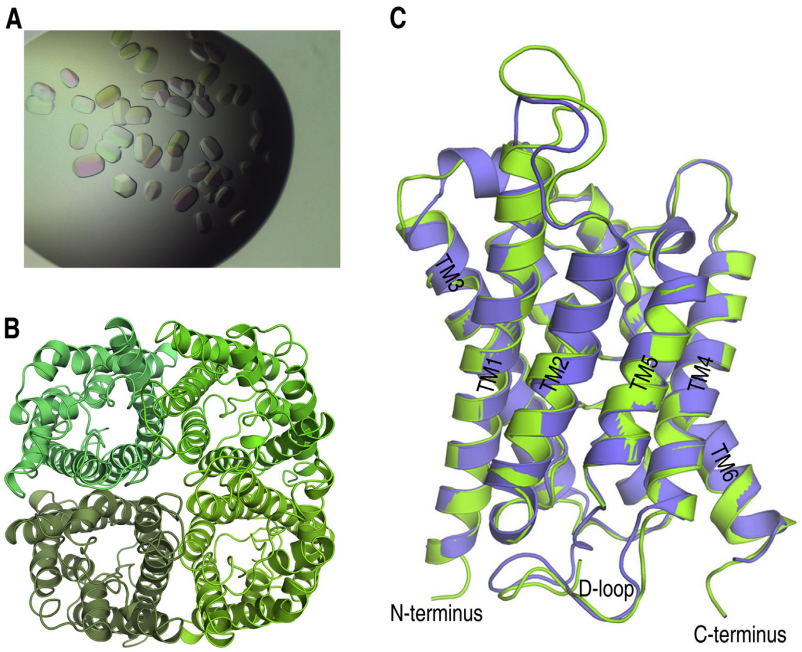

Fig. 6. Crystallization and structural determination of AtPIP2;4. (A) Optimized crystals of AtPI2;4 (28-279) purified to homogeneity. (B) 3D structure of AtPIP2;4 tetramer at 3.7 Å resolution as seen from the extracellular side. (C) The high-resolution structure of AtPIP2;4 (green) superimposed on the high-resolution structure of SoPIP2;1, closed conformation (pdb:1Z98) (purple).

Table 1
Data collection and refinement statistics of AtPIP2;4 (28-279). Statistics for the highest-resolution shell are shown in parentheses. The largest off-origin peak in the Patterson function is 4.83% of the height of the origin peak. No significant pseudotranslation is detected.

AtPIP2;4 (28-279)	
Data collection	
Wavelength (Å)	0.9666
Space group	P 63 22
Cell dimensions	
a, b, c (Å)	218.9 218.9 100.6
α, β, γ (°)	90 90 120
Resolution (Å)	48–3.7 (3.8–3.7)
R-meas	0.116 (1.8)
(I/sigma)	13 (1.3)
Completeness	98.2 (94.4)
Redundancy	14.2
Refinement	
Resolution (Å)	48.64–3.7 (3.832–3.7)
No. of reflections	15,438 (1506)
R_{work}/R_{free}	32.7/35.6 (36.7/35.3)
Mean I/sigma(I)	16.60 (4.25)
Wilson B-factor	137.35
No. of atoms	
Non-hydrogen atoms	3649
Protein	487
RMS (bonds)	0.004
RMS (angles)	0.81
Ramachandran favored (%)	89
Ramachandran outliers (%)	2.1

between SoPIP2;1 and hAqp1 does not show any obvious difference in the diameter of the pore despite the fact that the threonine is a cysteine in hAQP1 (Fig. 7C). Interestingly, from previous studies it has been suggested that water permeable aquaporins are also channels for hydrogen peroxide, but there might be variations in permeability for different isoforms. In the same study, it was also observed that the permeability for water as well as hydrogen peroxide was comparable despite differences in the pore diameter at the position of the specificity filter [51]. Therefore, based on our observations as well as previous studies, we cannot easily explain the observed differences in the water or hydrogen peroxide transport efficiencies of hAQP1, AtPIP2;4 and SoPIP2;1 by differences in the inner pore architecture. We rather speculate that isoform specific loop structures might contribute to the sieving of the molecules to be transported, thereby contributing to the variation in specificity observed among aquaporin homologues.

Comparing the sequences of hAQP1, AtPIP2;4 and SoPIP2;1 some differences are indeed observed in loop A and loop D (Fig. 7A). Loop A, as compared to AtPIP2;4, SoPIP2;1 is six amino acid residues shorter and hAQP1 four residues shorter. Since the three aquaporins are all rather different in loop A, it is not obvious that this loop is responsible for the observed differences in H_2O_2 transport between the aquaporin isoforms from plant and human, respectively (Fig. 4). Loop D, on the other hand, is highly similar between AtPIP2;4 and SoPIP2;1, 17 identical residues out of 19. In hAQP1, loop D is four residues shorter and it is also lacking the highly conserved leucine involved in channel regulation of PIPs, Leu197 in SoPIP2;1 [53]. It is therefore not excluded that Loop D could contribute to transporting molecules with different efficiencies for various aquaporin isoforms. Interestingly, for SoPIP2;1, a divalent cation, Cd^{2+} in the crystal structure and possibly Ca^{2+} in vivo, was pointed out to be critical for defining the closed structure by

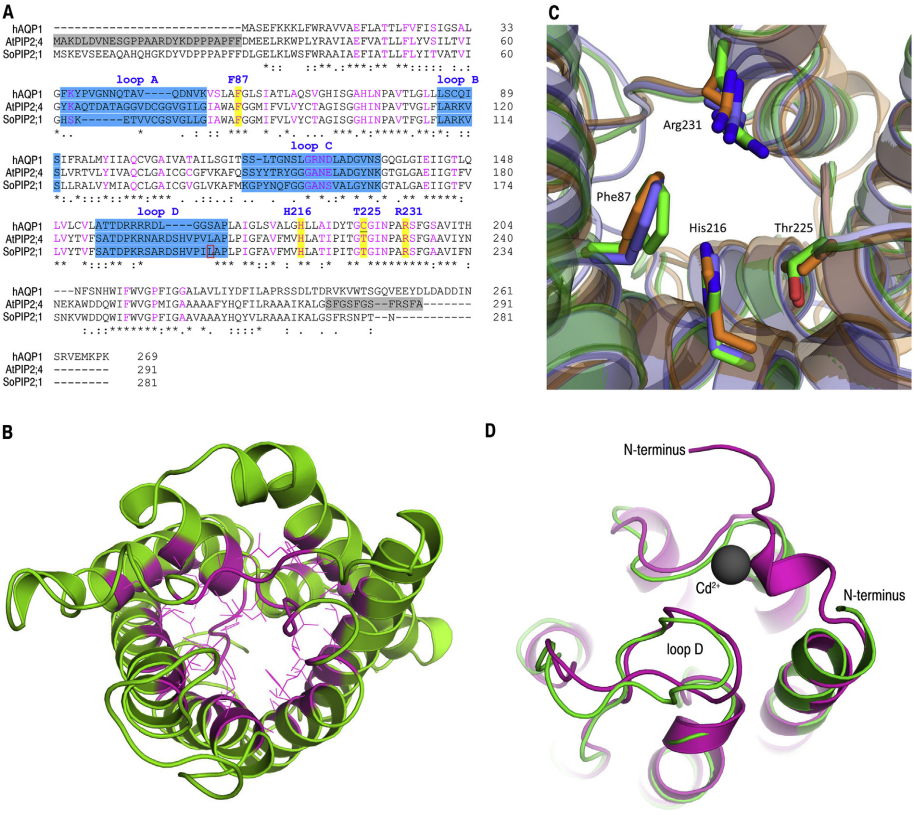

Fig. 7. The selectivity filter of AtPIP2;4. (A) Alignment of hAqp1, AtPIP2;4 and SoPIP2;1 indicating loop A, B, C and D (blue), respectively, as well as the four residues constituting the selectivity filter of the channel (yellow) where the numbering is the residues of AtPIP2;4 and the mercury sensitive cysteine is underlined. Pore lining residues of AtPIP2;4 are indicated (magenta) and Leu197 of SoPIP2;1 is indicated with a red box. The truncated form of the protein, AtPIP2;4 (28-279) are lacking parts of the N- and the C-terminus, respectively (grey). (B) Looking into the AtPIP2;4 channel from the extracellular side, highlighting the pore lining residues in magenta. (C) Superimposition of selectivity filter residues from AtPIP2;4, SoPIP2;1 and hAqp1. Residues are numbered according to sequence of AtPIP2;4 and depicted as sticks. Green: AtPIP2;4, orange: hAqp1 (pdb:1j4n), purple: SoPIP2;1, closed conformation (pdb:1Z98). (D) Loop D in AtPIP2;4 (green) and SoPIP2;1 (magenta), respectively, where the Cd^{2+} ion was recognized as essential for the closed conformation of the spinach aquaporin.

anchoring loop D [53,54]. In the 3.7 Å AtPIP2,4 structure, loop D is resolved in one of two monomers of the asymmetric unit, and, noteworthy, this loop adopts a very similar conformation implying a closed conformation also for this PIP from *A. thaliana*, despite the absence of the cation (Fig. 7D). Interestingly, this observation opens up for variations in the molecular mechanisms for plant aquaporin regulation.

The regulatory mechanism for water transport by the PIP proteins are rather well studied, especially well illustrated by the high-resolution structure of SoPIP2;1 providing a model for the gating mechanism based on phosphorylation and protonation [53]. Just like SoPIP2;1, the water transport of AtPIP2;1 has been suggested to be gated by divalent cations and protons [55] and regulation by phosphorylation has recently been presented for both water and hydrogen peroxide transport in AtPIP2;1 [56]. Altogether, these observations support a common gating mechanism for the highly homologues PIP proteins independent of specificity, suggesting that comparable regulation is also valid for AtPIP2;4. Nevertheless, observations from this study opens up for additional fine tuning of the regulation of the transport, where the loop regions possibly also influence the specificity of the aquaporin. For detailed analysis of the determinants of transport specificities among aquaporin homologues the hydrogen peroxide assay using proteoliposomes will be of great value, especially combined with mutational analysis.

5. Conclusions

In this study, we present a novel fluorescent based proteoliposome assay for the analysis of aquaporin facilitated hydrogen peroxide transport. Based on structural evaluation and water transport analysis, we suggest that the differences in efficiencies in transport for hydrogen peroxide between aquaporins cannot easily be explained by differences in the monomeric pore. To get a deeper understanding of the structural determinants for transport specificities for different aquaporin homologous, more isoforms need to be characterized, ideally for both structure and function, combined with mutational studies. Having quantitative protein assays for different specificities is indeed critical for this evaluation and pure protein is required. For the human aquaporin homologues, several of those are already produced in *P. pastoris*

[57] providing a setup for a broader evaluation and comparison. In conclusion, since we do not find any support from the structures and the analysis of the actual aquaporin pore explaining the differences in efficiencies for hydrogen peroxide transport observed for different aquaporin homologues, we speculate that the explanation could potentially be found in the loop regions. Further analysis would be needed to evaluate this hypothesis, and for such studies our proteoliposome assay for hydrogen peroxide will be of high value.

Transparency document

The Transparency document associated with this article can be found, in online version.

Declaration of competing interest

The authors declare that they have no conflicts of interest with the contents of this article.

Acknowledgements

The work presented in this study was supported from research grants from the Swedish research Council (VR-M, Structural studies of aquaporin:protein complexes) to Kristina Hedfalk, as well as from the China National Key Research and Development Plan (grant number 2017YFD0200901) and Natural Science Foundation of China (grant number 31772247) to Hansong Dong. We also acknowledge ESRF for crystallography beamtime at beamline ID23-2 and Weixiao Yuan Wahlgren for support with data collection.

The atomic coordinates and structure factors (codes 6QIM) have been deposited in the Protein Data Bank (http://wwpdb.org/).

Author contributions

The project presented in this manuscript is result of collaboration between University of Gothenburg, Sweden, and Nanjjing Agricultural University, China.

Hao Wang conducted the majority of the experiments (Data curation, Formal analysis, Methodology, Visualization, Writing - original draft).

Stefan Schoebel was involved in the development of the assay for hydrogen peroxide in liposomes as well as the structural determination (Conceptualization, Formal analysis, Methodology, Supervision, Validation, Visualization, Writing - review & editing).

Florian Schmitz made the majority of the experiments for water transport (Data curation, Formal analysis, Methodology, Visualization).

Hanson Dong is the initiator of the project (Conceptualization, Funding acquisition, Investigation, Project administration, Resources, Supervision, Writing - review & editing).

Kristina Hedfalk is the main supervisor of the path from protein production to characterization and she wrote the paper where all co-authors contributed to the writing process (Conceptualization, Data curation, Formal analysis, Funding acquisition, Investigation, Project administration, Resources, Supervision, Validation, Writing - review & editing).

Appendix A. Supplementary data

Supplementary data to this article can be found online at https://doi.org/10.1016/j.bbamem.2019.183065.

References

[1] K. Ishibashi, S. Hara, S. Kondo, Aquaporin water channels in mammals, Clin. Exp. Nephrol. 13 (2009) 107–117, https://doi.org/10.1007/s10157-008-0118-6.
[2] R. Mukhopadhyay, H. Bhattacharjee, B.P. Rosen, Aquaglyceroporins: generalized metalloid channels, Biochim. Biophys. Acta 1840 (2014) 1583–1591, https://doi.org/10.1016/j.bbagen.2013.11.021.
[3] J.S. Jung, G.M. Preston, B.L. Smith, W.B. Guggino, P. Agre, Molecular structure of the water channel through aquaporin CHIP. The hourglass model, J. Biol. Chem. 269 (1994) 14648–14654.
[4] E. Kruse, N. Uehlein, R. Kaldenhoff, The aquaporins, Genome Biol. 7 (2006) 206, https://doi.org/10.1186/gb-2006-7-2-206.
[5] A.N. van Hoek, et al., Functional unit of 30 kDa for proximal tubule water channels as revealed by radiation inactivation, J. Biol. Chem. 266 (1991) 16633–16635.
[6] S. Tornroth-Horsefield, K. Hedfalk, G. Fischer, K. Lindkvist-Petersson, R. Neutze, Structural insights into eukaryotic aquaporin regulation, FEBS Lett. 584 (2010) 2580–2588, https://doi.org/10.1016/j.febslet.2010.04.037.
[7] U.K. Eriksson, et al., Subangstrom resolution X-ray structure details aquaporin-water interactions, Science 340 (2013) 1346–1349, https://doi.org/10.1126/science.1234306.
[8] D. Fu, et al., Structure of a glycerol-conducting channel and the basis for its selectivity, Science 290 (2000) 481–486.
[9] H. Sui, B.G. Han, J.K. Lee, P. Walian, B.K. Jap, Structural basis of water-specific transport through the AQP1 water channel, Nature 414 (2001) 872–878, https://doi.org/10.1038/414872a.
[10] G.P. Bienert, J.K. Schjoerring, T.P. Jahn, Membrane transport of hydrogen peroxide, Biochim. Biophys. Acta 1758 (2006) 994–1003, https://doi.org/10.1016/j.bbamem.2006.02.015.
[11] U. Laforenza, et al., Aquaporin-mediated water and hydrogen peroxide transport is involved in normal human spermatozoa functioning, Int. J. Mol. Sci. 18 (2016), https://doi.org/10.3390/ijms18010066.
[12] S. Watanabe, C.S. Moniaga, S. Nielsen, M. Hara-Chikuma, Aquaporin-9 facilitates membrane transport of hydrogen peroxide in mammalian cells, Biochem. Biophys. Res. Commun. 471 (2016) 191–197, https://doi.org/10.1016/j.bbrc.2016.01.153.
[13] C. Hooijmaijers, et al., Hydrogen peroxide permeability of plasma membrane aquaporins of Arabidopsis thaliana, J. Plant Res. 125 (2012) 147–153, https://doi.org/10.1007/s10265-011-0413-2.
[14] D.E. Nordzieke, I. Medrano-Fernandez, The Plasma Membrane: A Platform for Intra- and Intercellular Redox Signaling. *Antioxidants (Basel)*, **7** (2018), https://doi.org/10.3390/antiox7110168.
[15] I. Direito, A. Madeira, M.A. Brito, G. Soveral, Aquaporin-5: from structure to function and dysfunction in cancer, Cell. Mol. Life Sci. 73 (2016) 1623–1640, https://doi.org/10.1007/s00018-016-2142-0.
[16] Quigley, F., Rosenberg, J. M., Shachar-Hill, Y. & Bohnert, H. J. From genome to function: the Arabidopsis aquaporins. Genome Biol. 3, RESEARCH0001 (2002).
[17] M.D. Bienert, T.A. Diehn, N. Richet, F. Chaumont, G.P. Bienert, Heterotetramerization of plant PIP1 and PIP2 aquaporins is an evolutionary ancient feature to guide PIP1 plasma membrane localization and function, Front. Plant Sci. 9 (2018) 382, https://doi.org/10.3389/fpls.2018.00382.
[18] A. Yaneff, V. Vitali, G. Amodeo, PIP1 aquaporins: intrinsic water channels or PIP2 aquaporin modulators? FEBS Lett. 589 (2015) 3508–3515, https://doi.org/10.1016/j.febslet.2015.10.018.
[19] M. Dynowski, G. Schaaf, D. Loque, O. Moran, U. Ludewig, Plant plasma membrane water channels conduct the signalling molecule H2O2, Biochem. J. 414 (2008) 53–61, https://doi.org/10.1042/BJ20080287.
[20] G.P. Bienert, F. Chaumont, Aquaporin-facilitated transmembrane diffusion of hydrogen peroxide, Biochim. Biophys. Acta 1840 (2014) 1596–1604, https://doi.org/10.1016/j.bbagen.2013.09.017.
[21] P. Niethammer, C. Grabher, A.T. Look, T.J. Mitchison, A tissue-scale gradient of hydrogen peroxide mediates rapid wound detection in zebrafish, Nature 459 (2009) 996–999, https://doi.org/10.1038/nature08119.
[22] M.A. Torres, ROS in biotic interactions, Physiol. Plant. 138 (2010) 414–429, https://doi.org/10.1111/j.1399-3054.2009.01326.x.
[23] M. Sagi, R. Fluhr, Production of reactive oxygen species by plant NADPH oxidases, Plant Physiol. 141 (2006) 336–340, https://doi.org/10.1104/pp.106.078089.
[24] C.K. Auh, T.M. Murphy, Plasma membrane redox enzyme is involved in the synthesis of O2- and H2O2 by Phytophthora elicitor-stimulated rose cells, Plant Physiol. 107 (1995) 1241–1247.
[25] T. Xing, V.J. Higgins, E. Blumwald, Race-specific elicitors of Cladosporium fulvum promote translocation of cytosolic components of NADPH oxidase to the plasma membrane of tomato cells, Plant Cell 9 (1997) 249–259, https://doi.org/10.1105/tpc.9.2.249.
[26] P. van Gestelen, H. Asard, N. Horemans, R.J. Caubergs, Superoxide producing NAD(P)H-oxides in plasma membrane vesicles from elicitor responsive bean plants, Physiol. Plant. 104 (2002) 653–660.
[27] H. Satooka, M. Hara-Chikuma, Aquaporin-3 controls breast cancer cell migration by regulating hydrogen peroxide transport and its downstream cell signaling, Mol. Cell. Biol. 36 (2016) 1206–1218, https://doi.org/10.1128/MCB.00971-15.
[28] J.R. Thiagarajah, J. Chang, J.A. Goettel, A.S. Verkman, W.I. Lencer, Aquaporin-3 mediates hydrogen peroxide-dependent responses to environmental stress in colonic epithelia, Proc. Natl. Acad. Sci. U. S. A. 114 (2017) 568–573, https://doi.org/10.1073/pnas.1612921114.
[29] S. Tian, et al., Plant aquaporin AtPIP1;4 links apoplastic H2O2 induction to disease immunity pathways, Plant Physiol. 171 (2016) 1635–1650, https://doi.org/10.1104/pp.15.01237.
[30] C. Maurel, et al., Aquaporins in plants, Physiol. Rev. 95 (2015) 1321–1358, https://doi.org/10.1152/physrev.00008.2015.
[31] G. Fischer, et al., Crystal structure of a yeast aquaporin at 1.15 angstrom reveals a novel gating mechanism, PLoS Biol. 7 (2009) e1000130, , https://doi.org/10.1371/journal.pbio.1000130.
[32] F. Oberg, J. Sjohamn, M.T. Conner, R.M. Bill, K. Hedfalk, Improving recombinant

eukaryotic membrane protein yields in Pichia pastoris: the importance of codon optimization and clone selection, Mol. Membr. Biol. 28 (2011) 398–411, https://doi.org/10.3109/09687688.2011.602219.
[33] E. Macierzynska, A. Grzelak, G. Bartosz, The effect of growth medium on the antioxidant defense of Saccharomyces cerevisiae, Cell Mol Biol Lett 12 (2007) 448–456, https://doi.org/10.2478/s11658-007-0017-y.
[34] M. Nyblom, et al., Exceptional overproduction of a functional human membrane protein, Protein Expr. Purif. 56 (2007) 110–120, https://doi.org/10.1016/j.pep.2007.07.007.
[35] A. Frick, et al., X-ray structure of human aquaporin 2 and its implications for nephrogenic diabetes insipidus and trafficking, Proc. Natl. Acad. Sci. U. S. A. 111 (2014) 6305–6310, https://doi.org/10.1073/pnas.1321406111.
[36] H.M. Piwonski, M. Goomanovsky, D. Bensimon, A. Horovitz, G. Haran, Allosteric inhibition of individual enzyme molecules trapped in lipid vesicles, Proc. Natl. Acad. Sci. U. S. A. 109 (2012) E1437–E1443, https://doi.org/10.1073/pnas.1116670109.
[37] F. Oberg, et al., Glycosylation increases the thermostability of human aquaporin 10 protein, J. Biol. Chem. 286 (2011) 31915–31923, https://doi.org/10.1074/jbc.M111.242677.
[38] M.P. van Heeswijk, C.H. van Os, Osmotic water permeabilities of brush border and basolateral membrane vesicles from rat renal cortex and small intestine, J. Membr. Biol. 92 (1986) 183–193.
[39] O. Svensson, M. Gilski, D. Nurizzo, M.W. Bowler, Multi-position data collection and dynamic beam sizing: recent improvements to the automatic data-collection algorithms on MASSIF-1, Acta Crystallogr D Struct Biol 74 (2018) 433–440, https://doi.org/10.1107/S2059798318003728.
[40] O. Svensson, S. Malbet-Monaco, A. Popov, D. Nurizzo, M.W. Bowler, Fully automatic characterization and data collection from crystals of biological macromolecules, Acta Crystallogr D Biol Crystallogr 71 (2015) 1757–1767, https://doi.org/10.1107/S1399004715011918.
[41] M.F. Incardona, et al., EDNA: a framework for plugin-based applications applied to X-ray experiment online data analysis, J. Synchrotron Radiat. 16 (2009) 872–879, https://doi.org/10.1107/S0909049509036681.
[42] W. Xds Kabsch, Acta Crystallogr D Biol Crystallogr 66 (2010) 125–132, https://doi.org/10.1107/S0907444909047337.
[43] Collaborative Computational Project, N, The CCP4 suite: programs for protein crystallography, Acta Crystallogr D Biol Crystallogr 50 (1994) 760–763, https://doi.org/10.1107/S0907444994003112.
[44] A. Frick, et al., Mercury increases water permeability of a plant aquaporin through a non-cysteine-related mechanism, Biochem. J. 454 (2013) 491–499, https://doi.org/10.1042/Bj20130377.
[45] P.D. Adams, et al., PHENIX: a comprehensive python-based system for macromolecular structure solution, Acta Crystallogr D Biol Crystallogr 66 (2010) 213–221, https://doi.org/10.1107/S0907444909052925.
[46] P. Emsley, K. Cowtan, Coot: model-building tools for molecular graphics, Acta Crystallogr D Biol Crystallogr 60 (2004) 2126–2132, https://doi.org/10.1107/S0907444904019158.
[47] P.V. Afonine, et al., Towards automated crystallographic structure refinement with phenix.refine, Acta Crystallogr D Biol Crystallogr 68 (2012) 352–367, https://doi.org/10.1107/S0907444912001308.
[48] C. Prata, S. Hrelia, D. Fiorentini, Peroxiporins in cancer, Int. J. Mol. Sci. 20 (2019), https://doi.org/10.3390/ijms20061371.
[49] V. Folmer, et al., H2O2 induces rapid biophysical and permeability changes in the plasma membrane of Saccharomyces cerevisiae, Biochim. Biophys. Acta 1778 (2008) 1141–1147, https://doi.org/10.1016/j.bbamem.2007.12.008.
[50] G.P. Bienert, et al., Specific aquaporins facilitate the diffusion of hydrogen peroxide across membranes, J. Biol. Chem. 282 (2007) 1183–1192, https://doi.org/10.1074/jbc.M603761200.
[51] A. Almasalmeh, D. Krenc, B. Wu, E. Beitz, Structural determinants of the hydrogen peroxide permeability of aquaporins, FEBS J. 281 (2014) 647–656, https://doi.org/10.1111/febs.12653.
[52] Y. Hirano, et al., Molecular mechanisms of how mercury inhibits water permeation through aquaporin-1: understanding by molecular dynamics simulation, Biophys. J. 98 (2010) 1512–1519, https://doi.org/10.1016/j.bpj.2009.12.4310.
[53] S. Tornroth-Horsefield, et al., Structural mechanism of plant aquaporin gating, Nature 439 (2006) 688–694, https://doi.org/10.1038/nature04316.
[54] S. Kreida, S. Tornroth-Horsefield, Structural insights into aquaporin selectivity and regulation, Curr. Opin. Struct. Biol. 33 (2015) 126–134, https://doi.org/10.1016/j.sbi.2015.08.004.
[55] L. Verdoucq, A. Grondin, C. Maurel, Structure-function analysis of plant aquaporin AtPIP2;1 gating by divalent cations and protons, Biochem. J. 415 (2008) 409–416, https://doi.org/10.1042/BJ20080275.
[56] O. Rodrigues, et al., Aquaporins facilitate hydrogen peroxide entry into guard cells to mediate ABA- and pathogen-triggered stomatal closure, Proc. Natl. Acad. Sci. U. S. A. 114 (2017) 9200–9205, https://doi.org/10.1073/pnas.1704754114.
[57] F. Oberg, K. Hedfalk, Recombinant production of the human aquaporins in the yeast Pichia pastoris (invited review), Mol. Membr. Biol. 30 (2013) 15–31, https://doi.org/10.3109/09687688.2012.665503.

PAPER IV

IV

MethodsX 7 (2020) 100816

Contents lists available at ScienceDirect

MethodsX

journal homepage: www.elsevier.com/locate/mex

Method Article

Quantitative analysis of H_2O_2 transport through purified membrane proteins

Hao Wang[a,b], Stefan Schoebel[b], Florian Schmitz[b], Hansong Dong[a,**], Kristina Hedfalk[b,*]

[a] Department of Plant Pathology, Nanjing Agricultural University, 1 Weigang, Nanjing 210095, China
[b] Department and Chemistry and Molecular Biology, Gothenburg University, Box 462, 405 30 Göteborg, Sweden

A B S T R A C T

Hydrogen peroxide (H_2O_2) is an important signal molecule produced in animal and plant cells. The balance of H_2O_2 between the intra- and extracellular space is regulated by integral membrane proteins, which thereby modulate signaling. Several methods have been established to analyze aquaporin mediated transport of H_2O_2 in whole cells with the intrinsic limitation that the amount of protein responsible for a certain activity cannot be standardized. As a consequence, the quantification of the transport and specific activity is difficult to extract making it problematic to compare isoforms and mutated variants of one specific target. Moreover, in cell-based assays, the expression of the target protein may alter the physiological processes of the host cell providing a complication and the risk of misleading results. To improve the measurements of protein based H_2O_2 transport, we have developed an assay allowing quantitative measurements.

- Using purified aquaporin reconstituted in proteoliposomes, transport of H_2O_2 can be accurately measured.
- Inside the liposomes, H_2O_2 catalyzes the reaction between Amplex Red and horseradish peroxidase (HRP) giving rise to the fluorescent product resorufin.
- Analysing pure protein provides direct biochemical evidence of a specific transport excluding putative cellular background.

A R T I C L E I N F O
Method name: Quantitative assay for H_2O_2 permeability of aquaporins
Keywords: Proteoliposomes, Hydrogen peroxide, Aquaporin, Permeability, Membrane protein structure
Article history: Received 15 November 2019; Accepted 1 February 2020; Available online 20 February 2020

DOI of original article: 10.1016/j.bbamem.2019.183065
* Corresponding author.
** Co-corresponding author.
E-mail addresses: 2014202001@njau.edu.cn (H. Wang), florian.schmitz@chem.gu.se (F. Schmitz), hsdong@njau.edu.cn (H. Dong), kristina.hedfalk@gu.se (K. Hedfalk).

https://doi.org/10.1016/j.mex.2020.100816

Specification table

Subject Area:	Biochemistry, Genetics and Molecular Biology
More specific subject area:	Function and specificity of membrane proteins
Method name:	Quantitative assay for H_2O_2 permeability of aquaporins
Name and reference of original method:	Piwonski, H. M., Goomanovsky, M., Bensimon, D., Horovitz, A. & Haran, G. Allosteric inhibition of individual enzyme molecules trapped in lipid vesicles. *Proc Natl Acad Sci U S A* **109**, E1437-1443, doi:10.1073/pnas.1116670109 (2012).
Resource availability:	Plate reader

Overview of the method

Cell-based methods for aquaporin mediated hydrogen peroxide transport include qualitative growth assays using yeast cells combined with fluorescent dyeing and fluorescent probe. These measurements rely on the expression of the channel proteins in the host cells, and, most importantly, proper localization of the recombinant protein to the cellular membrane [1–4], factors that are difficult to fully control and standardize. Noteworthy, recombinant production of the 13 highly homologues plasma membrane intrinsic proteins (PIPs) isoforms from *Arabidopsis thaliana* in *Saccharomyces cerevisiae* using the expression vector pYES2 [5] resulted in major variations in protein levels (Fig. 1). In conclusion, even when using the same promoter and growth conditions, comparing transport efficiencies and specificities for the AtPIP isoforms was non-trivial using the cell-based system [6]. Furthermore, working with cell-based systems, there is a substantial risk that background reactions within the complex intracellular environment of the host cell interfere with reaction of interest and influence the final results, an aspect that is also pronounced in less complex cells like yeast. In addition, the recombinant expression as such, aiming at producing a foreign protein within the cellular environment, might have a negative impact on endogenous physiological processes which could also interfere with the analysis giving misleading results.

To avoid possible complications and lack of reproducibility connected to the use of cell-based systems, a biochemical method for direct evidence of H_2O_2 transport mediated by selected membrane proteins has been developed using artificial liposomes as host system. It has previously been shown that the enzymatic reaction of horseradish peroxidase (HRP) can be assayed encapsulated in a lipid vesicle [7] and the method presented here is a development of this assay where integral membrane proteins reconstituted into the liposome have been included. In brief, the method relies on liposomes

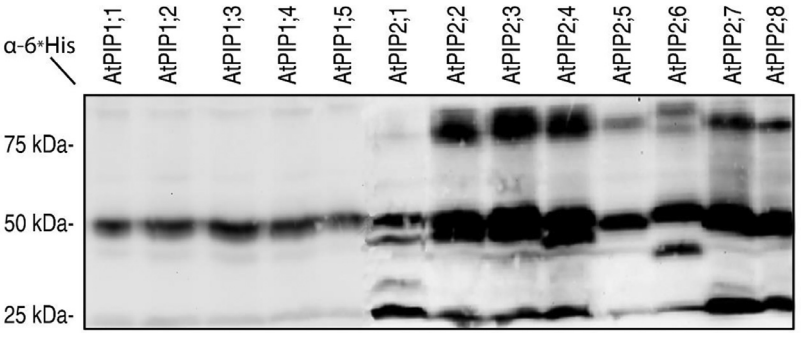

Fig. 1. Recombinant production of aquaporins in yeast for functional studies. Immunoblot showing the variation in production levels of the 13 AtPIPs expressed in yeast cells using the vector of pYES2. All AtPIP isoforms are fused to a C-teminal 6xHis tag and detected using an anti-His antibody. *Figure adapted from Wang et al 2020.*

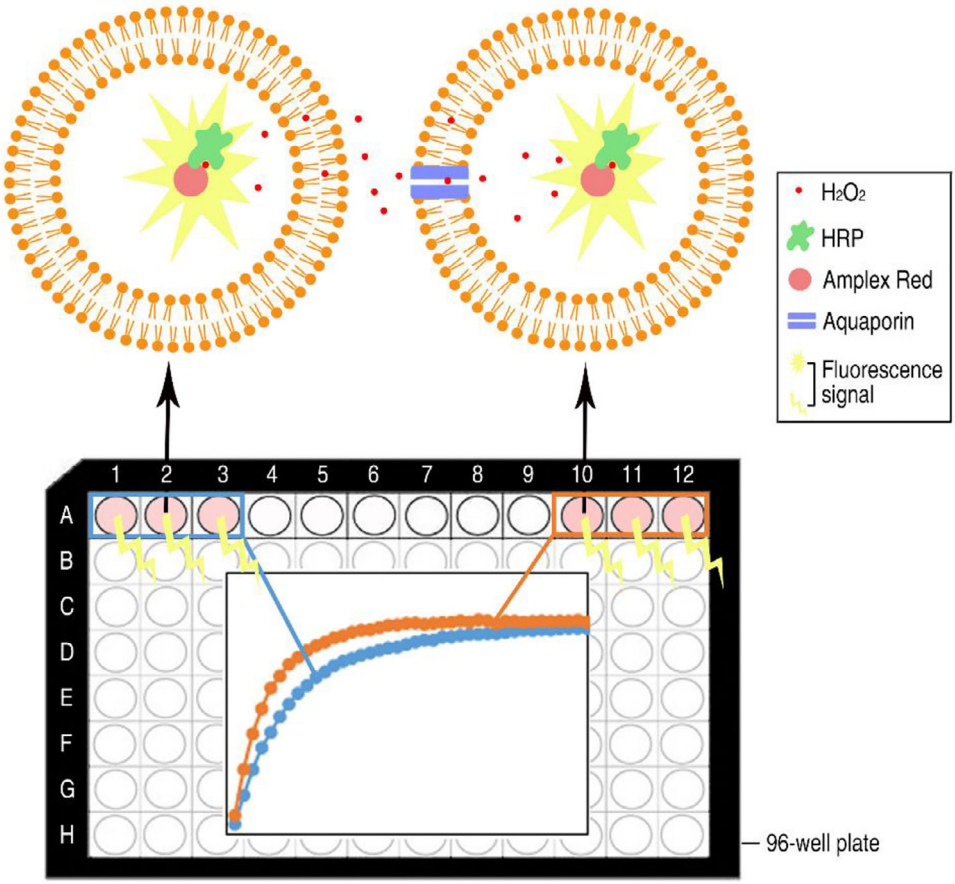

Fig. 2. Schematic figure of the proteoliposome assay with reconstituted aquaporin for functional analysis of H_2O_2 transport using a 96-well format. In order to provide the detection system for H_2O_2 transported via the lipid bilayer, Horseradish peroxidase (HRP) and Amplex Red are encapsulated in the lipid vesicles. The aquaporin mediated transport (orange trace) is more efficient than simple diffusion (blue trace) giving rise to a faster increase in the fluorescent signal as compared to background. *Figure adapted from Wang et al 2020.*

having HRP and Amplex Red (Invitrogen) trapped inside and, at time zero, a defined amount of H_2O_2 is added on the outside. By balancing the concentrations of internal HRP and Amplex Red, respectively, as well as optimizing the external concentration of H_2O_2, the transport efficiency of proteoliposomes as compared to liposomes can be evaluated. The externally added H_2O_2 penetrates the lipid membrane of the liposomes by simple diffusion, but importantly, the transport is more efficient via the aquaporin channel. When H_2O_2 reaches the inside of the vesicle, HRP catalyzes the reaction of Amplex Red and H_2O_2 forming the highly fluorescent product resorufin which could be quantified using a plate reader (Fig. 2). The main principle of the method is that a more efficient H_2O_2 transport over the membrane gives rise to a higher fluorescence. Thereby, the transport of different aquaporin isoforms can be quantified and accurately compared using empty liposomes as a reference. In principle, there is nothing hindering the evaluation of other membrane proteins using this method, providing a general method for H_2O_2 transport using proteoliposomes.

Experimental procedure

Protein purification and standardization of the amount

Purified protein is required for the reconstitution experiment. Noteworthy, purification of integral membrane proteins in high yields is challenging in itself, and it is well established that eukaryotic membrane proteins are the high-hanging fruits for recombinant protein production. Yeast, and especially the methylotrophic strain *Pichia pastoris*, has been shown to be a reliable host for challenging membrane protein targets [8]. High level production of stable protein is a prerequisite for subsequent purification, where the choice of detergent and purification protocol has to be optimized to suit each specific target. For AtPIP2;4, specifically, the key steps for the optimized protein purification procedure [6] is described below.

(a) For large scale production, *culture Pichia pastoris* transformed with recombinant aquaporin fused with a C-terminal 8xHis-tag in fermentor, harvest cells and keep at -20°C for future purification.
(b) For purification, thaw cells and resuspend them in buffer (20 mM Tris, 20 mM NaCl). For *cell breakage*, grind the cell resuspension in a bead beater (e.g Bio Spec) for 12 × 30 s, with 30 s cooling between each run. Collect unbroken cells by centrifugation.
(c) Collect the *membrane fraction* by ultracentrifugation (200,000 × g, 30 min, 4°C) and resuspend the membrane pellet in buffer (20 mM Tris-HCl, 200 mM NaCl, 10% glycerol).
(d) Perform a *detergent screen* to find the best solubilizing agent for the target of interest with respect to efficiency without compromising with protein function. It is recommended to screen the following detergents: 3-[(3-cholamidopropyl) dimethylammonio]-1-propanesulfonate (CHAPS), n-Dodecyl-β-DMaltopyranoside (DDM), n-Decyl-β-D-Maltopyranoside (DM), FosCholine-12 (fc12), n-Dodecyl-N,N-Dimethylamine-N-Oxide (LDAO), Lauryl Maltose Neopentyl Glycol (MNG), Decyl Glucose Neopentyl Glycol (NG) and n-Octyl-β-D-Glucopyranoside (β-OG). For the detergent screen, each detergent is added drop-wise to the membrane resuspension and the final mixture is incubated at 4°C for 2 h with rotation. Non-solubilized membranes are spun down at 160,000g for 30 min at 4°C and supernatant as well as pellet are collected for immunoblot analysis to evaluate the efficiency of each detergent.
(e) For *purification*, add 10 mM Imidazole to the solubilized material and incubate the solution with Ni-NTA agarose for 3 h at 4°C. Elute the target aquaporin in elution buffer (20 mM HCl, 200 mM NaCl, 10% glycerol, detergent, 300 mM imidazole) and concentrate the final protein sample using e.g VivaSpin 100 kDa concentration tube (Sartorius Stedim Biotech GmbH).
(f) If increased purity is required, a gel filtration step is advised using e.g a Superdex200 increase 10/300 GL column (GE Healtcare).

For proper comparison of the transport efficiencies, it is critical to standardize the amount of protein in each reconstitution experiment. In the case of H_2O_2 transport measurements via aquaporins, the concentration for each protein preparation was determined using the BCA protein assay or absorbance measurement (280 nm) using the protein specific extinction coefficients, and the concentration was then adjusted to 0.3 mM for each target.

Preparation of aquaporin-liposomes with encapsulated HRP

All reagents and equipment needed for the reconstitution experiment are listed in Box 1. It is highly recommended **to prepare all the reagents in advance.**

Box 1. Reagents and equipment*

Lipids (*E. coli* Polar Lipid Extract, Avanti Polar Lipids. inc)
Reconstitution buffer (50 mM NaCl, 50 mM Tris pH 8.0, with or without 1 mM EDTA)
10% OG (n-Octyl-β-D-Glucoside, Anatrace)
1 M NaCl
0.5 M Tris pH 8.0
200 U/ml HRP (type II, Sigma Aldrich)
GF buffer (the buffer used to elute the protein in the last purification step, in the case of aquaporins, 200 mM NaCl and 20 mM Tris pH 8.0 was used).
Bio-Beads (Bio-Beads® SM-2 Hydrophobic absorbents, Bio-Rad)
S400HR Column (GE Healthcare)
Ultracentrifuge (Beckman)
Roller table (kept at 4°C)

* Here we specify material successfully used for the aquaporin containing liposomes in Wang et al 2020, which does not exclude that alternatives could work equally well.

The experimental procedure for reconstitution of aquaporin in proteoliposomes is listed below as a-i. It is strongly advised to be thorough in the pipetting procedure so that equal amounts are added in each sample. Further, to avoid disruption of the preparation it is important to treat the samples as gentle as possible once the vesicles are formed.

(a) Mix lipid powder with Reconstitution buffer to a concentration of 25 mg/mL. Aliquot the homogenized mixture into 2 mL tubes, 160 µL in each. The aliquots could be stored at 4°C for up to two weeks.
(b) For the reconstitution experiment, add compounds to the 2 mL tubes as follows:

	Liposomes	Proteoliposomess
Lipid (25 mg/mL)	160 µL	160 µL
ddH_2O	610 µL	610 µL
1 M NaCl	42 µL	42 µL
0.5 M Tris pH 8.0	84 µL	84 µL
Mix gently		
10% OG	100 µL	100 µL
Mix them and let stand for 5 min, now the mixture should be clear.		
HRP (200 U/mL)	2 µL	2 µL
GF buffer	6.5 µL	-
Aquaporin (0.3 mM)	-	6.5 µL
Mix them gently and wait for 5 min		
Bio-Beads*	300 mg	300 mg

*Note: bio-beads should be activated by methanol, washed with mQ water two times and finally equilibrated with reconstitution buffer.

(c) Incubate the mixtures from step b) at 4°C for 3 h with rotation.
(d) To get rid of the bio-beads, centrifuge the mixture (13000xg, 4°C for 5 min) using a 0.22 µm spin filter.
(e) Mix the flow-through with 5 mL Reconstitution buffer (with 1 mM EDTA, all the reconstitution buffer used from this point should have EDTA added). Collect liposomes by ultracentrifugation (140,000xg, 4°C for 45min).
(f) Remove the supernatant and wash the liposomes with 5 mL Reconstitution buffer. Collect the liposomes by ultracentrifugation (140,000xg, 4°C for 45min). Discard the supernatant.
(g) Resuspend the liposomes in 200 µL Reconstitution buffer by gentle mixing. *Please note that the liposomes are fragile and break easily*.
(h) Wash residual HRP outside the liposomes away using the S400HR Column (GE Healthcare) [7], 100 µL of the liposome solution is spun at 700xg, 4°C for 30s.
(i) The final flow through is gently mixed with Reconstitution buffer, 500 uL. The liposomes/proteoliposomes are now ready for use.

Hydrogen peroxide transport assay

The actual measurements of hydrogen peroxide is performed in 96-well plates (Fig. 2) and the detailed procedure is listed in a-e below:

(a) Add 0.6 µL of Amplex Red (AR, Thermo Fisher SCIENTIFIC) stock solution (100 mM) to each of the prepared liposome samples and mix gently. In order to prepare a negative control, blocking the aquaporin transport with mercury, additionally 0.9 µL 200 mM $HgCl_2$ is added by gentle mixing.
(b) Add the liposome/proteoliposome mixture to black Matriplate 96 glass bottom plate (Brooks LIFE SCIENCE SYSTEMS), 150 µL in each well. For each sample, three repeats are prepared in individual wells. The plate is incubated at room temperature for 20 min before measurements.
(c) Meanwhile, prepare the H_2O_2 solution, 200 µM in Reconstitution buffer (0.2 µL 30% H_2O_2 to 10 mL Reconstitution buffer).
(d) Add the 200 µM H_2O_2 solution to the liposome/proteoliposome mixture, 50 µL in each well, using a multipipette.
(e) For fluorescent measurements, the plate is immediately put into a plate reader (e.g POLARstar Omega, BMG TECH). The fluorescent signal from the oxidation of Amplex Red by HRP and H_2O_2 inside the liposomes is collected for 40 cycles with an interval of 2 min, using the wavelength of 544 nm and 590 nm for excitation and emission, respectively. Since H_2O_2 penetrates the liposomes very fast, it is recommended to set up the program before adding H_2O_2.

Method validation

Optimizing the concentration of H_2O_2

To establish the method, different concentrations of H_2O_2 was evaluated to define conditions giving a clear signal to background as well as a distinction between the protein mediated transport and simple diffusion over the lipid bilayer. Using a low concentration of H_2O_2, 5 µM, resulted in a low fluorescent signal and a small difference between the liposomes and proteoliposomes, respectively. A high H_2O_2 concentration (200 µM), on the other hand, resulted in a fast increase of the fluorescent intensity with the concomitant risk to cover the difference in transport between liposomes and proteoliposomes. Noteworthy, using 50 µM H_2O_2 gave an intermediate velocity development for the fluorescent signal and also an acceptable ratio of signal to background, this concentration was therefore selected for all measurement of aquaporin mediated H_2O_2 transport as well as for the negative control with empty liposomes (Fig. 3A).

Confirming protein specific H_2O_2 transport

It is always possible that the actual reconstitution of a protein into the liposome alter the lipid bilayer and makes it leaky, giving the risk for misinterpretation of the transport in proteoliposomes. To exclude this possibility, and confirm that the observed H_2O_2 transport indeed was protein specific, an inhibitor for aquaporin was added to the proteoliposome preparation. Mercury is a well-established blocker for selected aquaporins, among those hAQP1, and this compound was therefore selected as inhibitor in the H_2O_2 transport assay. Noteworthy, by mercury addition, the H_2O_2 transport was fully abolished in the hAQP1 containing proteoliposomes and the curve overlaid the curve for the liposomes. To exclude that mercury had a negative effect on the lipid bilayer itself, a control experiment was performed by adding mercury to the empty liposomes, but no effect was observed confirming that the effect of mercury was protein specific (Fig. 3B). As an additional control experiment, a putative interference between mercury and the fluorescent reaction provided by AR, HRP and H_2O_2 was also investigated. Since no background reaction was observed, it was concluded that mercury is a compatible compound with the assay (Fig. 3C) and, over all, it was concluded that the observed increase of H_2O_2 transport in proteoliposomes was specifically due to the reconstituted aquaporin.

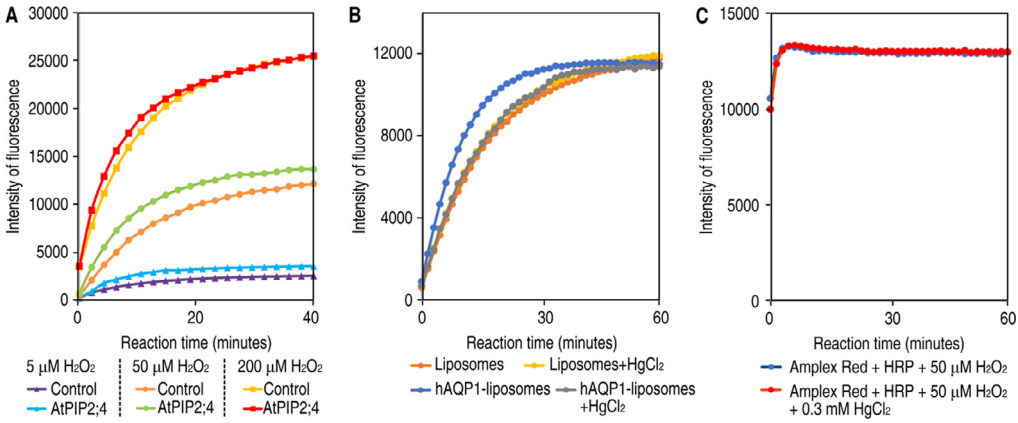

Fig. 3. Confirming protein specific H_2O_2 transport in proteoliposomes. (A) The fluorescent intensity curves of empty liposomes and AtPIP2;4-liposomes treated with 5 µM, 50 µM and 200 µM H_2O_2, respectively. (B) The fluorescent intensity curves of liposomes and hAQP1 containing proteoliposomes, with or without mercury added. (C) Control experiment for the detection system of hydrogen peroxide mixed with or without mercury. *Figure adapted from Wang et al 2020.*

Applicability of the assay for different aquaporin isoforms

In a first comparison, two highly homologues aquaporins from plant, SoPIP2;1 and AtPIP2;4, were evaluated using the H_2O_2 assay. Both aquaporins showed efficient transport of H_2O_2 and the fluorescence was clearly higher than the one in empty liposomes. To confirm that the observed transport was due to comparable amounts of reconstituted protein, the proteoliposome preparations were analyzed by SDS-PAGE (Fig. 4A). To compare aquaporins from different organisms, AtPIP2;4 was compared to hAQP1 in the same experiment. Interestingly, a difference in H_2O_2 transport was observed for these two aquaporins. Again, the proteoliposomes were analysed by SDS-PAGE, excluding that the difference in transport efficiencies were due to different amounts of reconstituted protein (Fig. 4B). Noteworthy, the result on aquaporin homologues from plant and human, respectively, indicated that this assay has the potential to compare differences in the capacity of H_2O_2 transport between different targets.

Comparison of the relative initial rate of H_2O_2 transport

The H_2O_2 assay is efficient in the sense that many samples can be compared simultaneously using the 96-well format. To quantitate the transport, the initial rate was evaluated for each target, having a minimum of three repeats. The Initial Rate (IR) was calculated by the equation

$$IR = dF/dt$$

where F(t) is the function fitted to the curve, F(0) is the fluorescent intensity at 0 min and t is the time in minutes. Due to slight deviations in pipetting of the H_2O_2 solution, there are minor variations between the rates observed for samples measured in different plates, an aspect difficult to avoid. Since the relative signal is consistent between different plates, however, relative initial rates were calculated for each sample by calculating the ratio of the initial rate of proteoliposomes to that of empty liposomes within the same plate. Using this approach, there is no theoretical limit for the number of samples that could be compared, all together providing a robust way to compare differences in H_2O_2 permeability among aquaporins. Further, to evaluate the significance of different transport efficiencies, ANOVA-test is applied giving that a difference is significant for a p value < 0.05 (Fig. 5).

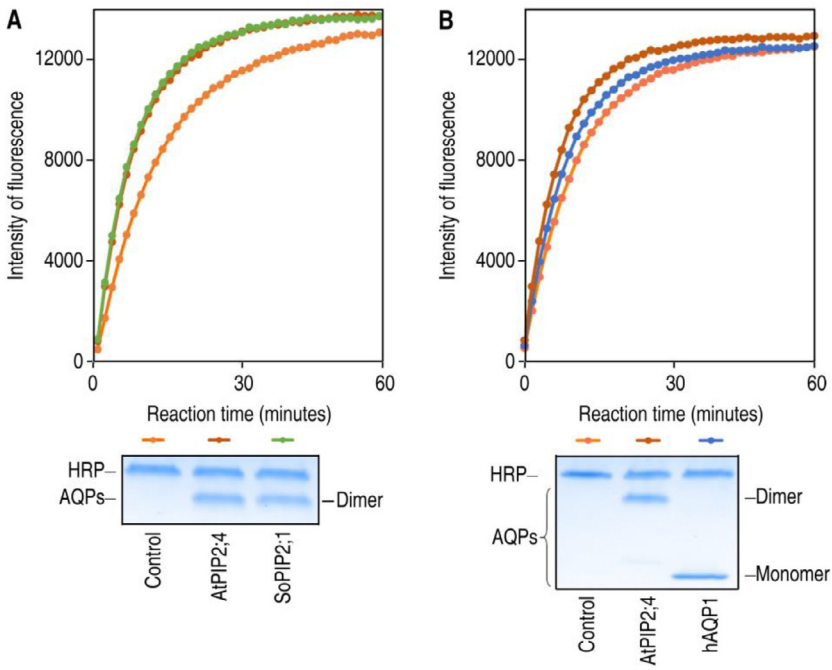

Fig. 4. Applicability of the assay for different aquaporin isoforms. (A) Comparing hydrogen peroxide transport for two aquaporin isoforms from plant, AtPIP2;4 and SoPIP2;1, respectively. (B) Comparing hydrogen peroxide transport for two aquaporin isoforms from different organisms, AtPIP2;4 and hAQP1, respectively. Fluorescent intensity curves as well as SDS-PAGE analysis are shown for each experiment. *Figure adapted from Wang et al 2020.*

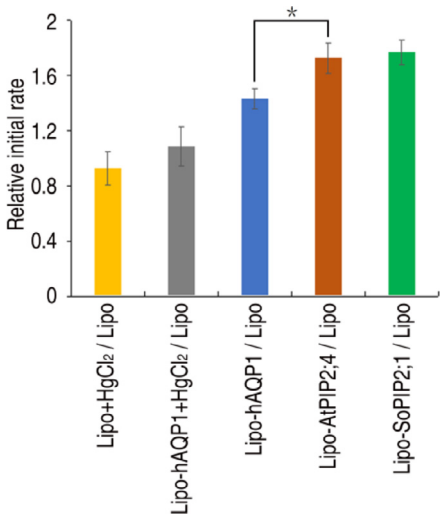

Fig. 5. Comparison of the relative initial rate of H_2O_2 transport. Columns of relative initial rate (n = 3-6) for various aquaporin homologues are shown where $*$ indicates significant difference. *Figure adapted from Wang et al 2020.*

Discussion

The method we established has been validated as a useful way to compare the capacity of various aquaporin isoforms in transporting H_2O_2 *in vitro*. Traditional methods for measuring H_2O_2 transport are normally based on living cell systems where expressing the aquaporins *in vivo* constitute an indispensable step. However, variations in production levels of individual protein targets as well as unavoidable interferences in the living cells make it non-trivial to accurately compare transport capacities between targets. Noteworthy, our method overcomes these disadvantages by reconstituting purified aquaporins in artificial liposomes.

The chemiluminescent probe used in the setup presented here is Amplex Red which is transformed to resorufin, catalyzed by HRP in the presence of H_2O_2. In fact, there are alternative fluorescent probes for detecting H_2O_2 which are established in cell-based assays. One of the most common probes to detect intracellular H_2O_2 is 2′,7′- Dichlorofluorescein diacetate (DCFH-DA) [9]. DCFH-DA permeates the cell membrane and is transformed to DCFH in the cell, catalyzed by esterase. However, in comparison to many other fluorescent probes, the transformation of DCFH to its fluorescent form requires the participation of additional compounds, like O_2, which cannot be controlled [4], and hereby we regard DCFH-DA as not suitable for our assay since problems with specificity and reproducibility can be expected. Another common chemical probe for hydrogen peroxide measurements is based on aryl boronate. Boronate esters of polycyclic aromatic compounds interact with H_2O_2 and release a highly fluorescent product [10,11]. However, the boronate esters a membrane permeable which makes it difficult to keep them inside the liposomes. A possible solution to this could be to bind the boronate esters to a protein target or some other impermeable compound, a reaction that might be difficult and costly. An additional disadvantage with the boronate esters is that the reaction between H_2O_2 is irreversible and that could possibly lead to inaccurate quantification of transient fluxes of hydrogen peroxide [12].

Furthermore, there are protein based fluorescent probes for H_2O_2 based on engineered proteins, including the commonly used HyPer. HyPer is based on the bacterial H_2O_2-sensing transcription factor OxyR and the circularly permuted yellow fluorescent protein (cpYFP) genetically inserted into the regulatory domain of OxyR [1]. The conformation of HyPer is altered by H_2O_2 which affects the disulfide bounds in the protein. A consequence is a shift in the fluorescent read out to an intensity at 500 nm. The fluorescent shift can also be detected *in vitro* by purified HyPer [1] and the protein can easily be encapsulated in liposomes, possibly providing an alternative system for hydrogen peroxide measurements. However, one concern to reflect upon is the necessity to keep the thiol group of HyPer reduced when encapsulated into liposomes, just to avoid the risk of disulfide bond formation in HyPer as a result from the interaction with H_2O_2. In the validation of this system, it would therefore be advisable to include an antioxidant, like the widely used β-mercaptoethanol, being aware of the paradox that the antioxidant itself could interfere with the reaction between HyPer and H_2O_2. Pointing this out, we do not exclude that HyPer could be a promising H_2O_2 sensor in the proteoliposome assay and it would be worth evaluating if this probe could improve the quantitative assay even further.

Acknowledgements

The work presented in this study was supported from research grants from the Swedish research Council (VR-M, Structural studies of aquaporin:protein complexes) to Kristina Hedfalk, as well as from the China National Key Research and Development Plan (grant number 2017YFD0200901) and Natural Science Foundation of China (grant number 31772247) to Hansong Dong.

Declaration of Competing Interest

The Authors confirm that there are no conflicts of interest.

References

[1] V.V. Belousov, et al., Genetically encoded fluorescent indicator for intracellular hydrogen peroxide, Nat. Methods 3 (2006) 281–286, doi:10.1038/nmeth866.
[2] G.P. Bienert, et al., Specific aquaporins facilitate the diffusion of hydrogen peroxide across membranes, J. Biol. Chem. 282 (2007) 1183–1192, doi:10.1074/jbc.M603761200.
[3] S. Dikalov, K.K. Griendling, D.G. Harrison, Measurement of reactive oxygen species in cardiovascular studies, Hypertension 49 (2007) 717–727, doi:10.1161/01.HYP.0000258594.87211.6b.
[4] B Kalyanaraman, et al., Measuring reactive oxygen and nitrogen species with fluorescent probes: challenges and limitations, Free Radic. Biol. Med. 52 (2012) 1–6, doi:10.1016/j.freeradbiomed.2011.09.030.
[5] A. Germaniuk, K. Liberek, J Marszalek, A bichaperone (Hsp70-Hsp78) system restores mitochondrial DNA synthesis following thermal inactivation of Mip1p polymerase, J. Biol. Chem. 277 (2002) 27801–27808, doi:10.1074/jbc.M201756200.
[6] H. Wang, S. Schoebel, F. Schmitz, H. Dong, K. Hedfalk, Characterization of aquaporin-driven hydrogen peroxide transport, Biochim. Biophys. Acta Biomembr. 1862 (2020) 183065, doi:10.1016/j.bbamem.2019.183065.
[7] H.M. Piwonski, M. Goomanovsky, D. Bensimon, A. Horovitz, G. Haran, Allosteric inhibition of individual enzyme molecules trapped in lipid vesicles, Proc. Natl. Acad. Sci. U.S.A. 109 (2012) E1437–E1443, doi:10.1073/pnas.1116670109.
[8] K. Hedfalk, Further advances in the production of membrane proteins in Pichia pastoris, Bioengineered (2013) 4.
[9] N.W. Kooy, J.A. Royall, H. Ischiropoulos, Oxidation of 2′,7′-dichlorofluorescin by peroxynitrite, Free Radic. Res. 27 (1997) 245–254, doi:10.3109/10715769709065763.
[10] H Maeda, et al., A design of fluorescent probes for superoxide based on a nonredox mechanism, J. Am. Chem. Soc. 127 (2005) 68–69, doi:10.1021/ja047018k.
[11] J.P. Miller, et al., Large-scale identification of yeast integral membrane protein interactions, Proc. Natl. Acad. Sci. U.S. A. 102 (2005) 12123–12128, doi:10.1073/pnas.0505482102.
[12] M.B. Grisham, Methods to detect hydrogen peroxide in living cells: Possibilities and pitfalls, Comp. Biochem. Physiol. A Mol. Integr. Physiol. 165 (2013) 429–438, doi:10.1016/j.cbpa.2013.02.003.

PAPER V

V

High-throughput screening combining bimolecular fluorescence with flow cytometry reveals constructive membrane protein complex formation

Florian Schmitz[1], Jessica Glas[1], Richard Neutze[1] & Kristina Hedfalk[1*]

[1]Department of Chemistry and Molecular Biology, Gothenburg University, Box 462, 405 30 Göteborg, Sweden

***Corresponding author:** Kristina Hedfalk, Department of Chemistry and Molecular Biology,

Gothenburg University, Box 463, 405 30 Göteborg, Sweden, +46-31-786 3923, kristina.hedfalk@gu.se

Interactions between membrane proteins in their cellular environment are determinants of the fine-tuned regulation crucial for all living cells. To shed light on the molecular mechanism of protein interactions, robust methods to screen and analyse protein complexes are of utmost importance where most available methods are designed for soluble proteins. The bimolecular fluorescence complementation (BiFC) assay is an approach which visualizes complex formation involving protein:protein interaction (PPI) partners *in vivo*, also for membrane protein complexes. In this study, we report the development of a high-throughput screening approach, using fluorescence-activated cell sorting (FACS) to characterize membrane protein interaction partners in the host *Saccharomyces cerevisiae*, allowing the discrimination between constructive complexes and random interaction. The approach developed in this study will make the use of manual screening obsolete and give the opportunity to efficiently screen for novel protein interaction partners *in vivo* in a high-through put setup.

The identification of protein-protein interactions (PPI) is the key for understanding cellular networks and their molecular processes in order to find effective treatments for the underlying diseases. Interaction between proteins are involved in critical functions such as signaling, posttranslational modification, trafficking and environmental communication. Derivation in function of the interactome is associated with various diseases such as autoimmune diseases and cancer.[1] The same fundamental role for cell functionality applies to membrane proteins, including aquaporins, which play a critical role in the development of a wide range of medical implications including, among others, neurological disorders[2-4], auto-immune diseases[5] and inflammatory related responses.[6, 7] Membrane proteins and their PPI networks are valuable drug targets[8] and there is a need for biochemical analysis and structural techniques which can give insight into their function. Since the progression in system biology and bioinformatics is fast, potential PPIs must be verified on a large-scale basis in less time, while aiming for high sensitivity, to provide targets for further characterization.

Several methods have been developed to detect PPIs based on different interaction effects[9], such as Surface Plasmon Resonance[10], Two-Hybrid methods[11], and biochemical approaches such as Co-Immunoprecipitation[12] and Pull-down assays.[13] For the various methods available to detect PPIs, biophysical, genetic or biochemical, it is necessary to assess whether the potential benefits of a technique outweigh its inherent disadvantages. In recent years, researchers have had access to a variety of methods[9, 14] for surveying the interactome, of which fluorescence-based techniques like fluorescence resonance energy transfer (FRET) and Bimolecular fluorescence complementation (BiFC) for high-throughput screening of PPIs in living cells[15, 16] have attracted attention. BiFC can readily be performed in different host systems, ranging from plant cells[17] to more complex mammalian cells like HEK293[18]. Complementation fluorescence was initially quantified using fluorescence microscopy[19], however, the benefits with flow cytometry for the analysis of fluorescence intensity became obvious[20] enabling high throughput screening while avoiding artefacts arising from manual readout. Independent of method used for evaluation of BiFC pair, the detection of PPIs has intrinsic challenges such as unspecific fluorescence background signal due to self-assembly of the fluorophore partner and possible tethering of BiFC partners during translation and translocation.[21] Thus, using BiFC, awareness of these limitations are needed and solutions to overcome them are highly attractive.

In a previous study, we have established the BiFC method to validate the direct protein-protein interaction between aquaporin tetramers and specifically the complex formed by human aquaporin 0 (hAQP0) and the regulatory protein Calmodulin (CaM) using the yeast host *Saccharomyces cerevisiae*, where this BiFC complex in addition aided the purification process.[22] In this specific study, each protein target is attached to a complementary YFP molecule and constructive BiFC complexes were verified[23], where the specific interaction between CaM and the C-terminus of hAQP0[24] brings the YFP fragments in close proximity. The native three-dimensional structure of YFP can be followed by the fluorescence read-out, providing a method for membrane protein complex screening where the *in vivo*

interaction can be analysed directly in its natural environment. The hAQP0-CaM complex was initially analysed by manual readout using fluorescence microscopy and complex formation was confirmed by Native Page.[22] In this study we aimed at developing the actual screening procedure applying population screening and quantification of the complex using FACS establishing the full procedure from transformation and growth of cells to the actual analysis of the fluorescent signal. Here we

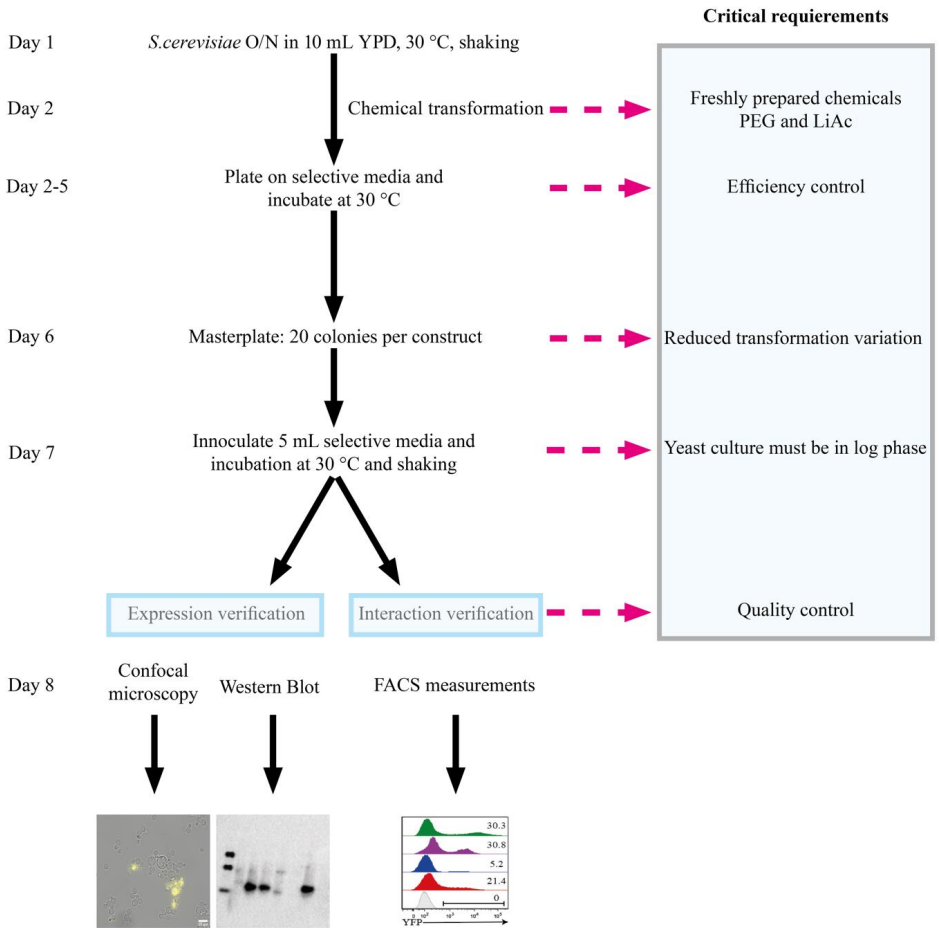

Figure 1: Schematic view of a standardized cell preparation scheme for qualitative and quantitative analysis of BiFC complexes produced in *Saccharomyces cerevisiae* cells. The schedule is optimized to finalize the whole screening process in less than 14 days. Optimization of critical steps throughout the whole procedure have been emphasized.

present a standardized method to perform reliable screening of the aquaporin BiFC complex using FACS allowing a high throughput and having the potential to screen for novel interactions. Additionally, we want to propose a second validation criterion as an indicator for authentic BiFC interaction, the relative fquency of the interaction.

Results

High throughput screening of aquaporin BiFC complexes produced in *S. cerevisiae*

Analyzing the expression and interaction of two membrane proteins described in this study with BiFC requires a robust experimental pathway design, which assures a consistent fluorescence signal for further investigation (**Figure 1**). The validation is based on at least three biological repeats based on individual chemical transformations. A first investigation of these transformation events via FACS measurements revealed an intrinsic fluorescence variation of the transformants. The intensity of fluorescence is correlated to a biological variation connected to the growth phase and natural variance of the yeast cells. For this reason, a protocol was established which standardizes the selection and growth of transformants to reduce the naturally occurring transformation variation.

By using fluorescence cytometry as a "pre-check" technique, ten colonies were screened directly from the growth plate after the transformation for fluorescence activity and thus for the evaluation of the transformation efficiency. The absence of fluorescence was considered as an unsuccessful transformation and therefore not used in this study. If fluorescence was detected from individual colonies the transformation was considered successful and 20 colonies were randomly picked and transferred to a fresh SC media agar plate, constituting the master plate. This procedure was performed for each individual biological replicate and finally ten colonies from each transformation were grown in liquid media to the log phase and analysed using flow cytometry. As negative controls, transformants containing only one plasmid of the BiFC paid were treated the same way as described above. However, non-fluorescence was not considered as an exclusion criterion when only one part of the YFP (Y_C or Y_N) fused with its target was transformed.

AQP0-CaM BiFC pairs are equally expressed in the cells

Before reading the fluorescence intensity of the BiFC complexes, it was verified that the BiFC constructs were correctly expressed in comparable amounts *in vivo*. For this purpose, standardized high density cell lysates of overnight cultures, loading the same OD_{600} units in each well, were separated by SDS-PAGE and the various BiFC pairs were analysed by immunoblot using anti-YFP and anti YFP split variant (YFP_C , YFP_N) antibodies, respectively, and the sizes of the bands evaluated (**Figure 2**). Using the antibody towards the YFP_C part, YFP_C-AQP0 (40 kDa) and YFP_C-CaM (28 kDa) could be identified at their expected molecular weights, lane 1-3 in **Figure 2A**. Furthermore, faint bands of oligomeric forms of YFP-AQP0 could be seen together with the negative and positive controls for this antibody, YFP_N-AQP0 and YFP_C-CaM in lane 5 and 6, same figure. Untransformed cells are loaded in lane 7. Similarly, using the antibody towards the YFP_N part, YFP_N-AQP0 (47 kDa) and YFP_N-AQP0Δ (41 kDa) could be identified a bit lower than

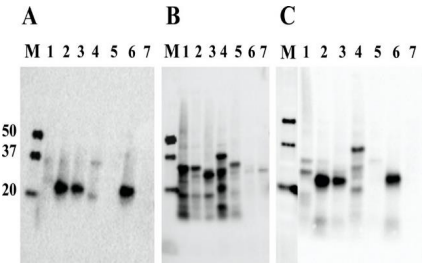

Figure 2: Immunoblot analysis of the various BiFC complexes obtained from cell lysates.. Samples were applied in the following order on all three blots (A-C): (M) Marker, molecular weight in kDa, (1) YFP_N-AQP0 + YFP_C-AQP0, (2) YFP_N-AQP0+ YFP_C–CaM, (3) YFP_N-AQP0Δ + YFP_C-CaM, (4) YFP-AQP0, (5) YFP_N-AQP0, (6) YFP_C –CaM, (7) non-transformed *S. cerevisiae* cells. Antibodies against YFP_C (A), YFP_N (B), or complemented YFP (C) were used.

their expected molecular weights, lane 1-3 in **Figure 2B**, which is not uncommon for membrane protein targets. Furthermore, the oligomeric states of YFP-AQP0 could be seen in lane 4 as well as the positive control, YFP_N-AQP0 in lane 5, and the two negative controls for this antibody, YFP_C-CaM and untransformed cells, in lane 6 and 7, respectively. Worth noting for the YFP_N antibody, is a faint background band between 20 and 37 kDa seen in all lanes (**Fig. 2B**). In addition, using the antibody against full YFP (**Fig. 2C**) gives very similar immunoblot pattern as the YFP_C antibody (**Fig. 2A**), indicating that the epitope for this antibody is located at the C-terminus. In summary, even though BiFC complexes are unambiguously produced in the cells analysed, the major immunoblot signals correspond to individual parts (lane 1-3) supporting an excess of fragments as compared to amount of complex actually formed (see also results below). In all blots, however, faint bands at higher molecular weight are also observed, possibly corresponding to full BiFC complexes. Noticeable also is the low expression of the YFP_C-AQP0 part of the YFP_N-AQP0 + YFP_C-AQP0 BiFC pair (**Fig 2A** and **B**, lane 1), which could possibly be related to the observed poor growth of that mutant, Nevertheless, by the immunoblot using various antibodies, the actual production of the BiFC parts in the host could be verified, as an important fundamental fact for further quantitative analysis of the fluorescent BiFC complex.

Log phase growth is important for accurate cytometry analysis

For the analysis of the BiFC complexes a suitable gate was created where 51% of all events ended up in the selected gate (**Fig 3A and B**). In order to establish a stable FACS analysis of biological samples, the actual pre-growth of the *S. cerevisiae* transformants were carefully evaluated. Initially, picking yeast cells directly from the SC agar plate was evaluated, however, the resulting fluorescence was relatively low (**Fig. 3C**). Hence, pre-selected fluorescent cultures grown to the log-phase (OD_{600} = 0.5) were evaluated assuring active growth of cells producing the BiFC complex. Indeed, a higher fluorescence was recorded, showing an additional peak in the chromatogram further up on the x-axis, as exemplified by the AQP0-CaM complex compared to the negative control just containing one of the fragments, YFP_N-AQP0 (**Fig. 3C**). Noteworthy, a higher percentage of cells also show fluorescence for cells pre-grown in liquid culture as compared to plate growth, indeed about four times higher for the AQP0-CaM complex, 21.4 as compared to 4.8. In conclusion, the cultivation of the transformed cells in liquid cultures up to the log phase was crucial for rationalization and standardization of the cytometry analysis. This control experiment led to an optimized growth scheme in liquid SC

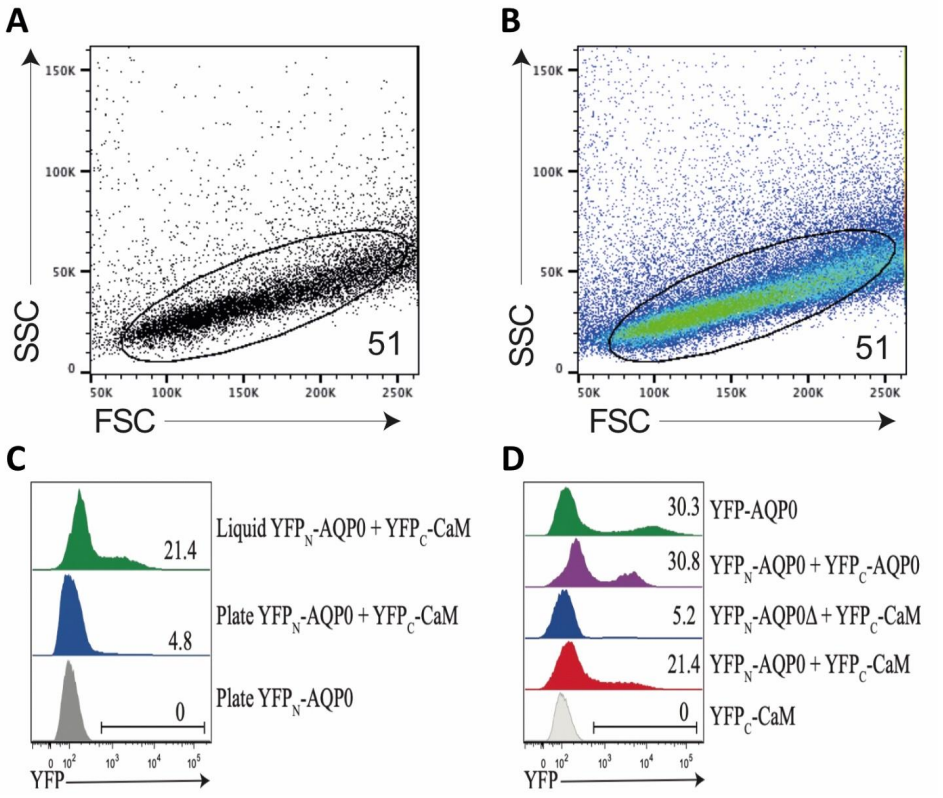

Figure 3. FACS evaluation of BiFC complexes. Applied gate showed as a dot plot with 16000 events in A) and a pseudo-color plot illustrating a heat-map of all events in B). SSC on the y-axes represents side scatter as indicator of complexity and FSC on the x-axes represents forward scatter as an indicator of size. The figure 51 means that 51% of all events ends up inside the gate. C) Representative YFP intensity flow cytometry readouts of the AQP0-CaM BiFC complex grown on SC media plates versus SC liquid growth to OD_{600} = 0.5. As a control, a non-fluorescent construct is shown as comparison. D) FACS analysis of the various BiFC pairs compared in this study together with a negative control (YFP_C-CaM). The figures show representing flow cytometry readouts of YFP intensities from different BiFC constructs and their individual fluorescent fraction in percentage.

media, which was applied to all cells analysed and their respective fluorescence intensities (**Fig. 3D**). As seen for the various complexes, transformants expressing the BiFC protein pairs showed a peak fluorescence on a logarithmic growth scale and the predefined growth conditions make the resulting intensity values more comparable. The exemplary representation of individual sample values (**Fig. 3D**) cannot show the variety of the analysis of the entire transformation range, but it is still possible to identify the different fluorescence intensities used for accounting and where the cut-off for the auto-fluorescent cells lies.

The highest fraction of fluorescent cells

was achieved for the positive control YFP-AQP0, which is in the same range as the control BiFC complex, AQP0-AQP0, 30.3 versus 30.8. For the AQP0-CaM complex, the fraction of fluorescent cells is a bit lower, 21.4, while the unconstructive complex where the binding site for CaM is deleted, only had a fraction of fluorescent cells of 5.2 (**Fig. 3D**). Summarizing these findings, for proper comparison of FACS signals, log phase cells should be compared and it is essential to evaluate the actual intensity of fluorescence as well as the fraction of fluorescent cells for each target.

BiFC complexes can be visualized by fluorescence microscopy

A qualitative examination of yeast transformants producing the BiFC complexes using fluorescence microscopy was performed to confirm the intracellular production complexes and the absence of fluorescent aggregates. A BiFC signal could indeed be successfully detected and varies between the different pairs. The strongest qualitative intensity signal was detected from the single plasmid transformant YFP-AQP0 (**Fig. 4**), which is possibly due to an easier uptake of a single plasmid by the yeast cells combined with the fact that a single fluorescent fusion protein is more likely to be fully translated and does not require a split YFP partner to be activated. BiFC complexes dependent on co-transformation, YFP_N-AQP0 + YFP_C -AQP0 and YFP_N - AQP0 + YFP_C –CaM, showed lower fluorescence intensities in comparison to the full length YFP-AQP0 control. That observation can be explained by the need for complex formation between the co-expressed proteins and the alignment of the YFP reporter protein. The single plasmid control, YFP_N-AQP0, was used as a negative control. On the other hand, the C-terminus deficient BiFC complex formation control, YFP_N-AQP0Δ + YFP_C–CaM, showed extremely low fluorescence intensities supporting that Fluorescent YFP will not form if the binding site for CaM on AQP0 is deleted. This observation is in good agreement with the FACS signal where the frequency of fluorescent cells was much higher for the YFP_N-AQP0 + YFP_C-CaM complex as compared to the YFP_N-AQP0Δ + YFP_C-CaM complex (21.4% versus 5.2 %, Fig. 3B). Thus, the qualitative microscope pictures already show the importance of an interaction-deficient mutant as internal control samples, since the coincidentally fluorescence intensity of the C-terminus deleted mutant is not completely suppressed.

Besides a qualitative check of fluorescence frequency and intensity, the observation of the general condition of the grown cells in the brightfield setup can provide information about the overall fitness of the yeast cells. Observed abnormal cell shapes can be an indicator for a strained cell and could indicate low replication rates. For example, we experienced low growth rates of the YFP_N-AQP0 + YFP_C-AQP0 cell line and examination via brightfield microscope showed an abnormal cell shape. In this specific case, we speculate whether the production could lead to dysfunctional osmotic balance regulation due to the aquaporin overexpression. Altogether, a microscopical confirmation allows the qualitative verification of targets for FACS evaluation where proper controls for the complex formation can be evaluated.

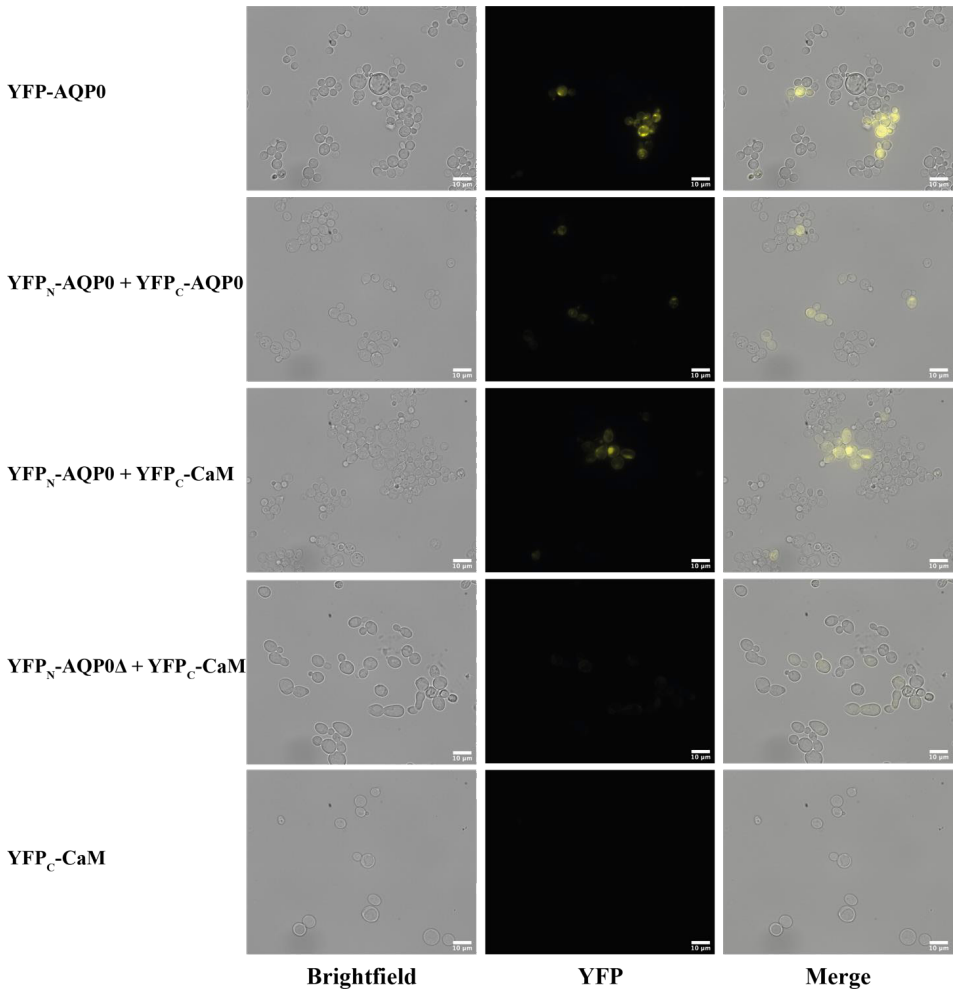

Figure 4: Bright field and fluorescence images of subcellular localisation of BiFC complexes produced in *Saccharomyces cerevisiae* cells. Highest fluorescence level was obtained from the positive control, cells producing the full length chromophor fused to human aquaporin 0, YFP-AQP0. Cells transformed with the split variants of YFP, YFP_N-AQP0 + YFP_C-AQP0 and YFP_N- AQP0 + YFP_C–CaM, respectively, showed an intermediate signal, while very faint fluorescence was observed for the negative AQP0-CaM complex, YFP_N-AQP0Δ + YFP_C-CaM complex. Cells expressing single plasmid were used as non-fluorescent controls.

The fraction of fluorescent cells is a critical parameter to evaluate successful BiFC formation

Even though the qualitative microscopy analysis provides a useful tool to evaluate BiFC complexes produced in *S. cerevisiae*, the method has intrinsic limitations due to risk and subjective evaluation as well as a large time demand. A more objective method having a high-through put is therefore of major interest where the median fluorescence intensity values can be quantitated with robust statistics, and FACS was therefore evaluated for screening of the BiFC membrane protein complexes produced in *S. cerevisiae*. Indeed, the readout of cells producing full length YFP-AQP0 expressing a single plasmid supports the results previously achieved from the microscope studies with the highest average median fluorescence units of 5645 +/- 660, n= 3 x 10 transformants (**Fig. 5A**), and thereby provides a robust standard as a positive fluorescence control using this method. In order to confirm that any auto fluorescence of cells in the selected gating (see **Figure 3A and B**) can be measured, single plasmid transformants (YFP_C-CaM and YFP_N-AQP0) were also included in the FACS evaluation to include proper negative controls. Furthermore, it is noticeable that all constructive BiFC pairs generally show similar average fluorescence intensities, while the higher YFP_N-AQP0Δ + YFP_C -CaM fluorescence derivation indicates a larger fraction of non-fluorescent cells. The constructive BiFC complexes, YFP_N -AQP0 + YFP_C-AQP0 and YFP_N-AQP0 + YFP_C-CaM, respectively, show average fluorescence intensities of 2185 +/- 685 and 1496 +/- 213, while the non-interactive construct YFP_N-AQP0Δ + YFP_C-CaM shows a higher oscillation of 976

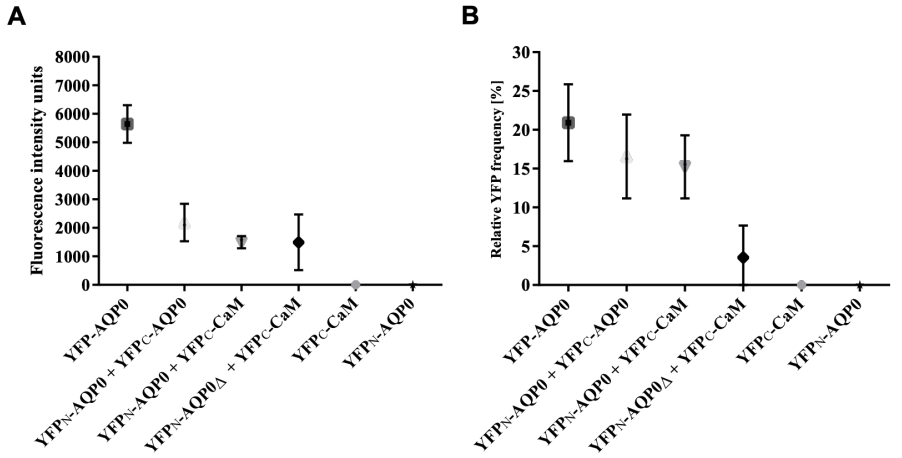

Figure 5. Fluorescence intensity and relative YFP frequency of BiFC complexes evaluated using FACS. A) Average fluorescence intensity is shown for each complex together with the standard error of the mean (n=10 technical repeats based on at least 3 biological repeats, i.e. independent transformation events). B)**.** The average of the fraction of fluorescent cells in percentage is shown for each complex together with standard error of the mean (n=10 technical repeats based on at least 3 biological repeats, i.e. independent transformation events).

fluorescence units around the standard deviation of 1493 units (**Fig. 5A, Table 1**). In order to exclude the obliterating effect of averaging all single measurements over different transformations, two transformations of each construct were also compared individually with respect to their intensity and relative frequency readouts. These results are not plotted separately, but a statistically significant difference was not observed. Furthermore, the low fluorescence readout for the single exemplary YFP_N-AQP0Δ + YFP_C-CaM construct (**Fig. 3B**) is having a similar but more volatile fluorescence readout comparing all transformation populations (**Fig. 5A**) indicating that randomly formed complexes are a more rare event, but when they are formed, they fluoresce as much as a constructive BiFC complex. This reveals the critical need for a second indicator to distinguish between constructive and non-constructive complementation.

To more accurately be able to distinguish constructive and non-constructive BiFC complexes we included another factor in the analysis of the BiFC complexes using FACS, namely the fraction of fluorescent cells. This criterion provides an additional quantitative criterion, besides the qualitative control by microscope examination, which makes it possible to distinguish between valid BiFC complementation and random background interactions. As expected, single plasmid transformants (YFP_N-AQP0 and YFP_C-CaM) did not show any analysable fluorescence fraction of cells (**Fig. 5B**), which is consistent with previous fluorescence intensity measurements (**Fig. 5A**). The same consensus was found for the YFP-AQP0 construct, which showed the highest average fluorescence intensity, in full agreement with the quantitation of the highest fraction of fluorescent cells at 20,91 % (**Fig. 5B**). The advantage of defining a second quantitative selection criterion for the selection of authentic complex formation becomes evident when the relative frequency of fluorescent cells of YFP_N -AQP0 + YFP_C-CaM, YFP_N-AQP0Δ + YFP_C -CaM is analysed. Focusing only on intensity levels, the YFP_N -AQP0Δ + YFP_C-CaM cells would be classified as a valid BiFC interaction sample showing fluorescence of comparable intensity (1496 units (YFP_N-AQP0 + YFP_C-CaM) versus 1493 units (YFP_N-AQP0Δ + YFP_C-CaM), **Fig. 5A**), while having a higher internal variation. Ahe integration of the relative frequency of fluorescent cells in the complementation analysis resulted in a more differentiated conception of how to interpret the analysis results. Since the cell preparation prior to analysis was the same for all constructs, the difference in fluorescence fractions ((15,23 % +/- 4,07 % (YFP_N-AQP0 + YFP_C-CaM) vs. 3,54 %+/- 4,12 % (YFP_N-AQP0Δ + YFP_C-CaM)) is a diagnostic tool to distinguish between constructive complex formation and background noise signal due to random interactions (**Table 1**).

Taken together, in this study we identified two criteria, the fluorescence frequency of occurrence in combination with intensities, as critical factors for proper evaluation of complex formation. The first criterion, the fraction of cells showing fluorescence, or the relative frequency, also provides a brief and reliable screening criterion to preclude potential constructs via the standardised growing scheme. Cells that didn't show any expression were eliminated for subsequent analysis, which preserves experimental time and reduces the risk of a decreased signal-to-noise ratio. In a subsequent analysis, the levels of relative fluorescence frequency of the different constructive constructs to each other were compared (**Fig. 5B**). The fraction of cells

Table 1. Overview table of fluorescence intensity and relative YFP frequency of BiFC complexes. Number of biological repeats (independent transformation event) and the sum of all technical repeats is shown for each construct. The average of the fluorescence intensity units is shown for each complex together with the variation (standard error of the mean). The average of the fraction of fluorescent cells in percentage is shown for each complex together with the standard error of the mean

Constructs	Biological Repeats	Technical Repeats	Average Fluorescence intensity units	Average YFP Frequency (%)	Variation Fluorescence intensity units	Variation YFP Frequency (%)
YFP-AQP0	3	31	5645.44	20.91	660.36	4.94
YFP_N-AQP0 + YFP_C-AQP0	3	32	2185.00	16.56	657.87	5.40
YFP_N-AQP0 + YFP_C-CaM	3	33	1495.87	25.23	213.24	4.07
YFP_N-AQP0Δ + YFP_C-CaM	3	44	1493.20	3.54	976.41	4.12
YFP_C-CaM	3	30	0	0	0	0
YFP_N-AQP0	3	30	0	0	0	0

containing the interaction-deficient plasmids YFP_N-AQP0Δ + YFP_C-CaM was defined as the threshold of use to identify and distinguish random interference from fluorescence complementation. From a practical point of view, the constructive complementation differed from random interactions when the relative fluorescence frequency was above the 7,66 % (YFP_N-AQP0Δ + YFP_C-CaM mean of 3,54 % + 4,12 % deviation, **Fig. 5B**) of the deficient control construct. This value can be considered as a threshold to distinguish between random interaction and complex formation.

All analysed transformants of full length YFP (YFP-AQP0) as well as all the two constructive BiFC pairs (YFP_N-AQP0 + YFP_C-AQP0, YFP_N-AQP0 + YFP_C-CaM) show a fluorescence frequency of more than 10 %, indicating a proper alignment of the two YFP fragments, which can be distinguished from the single plasmid controls and the YFP_N-AQPΔ mutant. A relative fraction of fluorescent cells above 10% could thus be an indicator of a constructive membrane protein complex when analysed using this method. Besides the relative frequency of cells showing fluorescence as a basal criterion, this study suggests the use of averaged fluorescence median intensities as a second quality selection criterion. The average median fluorescence intensity of the constructive BiFC pair YFP_N-AQP0 + YFP_C-AQP0 compounds to 2185 units +/- 658 (**Fig. 5A**), which is the highest average median of constructive BiFC combinations. The highest fluorescence level defines the exclusion limit, cells with a lower fluorescence display were considered as signal background. Given that the maximum obtainable fluorescence intensity is determined with 5645+/- 660 for YFP-AQP0, (**Fig. 5**), potential aquaporin BiFC studies with novel interaction partners should set the selection level to 4985 intensity units (**Table 1**).

Discussion

Previously, BiFC has been used to detect human aquaporin interaction partner *in vivo*[25], as well as the confirmation of aquaporin PPIs in living plant cells[26]. Furthermore, the use of different host systems has been developed, from prokaryotic cells[25] to eukaryotic yeast systems and human cell lines.[27] In the case of plant aquaporins, the complex formation could be confirmed by fluorescence microscopy.[28] The integration of flow cytometry readout into the analytical

process in recent years was a step forward towards high-throughput screening of molecular PPI processes, both in human cells[29] as well as in yeast cells[30, 31]. In this study, we have shown that human aquaporin-BiFC complexes produced in *S. cerevisiae* can be evaluated in a high throughput screening (HTS) manner via flow cytometry and we have established a detailed protocol for proper interaction studies. The present study rationalized the conditions prior to the HTS measurements while reducing unspecific BiFC background. A streamlined growth scheme ensures uniform cell populations in the logarithmic growth phase, where the expression of target proteins is optimal. The use of cytometry allows an objective screening of many populations in an HTS manner as well as the ability to measure several parameters in addition to the intensity of the quality checked cells.

While BiFC complementation is an established method for the detection and validation of protein:protein interactions, the intrinsic disadvantages of the technique, the distinction between background signal and valid molecular based signal and potential false-positive hits, are still a challenge. The development of advanced split fluorophores has led to an increased signal-to-noise ratio[32], but commonly, only the fluorescence intensities of complementation events are analysed. This seems to be natural, but this approach will favor the detection of events that show large differences in binding affinity and is only the indirect indicator of the association of two binding partner. Complementation events based on low PPI affinities or via two-step mechanisms do not occur often enough to be detected significantly. On the other hand, the false-positive rate would increase if too many of these events were locked via BiFC. Based on our evaluation, fluorescence intensities should not be interpreted in isolation from their molecular background. Even correctly designed negative controls such as YFP_N-AQP0Δ + YFP_C-CaM can show intensity levels that correspond the interaction controls, although with a higher variance. This is the reason to include the relative frequency of fluorescence in the evaluation of FACS complementation evaluations. The proportion of cells showing fluorescence is an indicator that allows the discrimination of non-constructive pairs from constructive complex formation. In conclusion, defining the proportion of fluorescent cells as the additional analysis criterion allows the investigation of PPIs with low affinity and/or complexes with cooperative complex formation, such as the AQP0-CaM complementation, while sorting random interactions away. Co-evaluation with relative fraction of fluorescent cells gives more information about the strength of the interactions, in the meaning and frequency of actual interaction events, and allows to distinguish between complexes with large differences in binding affinities and weak transient interactions. Furthermore, a weak two-step interaction could result in the potential fluorescence intensity never being reached because the molecules are not locked often or long enough to be separated from the background noise. Interaction processes like the binding of CaM to two AQP0 molecules is a cumulative process in which the first interaction favors the final interaction. Recent interaction studies with full length protein[24] indicate a low affinity binding of the AQP-CaM interaction illustrating that also weak interactions can be evaluated using FACS.

A general aspect of importance specifically for analysis of BiFC complexes is the requirement of proper internal controls[33] ,

which can be non-trivial to achieve for novel complexes where detailed biochemical information is missing. When designing controls, it is therefore of major importance to consider those lower interaction frequencies and include those in the analysis. When cells are screened for the detection of novel interaction partners, only clones with high fluorescence intensity and relative frequency that are individual for each protein target should be considered. Noteworthy, the results from this work emphasize the possibility of setting thresholds when screening for cells that show correct BiFC complementation based on the two criteria; fluorescence intensity combined with fraction of fluorescent cells.

Even though the FACS analysis satisfactorily identify fluorescent complexes, imaging is a relevant complement just to assure healthy cells are included in the analysis. Thus, besides the analysis of the BiFC intensities and relative frequencies, it is still encouraged to check the quality of the cells at least once for each designed construct. This aspect is especially relevant for membrane protein complexes where the actual localization can be observed and putative internal aggregates found. Worth noting is also that mutations designed for proper controls may be complementary at the molecular level, but can have an impact on the overall health of the cells. As a result, high fluorescence intensities can be read out, but a low percentage of fluorescent cells indicates a low rate of transformation and slow growth (see YFP_N -AQP0 + YFP_C -AQP0). Evaluation of the state of the cells with a confocal fluorescence microscope could exclude theoretical mutants that have a negative influence on the general health of the cells.

In summary, we present an approach combining quantitative and qualitative criteria for the screening of the biological variation that influences the evaluation of BiFC protein complex formation. The relative frequency of cells showing fluorescence is a complementary factor that supports constructive complex formation and lowers the number of false positive hits in the screening approach. This study presents a systematic screening process that can be utilized for high-throughput cDNA library screening of novel interaction partners[34] which opens up for understanding the underlying mechanics that are important for cellular functions associated with medical diseases.

Methods

Genes, vectors, and strains

The BiFC pairs, including human AQP0 and CaM, were cloned in the p423GPD and p426GPD vectors and transformed to *S. cerevisiae* (MYA-1662™ his3, ura3-52), as previously described (Sjöhamn et al. 2016). For this specific study the following constructive constructs were selected for evaluated by FACS screening; YFP-AQP0, YFP_N-AQP0 + YFP_C–AQP0, YFP_N-AQP0 + YFP_C -CaM, YFP_N -AQP0Δ + YFP_C -CaM, YFP_N -AQP0, YFP_N -AQP0 and YFP_C-CaM.

Chemical transformation of *S. cerevisiae*

For transformation of plasmids, *S. cerevisiae* cells with HIS or HIS/URA deficiency selection marker (MYA-1662™ strain) were inoculated in 5 ml YPD medium and grown overnight at 30˚C. The next day, the cells were inoculated in 50 ml YPD medium to a starting OD_{600} of 0.25 and grown at 30˚C to reach an OD_{600} between 0.7 and 1.0. For the chemical transformation, cells were fractionated into 50 μl batches and for a single plasmid transformation, each batch was mixed with 240 μl freshly prepared PEG4000 (50%),

36 µl 1 M freshly prepared LiAc, 50 µg freshly denatured salmon sperm , 1- 2 µg (maximum 10 µg) of plasmid DNA and mQ water was added to a final volume of 360 µl . In case of double plasmid transformation, a minimum of 2 µg (maximum 10 µg) of each plasmid DNA must be used. The mixture was incubated at 30˚C for 30 min with shaking and a subsequent heat shock followed for 25 min at 42˚C. The cells were spun down for 15 s at 5500 g. The pellet was resuspended in 200 µl mQ water, transformed cells were plated out on selective SC-agar plates and incubated at 30˚C. The single colonies were grown for at least three days, to become fully visible on the SC-agar plates. To verify efficient transformation for each target, ten colonies from each plate were randomly tested for fluorescence using FACS (see below). Before analysis, cells were resuspended in water and if the majority of the cells fluoresce, the transformation was judged as successful and cells selected for further analysis.

Growth of transformants producing the BiFC complexes

For successful transformations, master plates were prepared for each BiFC pair by re-streaking 20 single colonies on a fresh SC-agar plate, before re-growing the cultures in liquid selective me- dia. For each BiFC pair, or control, twelve colonies from the masterplate were regrown overnight in 5 ml SC medium at 30˚C with shaking. The following day, the cells from the overnight culture were diluted to OD_{600}=0.2 into a 12-well tissue culture plate and incubated at 30˚C to reach an OD_{600} of 0.5, assuring a generation time of two hours being a quality marker for being a culture of healthy cells. Cultures having a prolonged generation time were not included in the fluorescence analysis.

Fluorescence readout using FACS

Fluorescence intensities of the cell samples were evaluated using a FACSMelody (BD) flow cytometer (100 µm nozzle size, blue excitation laser at 488 nm). For the fluorescence measurements, 500 µl sample, cell culture of OD_{600}=0.5, was loaded into the FACS machine assuring a good resuspension of the cells. Debris and non-uniform cells were excluded and the fluorescence intensity of 100,000 cells of the live population was excited at 488 nm andevaluated on the FITC channel (527/32 bandpass filter).

Immunoblot analysis

To confirm proper and even production of the split YFP variants, YFP_N and YFP_C, respectively, fused to the targets of interest or the full-length YFP, cell lysates were evaluated using Immunoblot analysis. In brief, the cells of an overnight culture of the different constructs from the masterplate, same cells that we used for the FACS screening, were spun down (5,500g, 5 min.) and diluted in PBS to an OD_{600} of 5. Each sample was resuspended in 200 µl 1x SDS resuspension buffer (46 µL 4x Laemmli sample buffer (BioRad), 20 mM DTT, 150 µL mq H2O) and heated for 8 min at 95˚C. Cell debris were spun down (15000g, 5 min) and 14 µl of each sample were loaded on a SDS-PAGE gel (BioRad Protean TGX, 4-20%, 16 min, 300 V). A fast blotting procedure was performed (BioRad Trans-Blot Turbo, TGX Turbo protocol) to a PVDF membrane (Amersham Hybond PVDF). Three different antibodies were used in separate immunoblots directed towards the YFP split YFP variants (anti YFP_C: Roche Diagnostics #11814460001; anti YFP_N: BioLegend #902601) and the full length YFP (Thermo Scientific #CAB4211), respectively, using a Pierce Fast Western Blot kit (ECL substrate) from Thermo Scientific. The chemiluminescence

signal was detected via luminol enhancement from the kit. Fluorescence detection was manually performed and captured using a ChemiDoc MP imager from BioRad and Image Lab software.

Fluorescence microscopy and image analysis

Images of the transformants were generated with an exposure time of 200 ms at an inverted Zeiss Axio Observer.Z1 flurescence microscope with an Axiocam 506 camera. A Plan- Apochromat 100x/1.40 oil DIC M27 objective was fitted to the microscope. YFP excitation was performed at 508 nm, using a 450 - 490 nm filter with a HXP mercury short-arc lamp. The emitted fluorescence light at 524 nm was analysed after passing a 500 - 550 nm filter. Zeiss Zen blue software was used to capture and process the data.

References

[1] Safari-Alighiarloo, N., Taghizadeh, M., Rezaei-Tavirani, M., Goliaei, B., and Peyvandi, A. A. (2014) Protein-protein interaction networks (PPI) and complex diseases, *Gastroenterol Hepatol Bed Bench 7*, 17-31.

[2] Mader, S., and Brimberg, L. (2019) Aquaporin-4 Water Channel in the Brain and Its Implication for Health and Disease, *Cells 8*.

[3] Hubbard, J. A., Szu, J. I., and Binder, D. K. (2018) The role of aquaporin-4 in synaptic plasticity, memory and disease, *Brain Res Bull 136*, 118-129.

[4] Papadopoulos, M. C., and Verkman, A. S. (2013) Aquaporin water channels in the nervous system, *Nat Rev Neurosci 14*, 265-277.

[5] Weinshenker, B. G., and Wingerchuk, D. M. (2017) Neuromyelitis Spectrum Disorders, *Mayo Clin Proc 92*, 663-679.

[6] Meli, R., Pirozzi, C., and Pelagalli, A. (2018) New Perspectives on the Potential Role of Aquaporins (AQPs) in the Physiology of Inflammation, *Front Physiol 9*, 101.

[7] Sisto, M., Ribatti, D., and Lisi, S. (2019) Aquaporin water channels: New perspectives on the potential role in inflammation, *Adv Protein Chem Struct Biol 116*, 311-345.

[8] Yin, H., and Flynn, A. D. (2016) Drugging Membrane Protein Interactions, *Annu Rev Biomed Eng 18*, 51-76.

[9] Miura, K. (2018) An Overview of Current Methods to Confirm Protein-Protein Interactions, *Protein Pept Lett 25*, 728-733.

[10] Douzi, B. (2017) Protein-Protein Interactions: Surface Plasmon Resonance, *Methods Mol Biol 1615*, 257-275.

[11] Choi, S. G., Richardson, A., Lambourne, L., Hill, D. E., and Vidal, M. (2018) Protein Interactomics by Two-Hybrid Methods, *Methods Mol Biol 1794*, 1-14.

[12] Lin, J. S., and Lai, E. M. (2017) Protein-Protein Interactions: Co-Immunoprecipitation, *Methods Mol Biol 1615*, 211-219.

[13] Louche, A., Salcedo, S. P., and Bigot, S. (2017) Protein-Protein Interactions: Pull-Down Assays, *Methods Mol Biol 1615*, 247-255.

[14] Zhou, M., Li, Q., and Wang, R. (2016) Current Experimental Methods for Characterizing Protein-Protein Interactions, *ChemMedChem 11*, 738-756.

[15] Wade, M., Méndez, J., Coussens, N. P., Arkin, M. R., and Glicksman, M. A. (2017) Inhibition of protein-protein interactions: cell-based assays, In *Assay Guidance Manual [Internet]*, Eli Lilly & Company and the National Center for Advancing Translational Sciences.

[16] Wang, S., Ding, M., Xue, B., Hou, Y., and Sun, Y. (2018) Live Cell Visualization of Multiple Protein-Protein Interactions with BiFC Rainbow, *ACS Chem Biol 13*, 1180-1188.

[17] Berendzen, K. W., Bohmer, M., Wallmeroth, N., Peter, S., Vesic, M., Zhou, Y., Tiesler, F. K., Schleifenbaum, F., and Harter, K. (2012) Screening for in planta protein-protein interactions combining bimolecular fluorescence complementation with flow cytometry, *Plant Methods 8*, 25.

[18] Riese, F., Grinschgl, S., Gersbacher, M. T., Russi, N., Hock, C., Nitsch, R. M., and Konietzko, U. (2013) Visualization and quantification of APP intracellular domain-mediated nuclear signaling by bimolecular fluorescence complementation, *PLoS One 8*, e76094.

[19] Hu, C. D., Chinenov, Y., and Kerppola, T. K. (2002) Visualization of interactions among bZIP and Rel family proteins in living cells using bimolecular fluorescence complementation, *Mol Cell 9*, 789-798.

[20] Ozalp, C., Szczesna-Skorupa, E., and Kemper, B. (2005) Bimolecular fluorescence complementation analysis of cytochrome p450 2c2, 2e1, and NADPH-cytochrome p450 reductase molecular interactions in living cells, *Drug Metab Dispos 33*, 1382-1390.

[21] Tao, K., Waletich, J. R., Arredondo, F., and Tyler, B. M. (2019) Manipulating Endoplasmic Reticulum-Plasma Membrane Tethering in Plants Through Fluorescent Protein Complementation, *Front Plant Sci 10*, 635.

[22] Sjohamn, J., Bath, P., Neutze, R., and Hedfalk, K. (2016) Applying bimolecular fluorescence complementation to screen and purify aquaporin protein:protein complexes, *Protein Sci 25*, 2196-2208.

[23] Kerppola, T. K. (2006) Design and implementation of bimolecular fluorescence complementation (BiFC) assays for the visualization of protein interactions in living cells, *Nat Protoc 1*, 1278-1286.

[24] Kreida, S., Roche, J. V., Olsson, C., Linse, S., and Tornroth-Horsefield, S. (2018) Protein-protein interactions in AQP regulation - biophysical characterization of AQP0-CaM and AQP2-LIP5 complex formation, *Faraday Discuss 209*, 35-54.

[25] Hua, Y., Ju, J., Wang, X., Zhang, B., Zhao, W., Zhang, Q., Feng, Y., Ma, W., and Wan, C. (2018) Screening for host proteins interacting with Escherichia coli O157:H7 EspF using bimolecular fluorescence complementation, *Future Microbiol 13*, 37-58.

[26] Xin, S., Yu, G., Sun, L., Qiang, X., Xu, N., and Cheng, X. (2014) Expression of tomato SlTIP2;2 enhances the tolerance to salt stress in the transgenic Arabidopsis and interacts with target proteins, *J Plant Res 127*, 695-708.

[27] Weber-Boyvat, M., Li, S., Skarp, K. P., Olkkonen, V. M., Yan, D., and Jantti, J. (2015) Bimolecular fluorescence complementation (BiFC) technique in yeast Saccharomyces cerevisiae and mammalian cells, *Methods Mol Biol 1270*, 277-288.

[28] Hernández-Sánchez, I. E., Maruri-López, I., Molphe-Balch, E. P., Becerra-Flora, A., Jaimes-Miranda, F., and Jiménez-Bremont, J. F. (2019) Evidence for in vivo interactions between dehydrins and the aquaporin AtPIP2B, *Biochemical and biophysical research communications 510*, 545-550.

[29] Dirk, B. S., Jacob, R. A., Johnson, A. L., Pawlak, E. N., Cavanagh, P. C., Van Nynatten, L., Haeryfar, S. M., and Dikeakos, J. D. (2015) Viral bimolecular fluorescence complementation: a novel tool to study intracellular vesicular trafficking pathways, *PLoS One 10*, e0125619.

[30] Kojima, T., Karasawa, S., Miyawaki, A., Tsumuraya, T., and Fujii, I. (2011) Novel screening system for protein-protein interactions by bimolecular fluorescence complementation in Saccharomyces cerevisiae, *J Biosci Bioeng 111*, 397-401.

[31] Murozuka, E., Hanisch, S., Pomorski, T. G., Jahn, T. P., and Schjoerring, J. K. (2013) Bimolecular fluorescence complementation and interaction of various Arabidopsis major intrinsic proteins expressed in yeast, *Physiol Plant 148*, 422-431.
[32] Kodama, Y., and Hu, C. D. (2012) Bimolecular fluorescence complementation (BiFC): a 5-year update and future perspectives, *Biotechniques 53*, 285-298.
[33] Horstman, A., Tonaco, I. A., Boutilier, K., and Immink, R. G. (2014) A cautionary note on the use of split-YFP/BiFC in plant protein-protein interaction studies, *Int J Mol Sci 15*, 9628-9643.
[34] Miller, K. E., Kim, Y., Huh, W. K., and Park, H. O. (2015) Bimolecular Fluorescence Complementation (BiFC) Analysis: Advances and Recent Applications for Genome-Wide Interaction Studies, *J Mol Biol 427*, 2039-2055.

Acknowledgements

The work presented in this study was supported from research grants from the Swedish research Council (VR-M, Structural studies of aquaporin:protein complexes) and the Brain Foundation (FO2018-0231) as well as financial support from the Department of Chemistry and Molecular support to Kristina Hedfalk. We also acknowledge Ulf Yrlid, Samuel Alsén and Rebecca Andersson; Department of Microbiology and Immunology, Gothenburg University, for their kind assistance in the analysis of the flow cytometry data and Peter Dahl for providing the yeast strain.

Author Contribution

Florian Schmitz conducted the majority of the experiments and was involved in the development of the flow cytometry assay for membrane protein complexes (Data curation, Formal analysis, Methodology, Visualization, Writing - original draft & editing).
Jessica Glas conducted the majority of the experiments together with Florian Schmitz (Data curation, Formal analysis, Methodology, Validation, Visualization, Writing - review & editing).
Richard Neutze is the co-supervisor of the path from designing the constructs to evaluation using a high-through put method (Conceptualization, Data curation, Formal analysis, Funding acquisition, Investigation, Project administration, Resources, Supervision, Validation, Writing - review & editing).
Kristina Hedfalk is the main supervisor of the path from designing the constructs to evaluation using a high-through put method (Conceptualization, Data curation, Formal analysis, Funding acquisition, Investigation, Project administration, Resources, Supervision, Validation, Writing - review & editing).